ON NONLOCAL LAGRANGIAN-BASED MODELS AND APPLICATIONS TO MATERIAL FAILURE

A Dissertation

by

SEYED MOHSEN NOWRUZPOUR MEHRIAN

Submitted to the Office of Graduate and Professional Studies of
Texas A&M University
in partial fulfillment of the requirements for the degree of

DOCTOR OF PHILOSOPHY

Chair of Committee,	J. N. Reddy
Committee Members,	Alan D. Freed
	Anastasia Muliana
	Mary Beth Hueste
Head of Department,	Andreas A. Polycarpou

May 2020

Major Subject: Mechanical Engineering

ABSTRACT

Through this study, we present a discrete nonlocal Lagrangian approach called "tridynamics" which is designed at a length scale of interest to characterize the response of the body. As a basic unit to describe the interaction, instead of two particles required to define a bond in conventional discrete frameworks, we introduce three particles at the vertices of a triangular surface. The main idea is to understand the dynamics of a deformable body via a macro potential corresponding to a coupled interaction of rigid particles in the reduced dimension. Because the continuum limit is not taken, the framework automatically relaxes the requirement of differentiability of field variables. The discrete Lagrangian based approach is illustrated to derive equivalent Euler–Bernoulli beam model based upon the corresponding potential function. We also present a set of physical quantities that explain the deformation of Timoshenko beam and Mindlin plate, which help to derive the potential energy.

Although the construction of potential functions for basic elements such as beam and plate might be possible, it is challenging to create it in the generic case. For example, the behavior of carbon nanotube or a graphene sheet is very dependent upon molecular structure. Therefore a derivative-free balance law pertaining to a higher scale of interest has been developed based on the molecular level information, which might be useful in a continuum or discrete setting. Derived using a probabilistic projection technique, the law exploits certain microstructural information in a weakly unique manner. The projection generalizes the notion of directional derivative and, depending on the application, may be interpreted as a discrete Cauchy–Born map with the structure of the classical deformation gradient emerging in the infinitesimal limit. As an illustration, we use the Tersoff–Brenner potential and obtain a discrete macroscopic model for studying the deformation of a single-walled carbon nanotube (SWCNT). The macroscopic (or continuum) model shows the effect of chirality – a molecular phenomenon – in its deformation profile. We also demonstrate the deformation of a fractured SWCNT, which is a first-of-its-kind simulation, and predict

crack branching phenomena in agreement with molecular dynamics simulations. As another example, we have included simulation results for fractured SWCNT bundle with a view to establishing our claim regarding the efficacy of the proposed method.

The discrete Cauchy-Born rule with the principle of virtual work done are employed to formulate a generalized model with the hope to unify local and nonlocal continuum frameworks. We also found a compact mapping matrix which converts surface-based forces (stresses) to the nonlocal body-based forces. The transformation matrix allows reconstructing continuum models at a lower length scale in a discrete setting. Despite the conventional mapping of the microscopic bond from the undeformed configuration, the consistent derivation requires a transformation on the Average Deviation of Lattice (ADL) vector in the region of influence. The new conversion proffers flexibility to the framework for the analysis of nonuniform distribution of particles in the field. To see the credibility of the model, fracture evolution in SCB specimen made of Polymethyl methacrylate (PMMA) is simulated, and the results are compared with experiments.

DEDICATION

To my parents and my wife.

ACKNOWLEDGMENTS

I would like to express my sincere appreciation to my teacher, Professor J.N. Reddy, for his guidance, support, and most importantly care and patience during the course of my Ph.D. studies and research at Texas A&M University. I have been honored to study with Professor Reddy, who has dedicated to the field of applied and computational mechanics. Professor Reddy has always encouraged me to be an independent researcher with confidence. Without his guidance and persistent help this dissertation would not have been possible.

I would like to thank Dr. Alan D. Freed for his valuable comments as committee member and providing helpful resources through my course of study. Special appreciation is extended to Dr. Anastasia H. Muliana, and Dr.Mary Beth Hueste for serving on my Ph.D. committee. I would also like to thank Dr. Saikat Sarkar for the collaboration in this research work.

I am grateful for the financial support that was provided me during my Ph.D. studies by the Oscar S. Wyatt Endowed Chair, and the Aruna and J. N. Reddy Distinguished Fellowship in Computational Mechanics at Texas A&M University. I am thankful to all my seniors and colleagues at the Advanced Computational Mechanics Laboratory (ACML). I also thank Dr. Michael Powell for his kindness and helps to resolve problems to use the cluster at ACML.

I owe thanks to a very special person, my wife, Shahla for her continued and unfailing love, support and understanding during my pursuit of Ph.D degree that made the completion of thesis possible. She was always around at times I thought that it is impossible to continue, she helped me to keep things in perspective. I greatly value her contribution and deeply appreciate her love and unconditional support.

Finally, I acknowledge the people who mean a lot to me, my parents, Abdolhossein and Fatemeh, for showing faith in me. I salute you all for the selfless love, care, pain and sacrifice you did to shape my life. Also I express my thanks to my brother Abolfath who supported me since my childhood, and my sister Zeynab and Maryam for their prayers.

CONTRIBUTORS AND FUNDING SOURCES

This work was supported by a dissertation committee consisting of Professors J.N Reddy (committee chair), Alan D. Freed, and Anastasia H. Muliana of the Department of Mechanical Engineering and Professor Mary Beth Hueste of the Zachry Department of Civil Engineeing.

All other work conducted for the dissertation was completed by the student independently. Graduate study was supported by Oscar S. Wyatt Endowed Chair, and the Aruna and J. N. Reddy Distinguished Fellowship in Computational Mechanics at Texas A&M University.

NOMENCLATURE

ADL	Average Deviation of Lattice
NSPK	Nonlocal Second Piola Kirchhoff
NSPK	Nonlocal First Piola Kirchhoff
NSBP	Nonordinary State-Based Peridynamic
SBPD	State-Based Peridynamics
BBPD	Bond-Based Peridynamics
SB	Surface-Based
BB	Body-Based

TABLE OF CONTENTS

Page

LIST OF FIGURES

FIGURE Page

LIST OF TABLES

TABLE Page

1. INTRODUCTION

1.1 Background

A requirement of the state-of-the-art engineering application is to analyze complex phenomena like deformation of nano-structures, material failure, and so on. In small scale applications, these are solved using molecular dynamics (MD) simulations, which is essentially a discrete Lagrangian based approach. But from a practical point of view, MD simulation is quite inefficient due to the extreme computational overhead [1, 2]. Traditionally, differential continuum laws have been used in large scale system response analysis. As the spatio-temporal length scale of the forcing function or the response mechanisms become comparable to the internal length scale of the body, these classical models tend to diverge from experimental observations [3, 4]. This led to a series of developments of their non-local versions [5, 3, 6, 7, 8]. Samaei et al. [9] studied the effect of length scale on buckling behavior of a single-layer graphene sheet embedded in a Pasternak elastic medium using a nonlocal Mindlin plate theory. They also investigated the effect of small scale and van der Waals forces between adjacent tubes on the column buckling of multi-walled carbon nanotubes [9]. Unfortunately, some of these models show anomalies in responses for certain applications. For example, the Euler–Bernoulli beam model with Eringen type non-locality shows softening effect [10], while non-locality should ideally bring in a stiffening effect. This may be due to a lack of correspondence between these non-local models with their respective appropriate Lagrangian designed to represent physics of the problem.

It is important to establish correspondence between the evolution equation of a given problem and its associated Lagrangian, without which the model may generate energy artificially, like a *perpetual machine*. Besides, while some of these models have been useful in many engineering applications, they are ill-defined for problems that do not admit spatial derivatives of the field variables, for example, in fracture. Since the issue is with the differen-

tiability requirement of the field variable, it seems redundant to write the evolution equation in the continuum limit. Note that for most of the practical cases these continuum models cannot be solved analytically and they must be discretized back for simulation.

Even though we do not wish to use the microscopic potential function of material microstructure due to the computational restriction, some of the basic features of these functions may be useful in designing our Lagrangian at a length scale of interest. For example, many of them involves three-body interaction terms [11, 12]. One such potential is Brenner's potential [13] used to characterize deformation of graphene sheet. Under external influences, the equilibrium angles of crystal structures get changed, which contributes to the energy. This is typically incorporated within the potential via a three-body interaction term [14]. The three-body effects have significant contribution in understanding solid-liquid and vapor-liquid equilibrium of fluids [15, 16, 17, 18]. In certain protein DNA site recognition, while describing interaction between a DNA base and a protein residue with neighboring DNA base, three-body potential terms typically become dominant in comparison to its two-body counterpart [19]. Similarly, many of the macroscopic phenomena, for example, bending, torsion, etc. cannot be described by reduced dimensional models using two particle interaction without taking help of additional variables. Hence, one must characterize the reduced dimensional discrete Lagrangian based on three-body potential.

Silling [20] proposed a derivative-free framework capable of analyzing multi-dimensional problems. The PD framework may be considered as an intermediate route between the classical and molecular dynamics (MD) approaches. Since it characterizes spatial interaction via integration, a PD equation can solve problems with discontinuities without resorting to any special treatment [20]. Based on this advantage, the PD framework finds its application not only in mechanics [20] but also in areas like thermo-mechanics [21], electromigration [22], heat conduction in a body involving discontinuity [23] etc. However, its original bond-based (BBPD) version faces a serious limitation because of its restriction on Poisson's ratio. Besides, the BBPD does not distinguish between volumetric and distortional deformation.

The reason behind such limitations in BBPD is traced back to its assumption of equal and opposite pairwise forces between two particles within a bond. As an important step forward, Silling came up with a modification of the BBPD formalism and proposed state-based peridynamics (SBPD) (more precisely ordinary SBPD) in [24], which could resolve many of the issues associated with the original BBPD approach. Unlike the BBPD, the forces in a bond are unequal in ordinary SBPD [25]. However, the interaction forces within a bond are still considered as collinear. The SBPD framework is successfully applied in different areas of mechanics, e.g. plasticity [24], visco-elasticity [26], visco-plasticity [27], [28], dynamic brittle fracture [29], delamination in composite material [30], branching phenomena [31] etc. But owing to its assumption of collinear forces along a bond, the ordinary SBPD is not applicable to non-linear anisotropic materials [25]. Such limitation has led to further development, and non-ordinary SBPD has been proposed [25]. Unfortunately, the non-ordinary SBPD is also scourged with difficulties in implementations. It may suffer from instability arising from the weak coupling of particles in the definition of deformation gradient. Responses via the non-ordinary SBPD may also show zero energy modes [32].

1.2 Motivation and Scope of the Study

The contribution of the proposed study is novel and significant in the following seven respects [33, 34, 35]:

1. The new macroscopic framework provides flexibility in describing coupled dynamics of rigid multi-particles.

2. Macroscopic description of the Lagrangian avoids microscopic analysis and its computational overhead.

3. The differentiability requirement of field variable is automatically relaxed in the new framework since we do not take any continuum limit.

4. The new framework eliminates the necessity of any advanced mathematical tools such

as Fréchet derivative to construct the force function.

5. A new upscaling law (Discrete Cauchy-Born Rule) was developed to build up macroscopic potential based on molecular information.

6. A transformation matrix is developed that maps conventional stresses to nonlocal derivative-free body-based forces.

7. Numerical analyses are carried out to model crack propagation in carbon nanotube and experimental specimen using developed nonlocal theories.

2. A NONLOCAL LAGRANGIAN-BASED APPROACH TO MACROSCOPIC MODELLING [1]

2.1 Introduction

Lagrangian mechanics is typically considered as more convenient than Newtonian mechanics when it comes to analyzing complex dynamical behavior of rigid body systems [36, 37]. With an increase in the number of constraints, it may become cumbersome and error-prone to write down the laws of motion for such a system using the Newtonian approach. On the other hand, in Lagrangian mechanics, the whole information about the system is preserved within a scalar functional, thus making it easier to handle. For conservative systems, one can arrive at Newton's laws of motion from the Lagrangian via perturbation techniques. However, for non-conservative systems Lagrangian mechanics is not typically suited, even though Newton's equations allow non-conservative forces [38, 37]. This is owing to the fact that dissipation, being a microscopic phenomena, requires a huge number of degrees of freedom at the microscopic level for its characterization, which is not feasible for real-life studies. A more generic macroscopic way of handling non-conservative systems via Lagrangian approach [39, 40] is out of the scope of this study.

In this section, we propose a novel approach to describe the problem with a suitable discrete Lagrangian at a length scale of interest. The main idea is to understand the dynamics of a deformable body via a Lagrangian characterizing coupled interaction of rigid particles. A major advantage of adopting the Lagrangian characterization is its flexibility in describing coupled dynamics of rigid multi-particles. For large scale simulations, a macroscopic description of the Lagrangian is important, since we cannot directly solve the problem via variation of the Lagrangian defined at molecular level, owing to its computational overhead. The differentiability requirement of field variable is automatically relaxed since we do not take the

[1] Reprinted with permission from "A discrete Lagrangian based direct approach to macroscopic modelling." by Sarkar, Saikat, Mohsen Nowruzpour, J. N. Reddy, and A. R. Srinivasa. 2017 *Journal of the Mechanics and Physics of Solids* 98, 172-180. Copyright 2017 by Elsivier.

continuum limit. While constructing the Lagrangian, we must consider that a full-fledged 3D description of the body is not useful in many of the cases. Rather, for many problems, we would look for reduced dimensional descriptions (1D or 2D) via discrete Lagrangian equivalent to beam, plate, and shell models. We also have the advantage of choosing preferred coordinate systems, since one of the major advantages of Lagrangian approach is its flexibility in using a coordinate system. Even though we do not wish to use the microscopic potential function of material micro-structure due to the computational restriction, some of the basic features of these functions may be useful in designing our Lagrangian at a length scale of interest. For example, many of them involves three-body interaction terms [11, 12]. One such potential is Brenner's potential [13] used to characterize deformation of graphene sheet. Under external influences, the equilibrium angles of crystal structures get changed, which contributes to the energy. This is typically incorporated within the potential via a three-body interaction term [14]. The three-body effects have significant contribution in understanding solid-liquid and vapor-liquid equilibrium of fluids [15, 16, 17, 18]. In certain protein DNA site recognition, while describing interaction between a DNA base and a protein residue with neighboring DNA base, three-body potential terms typically become dominant in comparison to its two-body counterpart [19]. Similarly, many of the macroscopic phenomena, for example, bending, torsion, and so on cannot be described by reduced dimensional models using two particle interaction without taking help of additional variables. Hence, one must characterize the reduced dimensional discrete Lagrangian based on three-body potential. Incidentally, we would like to mention that a continuum limit on our model leads to peridynamic (PD) equations as special case [20, 24]. However, the generic structure may be hidden in PD formulation. Besides, PD interactions are classically defined in a cartesian coordinate system.

The rest of the section is organized as the follows. In Section 2, the inter-particle interaction is given a discrete Lagrangian based characterization and the discrete strain and kinetic energy terms are represented as summation of invariant local units (ILUs). In Section

3, the framework is applied to obtain a discrete law corresponding to the Euler–Bernoulli beam (EB) model. Some numerical results for the specific beam example are reported in Section 4. In this section, we also include simulation results of micro crack propagation on thin structures using the present formalism.

2.2 Euler-Lagrangian Equations for a Body

Consider a discrete system of N-particles $\{p_i\}_{i=1}^N$ at material points $\{\mathbf{x}_i\}_{i=1}^N$. As a basic unit to describe interaction, we introduce a three-particle based interaction model, keeping in mind that the displacement information of at least three particles are required to characterize bending behavior (otherwise, a rotation variable would be needed additionally). For convenience in describing the possible coupling in the inter-particle interaction, we consider that the three particles are at the vertices of a triangular surface (see Fig. 2.1). Since we start with a discrete system of particles, the triangular surface is nevertheless imaginary. Note that, such a construct has the potential of incorporating via the imaginary surface, finer length scale information that is ignored in the original discrete model. It may be customary to also mention that the three-particle based framework would include two-particle based interaction models as special cases. Particle p_i rests on one of the vertices of the triangle. The other two vertices span over all the particles in the neighbourhood of p_i. In Fig. 2.1, the evolution of the triangular element from reference to deformed configuration via a map $\boldsymbol{\chi}$ is shown pictorially. The ILU, denoted herein as ω_{ijk}, represents the coupling effect of particles p_j and p_k on p_i, and the functional dependence is written as

$$\omega_{ijk} = \omega_{ijk}\left(\mathbf{y}_i, \mathbf{y}_j, \mathbf{y}_k\right) \tag{2.1}$$

where $\mathbf{y}_i$ is the deformation vector of p_i in the deformed configuration. The discrete strain energy density, W_i, at $\mathbf{x}_i$ is characterized as

$$W_i = \sum_{j=1}^{N}\sum_{k=1}^{N} \frac{1}{3}\left(a_{jk}\omega_{ijk} + a_{ki}\omega_{jki} + a_{ij}\omega_{kij}\right) V_j V_k \tag{2.2}$$

Here V_i is the volume associated with the particle p_i. The fraction $\frac{1}{3}$ is introduced to account for the issue of over-counting; a_{jk} is the contribution factor of ω_{ijk} and is computed herein as a fraction of area as

$$a_{jk} = \frac{\Delta_{ojk}}{\Delta_{ijk}}, \quad a_{ki} = \frac{\Delta_{oki}}{\Delta_{jki}}, \quad a_{ij} = \frac{\Delta_{oij}}{\Delta_{kij}} \tag{2.3}$$

Point O is the centroid of the triangle Δ_{ijk} with $\mathbf{x}_i$, $\mathbf{x}_j$ and $\mathbf{x}_k$ as its vertices (see Fig. 2.1). This leads to a fixed value $\frac{1}{3}$ for a_{jk}, that is, giving each micro-potential corresponding to triangle Δ_{ijk} equal share of the surface area. A general way of computing a_{jk} may be explored by giving variable importance to different micro-potentials within a triangle, which is not done here to maintain simplicity of exposition. The total potential energy (U) may be written as

$$U = \sum_{i=1}^{N} W_i V_i - \sum_{i=1}^{N} \mathbf{f}_i^T \mathbf{u}_i V_i \tag{2.4}$$

$\mathbf{f}_i$ is the external force density applied on particle p_i. $\mathbf{u}_i$ is the displacement of p_i and is related to $\mathbf{y}_i$ as

$$\mathbf{y}_i = \mathbf{x}_i + \mathbf{u}_i \tag{2.5}$$

$\mathbf{x}_i$ is the initial position of particle p_i, that is, before external disturbance.

The total kinetic energy, T, of the discrete system may be generically described in terms of ILU, τ_i, via the following equation:

$$T = \sum_{i=1}^{N} \tau_i \left(\dot{\mathbf{u}}_i\right) V_i \tag{2.6}$$

where $\dot{\mathbf{u}}_i$ is the translational velocity vector at p_i. Note that τ_i may have contribution from its neighbouring particle velocities for some applications. This leads to the following

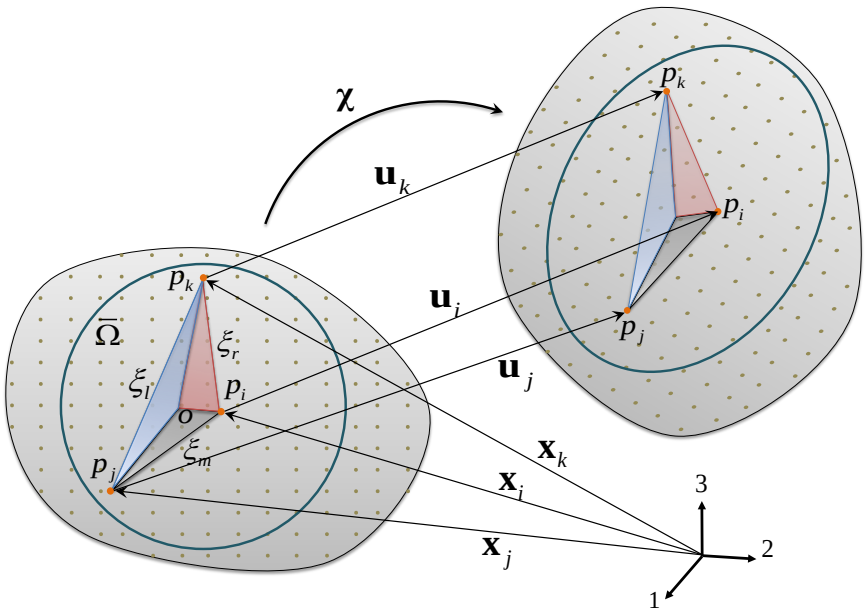

Figure 2.1: Evolution from reference configuration to deformed configuration

Lagrangian:

$$\begin{aligned} L &= T - U \\ &= \sum_{i=1}^{N} \tau_i \left(\dot{\mathbf{u}}_i\right) V_i - \sum_{i=1}^{N}\sum_{j=1}^{N}\sum_{k=1}^{N} \frac{1}{3} \left(a_{jk}\omega_{ijk} + a_{ki}\omega_{jki} + a_{ij}\omega_{kij}\right) V_j V_k V_i \\ &\quad + \sum_{i=1}^{N} \mathbf{f}_i^T \mathbf{u}_i V_i \end{aligned} \tag{2.7}$$

The Euler–Lagrange equations corresponding to $\mathbf{x}_i$ may be arrived at as follows:

$$\begin{aligned} \frac{\partial}{\partial t}\left(\frac{\partial \tau_i\left(\dot{\mathbf{u}}_i\right)}{\partial \dot{\mathbf{u}}_i}\right) V_i + \sum_{j=1}^{N}\sum_{k=1}^{N} \frac{\partial}{\partial \mathbf{u}_i}\left(a_{jk}\omega_{ijk}\right) V_j V_k V_i + \sum_{j=1}^{N}\sum_{k=1}^{N} \frac{\partial}{\partial \mathbf{u}_i}\left(a_{ki}\omega_{jki}\right) V_j V_k V_i \\ + \sum_{j=1}^{N}\sum_{k=1}^{N} \frac{\partial}{\partial \mathbf{u}_i}\left(a_{ij}\omega_{kij}\right) V_j V_k V_i = \mathbf{f}_i V_i \end{aligned} \tag{2.8}$$

Equation (2.8) is the desired evolution equation. Since it is a discrete model, this equation can be used to solve for defects. As we have mentioned earlier in this section a continuum

limit on Eq. (2.8) is useful, because for most of the practical problems of interest analytical solutions are not available. However, to see that, as special case, this equation recovers PD model in the continuum limit, we refer the reader to Appendix A.

2.3 Application to EB Beam Model

Consider a chain of discrete N-particles $\{p_i\}_{i=1}^N$ at material points $\{x_i\}_{i=1}^N$. x_i is taken as a scalar, because we wish to derive a beam model that is one-dimensional. In order to describe bending behavior of body in the present framework, the ILU for the potential energy is defined as the following (see Fig. 2.2):

$$\omega_{ijk} = \frac{1}{2}\beta\phi_{jk}\left(\boldsymbol{\theta}_{ijk}^T\boldsymbol{\theta}_{ijk} + \Psi_{ijk}\right) \tag{2.9}$$

$$\omega_{jki} = \frac{1}{2}\beta\phi_{ki}\left(\boldsymbol{\theta}_{jki}^T\boldsymbol{\theta}_{jki} + \Psi_{jki}\right) \tag{2.10}$$

$$\omega_{kij} = \frac{1}{2}\beta\phi_{ij}\left(\boldsymbol{\theta}_{kij}^T\boldsymbol{\theta}_{kij} + \Psi_{kij}\right) \tag{2.11}$$

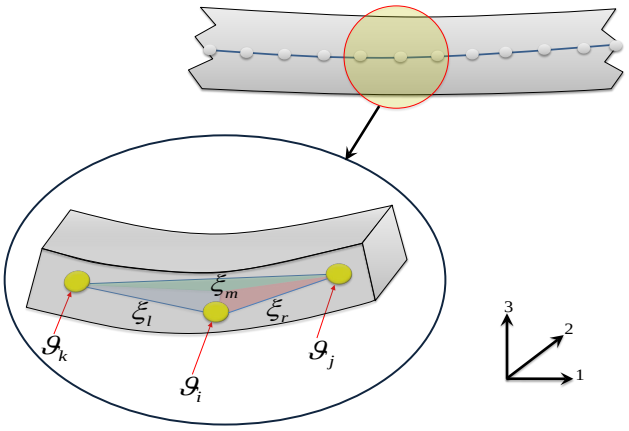

Figure 2.2: Beam element and surface normal

where ϕ_{jk} represents the influence of p_j and p_k on p_i, $\boldsymbol{\theta}_{ijk}$ is the angle of rotation of the

surface normal corresponding to Δ_{ijk} at x_i, and β is the material parameter to be determined via correspondence with classical energy function. The first terms on the right hand sides (RHS-s) of Eqs. (2.9), (2.10), and (2.11) represent pure bending effect, and Ψ_{ijk} is part of the micro-potential ω_{ijk}, effected by the translational vectors corresponding to Δ_{ijk}. A specific structure of Ψ_{ijk} is not required in the present derivation. The angels of rotation of the surface normals are computed for the discrete system as (see Fig. 2.2):

$$\boldsymbol{\theta}_{ijk} = \left(\frac{(\boldsymbol{\vartheta}_j - \boldsymbol{\vartheta}_i)}{\xi_r} + \frac{(\boldsymbol{\vartheta}_k - \boldsymbol{\vartheta}_i)}{\xi_l} \right)$$

$$\boldsymbol{\theta}_{jki} = \left(\frac{(\boldsymbol{\vartheta}_k - \boldsymbol{\vartheta}_j)}{\xi_m} + \frac{(\boldsymbol{\vartheta}_i - \boldsymbol{\vartheta}_j)}{\xi_r} \right)$$

$$\boldsymbol{\theta}_{kij} = \left(\frac{(\boldsymbol{\vartheta}_i - \boldsymbol{\vartheta}_k)}{\xi_l} + \frac{(\boldsymbol{\vartheta}_j - \boldsymbol{\vartheta}_k)}{\xi_m} \right)$$

Here, $\boldsymbol{\vartheta}_i$ is the surface normal vector at point x_i.

The kinetic energy of the discrete system of particles may be written as:

$$T = \sum_{i=1}^{N} \frac{1}{2} I_i \left(\frac{1}{r_i} \dot{w}_i + \dot{\theta}_i \right)^2 V_i \tag{2.12}$$

where w_i is the displacement along axis 3, θ_i is the rotation along axis 2 (see Fig. 2.2), r_i is the radius, and I_i the moment of inertia per unit volume of the particle p_i. Since we want to derive a beam equation, contribution from other components would be considered negligible. Here, we can see that a complicated structure of kinetic energy can be easily described in the discrete Lagrangian mechanics based framework. The Lagrangian, L, may be expressed

as

$$
\begin{aligned}
L &= T - U \\
&= \sum_{i=1}^{N} \frac{1}{2} I_i \left(\frac{1}{r_i} \dot{w}_i + \dot{\theta}_i \right)^2 V_i \\
&- \sum_{i=1}^{N} \sum_{j=1}^{N} \sum_{k=1}^{N} \frac{1}{6} \beta a_{jk} \phi_{jk} \left(\boldsymbol{\theta}_{ijk}^T \boldsymbol{\theta}_{ijk} + \Psi_{ijk} \right) V_i V_j V_k \\
&- \sum_{i=1}^{N} \sum_{j=1}^{N} \sum_{k=1}^{N} \frac{1}{6} \beta a_{ki} \phi_{ki} \left(\boldsymbol{\theta}_{jki}^T \boldsymbol{\theta}_{jki} + \Psi_{jki} \right) V_i V_j V_k \\
&- \sum_{i=1}^{N} \sum_{j=1}^{N} \sum_{k=1}^{N} \frac{1}{6} \beta a_{ij} \phi_{ij} \left(\boldsymbol{\theta}_{kij}^T \boldsymbol{\theta}_{kij} + \Psi_{kij} \right) V_i V_j V_k \\
&+ \sum_{i=1}^{N} \left(f_i c_i \right) \theta_i V_i + \sum_{i=1}^{N} \left(f_i w_i V_i \right)
\end{aligned}
\tag{2.13}
$$

where f_i is the body force in the direction of w_i, and c_i is the eccentricity of the body force f_i with respect to the centre of particle p_i. By taking derivative with respect to rotation of a surface normal at a material point, the associated Euler–Lagrange equation may be found as

$$
\begin{aligned}
I_i \left(\frac{1}{r_i} \ddot{w}_i + \ddot{\theta}_i \right) &= \frac{1}{3} \sum_j \sum_k \beta \phi_{x_j x_k} \left(\frac{(\theta_j - \theta_i)}{|x_j - x_i|} + \frac{(\theta_k - \theta_i)}{|x_k - x_i|} \right) V_{x_i} V_{x_k} \\
&- \frac{1}{3} \sum_j \sum_k \beta \phi_{x_j x_k} \left(\frac{(\theta_k - \theta_j)}{|x_k - x_j|} + \frac{(\theta_i - \theta_j)}{|x_i - x_j|} \right) V_{x_j} V_{x_k} \\
&- \frac{1}{3} \sum_j \sum_k \beta \phi_{x_j x_k} \left(\frac{(\theta_i - \theta_k)}{|x_i - x_k|} + \frac{(\theta_j - \theta_k)}{|x_j - x_k|} \right) V_{x_j} V_{x_k} \\
&+ f_i c_i
\end{aligned}
\tag{2.14}
$$

Under the assumption of $\frac{1}{r_i} >> 1$, we may drop the term $\ddot{\theta}_i$ from Eq. (2.14) for all practical purposes. This leads to the EB equation in the proposed framework as:

$$
\frac{I_i}{r_i c_i} \ddot{w}_i = \frac{2}{3} \sum_{x_i - \delta}^{x_i + \delta} \sum_{x_i - \delta}^{x_i + \delta} \hat{\beta} \phi_{x_j x_k} \left(\frac{(\theta_j - \theta_i)}{|x_j - x_i|} + \frac{(\theta_k - \theta_i)}{|x_k - x_i|} \right) V_j V_k + f_i \tag{2.15}
$$

where $\hat{\beta}$ is the new coefficient absorbing information regarding particle cross-sectional area and eccentricity, δ is the radius of the influence domain, and $\frac{I_i}{r_i c_i}$ represents the mass density. Note that if we do not drop the rotational inertia term, the equation may be called a

discrete version of Rayleigh beam without any spatial derivative. To the best of the authors' knowledge, this is the first derivation of non-local Rayleigh beam model. To solve Eq. (2.15), we need to establish a map between θ_i and w_i. This may be accomplished by the following definition of surface normal vector, $\boldsymbol{\vartheta}_i$, based on its physics:

$$\boldsymbol{\vartheta}_i = (-\mathbf{I} + \bigtriangledown_{x^-}\mathbf{u}_i) \times (-\mathbf{I} + \bigtriangledown_{x^+}\mathbf{u}_i) \tag{2.16}$$

where $\bigtriangledown_{x_i^-}\mathbf{u}_i$ is the gradient of $\mathbf{u}_i$ on the left limit and $\bigtriangledown_{x_i^+}\mathbf{u}_i$ on the right limit of $\mathbf{x}_i$ and $\mathbf{I} := \{1, 0, 0\}^T$. This specific definition captures bending behavior of body cancelling out other possibilities, for example, the rigid body motion. Using the formulae given by Eq. (2.16), we can solve Eq. (2.15).

Upon Taylor's expansion of θ_j and θ_k in Eq. (2.15) around θ_i and taking $\delta \to 0$, we can solve for the material parameter as

$$\frac{4}{3}\varsigma\hat{\beta}\xi^2\left[\frac{1}{\xi^2}\left(\bigtriangledown_{x_i^-}\theta_i + \bigtriangledown_{x_i^+}\theta_i\right)\right] = -\bar{E}\bar{I}\frac{\partial^4 w_i}{\partial x^4} \tag{2.17}$$

$$\varsigma = \sum_{x_i-\delta}^{x_i+\delta}\sum_{x_i}^{x_i+\delta}\phi_{x_j x_k}V_j V_k \tag{2.18}$$

Here $\bar{E}$ and $\bar{I}$ are Young's modulus of elasticity and moment of inertia of a classical EB model, respectively [37]. Following Eq. (2.17), we can write,

$$\hat{\beta} = -\frac{3\bar{E}\bar{I}}{4\xi^2\varsigma} \tag{2.19}$$

2.4 Numerical Results

2.4.1 Beam Model

We consider a beam of length unit length (1 m) and cross sectional area 0.05×0.001 m^2, and subjected to a uniform load of 5 N/m. The beam is initially at rest with zero velocity. Mass density and Young's modulus are taken as 8050 $\mathrm{kg/m}^3$ and 200×10^{11} $\mathrm{N/m}^2$,

Table 2.1: Material properties and numerical parameter values for isotropic beam and plate.

Parameters Values	Plate	Beam
X-direction discretization	500	100
Y-direction discretization	500	1
Boundary Velocity (m/s)	50.0	0.0
Boundary Loading (N/m^2)	0.0	5.0
Length (m)	0.05	1.00
Width (m)	0.05	0.05
Crack length (m)	0.01	0.0
δ (m) (Horizon radius)	3.01×10^{-4}	3.01×10^{-4}
ρ (kg/m^3)	8000.0	8050.0
Elasticity Modulus (N/m^3)	576×10^9	200×10^{11}
Area (m^2)	10^{-8}	5×10^{-8}
Time constant (s)	1.4×10^{-4}	2×10^{-3}

respectively. The required parameter values are presented in Table 2.1. With varying δ, we report the displacement profiles for three different cases: (1) simply supported (see Fig. 2.3), (2) clamped (see Fig. 2.4), and (3) cantilever (see Fig. 2.5) boundary conditions. The results are reported for time $t = 15$ s for simply supported and clamped beams and at $t = 22$ s for the cantilever beam. The numerical simulation is carried out with time step $\Delta t = 2 \times 10^{-3}$ s. While the choice of weight function is a matter of further investigation, here we consider a weight function that assumes a fixed value of unity within the influence domain and vanishes outside. Since the proposed framework, by construct, gives non-local models, it may be worth mentioning that the discrete EB model provides stiffer solution in comparison to classical EB model.

2.4.2 Micro-Crack Propagation in a Thin Structure

To show that, while this framework is demonstrated with an emphasis on three-body interaction, it includes two-body interactions as a special case, we simulate the problem of crack propagation in a thin plate structure via an appropriate potential function. The potential term is constructed at a length scale of interest, considering a coupled system of N

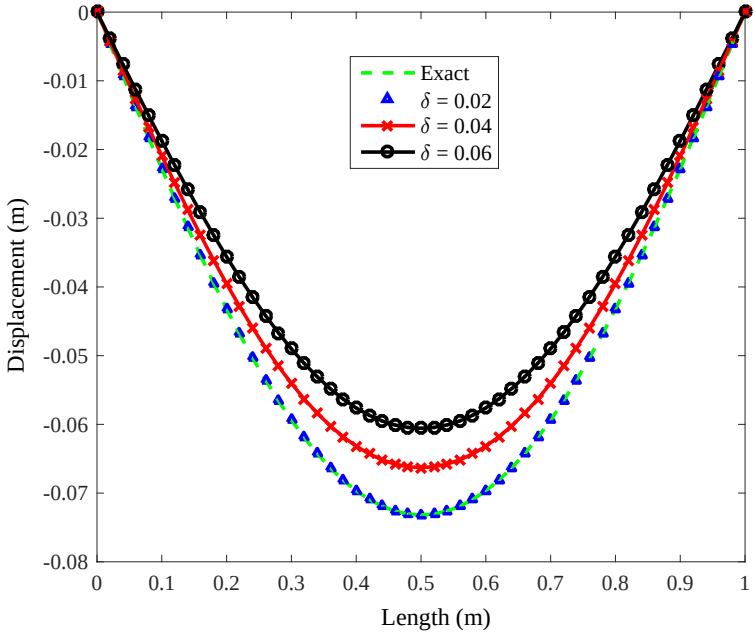

Figure 2.3: Displacement profiles with varying δ for simply support beam

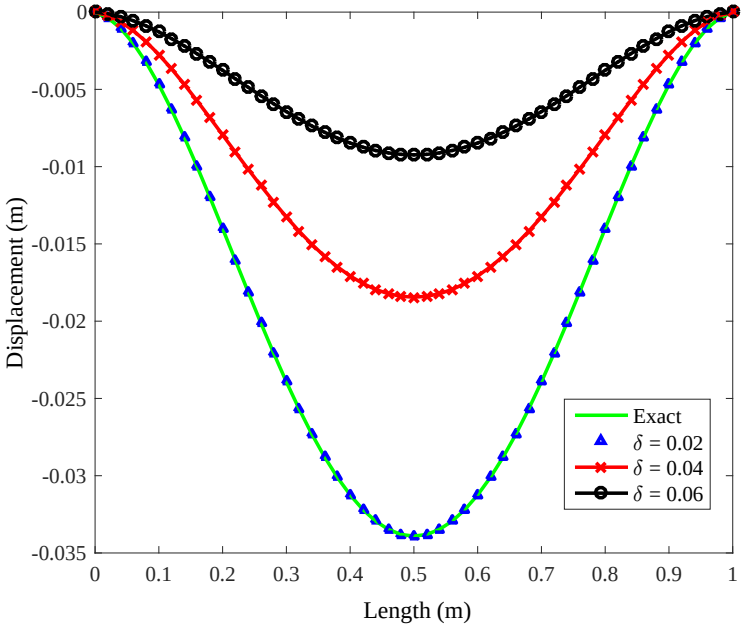

Figure 2.4: Displacement profiles with varying δ for clamped beam

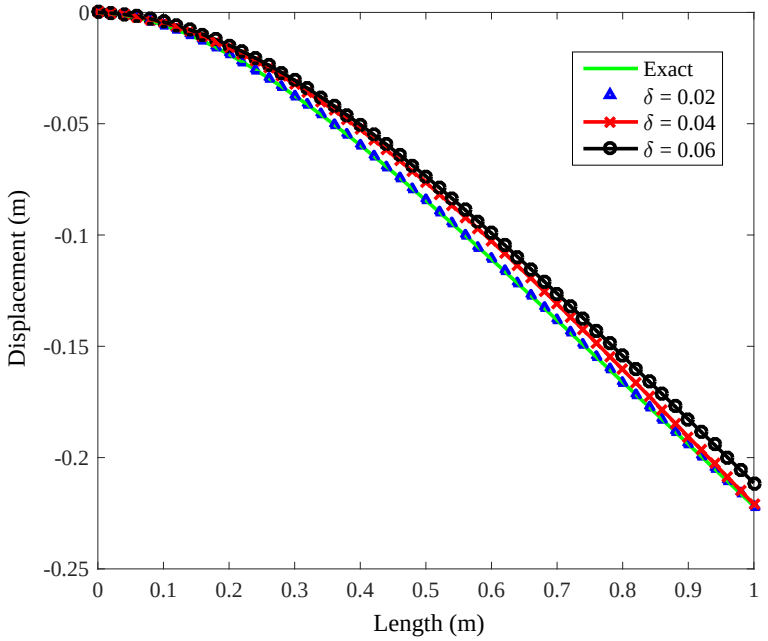

Figure 2.5: Displacement profiles with varying δ for cantilever beam

particles. The corresponding Lagrangian is taken as

$$L = \sum_{i=1}^{N} \frac{1}{2} \rho_i \mathbf{v}_i{}^T \mathbf{v}_i V_i - \sum_{i=1}^{N} \sum_{j=1}^{N} \frac{1}{2} \phi_{ij} k_{ij} l_{ij} \left(\frac{l'_{ij} - l_{ij}}{l_{ij}} \right)^2 V_i V_j \tag{2.20}$$

where $\mathbf{v}_i$ is the velocity of the particle p_i, l_{ij}, and l'_{ij} are Euclidean distances between particles p_i and p_j in undeformed and deformed conditions, respectively, k_{ij} is the associated stiffness, and ϕ_{ij} is the weight function. Through a material correspondence with a classical 2-D plate model, stiffness modulus may be found as, $k_{ij} = \frac{9E}{\pi \delta^4 (1-\nu)}$, where ν is Poisson's ratio. The crack is allowed to propagate once the stretch term ($s = \frac{l'_{ij} - l_{ij}}{l_{ij}}$) exceeds a critical stretch (s_c). The critical stretch is computed by comparing the work required to break all the interactions corresponding to a particle with the critical strain energy release rate (G_c) for a material.

Specifically, s_c is given as

$$s_c = 3\pi \sqrt{\frac{G_c\left(1-\nu^2\right)}{E\delta\left(24\nu + 27\pi\left(1-\nu\right) - 8\right)}} \tag{2.21}$$

We note that only brittle fracture is considered here. A plate of initial crack length 0.01 m is placed at the middle of the structure horizontally. We consider both isotropic and anisotropic materials. Along the y-axis (see Fig. 2.6 or 2.7), we apply 50 m/s and -50 m/s velocities on the left and the right edges, respectively, and the other edges are kept relaxed. The other required parameter values for the isotropic plate are given in Table 2.1. Figure 2.6 depicts the crack propagation snapshot on the isotropic material at time $t = 1.4 \times 10^{-5}$ s. From the simulation results (see Fig. 2.6 or 2.7), we can see that the isotropic plate does not show any micro-crack in its response.

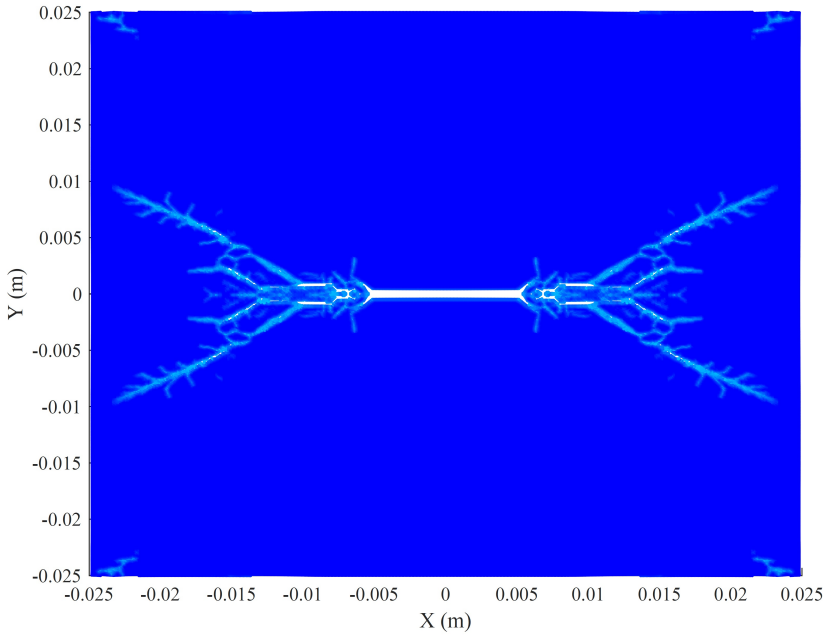

Figure 2.6: Crack propagation in an isotropic plate

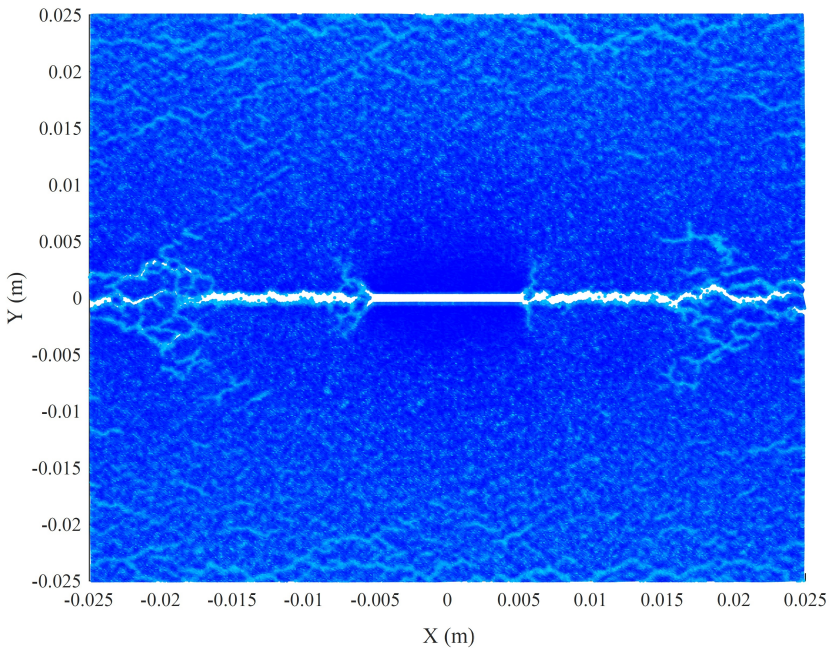

Figure 2.7: Crack propagation in an anisotropic plate

3. TRIDYNAMIC MODEL OF THE BEAM WITH TRANSVERSE SHEAR DEFORMATION

3.1 Introduction

The matter is fundamentally discrete, and due to this nature, Molecular Dynamics (MD) formulation could be employed to prognosticate the response. However, this formulation is not practical to be used in large scale due to heavy computation. On other hands, classical continuum theories (CCT) which assume continuity of matter has been successful in analyzing a wide range of engineering problem. However, these assumptions limit the reliability of the CCT to problems with no scale effect. Short wavelength excitation and analysis of nanomaterial such as carbon nanotube are some examples that CCT failed to describe them accurately [41].

The peridynamics (PD) framework is an intermediate approach between the classical and molecular dynamics model [20]. However, its original bond-based peridynamics (BBPD) suffers from the restriction on Poisson's ratio. Besides, the BBPD does not differentiate the volumetric and distortional deformation. These restrictions could be traced back to the assumption of forces developed between two particles within a bond which are equal and opposite. Unlike the BBPD, in ordinary State-Based PD (SBPD)[25] the forces in a bond may not be necessarily equal, and the interaction forces within a bond are still considered as collinear. The SBPD framework is successfully implemented in various mechanical problems, including plasticity [24], visco-plasticity [28], dynamic brittle fracture [29]. Diyaroglu et. al.[42] presents a comprehensive study on the BBPD model of Timoshenko beam and Mindlin plate. However, the results are valid for a thin plate or beam with a small height. Also, the presented approach will result in a linear behavior of frequency response in the axial direction.

In this section, we construct a tridynamic beam model which allows for transverse shear

deformation. Despite the prior presentation of deformation based upon surface normal as a mathematical concept, [33], we utilized the kinematic of the beam to suggest meaningful physical quantities in the framework. Since the interactions are described through three particles, we call this model "tridynamics." The new nonlocal formulations account for scale effects, and it permits recovering the classical model when the local limit is taken. A comparison of the localized equations of the tridynamics with the classical ones allows setting a relationship between the local and nonlocal parameters.

The rest of section is organized as follows: In Section 3.2 we characterize the nonlocal deformation basic unit based upon the kinetics of material particles within a triangular unit. In Section 3.3, the Lagrangian of the tridynamics beam is formulated. Through Section 3.4, we employ the Euler-Lagrange equation to derive the governing equation for the beam. We also include localization steps of the model to determine nonlocal parameters. In Section 3.6, we perform the dispersion analysis and find three modes of frequency and wave speed of the beam analytically. In Section 3.7, the dispersion curve of the beam are presented through a numerical implementation.

3.2 Tridynamic Kinematics

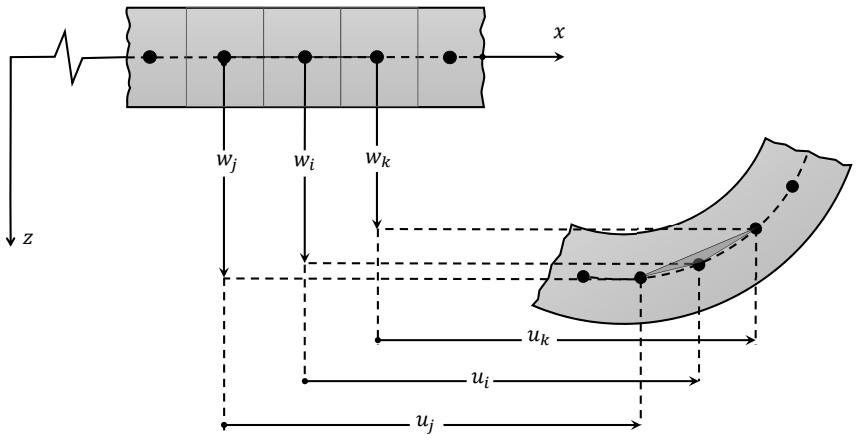

Figure 3.1: Kinematic of the discrete beam with transverse shear

In this section, a representative kinematic is described to model Timoshenko beam in the tridynamics framework. Unlike the previous description of Euler-Bernoulli beam through mathematical tools such as normal surface [33], here we solely use the kinematic of the system to define deformation of the basic unit. For that purpose, we consider a set of particles distributed uniformly along the x-axis. Fig. 3.1 shows a portion of the beam before and after deformation. Each particle is shown by a solid black circle where is embedded in the center of a rectangular unit. Although we have not shown particles above and below the central axis, the derivation throughout this section will remain valid for a beam with larger height. In the model, we include all three type of displacement, including axial, transverse, and rotational ones. To avoid complexity in illustration, the axial and transverse displacements are depicted in Fig. 3.1 and the rotational deformation is illustrated in Fig. 3.2 separately.The deformation at ith particle could be described by the construction of a basic triangular unit with three vertices i, j and k. In the tridynamics framework, the ith vertice represents the i^{th} particle, and it locates in the center of the influence domain. However, the other two vertices could be any two-particle in the horizon. For more elaboration of multi-body interaction, one may refer to [33].

In the analysis of beam, all edges of the triangle lie on x-axis before deformation. The triangle could be visible if the curvature of the beam changes. We are noting that this surface is imaginary and we are not going to make use of it in our analysis. However, one might use it as a nonlocal parameter (area scale).

To capture deformations of Timoshenko beam in this framework, we introduce three quantities that represent the stretch, curvature, and shear of the beam. The first quantity which presents the axial deformation at x_i could be given as:

$$\epsilon_{ijk} = \hat{u}_{ij} + \hat{u}_{ik},\ \epsilon_{jki} = \hat{u}_{jk} + \hat{u}_{ji},\ \epsilon_{kij} = \hat{u}_{kj} + \hat{u}_{ki} \tag{3.1}$$

The indices j and k are referring to particles, j, and k which are located in the influence

domain of particle i. $\hat{u}$ is the nonlocal axial strain and could be given:

$$\hat{u}_{ij} = \frac{u_j - u_i}{\xi_{ij}},\ \hat{u}_{ik} = \frac{u_k - u_i}{\xi_{ik}},\ \hat{u}_{jk} = \frac{u_k - u_j}{\xi_{jk}} \tag{3.2}$$

Noting that u_α indicates the axial displacement of particle α. The distance between particles α and β before deformation could be shown by $\xi_{\alpha\beta}$ as follows:

$$\xi_{ij} = \xi_{ji} = |x_j - x_i|\,,\ \xi_{ik} = \xi_{ki} = |x_k - x_i|\,,\ \xi_{jk} = \xi_{kj} = |x_k - x_j|\,, \tag{3.3}$$

One can easily find that $\hat{u}_{ji} = -\hat{u}_{ij},\ \hat{u}_{ki} = -\hat{u}_{ik},\ \hat{u}_{kj} = -\hat{u}_{jk}$.

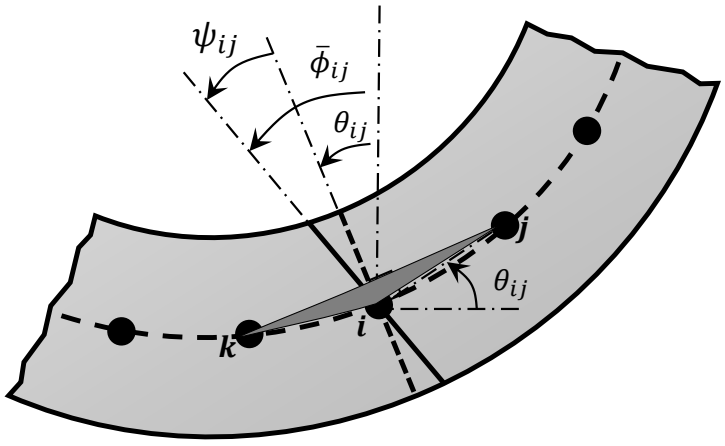

Figure 3.2: Angular deformation of the straight line in a unit.

In the following, we present the related deformation to curvature and shear of the beam. To avoid the complexity of figure, we illustrate rotational changes of i^{th}, j^{th} and k^{th} particles in three different plots (see figure. 3.2). Following classical Timoshenko beam theory, the straight line normal to the axis of the beam remains straight and inextensible (Timoshenko beam assumptions). Therefore, the curvature of the beam in this framework may be

characterized as:

$$\kappa_{ijk} = \hat{\phi}_{ij} + \hat{\phi}_{ik},\ \kappa_{jki} = \hat{\phi}_{jk} + \hat{\phi}_{ji},\ \kappa_{kij} = \hat{\phi}_{kj} + \hat{\phi}_{ki} \tag{3.4}$$

Noting that $\kappa_{\alpha\beta\gamma}$ is the curvature due to interaction of particle γ and β with particle α. Also $\hat{\phi}_{\alpha\beta}$ is one of the constituent components of the curvature due to rotational differences of particle β and α and can be given:

$$\hat{\phi}_{ij} = \frac{\phi_j - \phi_i}{\xi_{ij}},\ \hat{\phi}_{ik} = \frac{\phi_k - \phi_i}{\xi_{ik}},\ \hat{\phi}_{jk} = \frac{\phi_k - \phi_j}{\xi_{jk}}, \tag{3.5}$$

Here, ϕ_α is the rotation of the transverse straight line of particle α around y-axis (straight black line in Fig. 3.2). Noting that $\hat{\phi}_{ji} = -\hat{\phi}_{ij},\ \hat{\phi}_{ki} = -\hat{\phi}_{ik},\ \hat{\phi}_{kj} = -\hat{\phi}_{jk}$. The transverse shear deformation in the framework may be defined as:

$$\begin{aligned}
\psi_{ijk} &= \psi_{ij} + \psi_{ik} = \left(\theta_{ij} - \hat{n}_{ij}\bar{\phi}_{ij}\right) + \left(\theta_{ik} - \hat{n}_{ik}\bar{\phi}_{ik}\right), \\
\psi_{jki} &= \psi_{jk} + \psi_{ji} = \left(\theta_{jk} - \hat{n}_{jk}\bar{\phi}_{jk}\right) + \left(\theta_{ji} - \hat{n}_{ji}\bar{\phi}_{ji}\right), \\
\psi_{kij} &= \psi_{ki} + \psi_{kj} = \left(\theta_{kj} - \hat{n}_{kj}\bar{\phi}_{kj}\right) + \left(\theta_{ki} - \hat{n}_{ki}\bar{\phi}_{ki}\right)
\end{aligned} \tag{3.6}$$

Where $\theta_{\alpha\beta}$ is showing the slope of the beam at particle α and could be defined as:

$$\theta_{ij} = \frac{w_j - w_i}{\xi_{ij}},\ \theta_{ik} = \frac{w_k - w_i}{\xi_{ik}},\ \theta_{jk} = \frac{w_k - w_j}{\xi_{jk}} \tag{3.7}$$

and w_α is the transverse displacement of the particle α. In Eq. 3.6, $\bar{\phi}_{\alpha\beta}$ is the average rotation of the straight lines associated to α and β and it could be rewritten for particle i, j and k as:

$$\bar{\phi}_{ij} = \frac{\phi_j + \phi_i}{2},\ \bar{\phi}_{ik} = \frac{\phi_k + \phi_i}{2},\ \bar{\phi}_{jk} = \frac{\phi_k + \phi_j}{2} \tag{3.8}$$

The direction of the bond vector starting from particle α to particle β is shown by $\hat{n}_{\alpha\beta}$ and

could be express for i, j and k as:

$$\hat{n}_{ij} = \frac{x_j - x_i}{\xi_{ij}},\ \hat{n}_{ik} = \frac{x_k - x_i}{\xi_{ik}},\ \hat{n}_{jk} = \frac{x_k - x_j}{\xi_{jk}}, \tag{3.9}$$

The given definitions of deformations can help us to build up a proper Lagrangian of a system that incorporates three-particle interactions. Noting that the introduction of these physical quantities such as ϵ and κ could be vastly employed in other mechanical problems to properly describe changes of the field variables in this framework (for instance, the ϵ could be used as a discrete derivative-free temperature gradient in Fourier law, if we set temperature as our field variable).

It should be noted that , $\theta_{ji} = -\theta_{ij},\ \theta_{ki} = -\theta_{ik},\ \theta_{kj} = -\theta_{jk}$, and $\bar{\phi}_{ji} = \bar{\phi}_{ij},\ \bar{\phi}_{ki} = \bar{\phi}_{ik},\ \bar{\phi}_{kj} = \bar{\phi}_{jk}$. For the bond direction, we have; $\hat{n}_{ji} = -\hat{n}_{ij},\ \hat{n}_{ki} = -\hat{n}_{ik},\ \hat{n}_{kj} = -\hat{n}_{jk}$. We also can show that:

$$\begin{aligned} \epsilon_{ijk} + \epsilon_{jki} + \epsilon_{kij} &= 0 \\ \kappa_{ijk} + \kappa_{jki} + \kappa_{kij} &= 0 \\ \psi_{ijk} + \psi_{jki} + \psi_{kij} &= 0 \end{aligned} \tag{3.10}$$

In additions, in a three-particle basic unit, the order of interaction of two particles on the particle of interest does not matter. In other words, if $\Phi_{\alpha\beta\gamma}$ defines the interaction of particle β and γ with particle α, it will be the same as $\Phi_{\alpha\gamma\beta}$. This remains valid for all of the kinematical concepts in this section.

3.3 Lagrangian of the System

Consider a beam made of a chain of particles with length L, width b, and thickness h. The Lagrangian of the system could be calculated by summing up the potential and kinetic energy of the system. The potential energy for the structure could be divided into three smaller sub-potentials which are due to stretch, curvature, and shear effect of the beam:

$$U = U^{\epsilon} + U^{\kappa} + U^{\psi} \tag{3.11}$$

Here, U^{ϵ}, U^{κ} and U^{ψ} are respective portions of potential energies associated to the stretch, curvature and shear deformation of the beam. They also could be physically interpreted as the required energy to deform the edges and angles of the triangular unit. Each of these portions could be broken up into the smaller ones to directly show the contribution of individual particles in the basic:

$$\begin{aligned} U^{\epsilon} &= U^{\epsilon_i} + U^{\epsilon_j} + U^{\epsilon_k} = \sum_{i=1}^{N} \omega_i^{\epsilon_i} V_i + \sum_{i=1}^{N} \omega_i^{\epsilon_j} V_i + \sum_{i=1}^{N} \omega_i^{\epsilon_k} V_i \\ U^{\kappa} &= U^{\kappa_i} + U^{\kappa_j} + U^{\kappa_k} = \sum_{i=1}^{N} \omega_i^{\kappa_i} V_i + \sum_{i=1}^{N} \omega_i^{\kappa_j} V_i + \sum_{i=1}^{N} \omega_i^{\kappa_k} V_i \\ U^{\psi} &= U^{\psi_i} + U^{\psi_j} + U^{\psi_k} = \sum_{i=1}^{N} \omega_i^{\psi_i} V_i + \sum_{i=1}^{N} \omega_i^{\psi_j} V_i + \sum_{i=1}^{N} \omega_i^{\psi_k} V_i \end{aligned} \tag{3.12}$$

Where U^{ϵ_α} is a part of the axial potential energy that comes from the effect of the particles β and γ on the particle α due to stretch effect. Similarly, the corresponding curvature (κ) and shear (ψ) potential energies can be described. Noting that U^{ϵ_α}, U^{ϵ_β} and U^{ϵ_γ} can be rewritten in terms of their potential densities as given in Eq. 3.12. Here, V_i denotes the volume of the ith particle. The upper bound of the series (N) indicates the total number of particles in the beam. The potential energy density (ω) due to stretch, curvature, and shear of the beam could be defined as:

$$\begin{aligned} \omega_i^{\epsilon_i} &= \frac{1}{6} \sum_{j=1}^{M} \sum_{k=1}^{M} A_{ijk} \epsilon_{ijk} V_k V_j, \ \omega_i^{\epsilon_j} = \frac{1}{6} \sum_{j=1}^{M} \sum_{k=1}^{M} A_{jki} \epsilon_{jki} V_k V_j, \ \omega_i^{\epsilon_k} = \frac{1}{6} \sum_{j=1}^{M} \sum_{k=1}^{M} A_{kij} \epsilon_{kij} V_k V_j, \\ \omega_i^{\kappa_i} &= \frac{1}{6} \sum_{j=1}^{M} \sum_{k=1}^{M} B_{ijk} \kappa_{ijk} V_k V_j, \ \omega_i^{\kappa_j} = \frac{1}{6} \sum_{j=1}^{M} \sum_{k=1}^{M} B_{jki} \kappa_{jki} V_k V_j, \ \omega_i^{\kappa_k} = \frac{1}{6} \sum_{j=1}^{M} \sum_{k=1}^{M} B_{kij} \kappa_{kij} V_k V_j, \\ \omega_i^{\psi_i} &= \frac{1}{6} \sum_{j=1}^{M} \sum_{k=1}^{M} C_{ijk} \psi_{ijk} V_k V_j, \ \omega_i^{\psi_j} = \frac{1}{6} \sum_{j=1}^{M} \sum_{k=1}^{M} C_{jki} \psi_{jki} V_k V_j, \ \omega_i^{\psi_k} = \frac{1}{6} \sum_{j=1}^{M} \sum_{k=1}^{M} C_{kij} \psi_{kij} V_k V_j \end{aligned} \tag{3.13}$$

Where $A(N/m^8)$, $B(N/m^7)$, and $C(N/m^8)$ are the stretch, curvature and shear conjugate pairs of the ϵ, κ and ψ. The ratio of 1/6 is in equation to avoid the overcounting of each particle's contribution in basic units (the ratio of 1/3) and split the potential densities between two particles (the ratio of 1/2). Since the equations will be eventually calibrated

by using classical or experimental data, one may drop this ratio in the analysis. One of the clear differences of the tridynamics framework with peridynamics could be the introduction of the nanopotential function instead of micropotential to form the Lagrangian of the system. Such a description may help to analyze problems that need a smaller length scale. The total kinetic energy T of the system can be written as:

$$T = \frac{1}{2}\sum_{i=1}^{N} \rho \left[\dot{u_i}^2 + \frac{I}{A}\dot{\phi_i}^2 + 2z_i\dot{u_i}\dot{\phi_i} + \dot{w_i}^2 \right] V_i \tag{3.14}$$

Where ρ, A and I are the mass density, the moment of inertia and the cross-section area of the beam, respectively. Noting that the kinetic energy does not incorporate any length scale parameter. The ith particle that undergo the general two dimensional rigid body motion including axial (u), transverse (w) and rotational motion (ϕ). Such a insight may avoid phenomenological definition of kinetic energy with length scale parameter [43]. In this section, the word *particle* refers to a cubic volume V with mass density of ρ. In Eq. 3.14, the variable z is showing coordinates of the particles in z direction. For a very thin beam i.e. $h/L << 1$, the variable z could be approximated to zero, therefore, the coupling terms vanish. For keeping simplicity of the equations and avoiding more coupling terms in numerical part, we solely calculate the kinetic energy for particle i on the axial line. However the following derivations will remain valid for larger height. The Lagrangian of the Timoshenko beam in the framework could found using:

$$L = T - U \tag{3.15}$$

3.4 Equation of Motion of Tridynamic Beam

To derive the EOM of the system, the Euler-Lagrange equations can be employed. Since the system is conservative, the following set of equations could be derived. The time-dependent field variable used in the Lagrangian of the system is (u, w and ϕ); thus, we

have:

$$\frac{d}{dt}\left(\frac{\partial L}{\partial \dot{u}_i}\right) = \frac{\partial L}{\partial u_i}, \quad \frac{d}{dt}\left(\frac{\partial L}{\partial \dot{w}_i}\right) = \frac{\partial L}{\partial w_i}, \quad \frac{d}{dt}\left(\frac{\partial L}{\partial \dot{\phi}_i}\right) = \frac{\partial L}{\partial \phi_i} \tag{3.16}$$

Noting that T is the only quantity that involves the time derivative of the field variable while terms with displacement components appear in U. Substituting Lagrangian (Eq. 3.15) into the Euler-Lagrange (Eqs. 3.16) equations gives:

$$\frac{d}{dt}\left(\frac{\partial T}{\partial \dot{u}_i}\right) = -\frac{\partial U}{\partial u_i}, \quad \frac{d}{dt}\left(\frac{\partial T}{\partial \dot{w}_i}\right) = -\frac{\partial U}{\partial w_i}, \quad \frac{d}{dt}\left(\frac{\partial T}{\partial \dot{\phi}_i}\right) = -\frac{\partial U}{\partial \phi_i} \tag{3.17}$$

The left-hand side of Eq. (3.17) could be written as:

$$\begin{aligned}
\frac{d}{dt}\left(\frac{\partial T}{\partial \dot{u}_i}\right) &= \rho \ddot{u}_i + 2 z_i \rho \ddot{\phi}_i, \\
\frac{d}{dt}\left(\frac{\partial T}{\partial \dot{w}_i}\right) &= \rho \ddot{w}_i, \\
\frac{d}{dt}\left(\frac{\partial T}{\partial \dot{\phi}_i}\right) &= \rho \frac{I}{A} \ddot{\phi}_i + 2 z_i \rho \ddot{u}_i
\end{aligned} \tag{3.18}$$

and the right-hand side could be rewritten for all degrees of freedom (u, w and ϕ):

$$\begin{aligned}
\frac{\partial U}{\partial u_i} &= \frac{\partial U^{\epsilon}}{\partial u_i} + \frac{\partial U^{\kappa}}{\partial u_i} + \frac{\partial U^{\psi}}{\partial u_i} \\
\frac{\partial U}{\partial w_i} &= \frac{\partial U^{\epsilon}}{\partial w_i} + \frac{\partial U^{\kappa}}{\partial w_i} + \frac{\partial U^{\psi}}{\partial w_i} \\
\frac{\partial U}{\partial \phi_i} &= \frac{\partial U^{\epsilon}}{\partial \phi_i} + \frac{\partial U^{\kappa}}{\partial \phi_i} + \frac{\partial U^{\psi}}{\partial \phi_i}
\end{aligned} \tag{3.19}$$

It is clear from the mathematical description of κ and ψ that U^{κ} and U^{ψ} are independent of u_i. Therefore one can conclude $\partial U^{\kappa}/\partial u_i = 0$ and $\partial U^{\psi}/\partial u_i = 0$. Also, w_i only appears in U^{ψ}, consequently, U^{κ} and U^{ϵ} do not depend on w_i ($\partial U^{\kappa}/\partial w_i = 0$ and $\partial U^{\epsilon}/\partial w_i = 0$). Similarly, ϕ shows up in both U^{κ} and U^{ψ}, thus, $\partial U^{\epsilon}/\partial \phi_i$ could be dropped from our calculation.

The simplified form of the Eq. 3.19 based on potential densities could be given;

$$\begin{aligned}
\frac{\partial U}{\partial u_i} &= \frac{\partial U^{\epsilon}}{\partial u_i} = \frac{\partial \omega_i^{\epsilon_i}}{\partial u_i} + \frac{\partial \omega_i^{\epsilon_j}}{\partial u_i} + \frac{\partial \omega_i^{\epsilon_k}}{\partial u_i}, \\
\frac{\partial U}{\partial w_i} &= \frac{\partial U^{\psi}}{\partial w_i} = \frac{\partial \omega_i^{\psi_i}}{\partial w_i} + \frac{\partial \omega_i^{\psi_j}}{\partial w_i} + \frac{\partial \omega_i^{\psi_k}}{\partial w_i}, \\
\frac{\partial U}{\partial \phi_i} &= \frac{\partial U^{\kappa}}{\partial \phi_i} + \frac{\partial U^{\psi}}{\partial \phi_i} = \frac{\partial \omega_i^{\kappa_i}}{\partial \phi_i} + \frac{\partial \omega_i^{\kappa_j}}{\partial \phi_i} + \frac{\partial \omega_i^{\kappa_k}}{\partial \phi_i} + \frac{\partial \omega_i^{\psi_i}}{\partial \phi_i} + \frac{\partial \omega_i^{\psi_j}}{\partial \phi_i} + \frac{\partial \omega_i^{\psi_k}}{\partial \phi_i}
\end{aligned} \tag{3.20}$$

Noting that, in Eq. 3.20 the summation on i index was dropped due to taking derivative respect to ith particle i.e. ($\frac{\partial}{\partial u_k}\sum_{i=1}^{N}\omega_i^{\epsilon_i}V_i = \frac{\partial \omega_k^{\epsilon_k}}{\partial u_k}$). Then, partial derivative for each term of the potential energy density can be given as:

$$\begin{aligned}
\frac{\partial \omega_i^{\epsilon_i}}{\partial u_i} &= \frac{1}{6}\sum_{j=1}^{M}\sum_{k=1}^{M}\left[\frac{\partial\left(A_{ijk}\epsilon_{ijk}\right)}{\partial u_i}\right]V_kV_j, \ \frac{\partial \omega_i^{\epsilon_j}}{\partial u_i} = \frac{1}{6}\sum_{j=1}^{M}\sum_{k=1}^{M}\left[\frac{\partial\left(A_{jki}\epsilon_{jki}\right)}{\partial u_i}\right]V_kV_j, \\
\frac{\partial \omega_i^{\epsilon_k}}{\partial u_i} &= \frac{1}{6}\sum_{j=1}^{M}\sum_{k=1}^{M}\left[\frac{\partial\left(A_{kij}\epsilon_{kij}\right)}{\partial u_i}\right]V_kV_j, \ \frac{\partial \omega_i^{\psi_i}}{\partial w_i} = \frac{1}{6}\sum_{j=1}^{M}\sum_{k=1}^{M}\left[\frac{\partial\left(C_{ijk}\psi_{ijk}\right)}{\partial w_i}\right]V_kV_j, \\
\frac{\partial \omega_i^{\psi_j}}{\partial w_i} &= \frac{1}{6}\sum_{j=1}^{M}\sum_{k=1}^{M}\left[\frac{\partial\left(C_{jki}\psi_{jki}\right)}{\partial w_i}\right]V_kV_j, \ \frac{\partial \omega_i^{\psi_k}}{\partial w_i} = \frac{1}{6}\sum_{j=1}^{M}\sum_{k=1}^{M}\left[\frac{\partial\left(C_{kij}\psi_{kij}\right)}{\partial w_i}\right]V_kV_j, \\
\frac{\partial \omega_i^{\kappa_i}}{\partial \phi_i} &= \frac{1}{6}\sum_{j=1}^{M}\sum_{k=1}^{M}\left[\frac{\partial\left(B_{ijk}\kappa_{ijk}\right)}{\partial \phi_i}\right]V_kV_j, \ \frac{\partial \omega_i^{\kappa_j}}{\partial \phi_i} = \frac{1}{6}\sum_{j=1}^{M}\sum_{k=1}^{M}\left[\frac{\partial\left(B_{jki}\kappa_{jki}\right)}{\partial \phi_i}\right]V_kV_j, \\
\frac{\partial \omega_i^{\kappa_k}}{\partial \phi_i} &= \frac{1}{6}\sum_{j=1}^{M}\sum_{k=1}^{M}\left[\frac{\partial\left(B_{kij}\kappa_{kij}\right)}{\partial \phi_i}\right]V_kV_j, \ \frac{\partial \omega_i^{\psi_i}}{\partial \phi_i} = \frac{1}{6}\sum_{j=1}^{M}\sum_{k=1}^{M}\left[\frac{\partial\left(C_{ijk}\psi_{ijk}\right)}{\partial \phi_i}\right]V_kV_j, \\
\frac{\partial \omega_i^{\psi_j}}{\partial \phi_i} &= \frac{1}{6}\sum_{j=1}^{M}\sum_{k=1}^{M}\left[\frac{\partial\left(C_{jki}\psi_{jki}\right)}{\partial \phi_i}\right]V_kV_j, \ \frac{\partial \omega_i^{\psi_k}}{\partial \phi_i} = \frac{1}{6}\sum_{j=1}^{M}\sum_{k=1}^{M}\left[\frac{\partial\left(C_{kij}\psi_{kij}\right)}{\partial \phi_i}\right]V_kV_j
\end{aligned} \tag{3.21}$$

Here, A_{ijk}, B_{ijk} and C_{ijk} are existing forces in $i-j$ and $i-k$ bonds which result in the stretch, curvature and transverse shear of the beam. By permuting the indices, the forces in other bonds can be captured. These multi-body forces within the element may bring more flexibility to model other material classes, e.g., anisotropic materials. In this section, we

assume that the forces are a linear function of the corresponding deformation as:

$$\begin{aligned}
&A_{ijk} = K^{\epsilon}_{ijk}\epsilon_{ijk},\ A_{jki} = K^{\epsilon}_{jki}\epsilon_{jki},\ A_{kij} = K^{\epsilon}_{kij}\epsilon_{kij},\\
&B_{ijk} = K^{\phi}_{ijk}\kappa_{ijk},\ B_{jki} = K^{\phi}_{jki}\kappa_{jki},\ B_{kij} = K^{\phi}_{kij}\kappa_{kij},\\
&C_{ijk} = K^{\psi}_{ijk}\psi_{ijk},\ C_{jki} = K^{\psi}_{jki}\psi_{jki},\ C_{kij} = K^{\psi}_{kij}\psi_{kij}.
\end{aligned} \tag{3.22}$$

Where K^{ϵ}, K^{ϕ} and K^{ψ} are the resistances offered by the elastic beam against deformation. Using the chain rule, Eq. 3.21 for a linear material response could be simplified as:

$$\begin{aligned}
\frac{\partial\left(A_{ijk}\epsilon_{ijk}\right)}{\partial u_i} =& \frac{\partial\left(A_{ijk}\epsilon_{ijk}\right)}{\partial\epsilon_{ijk}}\frac{\partial\epsilon_{ijk}}{\partial u_i} = \left(2K^{\epsilon}_{ijk}\epsilon_{ijk}\right)\frac{\partial\epsilon_{ijk}}{\partial u_i} = -2K^{\epsilon}_{ijk}\left(\frac{1}{\xi_{ij}}+\frac{1}{\xi_{ik}}\right)\epsilon_{ijk},\\
\frac{\partial\left(A_{jki}\epsilon_{jki}\right)}{\partial u_i} =& \frac{\partial\left(A_{jki}\epsilon_{jki}\right)}{\partial\epsilon_{jki}}\frac{\partial\epsilon_{jki}}{\partial u_i} = \left(2K^{\epsilon}_{jki}\epsilon_{jki}\right)\frac{\partial\epsilon_{jki}}{\partial u_i} = 2K^{\epsilon}_{jki}\left(\frac{1}{\xi_{ij}}\right)\epsilon_{jki},\\
\frac{\partial\left(A_{kij}\epsilon_{kij}\right)}{\partial u_i} =& \frac{\partial\left(A_{kij}\epsilon_{kij}\right)}{\partial\epsilon_{kij}}\frac{\partial\epsilon_{kij}}{\partial u_i} = \left(2K^{\epsilon}_{kij}\epsilon_{kij}\right)\frac{\partial\epsilon_{kij}}{\partial u_i} = 2K^{\epsilon}_{kij}\left(\frac{1}{\xi_{ik}}\right)\epsilon_{kij}
\end{aligned} \tag{3.23}$$

$$\begin{aligned}
\frac{\partial\left(B_{ijk}\kappa_{ijk}\right)}{\partial\phi_i} &= \frac{\partial\left(B_{ijk}\kappa_{ijk}\right)}{\partial\kappa_{ijk}}\frac{\partial\kappa_{ijk}}{\partial\phi_i} = \left(2K^{\phi}_{ijk}\kappa_{ijk}\right)\frac{\partial\kappa_{ijk}}{\partial\phi_i} = -2K^{\phi}_{ijk}\left(\frac{1}{\xi_{ij}}+\frac{1}{\xi_{ik}}\right)\kappa_{ijk},\\
\frac{\partial\left(B_{jki}\kappa_{jki}\right)}{\partial\phi_i} &= \frac{\partial\left(B_{jki}\kappa_{jki}\right)}{\partial\kappa_{jki}}\frac{\partial\kappa_{jki}}{\partial\phi_i} = \left(2K^{\phi}_{jki}\kappa_{jki}\right)\frac{\partial\kappa_{jki}}{\partial\phi_i} = 2K^{\phi}_{jki}\left(\frac{1}{\xi_{ij}}\right)\kappa_{jki},\\
\frac{\partial\left(B_{kij}\kappa_{kij}\right)}{\partial\phi_i} &= \frac{\partial\left(B_{kij}\kappa_{kij}\right)}{\partial\kappa_{kij}}\frac{\partial\kappa_{kij}}{\partial\phi_i} = \left(2K^{\phi}_{kij}\kappa_{kij}\right)\frac{\partial\kappa_{kij}}{\partial\phi_i} = 2K^{\phi}_{kij}\left(\frac{1}{\xi_{ik}}\right)\kappa_{kij}
\end{aligned} \tag{3.24}$$

$$\begin{aligned}
\frac{\partial\left(C_{ijk}\psi_{ijk}\right)}{\partial w_i} &= \frac{\partial\left(C_{ijk}\psi_{ijk}\right)}{\partial\psi_{ijk}}\frac{\partial\psi_{ijk}}{\partial w_i} = \left(2K^{\psi}_{ijk}\psi_{ijk}\right)\frac{\partial\psi_{ijk}}{\partial w_i} = -2K^{\psi}_{ijk}\left(\frac{1}{\xi_{ij}}+\frac{1}{\xi_{ik}}\right)\psi_{ijk},\\
\frac{\partial\left(C_{jki}\psi_{jki}\right)}{\partial w_i} &= \frac{\partial\left(C_{jki}\psi_{jki}\right)}{\partial\psi_{jki}}\frac{\partial\psi_{jki}}{\partial w_i} = \left(2K^{\psi}_{jki}\psi_{jki}\right)\frac{\partial\psi_{jki}}{\partial w_i} = 2K^{\psi}_{jki}\left(\frac{1}{\xi_{ij}}\right)\psi_{jki},\\
\frac{\partial\left(C_{kij}\psi_{kij}\right)}{\partial w_i} &= \frac{\partial\left(C_{kij}\psi_{kij}\right)}{\partial\psi_{kij}}\frac{\partial\psi_{kij}}{\partial w_i} = \left(2K^{\psi}_{kij}\psi_{kij}\right)\frac{\partial\psi_{kij}}{\partial w_i} = 2K^{\psi}_{kij}\left(\frac{1}{\xi_{ik}}\right)\psi_{kij}
\end{aligned} \tag{3.25}$$

$$\begin{aligned}
\frac{\partial\left(C_{ijk}\psi_{ijk}\right)}{\partial\phi_i} &= \frac{\partial\left(C_{ijk}\psi_{ijk}\right)}{\partial\psi_{ijk}}\frac{\partial\psi_{ijk}}{\partial\phi_i} = \left(2K^{\psi}_{ijk}\psi_{ijk}\right)\frac{\partial\psi_{ijk}}{\partial\phi_i} = -K^{\psi}_{ijk}\left(\hat{n}_{ij}+\hat{n}_{ik}\right)\psi_{ijk},\\
\frac{\partial\left(C_{jki}\psi_{jki}\right)}{\partial\phi_i} &= \frac{\partial\left(C_{jki}\psi_{jki}\right)}{\partial\psi_{jki}}\frac{\partial\psi_{jki}}{\partial\phi_i} = \left(2K^{\psi}_{jki}\psi_{jki}\right)\frac{\partial\psi_{jki}}{\partial\phi_i} = K^{\psi}_{jki}\left(\hat{n}_{ij}\right)\psi_{jki},\\
\frac{\partial\left(C_{kij}\psi_{kij}\right)}{\partial\phi_i} &= \frac{\partial\left(C_{kij}\psi_{kij}\right)}{\partial\psi_{kij}}\frac{\partial\psi_{kij}}{\partial\phi_i} = \left(2K^{\psi}_{kij}\psi_{kij}\right)\frac{\partial\psi_{kij}}{\partial\phi_i} = K^{\psi}_{kij}\left(\hat{n}_{ik}\right)\psi_{jki}
\end{aligned} \tag{3.26}$$

Substituting Eqs. 3.4, 3.4, 3.4 and 3.4 into Eq. 3.20, and then using the results along with

the Eq. 3.18 in Eq. 3.17 give the EOMs for Timoshenko beam as:

$$\rho\ddot{u}_i + 2z_i\rho\ddot{\phi}_i = \frac{1}{3}\sum_{j=1}^{M}\sum_{k=1}^{M}\left[K^{\epsilon}_{ijk}\left(\frac{1}{\xi_{ij}}+\frac{1}{\xi_{ik}}\right)\epsilon_{ijk} - K^{\epsilon}_{jki}\left(\frac{1}{\xi_{ij}}\right)\epsilon_{jki} - K^{\epsilon}_{kij}\left(\frac{1}{\xi_{ik}}\right)\epsilon_{kij}\right]V_kV_j \tag{3.27}$$

$$\rho\ddot{w}_i = \frac{1}{3}\sum_{j=1}^{M}\sum_{k=1}^{M}\left[K^{\psi}_{ijk}\left(\frac{1}{\xi_{ij}}+\frac{1}{\xi_{ik}}\right)\psi_{ijk} - K^{\psi}_{jki}\left(\frac{1}{\xi_{ij}}\right)\psi_{jki} - K^{\psi}_{kij}\left(\frac{1}{\xi_{ik}}\right)\psi_{kij}\right]V_kV_j \tag{3.28}$$

$$\begin{aligned}\rho\frac{I}{A}\ddot{\phi}_i + 2z_i\rho\ddot{u}_i = &\frac{1}{3}\sum_{j=1}^{M}\sum_{k=1}^{M}\left[K^{\phi}_{ijk}\left(\frac{1}{\xi_{ij}}+\frac{1}{\xi_{ik}}\right)\kappa_{ijk} - K^{\phi}_{jki}\left(\frac{1}{\xi_{ij}}\right)\kappa_{jki} - K^{\phi}_{kij}\left(\frac{1}{\xi_{ik}}\right)\kappa_{kij}\right]V_kV_j \\ &+ \frac{1}{6}\sum_{j=1}^{M}\sum_{k=1}^{M}\left[K^{\psi}_{ijk}\left(\hat{n}_{ij}+\hat{n}_{ik}\right)\psi_{ijk} - K^{\psi}_{jki}\left(\hat{n}_{ij}\right)\psi_{jki} - K^{\psi}_{kij}\left(\hat{n}_{ik}\right)\psi_{kij}\right]V_kV_j\end{aligned} \tag{3.29}$$

Assuming that the beam is made of isotropic materials, the directional dependence of interaction could be relaxed as:

$$\begin{aligned}K^{\epsilon}_{ijk} =& K^{\epsilon}_{jki} = K^{\epsilon}_{kij} = K^{\epsilon},\\ K^{\phi}_{ijk} =& K^{\phi}_{jki} = K^{\phi}_{kij} = K^{\phi},\\ K^{\psi}_{ijk} =& K^{\psi}_{jki} = K^{\psi}_{kij} = K^{\psi}\end{aligned} \tag{3.30}$$

Noting that K^{ϵ}, K^{ϕ} and K^{ψ} are material nonlocal parameters that should be determined by localization of the governing equations (Eqs. 3.27, 3.28, 3.29) and comparing with the classical counterparts.

3.5 Localization of the Equation of Motion

Since we are working with a discrete system of equations, the local limit could be explained as the case in which particles can only interact with their closest neighbors. Therefore, one could conclude that $\xi_{ij} = \xi_{ik} = \xi$. Using Eqs. 3.10 along with other index properties in Section 3.2, the localized form of the developed nonlocal beam equations are given as:

$$\rho\ddot{u}_i + 2z_i\rho\ddot{\phi}_i = \lim_{\delta\to\delta_l}\left(\frac{\epsilon_{ijk}}{\xi}\right)K^{\epsilon}\sum_{j=1}^{m}\sum_{k=1}^{m}V_kV_j \tag{3.31}$$

$$\rho\ddot{w}_i = \lim_{\delta\to\delta_l}\left(\frac{\psi_{ijk}}{\xi}\right)K^{\psi}\sum_{j=1}^{m}\sum_{k=1}^{m}V_kV_j \tag{3.32}$$

$$\rho\frac{I}{A}\ddot{\phi}_i + 2z_i\rho\ddot{u}_i = \lim_{\delta\to\delta_l}\left(\frac{K^{\psi}}{6}\sum_{j=1}^{m}\sum_{k=1}^{m}\left[\left(\hat{n}_{ij}+\hat{n}_{ik}\right)\psi_{ijk} - \hat{n}_{ij}\psi_{jki} - \hat{n}_{ik}\psi_{kij}\right]V_kV_j\right) + \lim_{\delta\to\delta_l}\left(\frac{\epsilon_{ijk}}{\xi}\right)K^{\phi}\sum_{j=1}^{m}\sum_{k=1}^{m}V_kV_j \tag{3.33}$$

In the local limit, we change the upper bond of the series from N to m to emphasis on the immediate neighbor. We also assume that the values of ϵ, κ and ψ are constant in the local horizon. Therefore, they could be taken out of the series. To have a set of equations that are decoupled (respect to u), we assume that the thickness of the beam is sufficiently small in comparison to the length of the beam ($h/L < 0.01$), i.e., the particles are scattered uniformly on the x-axis, and other particles above or below the x-axis have very small z value. Thus, we are able to drop terms with z in the kinetic part of EOMs (Eqs. 3.27 and Eq. 3.29). The details of localization of the discrete equations are given in Appendix C. It could be easily shown the followings relations in local limit:

$$\lim_{\delta\to\delta_l}\left(\frac{\epsilon_{ijk}}{\xi}\right) = u_i'' \tag{3.34a}$$

$$\lim_{\delta\to\delta_l}\left(\frac{\psi_{ijk}}{\xi}\right) = w_i'' - \phi_i' \tag{3.34b}$$

$$\lim_{\delta\to\delta_l}\left(\frac{\kappa_{ijk}}{\xi}\right) = \phi_i'' \tag{3.34c}$$

Therefore, the localized form of the equations could be given as:

$$\rho\ddot{u}_i = K^{\epsilon}V_T^2u_i'' \tag{3.35a}$$

$$\rho\ddot{w}_i = K^{\psi}V_T^2(w_i'' - \phi_i') \tag{3.35b}$$

$$\rho\frac{I}{A}\ddot{\phi}_i = K^{\phi}V_T^2(\phi_i'') + K^{\psi}V_T^2(w_i' - \phi_i) \tag{3.35c}$$

Where V_T denotes the total volume of the domain associated to the horizon and can be calculated through the following:

$$V_T = \sum_{j=1}^{m}V_j \tag{3.36}$$

Noting that V_T is equal to $2V$ in the local limit for the beam model. The Eq. 3.36 is valid to be used in governing equations if we have "m" as upper bounds for both series. Noting that the classical EOMs for Timoshenko beam theory can be given as:

$$\rho\ddot{u} + 2z\rho\ddot{\phi} = Eu^{''} \tag{3.37a}$$

$$\rho\ddot{w} = \kappa_s G\left(w^{''} - \phi^{'}\right) \tag{3.37b}$$

$$\rho\frac{I}{A}\ddot{\phi} + 2z\rho\ddot{u} = \frac{EI}{A}\phi^{''} + \kappa_s G\left(w^{'} - \phi\right) \tag{3.37c}$$

Where κ_s is the shear correction coefficient and depends on the cross-section of the beam. This value for a rectangular cross-section is $5/6$. The material parameters can be obtained by comparing the localized form of the tridynamics beam EOMs with the classical Timoshenko beam theory as:

$$\begin{aligned} K^{\epsilon} =& \frac{E}{V_T^2} \\ K^{\psi} =& \frac{\kappa_s \mu}{V_T^2} \\ K^{\phi} =& \frac{EI}{AV_T^2} \end{aligned} \tag{3.38}$$

Here, E, μ, A and I are respectively Young's modulus, shear modulus, cross-sectional area and the second moment of inertia of the beam.

3.6 Dispersion Analysis

To see how the model performs in comparison to classical and peridynamics, we will carry out dispersion analysis. Noting that we try to derive our dispersion equations without setting $z = 0$ in the EOMs i.e. the beam is not thin. Since our equations are written in discrete form, we are interested in using the discrete format of wave propagation for all DOFs as follows:

$$\begin{aligned} u_i =& u(x_i, t) = u_0 e^{\hat{i}(\kappa x_i - \omega t + \hat{n}_{ii}\kappa\xi_{ii})} = u_0 X_i \Lambda_{ii} = u_0 X_i \\ u_j =& u(x_j, t) = u_0 e^{\hat{i}(\kappa x_i - \omega t + \hat{n}_{ij}\kappa\xi_{ij})} = u_0 X_i \Lambda_{ij} \\ u_k =& u(x_k, t) = u_0 e^{\hat{i}(\kappa x_i - \omega t + \hat{n}_{ik}\kappa\xi_{ik})} = u_0 X_i \Lambda_{ik} \end{aligned} \tag{3.39}$$

$$
\begin{aligned}
w_i =& w(x_i,t) = w_0 e^{\hat{i}(\kappa x_i - \omega t + \hat{n}_{ii}\kappa\xi_{ii})} = w_0 X_i \Lambda_{ii} = w_0 X_i \\
w_j =& w(x_j,t) = w_0 e^{\hat{i}(\kappa x_i - \omega t + \hat{n}_{ij}\kappa\xi_{ij})} = w_0 X_i \Lambda_{ij} \\
w_k =& w(x_k,t) = w_0 e^{\hat{i}(\kappa x_i - \omega t + \hat{n}_{ik}\kappa\xi_{ik})} = w_0 X_i \Lambda_{ik}
\end{aligned} \tag{3.40}
$$

$$
\begin{aligned}
\phi_i =& \phi(x_i,t) = \phi_0 e^{\hat{i}(\kappa x_i - \omega t + \hat{n}_{ii}\kappa\xi_{ii})} = \phi_0 X_i \Lambda_{ii} = \phi_0 X_i \\
\phi_j =& \phi(x_j,t) = \phi_0 e^{\hat{i}(\kappa x_i - \omega t + \hat{n}_{ij}\kappa\xi_{ij})} = \phi_0 X_i \Lambda_{ij} \\
\phi_k =& \phi(x_k,t) = \phi_0 e^{\hat{i}(\kappa x_i - \omega t + \hat{n}_{ik}\kappa\xi_{ik})} = \phi_0 X_i \Lambda_{ik}
\end{aligned} \tag{3.41}
$$

Where κ is the wave number and ω is the wave frequency. The axial coordinate of particles is shown by x_i and the variable t indicates time. u_0, w_0 and ϕ_0 are the amplitude of the waves in the axial, traverse and rotation in y plane. Here $\hat{i}$ is showing the imaginary part ($\hat{i} = \sqrt{-1}$). It should be noted that $X_i = e^{\hat{i}(\kappa x_i - \omega t)}$ is the wave equation associate to i^{th} particle. The phase difference of the particle i with particle j and k could be given by $\kappa\hat{n}_{ij}\xi_{ij}$ and $\kappa\hat{n}_{ik}\xi_{ik}$ respectively. Form the definition of $\Lambda_{i\alpha} = e^{i(\kappa\hat{n}_{i\alpha}\xi_{i\alpha}t)}$ where $\alpha = i, j, k$, one can easily find that $\Lambda_{ii} = 1$ i.e, no phase difference with the ith particle. Substituting Eq. 3.39, in definition of stretch (Eq. 3.1) results into;

$$
\epsilon_{\alpha\beta\gamma} = u_0 X_i \left(\frac{1}{\xi_{\alpha\beta}} \left(\Lambda_{i\beta} - \Lambda_{i\alpha} \right) + \frac{1}{\xi_{\alpha\gamma}} \left(\Lambda_{i\gamma} - \Lambda_{i\alpha} \right) \right) = u_0 X_i T_{\alpha\beta\gamma} \tag{3.42}
$$

Noting that $T_{\alpha\beta\gamma} = \frac{1}{\xi_{\alpha\beta}} \left(\Lambda_{i\beta} - \Lambda_{i\alpha} \right) + \frac{1}{\xi_{\alpha\gamma}} \left(\Lambda_{i\gamma} - \Lambda_{i\alpha} \right)$ Therefore, we could have the following equations when α and β are i, j and k indices:

$$
\begin{aligned}
\epsilon_{ijk} =& u_0 X_i \left(\frac{1}{\xi_{ij}} \left(\Lambda_{ij} - 1 \right) + \frac{1}{\xi_{ik}} \left(\Lambda_{ik} - 1 \right) \right) = u_0 X_i T_{ijk} \\
\epsilon_{jki} =& u_0 X_i \left(\frac{1}{\xi_{jk}} \left(\Lambda_{ik} - \Lambda_{ij} \right) + \frac{1}{\xi_{ji}} \left(1 - \Lambda_{ij} \right) \right) = u_0 X_i T_{jki} \\
\epsilon_{kij} =& u_0 X_i \left(\frac{1}{\xi_{ki}} \left(1 - \Lambda_{ik} \right) + \frac{1}{\xi_{kj}} \left(\Lambda_{ij} - \Lambda_{ik} \right) \right) = u_0 X_i T_{kij}
\end{aligned} \tag{3.43}
$$

Similarly, we can find it for $\kappa_{\alpha\beta\gamma}$ and $\psi_{\alpha\beta\gamma}$ by substituting 3.40 and 3.41 into their definitions

(Eqs. 3.4 and 3.6) as:

$$\kappa_{\alpha\beta\gamma} = \phi_0 X_i \left(\frac{1}{\xi_{\alpha\beta}} \left(\Lambda_{i\beta} - \Lambda_{i\alpha} \right) + \frac{1}{\xi_{\alpha\gamma}} \left(\Lambda_{i\gamma} - \Lambda_{i\alpha} \right) \right) = \phi_0 X_i J_{\alpha\beta\gamma} \tag{3.44}$$

Noting that $J_{\alpha\beta\gamma} = \frac{1}{\xi_{\alpha\beta}} \left(\Lambda_{i\beta} - \Lambda_{i\alpha} \right) + \frac{1}{\xi_{\alpha\gamma}} \left(\Lambda_{i\gamma} - \Lambda_{i\alpha} \right)$. We could have the followings for the indices i, j and k:

$$\begin{aligned}
\kappa_{ijk} =& \phi_0 X_i \left(\frac{1}{\xi_{ij}} \left(\Lambda_{ij} - 1 \right) + \frac{1}{\xi_{ik}} \left(\Lambda_{ik} - 1 \right) \right) = \phi_0 X_i J_{ijk} \\
\kappa_{jki} =& \phi_0 X_i \left(\frac{1}{\xi_{jk}} \left(\Lambda_{ik} - \Lambda_{ij} \right) + \frac{1}{\xi_{ji}} \left(1 - \Lambda_{ij} \right) \right) = \phi_0 X_i J_{jki} \\
\kappa_{kij} =& \phi_0 X_i \left(\frac{1}{\xi_{ki}} \left(1 - \Lambda_{ik} \right) + \frac{1}{\xi_{kj}} \left(\Lambda_{ij} - \Lambda_{ik} \right) \right) = \phi_0 X_i J_{kij}
\end{aligned} \tag{3.45}$$

In a similar fashion, we may get the following relations for $\psi_{\alpha\beta\gamma}$

$$\psi_{\alpha\beta\gamma} = w_0 X_i P_{\alpha\beta\gamma} + \phi_0 X_i Q_{\alpha\beta\gamma} \tag{3.46}$$

where

$$\begin{aligned}
P_{\alpha\beta\gamma} &= \frac{1}{\xi_{\alpha\beta}} \left(\Lambda_{i\beta} - \Lambda_{i\alpha} \right) + \frac{1}{\xi_{\alpha\gamma}} \left(\Lambda_{i\gamma} - \Lambda_{i\alpha} \right) \\
Q_{\alpha\beta\gamma} &= -\frac{n_{\alpha\beta}}{2} \left(\Lambda_{i\alpha} + \Lambda_{i\beta} \right) - \frac{n_{\alpha\gamma}}{2} \left(\Lambda_{i\gamma} + \Lambda_{i\alpha} \right)
\end{aligned} \tag{3.47}$$

The term ψ_{ijk}, ψ_{jki} and ψ_{kij} can be given as:

$$\begin{aligned}
\psi_{ijk} =& w_0 X_i \left(\frac{1}{\xi_{ij}} \left(\Lambda_{ij} - 1 \right) + \frac{1}{\xi_{ik}} \left(\Lambda_{ik} - 1 \right) \right) + \phi_0 X_i \left(-\frac{\hat{n}_{ij}}{2} \left(1 + \Lambda_{ij} \right) - \frac{\hat{n}_{ik}}{2} \left(1 + \Lambda_{ik} \right) \right) \\
\psi_{jki} =& w_0 X_i \left(\frac{1}{\xi_{jk}} \left(\Lambda_{ik} - \Lambda_{ij} \right) + \frac{1}{\xi_{ji}} \left(1 - \Lambda_{ij} \right) \right) + \phi_0 X_i \left(-\frac{\hat{n}_{jk}}{2} \left(\Lambda_{ij} + \Lambda_{ik} \right) - \frac{\hat{n}_{ji}}{2} \left(1 + \Lambda_{ij} \right) \right) \\
\psi_{kij} =& w_0 X_i \left(\frac{1}{\xi_{ki}} \left(1 - \Lambda_{ik} \right) + \frac{1}{\xi_{kj}} \left(\Lambda_{ij} - \Lambda_{ik} \right) \right) + \phi_0 X_i \left(-\frac{\hat{n}_{ki}}{2} \left(1 + \Lambda_{ik} \right) - \frac{\hat{n}_{kj}}{2} \left(\Lambda_{ij} + \Lambda_{ik} \right) \right)
\end{aligned} \tag{3.48}$$

For sake of simplicity, we rewrite the equations in the following forms:

$$\begin{aligned}\psi_{ijk} &= w_0 X_i P_{ijk} + \phi_0 X_i Q_{ijk} \\ \psi_{jki} &= w_0 X_i P_{jki} + \phi_0 X_i Q_{jki} \\ \psi_{kij} &= w_0 X_i P_{kij} + \phi_0 X_i Q_{kij}\end{aligned} \tag{3.49}$$

Substituting Eqs. 3.43, 3.45 and 3.48 in the EOMs 3.27, 3.28 and 3.29 will give:

$$\begin{aligned}&\left(\rho\omega^2 + K^t A_1\right) u_0 + \left(A_2\omega^2\right)\phi_0 = 0 \\ &\left(\rho\omega^2 + K^\psi B_1\right) w_0 + \left(K^\psi B_2\right)\phi_0 = 0 \\ &\left(C_1\rho\omega^2\right) u_0 + \left(K^\psi C_2\right) w_0 + \left(\frac{\rho I}{A}\omega^2 + K^\psi C_3 + K^\phi C_4\right)\phi_0 = 0\end{aligned} \tag{3.50}$$

where:

$$\begin{aligned}A_1 =& \frac{1}{3}\sum_{j=1}^{M}\sum_{k=1}^{M}\left[\left(\frac{1}{\xi_{ij}} + \frac{1}{\xi_{ik}}\right) T_{ijk} - \left(\frac{1}{\xi_{ij}}\right) T_{jki} - \left(\frac{1}{\xi_{ik}}\right) T_{kij}\right] V_k V_j \\ A_2 =& 2 z_i \\ B1 =& \frac{1}{3}\sum_{j=1}^{M}\sum_{k=1}^{M}\left[\left(\frac{1}{\xi_{ij}} + \frac{1}{\xi_{ik}}\right) P_{ijk} - \left(\frac{1}{\xi_{ij}}\right) P_{jki} - \left(\frac{1}{\xi_{ik}}\right) P_{kij}\right] V_k V_j \\ B_2 =& \frac{1}{3}\sum_{j=1}^{M}\sum_{k=1}^{M}\left[\left(\frac{1}{\xi_{ij}} + \frac{1}{\xi_{ik}}\right) Q_{ijk} - \left(\frac{1}{\xi_{ij}}\right) Q_{jki} - \left(\frac{1}{\xi_{ik}}\right) Q_{kij}\right] V_k V_j \\ C_1 =& 2 z_i \\ C_2 =& \frac{1}{6}\sum_{j=1}^{M}\sum_{k=1}^{M}\left[\left(\hat{n}_{ij} + \hat{n}_{ik}\right) P_{ijk} - \left(\hat{n}_{ij}\right) P_{jki} - \left(\hat{n}_{ik}\right) P_{kij}\right] V_k V_j \\ C_3 =& \frac{1}{6}\sum_{j=1}^{M}\sum_{k=1}^{M}\left[\left(\hat{n}_{ij} + \hat{n}_{ik}\right) Q_{ijk} - \left(\hat{n}_{ij}\right) Q_{jki} - \left(\hat{n}_{ik}\right) Q_{kij}\right] V_k V_j \\ C_4 =& \frac{1}{3}\sum_{j=1}^{M}\sum_{k=1}^{M}\left[\left(\frac{1}{\xi_{ij}} + \frac{1}{\xi_{ik}}\right) J_{ijk} - \left(\frac{1}{\xi_{ij}}\right) J_{jki} - \left(\frac{1}{\xi_{ik}}\right) J_{kij}\right] V_k V_j\end{aligned} \tag{3.51}$$

For a non-trivial solution, the determinant of the coefficients u_0, w_0 and ϕ_0 should be zero:

$$\begin{vmatrix} \rho\omega^2 + K^t A_1 & 0 & A_2\omega^2 \\ 0 & \rho\omega^2 + K^\psi B_1 & K^\psi B_2 \\ C_1\rho\omega^2 & K^\psi C_2 & \frac{\rho I}{A}\omega^2 + K^\psi C_3 + K^\phi C_4 \end{vmatrix} = 0 \tag{3.52}$$

Which leads to the following sixth order polynomial equation as:

$$\begin{aligned} &\left(I\rho^3 - AA_2C_1\rho^2\right)\omega^6 \\ &+ \left(AC_4K^\phi\rho^2 + AC_3K^\psi\rho^2 + A_1IK^t\rho^2 + B_1IK^\psi\rho^2 - AA_2B_1C_1K^\psi\rho\right)\omega^4 \\ &+ (AB_1C_3{K^\psi}^2\rho - AB_2C_2{K^\psi}^2\rho + AA_1C_4K^\phi K^t\rho + AA_1C_3K^\psi K^t\rho \\ &+ AB_1C_4K^\phi K^\psi\rho + A_1B_1IK^\psi K^t\rho)\omega^2 \\ &+ \left(AA_1B_1C_3{K^\psi}^2K^t - AA_1B_2C_2{K^\psi}^2K^t + AA_1B_1C_4K^\phi K^\psi K^t\right) = 0 \end{aligned} \tag{3.53}$$

Here we impose the assumption for thin beam; therefore, the terms in the equation with z could be dropped (C_1 and C_4). Therefore, we could find axial wave frequency (mode I) as:

$$\omega^2 = \frac{K^t A_1}{\rho} \tag{3.54}$$

Noting that the dispersion analysis for peridynamics bar could be given as:

$$\omega_p = \kappa\sqrt{\frac{E}{\rho}}\left[1 - \frac{\kappa^2\delta^2}{24}\right]^{1/2} \tag{3.55}$$

The details of derivation of peridynamics and classical models could be found in C.2 and C.3. The determinant of the coefficient for the other two equations can be given as:

$$\begin{vmatrix} \rho\omega^2 + K^{\psi}B_1 & K^{\psi}B_2 \\ K^{\psi}C_2 & \frac{\rho I}{A}\omega^2 + K^{\psi}C_3 + K^{\phi}C_4 \end{vmatrix} = 0 \tag{3.56}$$

which leads to the following polynomial equations.

$$\begin{aligned} &\left(I\rho^2\right)\omega^4 + \left(AC_4K^{\phi}\rho + AC_3K^{\psi}\rho + B_1IK^{\psi}\rho\right)\omega^2 \\ &+ \left(AB_1C_3{K^{\psi}}^2 - AB_2C_2{K^{\psi}}^2 + AB_1C_4K^{\phi}K^{\psi}\right) = 0 \end{aligned} \tag{3.57}$$

The solution of the equation provides the mode II and mode III wave frequency of the thin beam.

3.7 Numerical Results

In this section, we provide the results from the numerical implementation of the tridynamics beam and compare them other local and nonlocal Timoshenko models. The material properties are chosen similar to reference [42]:

$$E = 200GPa, \quad \rho = 7850\frac{kg}{m^3}, \quad ,\kappa_s = 5/6 \quad h = 10^{-7}m, \quad \nu = 0.3, \quad \delta = 10^{-8}m. \tag{3.58}$$

All parameters, including A_1, B_1, B_2, C_2, C_3 and C_4 are calculated numerically using a MATLAB code. Figure. 3.3 shows the variation of the wave frequency in the axial direction for different normalized wave numbers. Noting that in the figure, the wave number has been normalized by dividing $2\pi/\delta$. It is worth-noting that since the axial direction is decoupled, the solution could be valid for bar element as well. Figure. 3.3 shows that both Peridynamics and classical theory exhibits a linear behavior for shown normalized wave numbers. However, the tridynamics model illustrates a nonlinear response.

Figure. 3.4 illustrates variation of normalized phase speed $\Omega/\left(\zeta\sqrt{\kappa_s}\right)$versus the normalized wave number. Noting that κ_s is the shear correction factor and $\zeta = \kappa h$ where h is

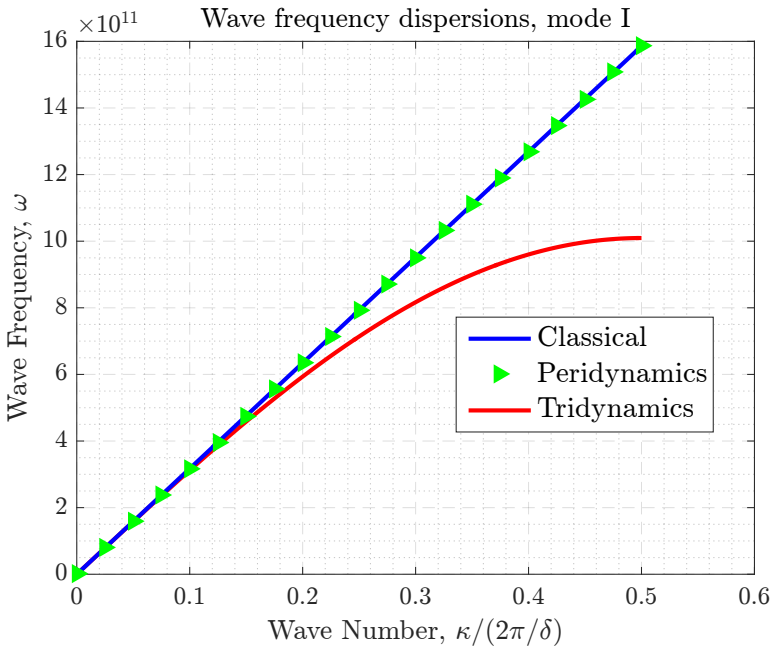

Figure 3.3: Variation of wave frequency (mode I) with the normalized wave number in different frameworks.

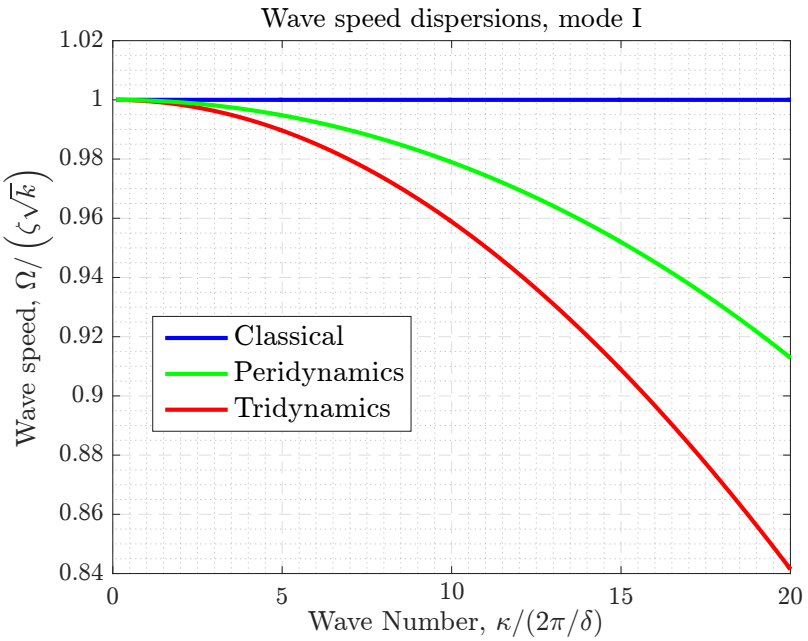

Figure 3.4: Variation of wave speed (mode I) with the normalized wave number in different frameworks.

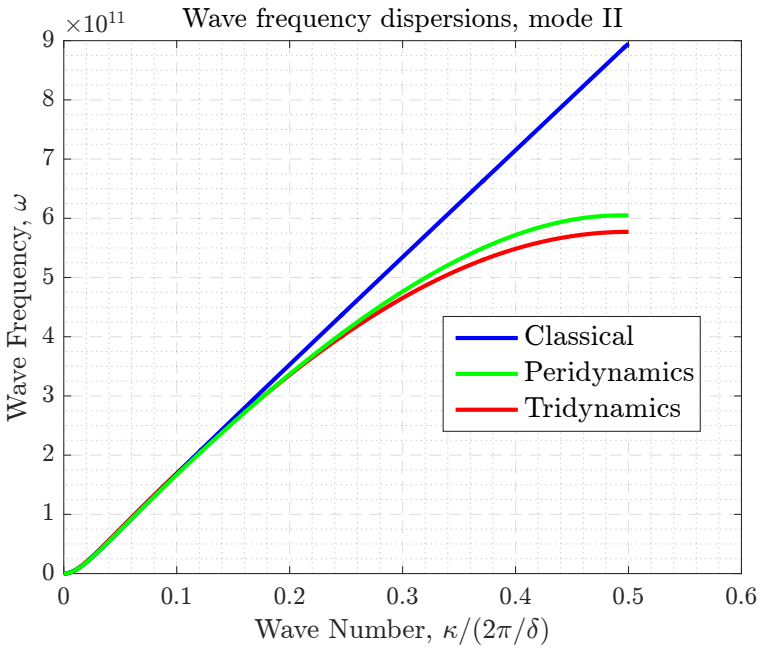

Figure 3.5: Variation of wave frequency (mode II) with the normalized wave number in different frameworks.

the height of the beam. The normalized frequency $\Omega = \omega h/v_s$ and $v_s = \sqrt{G/\rho}$ is the shear wave speed. The figure shows that both peridynamics and tridynamics do not follow a linear variation, however the classical shows a constant value.

Fig. 3.5 and Fig. 3.6 depict the mode II and III wave frequency as a function of the normalized wave numbers in different frameworks. The mode II and III are being influenced by both DOFs; (w) and ϕ. However, mode II is dominantly affected by w and mode III is mostly influenced by ϕ. Fig. 3.5 shows that unlike the wave frequency response in mode III, both peridynamics and tridynamics relatively have a similar response for mode II. One of the reasons that may cause a larger difference in mode III in comparison to mode II is the way that framework prescribes interaction of particle. In tridynamics, we associate particle at x_i with three different rotational terms κ_{ijk}, κ_{jki} and κ_{kij}. However, peridynamics only involves one rotational term at x_i. The other reason could be due to the order of nonlinearity in each case. We could have the same argument for these two figures, as it was expected.

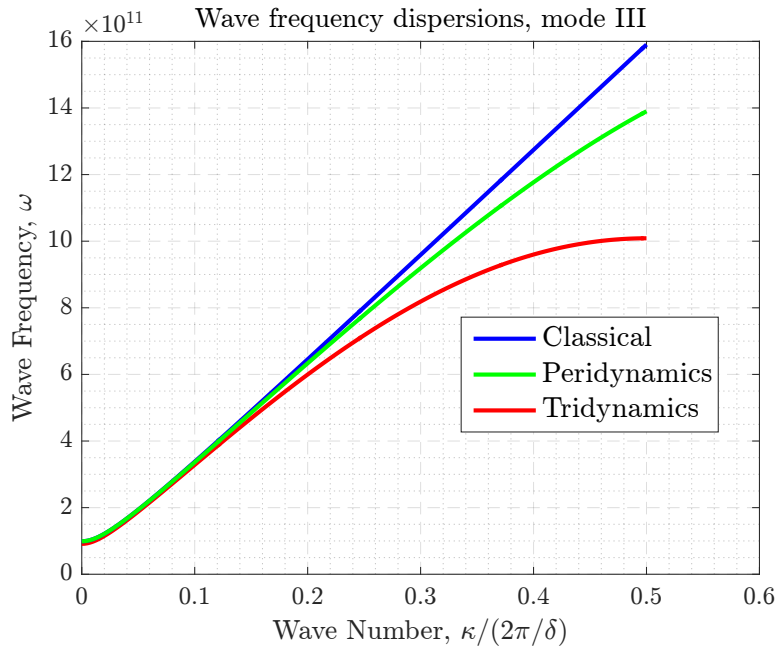

Figure 3.6: Variation of wave frequency (mode III) with the normalized wave number in different frameworks.

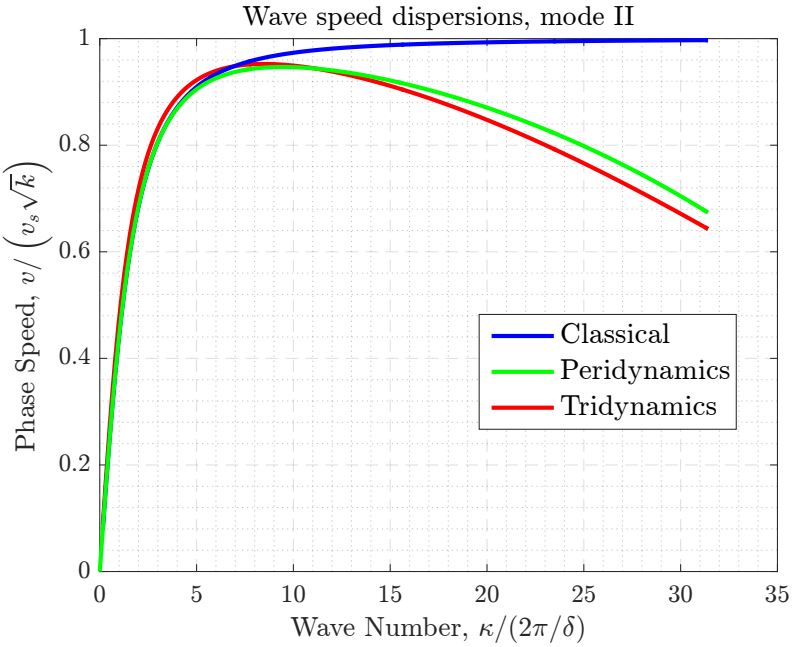

Figure 3.7: Variation of wave speed (mode II) with the normalized wave number in different frameworks.

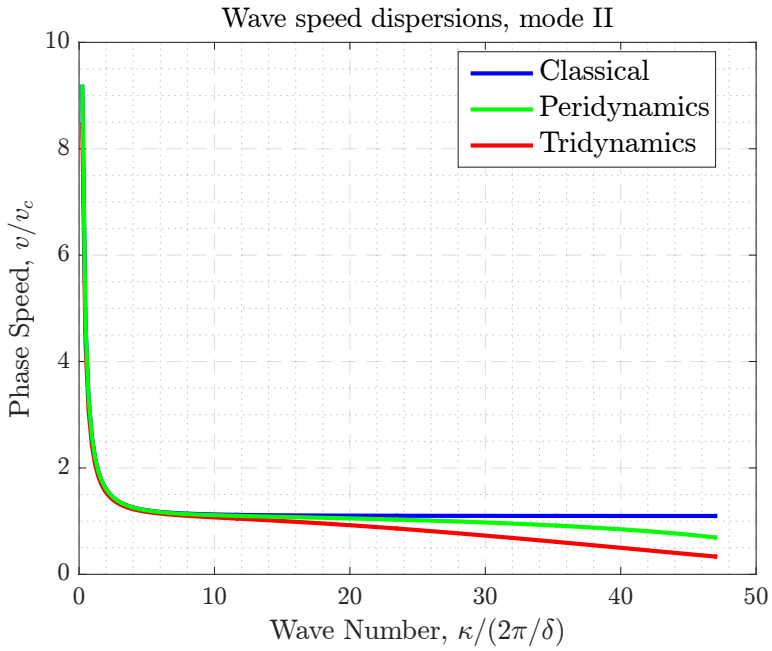

Figure 3.8: Variation of wave speed (mode III) with the normalized wave number in different frameworks.

Fig. 3.7 and 3.8 show the changes of phase speed as the normalized wave number varies.

4. TRIDYNAMIC MODEL OF THE PLATE UNDER ASSUMPTION OF FIRST-ORDER SHEAR DEFORMATION THEORY (FSDT)

4.1 Introduction

This section is in the continuation of the previous section, and we develop the tridynamic model of the plate under the assumption of first-order shear deformation theory (FSDT). In Section 4.2, we characterize the nonlocal deformation of the basic unit based upon the kinematics of material particles within the triangular unit. In Section 4.3, the Lagrangian of the tridynamics plate is formulated. Through Section 4.4, we employ the Euler-Lagrange equation to derive the governing equation for the plate. We also include localization of the model to determine nonlocal parameters.

4.2 Kinematics of Tridynamic FSDT Plate

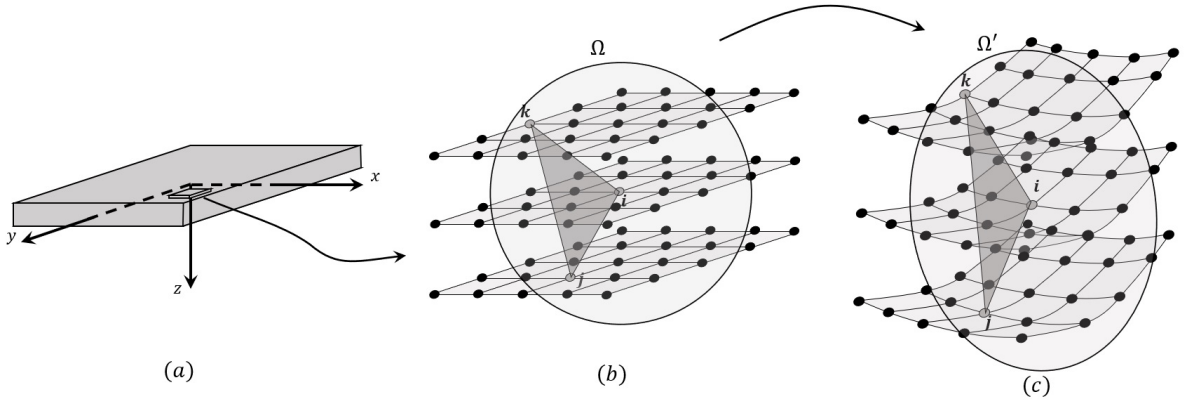

Figure 4.1: Evolution of basic unit in the plate element.

In this section, a representative kinematic is described to model first-order plate in the tridynamics framework. Let us consider a collection of particles distributed uniformly along

the x, y, and z-axis. Fig. 4.1 shows a chunk of a discrete plate in the undeformed and deformed configuration. Each particle is indicated by a solid black sphere. For the sake of illustration, we only depict three layers of material particles. The deformation at ith particle could be expressed by building a triangular unit with three vertices i, j and k. The ith vertice represents the i^{th} particle, and it locates in the center of the influence domain Ω. However, the other two vertices could be any two particles in the horizon. Fig. 1 shows only the case that i^th and j^th particles are from lower and upper material layers. However, i and j could be both from the upper or lower layer. Noting that in the deformed configuration, the influence domain turns into ellipse $\Omega^{'}$. Fig. 4.1 depicts the formation of a triangle in general three-dimensional space. However, in the following, we employ the planar triangles in x and y plane to model the plate.

In the analysis of plate, all edges of the triangle lie on x-axis or y-axis before deformation. The triangle could be visible if the curvature in x or y plane changes.
To capture deformations of the first-order plate in this framework, we introduce three quantities that represent the stretch, curvature (in x and y plane), and shear of the plate (in x and y plane). The first quantity which presents the axial deformation at x_i (x and y-axis) could be given as:

$$\begin{aligned}
&\epsilon^{xx}_{ijk} = \hat{u}^x_{ij} + \hat{u}^x_{ik}, \quad \epsilon^{xx}_{jki} = \hat{u}^x_{jk} + \hat{u}^x_{ji}, \quad \epsilon^{xx}_{kij} = \hat{u}^x_{kj} + \hat{u}^x_{ki} \\
&\epsilon^{yy}_{ijk} = \hat{v}^y_{ij} + \hat{v}^y_{ik}, \quad \epsilon^{yy}_{jki} = \hat{v}^y_{jk} + \hat{v}^y_{ji}, \quad \epsilon^{yy}_{kij} = \hat{v}^y_{kj} + \hat{v}^y_{ki}
\end{aligned} \tag{4.1}$$

Noting that ϵ^{xx}_{ijk} and ϵ^{yy}_{ijk} could be found through deformation of triangle i, k, j and l, m, j respectively (see Fig. 4.1). The planar angular deformation in x-y plane could be given as;

$$\begin{aligned}
\epsilon^{xy}_{ijk} &= {}^1\epsilon^{xy}_{ijk} + {}^2\epsilon^{xy}_{ijk} = \left(\hat{u}^y_{ij} + \hat{u}^y_{ik}\right) + \left(\hat{v}^x_{ij} + \hat{v}^x_{ik}\right) \\
\epsilon^{xy}_{jki} &= {}^1\epsilon^{xy}_{jki} + {}^2\epsilon^{xy}_{jki} = \left(\hat{u}^y_{jk} + \hat{u}^y_{ji}\right) + \left(\hat{v}^x_{ji} + \hat{v}^x_{ji}\right) \\
\epsilon^{xy}_{kij} &= {}^1\epsilon^{xy}_{kij} + {}^2\epsilon^{xy}_{kij} = \left(\hat{u}^y_{ki} + \hat{u}^y_{kj}\right) + \left(\hat{v}^x_{ki} + \hat{v}^x_{kj}\right)
\end{aligned} \tag{4.2}$$

The axial stretch in the x-direction could be given as;

$$\begin{aligned}
\hat{u}^x_{ij} =& \frac{u_j - u_i}{\xi^x_{ij}}, \quad \hat{u}^x_{ik} = \frac{u_k - u_i}{\xi^x_{ik}}, \quad \hat{u}^x_{jk} = \frac{u_k - u_j}{\xi^x_{jk}} \\
\hat{u}^y_{ij} =& \frac{u_j - u_i}{\xi^y_{ij}}, \quad \hat{u}^y_{ik} = \frac{u_k - u_i}{\xi^y_{ik}}, \quad \hat{u}^y_{jk} = \frac{u_k - u_j}{\xi^y_{jk}}
\end{aligned} \tag{4.3}$$

Similarly, the stretch in y direction could be given as;

$$\begin{aligned}
\hat{v}^x_{ij} =& \frac{v_j - v_i}{\xi^x_{ij}}, \quad \hat{v}^x_{ik} = \frac{v_k - v_i}{\xi^x_{ik}}, \quad \hat{v}^x_{jk} = \frac{v_k - v_j}{\xi^x_{jk}} \\
\hat{v}^y_{ij} =& \frac{v_j - v_i}{\xi^y_{ij}}, \quad \hat{v}^y_{ik} = \frac{v_k - v_i}{\xi^y_{ik}}, \quad \hat{v}^y_{jk} = \frac{v_k - v_j}{\xi^y_{jk}}
\end{aligned} \tag{4.4}$$

Noting that u_α and v_α indicate the displacement of particle α in x and y direction respectively. The initial planar distance between particles α and β in direction of n could be shown by $\xi^{e_i}_{\alpha\beta}$, where e_i could be x or y direction and it can be given as:

$$\begin{aligned}
\xi^x_{ij} =& \xi^x_{ji} = |x_j - x_i|, \quad \xi^x_{ik} = \xi^x_{ki} = |x_k - x_i|, \quad \xi^x_{jk} = \xi^x_{kj} = |x_k - x_j|, \\
\xi^y_{ij} =& \xi^y_{ji} = |y_j - y_i|, \quad \xi^y_{ik} = \xi^y_{ki} = |y_k - y_i|, \quad \xi^y_{jk} = \xi^y_{kj} = |y_k - y_j|
\end{aligned} \tag{4.5}$$

One can easily find that $\hat{u}^x_{ji} = -\hat{u}^x_{ij}$, $\hat{u}^x_{ki} = -\hat{u}^x_{ik}$, $\hat{u}^x_{kj} = -\hat{u}^x_{jk}, \hat{v}^y_{ji} = -\hat{v}^y_{ij}$, $\hat{v}^y_{ki} = -\hat{v}^y_{ik}$, $\hat{v}^y_{kj} = -\hat{v}^y_{jk}, \hat{u}^y_{ji} = -\hat{u}^y_{ij}$, $\hat{u}^y_{ki} = -\hat{u}^y_{ik}$, $\hat{u}^y_{kj} = -\hat{u}^y_{jk}, \hat{v}^x_{ji} = -\hat{v}^x_{ij}$, $\hat{v}^x_{ki} = -\hat{v}^x_{ik}$, $\hat{v}^x_{kj} = -\hat{v}^x_{jk}$,.

In the following, we present the related deformation to curvature and shear of the plate. In Fig. 4.2, transverse displacements, as well as axial and rotational deformation, are illustrated. Following classical first-order plate theory, straight lines perpendicular to the mid-surface (i.e., transverse normals) remains straight and inextensible. These lines are shown by solid black lines that go through the i, j, k, l, and m particles located on the lateral side of the plate element shown in Fig. 4.2. These lines are shown in the deformed configuration and they make the angle ϕ^x and ϕ^y with their initial position (shown by thin dash-dot lines in

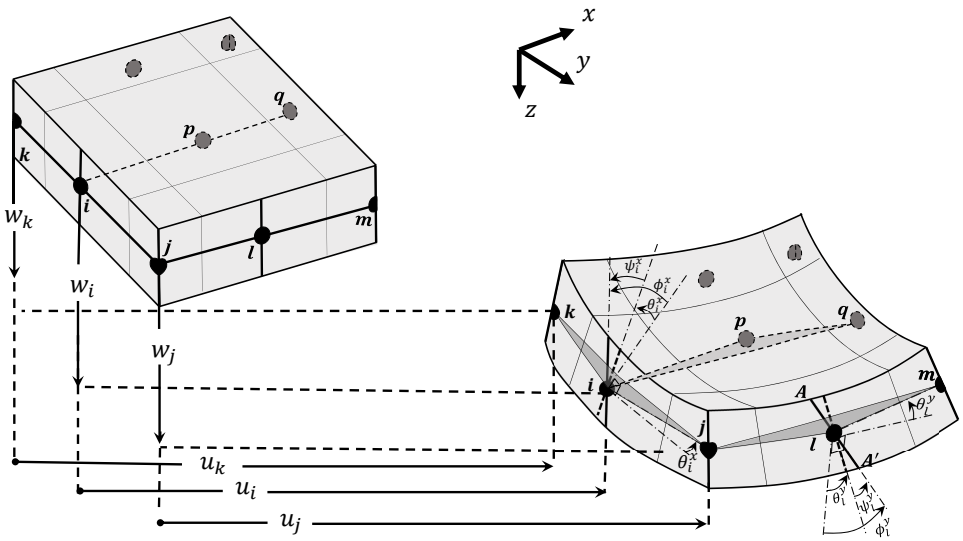

Figure 4.2: Illustration of axial, transverse and angular deformation in plane x and y.

the deformed configurations) Therefore, the curvature of the plate may be characterized as:

$$\begin{aligned}
\kappa_{ijk}^{xx} &= \hat{\phi}_{ij}^{xx} + \hat{\phi}_{ik}^{xx},\ \kappa_{jki}^{xx} = \hat{\phi}_{jk}^{xx} + \hat{\phi}_{ji}^{xx},\ \kappa_{kij}^{xx} = \hat{\phi}_{kj}^{xx} + \hat{\phi}_{ki}^{xx} \\
\kappa_{ijk}^{yy} &= \hat{\phi}_{ij}^{yy} + \hat{\phi}_{ik}^{yy},\ \kappa_{jki}^{yy} = \hat{\phi}_{jk}^{yy} + \hat{\phi}_{ji}^{yy},\ \kappa_{kij}^{yy} = \hat{\phi}_{kj}^{yy} + \hat{\phi}_{ki}^{yy}
\end{aligned} \tag{4.6}$$

According to first-order shear deformation theory, since we also have in-plane shear effect, the following could be defined;

$$\begin{aligned}
\kappa_{ijk}^{xy} &= {}^1\kappa_{ijk}^{xy} + {}^2\kappa_{ijk}^{yx} = \left(\hat{\phi}_{ij}^{xy} + \hat{\phi}_{ik}^{xy}\right) + \left(\hat{\phi}_{ij}^{yx} + \hat{\phi}_{ik}^{yx}\right) \\
\kappa_{jki}^{xy} &= {}^1\kappa_{jki}^{xy} + {}^2\kappa_{jki}^{yx} = \left(\hat{\phi}_{jk}^{xy} + \hat{\phi}_{ji}^{xy}\right) + \left(\hat{\phi}_{jk}^{yx} + \hat{\phi}_{ji}^{yx}\right) \\
\kappa_{kij}^{xy} &= {}^1\kappa_{kij}^{xy} + {}^2\kappa_{kij}^{yx} = \left(\hat{\phi}_{kj}^{xy} + \hat{\phi}_{ki}^{xy}\right) + \left(\hat{\phi}_{kj}^{yx} + \hat{\phi}_{ki}^{yx}\right)
\end{aligned} \tag{4.7}$$

Noting that $\kappa_{\alpha\beta\gamma}^{xy}$ is the curvature in XY-plane due to the interaction of particle γ and β with particle α. The changes of rotation of the perpendicular lines in x plane with respect

to both direction of x and y can be given as;

$$\begin{aligned}\hat{\phi}^{xx}_{ij} =&\frac{\phi^x_j-\phi^x_i}{\xi^x_{ij}},\ \hat{\phi}^{xx}_{ik}=\frac{\phi^x_k-\phi^x_i}{\xi^x_{ik}},\ \hat{\phi}^{xx}_{jk}=\frac{\phi^x_k-\phi^x_j}{\xi^x_{jk}},\\ \hat{\phi}^{xy}_{ij} =&\frac{\phi^x_j-\phi^x_i}{\xi^y_{ij}},\ \hat{\phi}^{xy}_{ik}=\frac{\phi^x_k-\phi^x_i}{\xi^y_{ik}},\ \hat{\phi}^{xy}_{jk}=\frac{\phi^x_k-\phi^x_j}{\xi^y_{jk}}\end{aligned} \tag{4.8}$$

Similarly, we can have the following for the rotational changes in y plane with respect to y and x direction as:

$$\begin{aligned}\hat{\phi}^{yy}_{ij} =&\frac{\phi^y_j-\phi^y_i}{\xi^y_{ij}},\ \hat{\phi}^{yy}_{ik}=\frac{\phi^y_k-\phi^y_i}{\xi^y_{ik}},\ \hat{\phi}^{yy}_{jk}=\frac{\phi^y_k-\phi^y_j}{\xi^y_{jk}},\\ \hat{\phi}^{yx}_{ij} =&\frac{\phi^y_j-\phi^y_i}{\xi^x_{ij}},\ \hat{\phi}^{yx}_{ik}=\frac{\phi^y_k-\phi^y_i}{\xi^x_{ik}},\ \hat{\phi}^{yx}_{jk}=\frac{\phi^y_k-\phi^y_j}{\xi^x_{jk}}\end{aligned} \tag{4.9}$$

Here, $\phi^{e_i}_\alpha$ is the rotation of the transverse straight line of particle α in e_i-plane. Noting that $\hat{\phi}^{e_ie_j}_{\alpha\beta}=-\hat{\phi}^{e_je_i}_{\alpha\beta}$. The transverse shear deformation in the e_i-plane may be defined as:

$$\begin{aligned}\psi^x_{ijk}&=\left(\theta^x_{ij}-\hat{n_i}^x_{ij}\bar{\phi}^x_{ij}\right)+\left(\theta^x_{ik}-\hat{n_i}^x_{ik}\bar{\phi}^x_{ik}\right)\\ \psi^x_{jki}&=\left(\theta^x_{jk}-\hat{n_i}^x_{jk}\bar{\phi}^x_{jk}\right)+\left(\theta^x_{ji}-\hat{n_i}^x_{ji}\bar{\phi}^x_{ji}\right)\\ \psi^x_{kij}&=\left(\theta^x_{kj}-\hat{n_i}^x_{kj}\bar{\phi}^x_{kj}\right)+\left(\theta^x_{ki}-\hat{n_i}^x_{ki}\bar{\phi}^x_{ki}\right)\end{aligned} \tag{4.10}$$

In similar fashion, we could defined the shear deformation in y plane as:

$$\begin{aligned}\psi^y_{ijk}&=\left(\theta^y_{ij}-\hat{n_i}^y_{ij}\bar{\phi}^y_{ij}\right)+\left(\theta^y_{ik}-\hat{n_i}^y_{ik}\bar{\phi}^y_{ik}\right)\\ \psi^y_{jki}&=\left(\theta^y_{jk}-\hat{n_i}^y_{jk}\bar{\phi}^y_{jk}\right)+\left(\theta^y_{ji}-\hat{n_i}^y_{ji}\bar{\phi}^y_{ji}\right)\\ \psi^y_{kij}&=\left(\theta^y_{kj}-\hat{n_i}^y_{kj}\bar{\phi}^y_{kj}\right)+\left(\theta^y_{ki}-\hat{n_i}^y_{ki}\bar{\phi}^y_{ki}\right)\end{aligned} \tag{4.11}$$

where $\theta^{e_i}_{\alpha\beta}$ is showing the slope of the line that connects particle α to particle β in e_i-plane

and could be given as:

$$\begin{aligned}\theta^x_{ij} =&\frac{w_j - w_i}{\xi^x_{ij}},\ \theta^x_{ik} = \frac{w_k - w_i}{\xi^x_{ik}},\ \theta^x_{jk} = \frac{w_k - w_j}{\xi^x_{jk}}\\ \theta^y_{ij} =&\frac{w_j - w_i}{\xi^y_{ij}},\ \theta^y_{ik} = \frac{w_k - w_i}{\xi^y_{ik}},\ \theta^y_{jk} = \frac{w_k - w_j}{\xi^y_{jk}}\end{aligned} \tag{4.12}$$

and w_α is the transverse displacement of the particle α. In Eq. 4.11, $\bar{\phi}^{e_i}_{\alpha\beta}$ is the average rotation of the straight lines associated to α and β in e_i plane and it could be rewritten for particle i, j and k as:

$$\begin{aligned}\bar{\phi}^x_{ij} =&\frac{\phi^x_j + \phi^x_i}{2},\ \bar{\phi}^x_{ik} = \frac{\phi^x_k + \phi^x_i}{2},\ \bar{\phi}^x_{jk} = \frac{\phi^x_k + \phi^x_j}{2}\\ \bar{\phi}^y_{ij} =&\frac{\phi^y_j + \phi^y_i}{2},\ \bar{\phi}^y_{ik} = \frac{\phi^y_k + \phi^y_i}{2},\ \bar{\phi}^y_{jk} = \frac{\phi^y_k + \phi^y_j}{2},\end{aligned} \tag{4.13}$$

The direction of the bond vector starting from particle α to particle β in e-plane is shown by $\hat{n_i}^e_{\alpha\beta}$ and could be express for i, j and k in x and y direction as:

$$\begin{aligned}\hat{n}^y_{ij} =&\frac{y_j - y_i}{\xi^y_{ij}},\ \hat{n}^y_{ik} = \frac{y_k - y_i}{\xi^y_{ik}},\ \hat{n}^y_{jk} = \frac{y_k - y_j}{\xi^y_{jk}}\\ \hat{n}^x_{ij} =&\frac{x_j - x_i}{\xi^x_{ij}},\ \hat{n}^x_{ik} = \frac{x_k - x_i}{\xi^x_{ik}},\ \hat{n}^x_{jk} = \frac{x_k - x_j}{\xi^x_{jk}},\end{aligned} \tag{4.14}$$

Noting that the introduction of these physical quantities such as ϵ and κ could be vastly employed in other mechanical problems to properly describe changes of the field variables in this framework (for instance, the ϵ could be used as a discrete derivative-free temperature gradient in two dimensional Fourier law, if we set temperature as our field variable).
It should be noted that , $\theta^{e_i}_{\alpha\beta} = -\theta^{e_i}_{\beta\alpha}$ and $\bar{\phi}^{e_i}_{\alpha\beta} = \bar{\phi}^{e_i}_{\beta\alpha}$ and $\hat{n_i}^{e_j}_{\alpha\beta} = -\hat{n_i}^{e_j}_{\beta\alpha},\ \theta^{e_i}_{\alpha\beta} = -\theta^{e_i}_{\beta\alpha}$

$$\begin{aligned}&\epsilon^{e_ie_j}_{\alpha\beta\gamma} + \epsilon^{e_ie_j}_{\beta\gamma\alpha} + \epsilon^{e_ie_j}_{\gamma\alpha\beta} = 0\\ &\kappa^{e_ie_j}_{\alpha\beta\gamma} + \kappa^{e_ie_j}_{\beta\gamma\alpha} + \kappa^{e_ie_j}_{\gamma\alpha\beta} = 0\\ &\psi^{e_i}_{\alpha\beta\gamma} + \psi^{e_i}_{\beta\gamma\alpha} + \psi^{e_i}_{\gamma\alpha\beta} = 0\end{aligned} \tag{4.15}$$

In additions, in a three-particle basic unit, the order of interaction of two particles on the particle of interest does not matter. In other words, if $\Phi^{e_i e_j}_{\alpha\beta\gamma}$ defines the interaction of particle β and γ with particle α in plane n, it will be the same as $\Phi^{e_i e_j}_{\alpha\gamma\beta}$. This remains valid for all of the kinematical concepts in this section.

4.3 Lagrangian of the FSDT Plate

Consider a plate made of a finite number of particles with the length of L and width W and thickness of h. The Lagrangian of the system could be calculated by summing up the potential and kinetic energy of the system. The potential energy for the structure could be divided into smaller sub-potentials which are due to stretch, curvature, and shear effect in different planes as:

$$U = U^{\epsilon} + U^{\kappa} + U^{\psi} \tag{4.16}$$

where each component could be described as:

$$\begin{aligned} U^{\epsilon} &= U^{\epsilon^{xx}} + U^{\epsilon^{yy}} + U^{\epsilon^{xy}} \\ U^{\kappa} &= U^{\kappa^{xx}} + U^{\kappa^{yy}} + U^{\kappa^{xy}} \\ U^{\psi} &= U^{\psi^{x}} + U^{\psi^{y}} \end{aligned} \tag{4.17}$$

Here, $U^{\epsilon^{xx}}$, $U^{\epsilon^{yy}}$, $U^{\kappa^{xx}}$, $U^{\kappa^{yy}}$,$U^{\epsilon^{xy}}$, $U^{\psi^{x}}$, $U^{\psi^{y}}$ and $U^{\kappa^{xy}}$ are respective portions of potential energies associated to the stretch in x and y direction, curvature in x, y, and xy-plane, shear deformation of the plate in x, y and xy-plane. They also could be physically interpreted as the required energy to deform the edges and angles of the triangular unit in different planes. Each of these portions could be broken up into the smaller pieces to directly show the contribution of individual particles in the basic unit. For the axial stretches and in plane

angular deformation, we could have the followings:

$$
\begin{aligned}
U^{\epsilon^{xx}} &= U^{\epsilon_i^{xx}} + U^{\epsilon_j^{xx}} + U^{\epsilon_k^{xx}} = \sum_{i=1}^{N} \omega_i^{\epsilon_i^{xx}} V_i + \sum_{i=1}^{N} \omega_i^{\epsilon_j^{xx}} V_i + \sum_{i=1}^{N} \omega_i^{\epsilon_k^{xx}} V_i \\
U^{\epsilon^{yy}} &= U^{\epsilon_i^{yy}} + U^{\epsilon_j^{yy}} + U^{\epsilon_k^{yy}} = \sum_{i=1}^{N} \omega_i^{\epsilon_i^{yy}} V_i + \sum_{i=1}^{N} \omega_i^{\epsilon_j^{yy}} V_i + \sum_{i=1}^{N} \omega_i^{\epsilon_k^{yy}} V_i \\
U^{\epsilon^{xy}} &= U^{\epsilon_i^{xy}} + U^{\epsilon_j^{xy}} + U^{\epsilon_k^{xy}} = \sum_{i=1}^{N} \omega_i^{\epsilon_i^{xy}} V_i + \sum_{i=1}^{N} \omega_i^{\epsilon_j^{xy}} V_i + \sum_{i=1}^{N} \omega_i^{\epsilon_k^{xy}} V_i
\end{aligned}
\tag{4.18}
$$

The potential due to curvature can be given by:

$$
\begin{aligned}
U^{\kappa^{xx}} &= U^{\kappa_i^{xx}} + U^{\kappa_j^{xx}} + U^{\kappa_k^{xx}} = \sum_{i=1}^{N} \omega_i^{\kappa_i^{xx}} V_i + \sum_{i=1}^{N} \omega_i^{\kappa_j^{xx}} V_i + \sum_{i=1}^{N} \omega_i^{\kappa_k^{xx}} V_i \\
U^{\kappa^{yy}} &= U^{\kappa_i^{yy}} + U^{\kappa_j^{yy}} + U^{\kappa_k^{yy}} = \sum_{i=1}^{N} \omega_i^{\kappa_i^{yy}} V_i + \sum_{i=1}^{N} \omega_i^{\kappa_j^{yy}} V_i + \sum_{i=1}^{N} \omega_i^{\kappa_k^{yy}} V_i \\
U^{\kappa^{xy}} &= U^{\kappa_i^{xy}} + U^{\kappa_j^{xy}} + U^{\kappa_k^{xy}} = \sum_{i=1}^{N} \omega_i^{\kappa_i^{xy}} V_i + \sum_{i=1}^{N} \omega_i^{\kappa_j^{xy}} V_i + \sum_{i=1}^{N} \omega_i^{\kappa_k^{xy}} V_i
\end{aligned}
\tag{4.19}
$$

We also can give the potential due to shear effect in two different planes as:

$$
\begin{aligned}
U^{\psi^{x}} &= U^{\psi_i^{x}} + U^{\psi_j^{x}} + U^{\psi_k^{x}} = \sum_{i=1}^{N} \omega_i^{\psi_i^{x}} V_i + \sum_{i=1}^{N} \omega_i^{\psi_j^{x}} V_i + \sum_{i=1}^{N} \omega_i^{\psi_k^{x}} V_i \\
U^{\psi^{y}} &= U^{\psi_i^{y}} + U^{\psi_j^{y}} + U^{\psi_k^{y}} = \sum_{i=1}^{N} \omega_i^{\psi_i^{y}} V_i + \sum_{i=1}^{N} \omega_i^{\psi_j^{y}} V_i + \sum_{i=1}^{N} \omega_i^{\psi_k^{y}} V_i
\end{aligned}
\tag{4.20}
$$

where $U^{\epsilon_\alpha^{e_i e_j}}$ is a part of the axial potential energy that comes from the effect of the particles β and γ on the particle α due to stretches of the triangle edges $e_i e_j$-plane. Similarly, the corresponding curvature (κ) and shear (ψ) potential energies can be described. Noting that U^{ϵ_α}, U^{ϵ_β} and U^{ϵ_γ} can be rewritten in terms of their potential densities as given in Eq. 4.18. Here, V_i denotes the volume of the ith particle. The upper bound of the series (N) indicates the total number of particles in the plate. The potential energy density (ω) due to stretch, curvature, and shear of the plate in different planes could be defined in Eqs. 4.21,

4.22 and 4.23:

$$\omega_i^{\epsilon_i^{xx}} = \frac{1}{6}\sum_{j=1}^{N}\sum_{k=1}^{N} A^1_{ijk}\epsilon^{xx}_{ijk}V_kV_j,\ \omega_i^{\epsilon_j^{xx}} = \frac{1}{6}\sum_{j=1}^{N}\sum_{k=1}^{N} A^1_{jki}\epsilon^{xx}_{jki}V_kV_j,\ \omega_i^{\epsilon_k^{xx}} = \frac{1}{6}\sum_{j=1}^{N}\sum_{k=1}^{N} A^1_{kij}\epsilon^{xx}_{kij}V_kV_j,$$
$$\omega_i^{\epsilon_i^{yy}} = \frac{1}{6}\sum_{j=1}^{N}\sum_{k=1}^{N} A^2_{ijk}\epsilon^{yy}_{ijk}V_kV_j,\ \omega_i^{\epsilon_j^{yy}} = \frac{1}{6}\sum_{j=1}^{N}\sum_{k=1}^{N} A^2_{jki}\epsilon^{yy}_{jki}V_kV_j,\ \omega_i^{\epsilon_k^{yy}} = \frac{1}{6}\sum_{j=1}^{N}\sum_{k=1}^{N} A^2_{kij}\epsilon^{yy}_{kij}V_kV_j,$$
$$\omega_i^{\epsilon_i^{xy}} = \frac{1}{6}\sum_{j=1}^{N}\sum_{k=1}^{N} A^3_{ijk}\epsilon^{xy}_{ijk}V_kV_j,\ \omega_i^{\epsilon_j^{xy}} = \frac{1}{6}\sum_{j=1}^{N}\sum_{k=1}^{N} A^3_{jki}\epsilon^{xy}_{jki}V_kV_j,\ \omega_i^{\epsilon_k^{xy}} = \frac{1}{6}\sum_{j=1}^{N}\sum_{k=1}^{N} A^3_{kij}\epsilon^{xy}_{kij}V_kV_j \tag{4.21}$$

$$\omega_i^{\kappa_i^{xx}} = \frac{1}{6}\sum_{j=1}^{N}\sum_{k=1}^{N} B^1_{ijk}\kappa^{xx}_{ijk}V_kV_j,\ \omega_i^{\kappa_j^{xx}} = \frac{1}{6}\sum_{j=1}^{N}\sum_{k=1}^{N} B^1_{jki}\kappa^{xx}_{jki}V_kV_j,\ \omega_i^{\kappa_k^{xx}} = \frac{1}{6}\sum_{j=1}^{N}\sum_{k=1}^{N} B^1_{kij}\kappa^{xx}_{kij}V_kV_j,$$
$$\omega_i^{\kappa_i^{yy}} = \frac{1}{6}\sum_{j=1}^{N}\sum_{k=1}^{N} B^2_{ijk}\kappa^{yy}_{ijk}V_kV_j,\ \omega_i^{\kappa_j^{yy}} = \frac{1}{6}\sum_{j=1}^{N}\sum_{k=1}^{N} B^2_{jki}\kappa^{yy}_{jki}V_kV_j,\ \omega_i^{\kappa_k^{yy}} = \frac{1}{6}\sum_{j=1}^{N}\sum_{k=1}^{N} B^2_{kij}\kappa^{yy}_{kij}V_kV_j,$$
$$\omega_i^{\kappa_i^{xy}} = \frac{1}{6}\sum_{j=1}^{N}\sum_{k=1}^{N} B^3_{ijk}\kappa^{xy}_{ijk}V_kV_j,\ \omega_i^{\kappa_j^{xy}} = \frac{1}{6}\sum_{j=1}^{N}\sum_{k=1}^{N} B^3_{jki}\kappa^{xy}_{jki}V_kV_j,\ \omega_i^{\kappa_k^{xy}} = \frac{1}{6}\sum_{j=1}^{N}\sum_{k=1}^{N} B^3_{kij}\kappa^{xy}_{kij}V_kV_j \tag{4.22}$$

$$\omega_i^{\psi_i^{x}} = \frac{1}{6}\sum_{j=1}^{N}\sum_{k=1}^{N} C^1_{ijk}\psi^{x}_{ijk}V_kV_j,\ \omega_i^{\psi_j^{x}} = \frac{1}{6}\sum_{j=1}^{N}\sum_{k=1}^{N} C^1_{jki}\psi^{x}_{jki}V_kV_j,\ \omega_i^{\psi_k^{x}} = \frac{1}{6}\sum_{j=1}^{N}\sum_{k=1}^{N} C^1_{kij}\psi^{x}_{kij}V_kV_j,$$
$$\omega_i^{\psi_i^{y}} = \frac{1}{6}\sum_{j=1}^{N}\sum_{k=1}^{N} C^2_{ijk}\psi^{y}_{ijk}V_kV_j,\ \omega_i^{\psi_j^{y}} = \frac{1}{6}\sum_{j=1}^{N}\sum_{k=1}^{N} C^2_{jki}\psi^{y}_{jki}V_kV_j,\ \omega_i^{\psi_k^{y}} = \frac{1}{6}\sum_{j=1}^{N}\sum_{k=1}^{N} C^2_{kij}\psi^{y}_{kij}V_kV_j \tag{4.23}$$

where $A(N/m^8)$, $B(N/m^7)$, and $C(N/m^8)$ are the stretch, curvature and shear conjugate pairs of the ϵ, κ and ψ, the ratio of 1/6 is in the equation to avoid the overcounting of each particle's contribution in basic units (the ratio of 1/3) and split the potential densities between two particles (the ratio of 1/2). However, one may drop this ratio from the derivation since the equations will be eventually calibrated by using classical or experimental data. One of the clear differences of the tridynamics framework with peridynamics could be the introduction of the nanopotential function instead of micropotential to form the Lagrangian of the system. Such a description may help to analyze problems that need a smaller length scale. Noting that due to coupling effect in the plate model, A^1 contributes in the stretches of mid-plane in the x-direction. Similarly, A^2 causes the axial deformation in the y-direction.

For the in-plane shear deformation, all forces A^1, A^2 play role independently. The coupling deformation effect comes from A^3. It is worth noting that A^1 is a function of ϵ^{xx}, and A^2 is a function of ϵ^{yy}. By a similar interpretation, B^1 and B^2 are the loads that result in curvatures κ^{xx} and κ^{yy}, respectively. It should be noted that B^1 is presented as a function of κ^{xx}, and B^2 is given as a function of κ^{yy}. In addition, B^3 results into twisting of the plate in XY-plane (κ^{xy}). We also introduce the C^1 and C^2 due to the shear effect that respectively make ψ^x and ψ^y.

As another part of Lagrangian of the system, we need to construct the total kinetic energy T of the system as:

$$T = \frac{1}{2}\sum_{i=1}^{N} \rho \left[\dot{u_i}^2 + \frac{I}{A}(\dot{\phi_i^x})^2 + 2z\dot{u_i}\dot{\phi_i^x} + \dot{v_i}^2 + \frac{I}{A}(\dot{\phi_i^y})^2 + 2z\dot{v_i}\dot{\phi_i^y} + \dot{w_i}^2 \right] V_i \tag{4.24}$$

where ρ, A and I are the mass density, the moment of inertia and the cross-section area of the plate, respectively. Noting that the kinetic energy does not incorporate any length scale parameter. The ith particle that undergo the general two dimensional rigid body motion including axial (u), transverse (w) and rotational motion (ϕ). Such a insight may avoid phenomenological definition of kinetic energy with length scale parameter [43]. In this section, the word *particle* refers to a cubic volume V with mass density of ρ. In Eq. 4.24, the variable z is showing coordinates of the particles in z direction. For a very thin plate i.e. $h/L << 1$, the variable z could be approximated to zero, therefore, the coupling terms vanish. For keeping simplicity of the equations and avoiding more coupling terms in numerical part, we solely calculate the kinetic energy for particle i on the axial line. However the following derivations will remain valid for larger height. The Lagrangian of the FSDT plate in the framework could found using:

$$L = T - U \tag{4.25}$$

4.4 Equation of Motion of the Plate

To derive the EOM of the system, the Euler-Lagrange equations can be employed. Since the system is conservative, the following set of equations could be derived. The time-dependent field variable used in the Lagrangian of the system is (u, w and ϕ); thus, we have:

$$\begin{aligned}
&\frac{d}{dt}\left(\frac{\partial L}{\partial \dot{u}_i}\right) = \frac{\partial L}{\partial u_i}, \quad \frac{d}{dt}\left(\frac{\partial L}{\partial \dot{v}_i}\right) = \frac{\partial L}{\partial v_i}, \quad \frac{d}{dt}\left(\frac{\partial L}{\partial \dot{w}_i}\right) = \frac{\partial L}{\partial w_i} \\
&\frac{d}{dt}\left(\frac{\partial L}{\partial \dot{\phi}_i^x}\right) = \frac{\partial L}{\partial \phi_i^x}, \frac{d}{dt}\left(\frac{\partial L}{\partial \dot{\phi}_i^y}\right) = \frac{\partial L}{\partial \phi_i^y}
\end{aligned} \tag{4.26}$$

Noting that T is the only quantity that involves the time derivative of the field variable while terms with displacement components appear in U. Substituting Lagrangian (Eq. 4.25) into the Euler-Lagrange (Eqs. 4.26) equations gives:

$$\begin{aligned}
&\frac{d}{dt}\left(\frac{\partial T}{\partial \dot{u}_i}\right) = -\frac{\partial U}{\partial u_i}, \ \frac{d}{dt}\left(\frac{\partial T}{\partial \dot{v}_i}\right) = -\frac{\partial U}{\partial v_i}, \ \frac{d}{dt}\left(\frac{\partial T}{\partial \dot{w}_i}\right) = -\frac{\partial U}{\partial w_i}, \\
&\frac{d}{dt}\left(\frac{\partial T}{\partial \dot{\phi}_i^x}\right) = -\frac{\partial U}{\partial \phi_i^x}, \ \frac{d}{dt}\left(\frac{\partial T}{\partial \dot{\phi}_i^y}\right) = -\frac{\partial U}{\partial \phi_i^y}
\end{aligned} \tag{4.27}$$

The left-hand side of Eq. 4.27 could be written as:

$$\begin{aligned}
&\frac{d}{dt}\left(\frac{\partial T}{\partial \dot{u}_i}\right) = \rho\ddot{u}_i + 2z_i\rho\ddot{\phi}_i^x, \quad \frac{d}{dt}\left(\frac{\partial T}{\partial \dot{v}_i}\right) = \rho\ddot{v}_i + 2z_i\rho\ddot{\phi}_i^y, \quad \frac{d}{dt}\left(\frac{\partial T}{\partial \dot{w}_i}\right) = \rho\ddot{w}_i, \\
&\frac{d}{dt}\left(\frac{\partial T}{\partial \dot{\phi}_i^x}\right) = \rho\frac{I}{A}\ddot{\phi}_i^x + 2z_i\rho\ddot{u}_i, \quad \frac{d}{dt}\left(\frac{\partial T}{\partial \dot{\phi}_i^y}\right) = \rho\frac{I}{A}\ddot{\phi}_i^y + 2z_i\rho\ddot{v}_i
\end{aligned} \tag{4.28}$$

and the right-hand side could be rewritten for all degrees of freedom (u, w and ϕ):

$$\begin{aligned}
&\frac{\partial U}{\partial u_i} = \frac{\partial U^\epsilon}{\partial u_i} + \frac{\partial U^\kappa}{\partial u_i} + \frac{\partial U^\psi}{\partial u_i} \quad \frac{\partial U}{\partial v_i} = \frac{\partial U^\epsilon}{\partial v_i} + \frac{\partial U^\kappa}{\partial v_i} + \frac{\partial U^\psi}{\partial v_i}, \quad \frac{\partial U}{\partial w_i} = \frac{\partial U^\epsilon}{\partial w_i} + \frac{\partial U^\kappa}{\partial w_i} + \frac{\partial U^\psi}{\partial w_i} \\
&\frac{\partial U}{\partial \phi_i^x} = \frac{\partial U^\epsilon}{\partial \phi_i^x} + \frac{\partial U^\kappa}{\partial \phi_i^x} + \frac{\partial U^\psi}{\partial \phi_i^x}, \quad \frac{\partial U}{\partial \phi_i^y} = \frac{\partial U^\epsilon}{\partial \phi_i^y} + \frac{\partial U^\kappa}{\partial \phi_i^y} + \frac{\partial U^\psi}{\partial \phi_i^y}
\end{aligned} \tag{4.29}$$

It is clear from the mathematical description of κ and ψ that the potential energy, U^κ and U^ψ are independent of u_i and v_i. Therefore one can conclude

$$\frac{\partial U^{\kappa}}{\partial u_i} = 0, \quad \frac{\partial U^{\kappa}}{\partial v_i} = 0, \quad \frac{\partial U^{\psi}}{\partial u_i} = 0, \quad \frac{\partial U^{\psi}}{\partial v_i} = 0. \tag{4.30}$$

In addition, w_i only appears in U^{ψ}, consequently, U^{κ} and U^{ϵ} do not depend on w_i:

$$\frac{\partial U^{\kappa}}{\partial w_i} = 0, \quad \frac{\partial U^{\epsilon}}{\partial w_i} = 0. \tag{4.31}$$

Similarly, ϕ shows up in both U^{κ} and U^{ψ}, thus:

$$\frac{\partial U^{\epsilon}}{\partial \phi_i^x} = 0, \quad \frac{\partial U^{\epsilon}}{\partial \phi_i^y} = 0. \tag{4.32}$$

$$\frac{\partial U}{\partial u_i} = \frac{\partial U^{\epsilon}}{\partial u_i} + \frac{\partial U^{\epsilon}}{\partial v_i} + \frac{\partial U^{\kappa}}{\partial \phi_i^x} + \frac{\partial U^{\kappa}}{\partial \phi_i^y} + \frac{\partial U^{\psi}}{\partial w_i} + \frac{\partial U^{\psi}}{\partial \phi_i^x} + \frac{\partial U^{\psi}}{\partial \phi_i^y} \tag{4.33}$$

The simplified form of the Eq. 4.29 based on potential densities could be given;

$$\frac{\partial U^{\epsilon}}{\partial u_i} = \left(\frac{\partial \omega_i^{\epsilon_i^{xx}}}{\partial u_i} + \frac{\partial \omega_i^{\epsilon_j^{xx}}}{\partial u_i} + \frac{\partial \omega_i^{\epsilon_k^{xx}}}{\partial u_i} \right) + \left(\frac{\partial \omega_i^{\epsilon_i^{xy}}}{\partial u_i} + \frac{\partial \omega_i^{\epsilon_j^{xy}}}{\partial u_i} + \frac{\partial \omega_i^{\epsilon_k^{xy}}}{\partial u_i} \right) \tag{4.34a}$$

$$\frac{\partial U^{\epsilon}}{\partial v_i} = \left(\frac{\partial \omega_i^{\epsilon_i^{yy}}}{\partial v_i} + \frac{\partial \omega_i^{\epsilon_j^{yy}}}{\partial v_i} + \frac{\partial \omega_i^{\epsilon_k^{yy}}}{\partial v_i} \right) + \left(\frac{\partial \omega_i^{\epsilon_i^{xy}}}{\partial v_i} + \frac{\partial \omega_i^{\epsilon_j^{xy}}}{\partial v_i} + \frac{\partial \omega_i^{\epsilon_k^{xy}}}{\partial v_i} \right), \tag{4.34b}$$

$$\frac{\partial U^{\psi}}{\partial w_i} = \left(\frac{\partial \omega_i^{\psi_i^{x}}}{\partial w_i} + \frac{\partial \omega_i^{\psi_j^{x}}}{\partial w_i} + \frac{\partial \omega_i^{\psi_k^{x}}}{\partial w_i} \right) + \left(\frac{\partial \omega_i^{\psi_i^{y}}}{\partial w_i} + \frac{\partial \omega_i^{\psi_j^{y}}}{\partial w_i} + \frac{\partial \omega_i^{\psi_k^{y}}}{\partial w_i} \right), \tag{4.34c}$$

$$\frac{\partial U^{\kappa}}{\partial \phi_i^x} = \left(\frac{\partial \omega_i^{\kappa_i^{x}}}{\partial \phi_i^x} + \frac{\partial \omega_i^{\kappa_j^{x}}}{\partial \phi_i^x} + \frac{\partial \omega_i^{\kappa_k^{x}}}{\partial \phi_i^x} \right) + \left(\frac{\partial \omega_i^{\kappa_i^{xy}}}{\partial \phi_i^x} + \frac{\partial \omega_i^{\kappa_j^{xy}}}{\partial \phi_i^x} + \frac{\partial \omega_i^{\kappa_k^{xy}}}{\partial \phi_i^x} \right) \tag{4.34d}$$

$$\frac{\partial U^{\kappa}}{\partial \phi_i^y} = \left(\frac{\partial \omega_i^{\kappa_i^{y}}}{\partial \phi_i^y} + \frac{\partial \omega_i^{\kappa_j^{y}}}{\partial \phi_i^y} + \frac{\partial \omega_i^{\kappa_k^{y}}}{\partial \phi_i^y} \right) + \left(\frac{\partial \omega_i^{\kappa_i^{xy}}}{\partial \phi_i^y} + \frac{\partial \omega_i^{\kappa_j^{xy}}}{\partial \phi_i^y} + \frac{\partial \omega_i^{\kappa_k^{xy}}}{\partial \phi_i^y} \right) \tag{4.34e}$$

$$\frac{\partial U^{\psi}}{\partial \phi_i^x} = \left(\frac{\partial \omega_i^{\psi_i^{x}}}{\partial \phi_i^x} + \frac{\partial \omega_i^{\psi_j^{x}}}{\partial \phi_i^x} + \frac{\partial \omega_i^{\psi_k^{x}}}{\partial \phi_i^x} \right) \tag{4.34f}$$

$$\frac{\partial U^{\psi}}{\partial \phi_i^y} = \left(\frac{\partial \omega_i^{\psi_i^{y}}}{\partial \phi_i^y} + \frac{\partial \omega_i^{\psi_j^{y}}}{\partial \phi_i^y} + \frac{\partial \omega_i^{\psi_k^{y}}}{\partial \phi_i^y} \right) \tag{4.34g}$$

Noting that, in Eq. 4.34 the summation on i index was dropped due to taking derivative respect to ith particle i.e. $\frac{\partial}{\partial u_k} \sum_{i=1}^{N} \omega_i^{\epsilon_i} V_i = \frac{\partial \omega_k^{\epsilon_k}}{\partial u_k}$. In this section, we assume that the forces

are a linear function of the corresponding deformation as:

$$
\begin{aligned}
&A^1_{ijk} = K^{\epsilon^{xx}}_{ijk}\epsilon^{xx}_{ijk},\ A^2_{ijk} = K^{\epsilon^{yy}}_{ijk}\epsilon^{yy}_{ijk},\ A^3_{ijk} = K^{{}^1\epsilon^{xy}1}_{ijk}\epsilon^{xy}_{ijk} + K^{{}^2\epsilon^{xy}2}_{ijk}\epsilon^{xy}_{ijk} \\
&B^1_{ijk} = K^{\phi^{xx}}_{ijk}\kappa^{xx}_{ijk},\ B^2_{ijk} = K^{\phi^{yy}}_{ijk}\kappa^{yy}_{ijk},\ B^3_{ijk} = K^{{}^1\phi^{xy}1}_{ijk}\kappa^{xy}_{ijk} + K^{{}^2\phi^{xy}2}_{ijk}\kappa^{xy}_{ijk} \\
&C^1_{ijk} = K^{\psi^x}_{ijk}\psi^x_{ijk},\ C^2_{ijk} = K^{\psi^y}_{ijk}\psi^y_{ijk}
\end{aligned}
\tag{4.35}
$$

partial derivative for each term of the potential energy density can be given as:

$$
\begin{aligned}
\frac{\partial \omega_i^{\epsilon_i^{xx}}}{\partial u_i} &= \frac{1}{6}\sum_{j=1}^{N}\sum_{k=1}^{N}\frac{\partial\left(A^1_{ijk}\epsilon^{xx}_{ijk}\right)}{\partial u_i}V_kV_j = \frac{1}{6}\sum_{j=1}^{N}\sum_{k=1}^{N}\frac{\partial\left(A^1_{ijk}\epsilon^{xx}_{ijk}\right)}{\partial \epsilon^{xx}_{ijk}}\frac{\partial\epsilon^{xx}_{ijk}}{\partial u_i}V_kV_j \\
&= -\frac{1}{3}\sum_{j=1}^{N}\sum_{k=1}^{N}\left[K^{\epsilon_{xx}}_{ijk}\epsilon^{xx}_{ijk}\left(\frac{1}{\xi^x_{ij}}+\frac{1}{\xi^x_{ik}}\right)\right]V_kV_j
\end{aligned}
\tag{4.36}
$$

$$
\begin{aligned}
\frac{\partial \omega_i^{\epsilon_i^{yy}}}{\partial v_i} &= \frac{1}{6}\sum_{j=1}^{N}\sum_{k=1}^{N}\frac{\partial\left(A^2_{ijk}\epsilon^{yy}_{ijk}\right)}{\partial v_i}V_kV_j = \frac{1}{6}\sum_{j=1}^{N}\sum_{k=1}^{N}\frac{\partial\left(A^2_{ijk}\epsilon^{yy}_{ijk}\right)}{\partial \epsilon^{yy}_{ijk}}\frac{\partial\epsilon^{yy}_{ijk}}{\partial v_i}V_kV_j \\
&= -\frac{1}{3}\sum_{j=1}^{N}\sum_{k=1}^{N}\left[K^{\epsilon_{yy}}_{ijk}\epsilon^{yy}_{ijk}\left(\frac{1}{\xi^y_{ij}}+\frac{1}{\xi^y_{ik}}\right)\right]V_kV_j
\end{aligned}
\tag{4.37}
$$

$$
\begin{aligned}
\frac{\partial \omega_i^{\epsilon_i^{xy}}}{\partial u_i} &= \frac{1}{6}\sum_{j=1}^{N}\sum_{k=1}^{N}\frac{\partial\left(A^3_{ijk}\epsilon^{xy}_{ijk}\right)}{\partial v_i}V_kV_j = \frac{1}{6}\sum_{j=1}^{N}\sum_{k=1}^{N}\frac{\partial\left(A^3_{ijk}\epsilon^{xy}_{ijk}\right)}{\partial \epsilon^{xy}_{ijk}}\frac{\partial\epsilon^{xy}_{ijk}}{\partial u_i}V_kV_j \\
&= -\frac{1}{3}\sum_{j=1}^{N}\sum_{k=1}^{N}\left[\left(K^{{}^1\epsilon^{xy}1}_{ijk}\epsilon^{xy}_{ijk} + \left(K^{{}^1\epsilon^{xy}}_{ijk} + K^{{}^2\epsilon^{xy}}_{ijk}\right){}^2\epsilon^{xy}_{ijk}\right)\left(\frac{1}{\xi^y_{ij}}+\frac{1}{\xi^y_{ik}}\right)\right]V_kV_j
\end{aligned}
\tag{4.38}
$$

$$
\begin{aligned}
\frac{\partial \omega_i^{\epsilon_i^{xy}}}{\partial v_i} &= \frac{1}{6}\sum_{j=1}^{N}\sum_{k=1}^{N}\frac{\partial\left(A^3_{ijk}\epsilon^{xy}_{ijk}\right)}{\partial v_i}V_kV_j = \frac{1}{6}\sum_{j=1}^{N}\sum_{k=1}^{N}\frac{\partial\left(A^3_{ijk}\epsilon^{xy}_{ijk}\right)}{\partial \epsilon^{xy}_{ijk}}\frac{\partial\epsilon^{xy}_{ijk}}{\partial v_i}V_kV_j \\
&= -\frac{1}{3}\sum_{j=1}^{N}\sum_{k=1}^{N}\left[\left(K^{{}^1\epsilon^{xy}1}_{ijk}\epsilon^{xy}_{ijk} + \left(K^{{}^1\epsilon^{xy}}_{ijk} + K^{{}^2\epsilon^{xy}}_{ijk}\right){}^2\epsilon^{xy}_{ijk}\right)\left(\frac{1}{\xi^x_{ij}}+\frac{1}{\xi^x_{ik}}\right)\right]V_kV_j
\end{aligned}
\tag{4.39}
$$

$$
\begin{aligned}
\frac{\partial \omega_i^{\psi_i^{x}}}{\partial w_i} &= \frac{1}{6}\sum_{j=1}^{N}\sum_{k=1}^{N}\frac{\partial\left(C^1_{ijk}\psi^x_{ijk}\right)}{\partial w_i}V_kV_j = \frac{1}{6}\sum_{j=1}^{N}\sum_{k=1}^{N}\frac{\partial\left(C^1_{ijk}\psi^x_{ijk}\right)}{\partial \psi^x_{ijk}}\frac{\partial\psi^x_{ijk}}{\partial w_i}V_kV_j \\
&= -\frac{1}{3}\sum_{j=1}^{N}\sum_{k=1}^{N}\left[K^{\psi^x,w}_{ijk}\psi^x_{ijk}\left(\frac{1}{\xi^x_{ij}}+\frac{1}{\xi^x_{ik}}\right)\right]V_kV_j
\end{aligned}
\tag{4.40}
$$

$$\frac{\partial \omega_i^{\psi^y}}{\partial w_i} = \frac{1}{6}\sum_{j=1}^{N}\sum_{k=1}^{N}\frac{\partial\left(C_{ijk}^1\psi_{ijk}^y\right)}{\partial w_i}V_kV_j = \frac{1}{6}\sum_{j=1}^{N}\sum_{k=1}^{N}\frac{\partial\left(C_{ijk}^1\psi_{ijk}^y\right)}{\partial \psi_{ijk}^y}\frac{\partial\psi_{ijk}^y}{\partial w_i}V_kV_j$$
$$= -\frac{1}{3}\sum_{j=1}^{N}\sum_{k=1}^{N}\left[K_{ijk}^{\psi^y,w}\psi_{ijk}^y\left(\frac{1}{\xi_{ij}^y}+\frac{1}{\xi_{ik}^y}\right)\right]V_kV_j \tag{4.41}$$

$$\frac{\partial \omega_i^{\psi^x}}{\partial \phi_i^x} = \frac{1}{6}\sum_{j=1}^{N}\sum_{k=1}^{N}\frac{\partial\left(C_{ijk}^1\psi_{ijk}^x\right)}{\partial \phi_i^x}V_kV_j = \frac{1}{6}\sum_{j=1}^{N}\sum_{k=1}^{N}\frac{\partial\left(C_{ijk}^1\psi_{ijk}^x\right)}{\partial \psi_{ijk}^x}\frac{\partial\psi_{ijk}^x}{\partial \phi_i^x}V_kV_j$$
$$= -\frac{1}{6}\sum_{j=1}^{N}\sum_{k=1}^{N}\left[K_{ijk}^{\psi^x}\psi_{ijk}^x\left(\hat{n}_{iij}^x+\hat{n}_{iik}^x\right)\right]V_kV_j \tag{4.42}$$

$$\frac{\partial \omega_i^{\psi^y}}{\partial \phi_i^y} = \frac{1}{6}\sum_{j=1}^{N}\sum_{k=1}^{N}\frac{\partial\left(C_{ijk}^2\psi_{ijk}^y\right)}{\partial \psi_i^y}V_kV_j = \frac{1}{6}\sum_{j=1}^{N}\sum_{k=1}^{N}\frac{\partial\left(C_{ijk}^2\psi_{ijk}^y\right)}{\partial \psi_{ijk}^y}\frac{\partial\psi_{ijk}^y}{\partial \psi_i^y}V_kV_j$$
$$= -\frac{1}{6}\sum_{j=1}^{N}\sum_{k=1}^{N}\left[K_{ijk}^{\psi^y}\psi_{ijk}^y\left(\hat{n}_{iij}^y+\hat{n}_{iik}^y\right)\right]V_kV_j \tag{4.43}$$

$$\frac{\partial \omega_i^{\kappa^{xx}}}{\partial \phi_i^x} = \frac{1}{6}\sum_{j=1}^{N}\sum_{k=1}^{N}\frac{\partial\left(B_{ijk}^1\kappa_{ijk}^{xx}\right)}{\partial \phi_i^x}V_kV_j = \frac{1}{6}\sum_{j=1}^{N}\sum_{k=1}^{N}\frac{\partial\left(B_{ijk}^1\kappa_{ijk}^{xx}\right)}{\partial \kappa_{ijk}^{xx}}\frac{\partial\kappa_{ijk}^{xx}}{\partial \phi_i^x}V_kV_j$$
$$= -\frac{1}{3}\sum_{j=1}^{N}\sum_{k=1}^{N}\left[K_{ijk}^{\phi^{xx}}\kappa_{ijk}^{xx}\left(\frac{1}{\xi_{ij}^x}+\frac{1}{\xi_{ik}^x}\right)\right]V_kV_j \tag{4.44}$$

$$\frac{\partial \omega_i^{\kappa^{xy}}}{\partial \phi_i^x} = \frac{1}{6}\sum_{j=1}^{N}\sum_{k=1}^{N}\frac{\partial\left(B_{ijk}^3\kappa_{ijk}^{xy}\right)}{\partial \phi_i^x}V_kV_j = \frac{1}{6}\sum_{j=1}^{N}\sum_{k=1}^{N}\frac{\partial\left(B_{ijk}^3\kappa_{ijk}^{xy}\right)}{\partial \kappa_{ijk}^{xy}}\frac{\partial\kappa_{ijk}^{xy}}{\partial \phi_i^x}V_kV_j$$
$$= -\frac{1}{3}\sum_{j=1}^{N}\sum_{k=1}^{N}\left[\Gamma_1 K_{ijk}^{\phi^{xx}}\kappa_{ijk}^{xy}\left(\frac{1}{\xi_{ij}^y}+\frac{1}{\xi_{ik}^y}\right)\right]V_kV_j \tag{4.45}$$

$$\frac{\partial \omega_i^{\kappa^{yy}}}{\partial \phi_i^y} = \frac{1}{6}\sum_{j=1}^{N}\sum_{k=1}^{N}\frac{\partial\left(B_{ijk}^2\kappa_{ijk}^{yy}\right)}{\partial \phi_i^y}V_kV_j = \frac{1}{6}\sum_{j=1}^{N}\sum_{k=1}^{N}\frac{\partial\left(B_{ijk}^2\kappa_{ijk}^{yy}\right)}{\partial \kappa_{ijk}^{yy}}\frac{\partial\kappa_{ijk}^{yy}}{\partial \phi_i^y}V_kV_j$$
$$= -\frac{1}{3}\sum_{j=1}^{N}\sum_{k=1}^{N}\left[K_{ijk}^{\phi^{yy}}\kappa_{ijk}^{yy}\left(\frac{1}{\xi_{ij}^y}+\frac{1}{\xi_{ik}^y}\right)\right]V_kV_j \tag{4.46}$$

$$\frac{\partial \omega_i^{\kappa^{xy}}}{\partial \phi_i^y} = \frac{1}{6}\sum_{j=1}^{N}\sum_{k=1}^{N}\frac{\partial\left(B_{ijk}^2\kappa_{ijk}^{xy}\right)}{\partial \phi_i^y}V_kV_j = \frac{1}{6}\sum_{j=1}^{N}\sum_{k=1}^{N}\frac{\partial\left(B_{ijk}^2\kappa_{ijk}^{xy}\right)}{\partial \kappa_{ijk}^{xy}}\frac{\partial\kappa_{ijk}^{xy}}{\partial \phi_i^y}V_kV_j$$
$$= -\frac{1}{3}\sum_{j=1}^{N}\sum_{k=1}^{N}\left[\Gamma_2 K_{ijk}^{\phi^{yy}}\kappa_{ijk}^{xy}\left(\frac{1}{\xi_{ij}^y}+\frac{1}{\xi_{ik}^y}\right)\right]V_kV_j \tag{4.47}$$

Note that all relations are written only for index i for the sake of brevity, while, the relations can easily be generalized for indices j and k. The rest of derivations for particles j^th and k^th

are given in D. Here, A_{ijk}, B_{ijk} and C_{ijk} are existing forces in $i-j$ and $i-k$ bonds which result in the stretch, curvature and transverse shear of the plate. By permuting the indices, the forces in other bonds can be shown. These multi-body forces within the element may bring more flexibility to model other material classes, e.g., anisotropic materials. Therefore, the equation of motion of plate under FSDT assumption can be given as;

$$\begin{aligned}
\rho\ddot{u}_i + 2z_i\rho\ddot{\phi}_i^x =& \frac{1}{3}\sum_{j=1}^{M}\sum_{k=1}^{M}\left[K_{ijk}^{\epsilon^{xx}}\left(\frac{1}{\xi_{ij}^x}+\frac{1}{\xi_{ik}^x}\right)\epsilon_{ijk}^{xx} - K_{jki}^{\epsilon^{xx}}\left(\frac{1}{\xi_{ij}^x}\right)\epsilon_{jki}^{xx} - K_{kij}^{\epsilon^{xx}}\left(\frac{1}{\xi_{ik}^x}\right)\epsilon_{kij}^{xx}\right]V_kV_j \\
&+\frac{1}{3}\sum_{j=1}^{M}\sum_{k=1}^{M}\left[\left(2K_{ijk}^{{}^1\epsilon^{xy}}{}^1\epsilon_{ijk}^{xy} + \left(K_{ijk}^{{}^1\epsilon^{xy}} + K_{ijk}^{{}^2\epsilon^{xy}}\right){}^2\epsilon_{ijk}^{xy}\right)\left(\frac{1}{\xi_{ij}^y}+\frac{1}{\xi_{ik}^y}\right)\right]V_kV_j \\
&-\frac{1}{3}\sum_{j=1}^{M}\sum_{k=1}^{M}\left[\left(2K_{jki}^{{}^1\epsilon^{xy}}{}^1\epsilon_{jki}^{xy} + \left(K_{jki}^{{}^1\epsilon^{xy}} + K_{jki}^{{}^2\epsilon^{xy}}\right){}^2\epsilon_{jki}^{xy}\right)\left(\frac{1}{\xi_{ij}^y}\right)\right]V_kV_j \\
&-\frac{1}{3}\sum_{j=1}^{M}\sum_{k=1}^{M}\left[\left(2K_{kij}^{{}^1\epsilon^{xy}}{}^1\epsilon_{kij}^{xy} + \left(K_{kij}^{{}^1\epsilon^{xy}} + K_{kij}^{{}^2\epsilon^{xy}}\right){}^2\epsilon_{kij}^{xy}\right)\left(\frac{1}{\xi_{ik}^y}\right)\right]V_kV_j
\end{aligned} \tag{4.48}$$

$$\begin{aligned}
\rho\ddot{v}_i + 2z_i\rho\ddot{\phi}_i^y =& \frac{1}{3}\sum_{j=1}^{M}\sum_{k=1}^{M}\left[K_{ijk}^{\epsilon^{yy}}\left(\frac{1}{\xi_{ij}^y}+\frac{1}{\xi_{ik}^y}\right)\epsilon_{ijk}^{yy} - K_{jki}^{\epsilon^{yy}}\left(\frac{1}{\xi_{ij}^y}\right)\epsilon_{jki}^{yy} - K_{kij}^{\epsilon^{yy}}\left(\frac{1}{\xi_{ik}^y}\right)\epsilon_{kij}^{yy}\right]V_kV_j \\
&+\frac{1}{3}\sum_{j=1}^{M}\sum_{k=1}^{M}\left[\left(2K_{ijk}^{{}^2\epsilon^{xy}}{}^2\epsilon_{ijk}^{xy} + \left(K_{ijk}^{{}^1\epsilon^{xy}} + K_{ijk}^{{}^2\epsilon^{xy}}\right){}^1\epsilon_{ijk}^{xy}\right)\left(\frac{1}{\xi_{ij}^x}+\frac{1}{\xi_{ik}^x}\right)\right]V_kV_j \\
&-\frac{1}{3}\sum_{j=1}^{M}\sum_{k=1}^{M}\left[\left(2K_{jki}^{{}^2\epsilon^{xy}}{}^2\epsilon_{jki}^{xy} + \left(K_{jki}^{{}^1\epsilon^{xy}} + K_{jki}^{{}^2\epsilon^{xy}}\right){}^1\epsilon_{jki}^{xy}\right)\left(\frac{1}{\xi_{ij}^x}\right)\right]V_kV_j \\
&-\frac{1}{3}\sum_{j=1}^{M}\sum_{k=1}^{M}\left[\left(2K_{kij}^{{}^2\epsilon^{xy}}{}^2\epsilon_{kij}^{xy} + \left(K_{kij}^{{}^1\epsilon^{xy}} + K_{kij}^{{}^2\epsilon^{xy}}\right){}^1\epsilon_{kij}^{xy}\right)\left(\frac{1}{\xi_{ik}^x}\right)\right]V_kV_j
\end{aligned} \tag{4.49}$$

$$\begin{aligned}
\rho\ddot{w}_i \quad =& \quad \frac{1}{3}\sum_{j=1}^{M}\sum_{k=1}^{M}\left[K_{ijk}^{\psi_x}\left(\frac{1}{\xi_{ij}^x}+\frac{1}{\xi_{ik}^x}\right)\psi_{ijk}^x - K_{jki}^{\psi_x}\left(\frac{1}{\xi_{ij}^x}\right)\psi_{jki}^x - K_{kij}^{\psi_x}\left(\frac{1}{\xi_{ik}^x}\right)\psi_{kij}^x\right]V_kV_j \\
&+\frac{1}{3}\sum_{j=1}^{M}\sum_{k=1}^{M}\left[K_{ijk}^{\psi_y}\left(\frac{1}{\xi_{ij}^y}+\frac{1}{\xi_{ik}^y}\right)\psi_{ijk}^y - K_{jki}^{\psi_y}\left(\frac{1}{\xi_{ij}^y}\right)\psi_{jki}^y - K_{kij}^{\psi_y}\left(\frac{1}{\xi_{ik}^y}\right)\psi_{kij}^y\right]V_kV_j
\end{aligned} \tag{4.50}$$

$$\rho\frac{I}{A}\ddot{\phi}_i^x + 2z_i\rho\ddot{u}_i = +\frac{1}{3}\sum_{j=1}^{M}\sum_{k=1}^{M}\left[K_{ijk}^{\phi^{xx}}\left(\frac{1}{\xi_{ij}^x}+\frac{1}{\xi_{ik}^x}\right)\kappa_{ijk}^{xx} - K_{jki}^{\phi^{xx}}\left(\frac{1}{\xi_{ij}^x}\right)\kappa_{jki}^{xx} - K_{kij}^{\phi^{xx}}\left(\frac{1}{\xi_{ik}^x}\right)\kappa_{kij}^{xx}\right]V_kV_j$$
$$+\frac{1}{3}\sum_{j=1}^{M}\sum_{k=1}^{M}\left[\left(2K_{ijk}^{{}^1\phi^{xy}}{}^1\kappa_{ijk}^{xy} + \left(K_{ijk}^{{}^1\phi^{xy}} + K_{ijk}^{{}^2\phi^{xy}}\right){}^2\kappa_{ijk}^{xy}\right)\left(\frac{1}{\xi_{ij}^y}+\frac{1}{\xi_{ik}^y}\right)\right]V_kV_j$$
$$-\frac{1}{3}\sum_{j=1}^{M}\sum_{k=1}^{M}\left[\left(2K_{jki}^{{}^1\phi^{xy}}{}^1\kappa_{jki}^{xy} + \left(K_{jki}^{{}^1\phi^{xy}} + K_{jki}^{{}^2\phi^{xy}}\right){}^2\kappa_{jki}^{xy}\right)\left(\frac{1}{\xi_{ij}^y}\right)\right]V_kV_j$$
$$-\frac{1}{3}\sum_{j=1}^{M}\sum_{k=1}^{M}\left[\left(2K_{kij}^{{}^1\phi^{xy}}{}^1\kappa_{kij}^{xy} + \left(K_{kij}^{{}^1\phi^{xy}} + K_{kij}^{{}^2\phi^{xy}}\right){}^2\kappa_{kij}^{xy}\right)\left(\frac{1}{\xi_{ik}^y}\right)\right]V_kV_j$$
$$+\frac{1}{6}\sum_{j=1}^{M}\sum_{k=1}^{M}\left[K_{ijk}^{\psi^x}\psi_{ijk}^x\left(\hat{n}_{iij}^{\ x}+\hat{n}_{iik}^{\ x}\right) - K_{jki}^{\psi^x}\psi_{jki}^x\left(\hat{n}_{iij}^{\ x}\right) - K_{kij}^{\psi^x}\psi_{kij}^x\left(\hat{n}_{iik}^{\ x}\right)\right]V_kV_j \tag{4.51}$$

$$\rho\frac{I}{A}\ddot{\phi}_i^y + 2z_i\rho\ddot{v}_i = +\frac{1}{3}\sum_{j=1}^{M}\sum_{k=1}^{M}\left[K_{ijk}^{\phi^{yy}}\left(\frac{1}{\xi_{ij}^y}+\frac{1}{\xi_{ik}^y}\right)\kappa_{ijk}^{yy} - K_{jki}^{\phi^{yy}}\left(\frac{1}{\xi_{ij}^y}\right)\kappa_{jki}^{yy} - K_{kij}^{\phi^{yy}}\left(\frac{1}{\xi_{ik}^y}\right)\kappa_{kij}^{yy}\right]V_kV_j$$
$$+\frac{1}{3}\sum_{j=1}^{M}\sum_{k=1}^{M}\left[\left(2K_{ijk}^{{}^2\phi^{xy}}{}^2\kappa_{ijk}^{xy} + \left(K_{ijk}^{{}^1\phi^{xy}} + K_{ijk}^{{}^2\phi^{xy}}\right){}^1\kappa_{ijk}^{xy}\right)\left(\frac{1}{\xi_{ij}^x}+\frac{1}{\xi_{ik}^x}\right)\right]V_kV_j$$
$$-\frac{1}{3}\sum_{j=1}^{M}\sum_{k=1}^{M}\left[\left(2K_{jki}^{{}^2\phi^{xy}}{}^2\kappa_{jki}^{xy} + \left(K_{jki}^{{}^1\phi^{xy}} + K_{jki}^{{}^2\phi^{xy}}\right){}^1\kappa_{jki}^{xy}\right)\left(\frac{1}{\xi_{ij}^x}\right)\right]V_kV_j$$
$$-\frac{1}{3}\sum_{j=1}^{M}\sum_{k=1}^{M}\left[\left(2K_{kij}^{{}^2\phi^{xy}}{}^2\kappa_{kij}^{xy} + \left(K_{kij}^{{}^1\phi^{xy}} + K_{kij}^{{}^2\phi^{xy}}\right){}^1\kappa_{kij}^{xy}\right)\left(\frac{1}{\xi_{ik}^x}\right)\right]V_kV_j$$
$$+\frac{1}{6}\sum_{j=1}^{M}\sum_{k=1}^{M}\left[K_{ijk}^{\psi^y}\psi_{ijk}^y\left(\hat{n}_{iij}^{\ y}+\hat{n}_{iik}^{\ y}\right) - K_{jki}^{\psi^y}\psi_{jki}^y\left(\hat{n}_{iij}^{\ y}\right) - K_{kij}^{\psi^y}\psi_{kij}^y\left(\hat{n}_{iik}^{\ y}\right)\right]V_kV_j \tag{4.52}$$

Assuming that the plate is made of isotropic materials, The nonlocal material properties could be given as:

$$\begin{aligned} K_{ijk}^{\epsilon^{mn}} &= K_{jki}^{\epsilon^{mn}} = K_{kij}^{\epsilon^{mn}} = K^{\epsilon^{mn}} \\ K_{ijk}^{\phi^{mn}} &= K_{jki}^{\phi^{mn}} = K_{kij}^{\phi^{mn}} = K^{\phi^{mn}} \\ K_{ijk}^{\psi^{e_j}} &= K_{jki}^{\psi^{e_j}} = K_{kij}^{\psi^{e_j}} = K^{\psi^{mn}} \end{aligned} \tag{4.53}$$

where m and n could be x, y.

4.5 Localization of the Equation of Motion

Since we are working with a discrete system of equations, the local limit could be imagined when particles only interact with their closest neighbors. Therefore, one could conclude that

$\xi^x_{ij} = \xi^x_{ik} = \xi^x$ and $\xi^y_{ij} = \xi^y_{ik} = \xi^y$. Using Eqs. 4.15 along with other index properties mentioned in Section 4.2, the localized form of the developed nonlocal plate equations are given as:

$$\begin{aligned}\rho\ddot{u}_i + 2z_i\rho\ddot{\epsilon}^x_i = &\left[K^{\epsilon^{xx}} \lim_{\delta\to\delta_l}\left(\frac{\epsilon^{xx}_{ijk}}{\xi^x}\right) + 2\left({}^1K^{\epsilon^{xy}}\right)\lim_{\delta\to\delta_l}\left(\frac{{}^1\epsilon^{xy}_{ijk}}{\xi^y}\right)\right]\lim_{\delta\to\delta_l}\left(\sum_{j=1}^{M}\sum_{k=1}^{M}V_kV_j\right)\\ &+\left[\left({}^1K^{\epsilon^{xy}} + {}^2K^{\epsilon^{xy}}\right)\lim_{\delta\to\delta_l}\left(\frac{{}^2\epsilon^{xy}_{ijk}}{\xi^y}\right)\right]\lim_{\delta\to\delta_l}\left(\sum_{j=1}^{M}\sum_{k=1}^{M}V_kV_j\right)\end{aligned} \tag{4.54}$$

$$\begin{aligned}\rho\ddot{v}_i + 2z_i\rho\ddot{\phi}^y_i = &\left[K^{\epsilon^{yy}} \lim_{\delta\to\delta_l}\left(\frac{\epsilon^{yy}_{ijk}}{\xi^y}\right) + 2\left({}^2K^{\epsilon^{xy}}\right)\lim_{\delta\to\delta_l}\left(\frac{{}^2\epsilon^{xy}_{ijk}}{\xi^x}\right)\right]\lim_{\delta\to\delta_l}\left(\sum_{j=1}^{M}\sum_{k=1}^{M}V_kV_j\right)\\ &+\left[\left({}^1K^{\epsilon^{xy}} + {}^2K^{\epsilon^{xy}}\right)\lim_{\delta\to\delta_l}\left(\frac{{}^1\epsilon^{xy}_{ijk}}{\xi^x}\right)\right]\lim_{\delta\to\delta_l}\left(\sum_{j=1}^{M}\sum_{k=1}^{M}V_kV_j\right)\end{aligned} \tag{4.55}$$

$$\rho\ddot{w}_i = \left[K^{\psi^x}\lim_{\delta\to\delta_l}\left(\frac{\psi^x_{ijk}}{\xi^x}\right) + K^{\psi^y}\lim_{\delta\to\delta_l}\left(\frac{\psi^y_{ijk}}{\xi^y}\right)\right]\lim_{\delta\to\delta_l}\left(\sum_{j=1}^{M}\sum_{k=1}^{M}V_kV_j\right) \tag{4.56}$$

$$\begin{aligned}\rho\frac{I}{A}\ddot{\phi}^x_i + 2z_i\rho\ddot{u}_i = &\left[K^{\phi^{xx}} \lim_{\delta\to\delta_l}\left(\frac{\kappa^{xx}_{ijk}}{\xi^x}\right) + 2\left({}^1K^{\phi^{xy}}\right)\lim_{\delta\to\delta_l}\left(\frac{{}^1\kappa^{xy}_{ijk}}{\xi^y}\right)\right]\lim_{\delta\to\delta_l}\left(\sum_{j=1}^{M}\sum_{k=1}^{M}V_kV_j\right)\\ &+\left[\left({}^1K^{\phi^{xy}} + {}^2K^{\phi^{xy}}\right)\lim_{\delta\to\delta_l}\left(\frac{{}^2\kappa^{xy}_{ijk}}{\xi^y}\right)\right]\lim_{\delta\to\delta_l}\left(\sum_{j=1}^{M}\sum_{k=1}^{M}V_kV_j\right)\\ &+\frac{K^{\psi^x}}{6}\lim_{\delta\to\delta_l}\left(\sum_{j=1}^{M}\sum_{k=1}^{M}\left[\psi^x_{ijk}\left(\hat{n}^x_{iij}+\hat{n}^x_{iik}\right) - \psi^x_{jki}\left(\hat{n}^x_{iij}\right) - \psi^x_{kij}\left(\hat{n}^x_{iik}\right)\right]V_kV_j\right)\end{aligned} \tag{4.57}$$

$$\begin{aligned}\rho\frac{I}{A}\ddot{\phi}^y_i + 2z_i\rho\ddot{v}_i = &\left[K^{\phi^{yy}} \lim_{\delta\to\delta_l}\left(\frac{\kappa^{yy}_{ijk}}{\xi^y}\right) + 2\left({}^2K^{\phi^{xy}}\right)\lim_{\delta\to\delta_l}\left(\frac{{}^2\kappa^{xy}_{ijk}}{\xi^x}\right)\right]\lim_{\delta\to\delta_l}\left(\sum_{j=1}^{M}\sum_{k=1}^{M}V_kV_j\right)\\ &+\left[\left({}^1K^{\phi^{xy}} + {}^2K^{\phi^{xy}}\right)\lim_{\delta\to\delta_l}\left(\frac{{}^1\kappa^{xy}_{ijk}}{\xi^x}\right)\right]\lim_{\delta\to\delta_l}\left(\sum_{j=1}^{M}\sum_{k=1}^{M}V_kV_j\right)\\ &+\frac{K^{\psi^y}}{6}\lim_{\delta\to\delta_l}\left(\sum_{j=1}^{M}\sum_{k=1}^{M}\left[\psi^y_{ijk}\left(\hat{n}^y_{iij}+\hat{n}^y_{iik}\right) - \psi^y_{jki}\left(\hat{n}^y_{iij}\right) - \psi^y_{kij}\left(\hat{n}^y_{iik}\right)\right]V_kV_j\right)\end{aligned} \tag{4.58}$$

In the local limit, we change the upper bond of the series from N to m to emphasis on the particles in the immediate neighbor. We also assume that the values of ϵ, κ and ψ are constant in the local horizon. Therefore, they could be taken out of the series. To have a set of equations that are decoupled (respect to u), we assume that the thickness of the plate is sufficiently small in comparison to other in-plane dimensions ($h/L < 0.01$), i.e., the particles are scattered uniformly on the XY-plane, and other particles above or below the XY-plane have very small z_i. Thus, we are able to drop terms with z in the kinetic part of EOMs (Eqs. 4.48, 4.49, 4.51 and 4.52). It could be easily shown the followings relations in local limit:

$$\lim_{\delta\to\delta_l}\left(\frac{\epsilon^{xx}_{ijk}}{\xi^x}\right) = u_{,xx} \quad , \lim_{\delta\to\delta_l}\left(\frac{{}^1\epsilon^{xy}_{ijk}}{\xi^y}\right) = u_{,yy}, \quad \lim_{\delta\to\delta_l}\left(\frac{{}^2\epsilon^{xy}_{ijk}}{\xi^y}\right) = v_{,xy}, \tag{4.59a}$$

$$\lim_{\delta\to\delta_l}\left(\frac{\epsilon^{yy}_{ijk}}{\xi^y}\right) = v_{,yy}, \quad \lim_{\delta\to\delta_l}\left(\frac{{}^1\epsilon^{xy}_{ijk}}{\xi^x}\right) = u_{,xy}, \quad \lim_{\delta\to\delta_l}\left(\frac{{}^2\epsilon^{xy}_{ijk}}{\xi^x}\right) = v_{,xx} \tag{4.59b}$$

$$\lim_{\delta\to\delta_l}\left(\frac{\kappa^{xx}_{ijk}}{\xi^x}\right) = \phi_{x,xx} \quad , \lim_{\delta\to\delta_l}\left(\frac{{}^1\kappa^{xy}_{ijk}}{\xi^y}\right) = \phi_{x,yy}, \quad \lim_{\delta\to\delta_l}\left(\frac{{}^2\kappa^{xy}_{ijk}}{\xi^y}\right) = \phi_{y,xy}, \tag{4.59c}$$

$$\lim_{\delta\to\delta_l}\left(\frac{\kappa^{yy}_{ijk}}{\xi^y}\right) = \phi_{y,yy}, \quad \lim_{\delta\to\delta_l}\left(\frac{{}^1\kappa^{xy}_{ijk}}{\xi^x}\right) = \phi_{x,xy}, \quad \lim_{\delta\to\delta_l}\left(\frac{{}^2\kappa^{xy}_{ijk}}{\xi^x}\right) = \phi_{y,xx} \tag{4.59d}$$

$$\lim_{\delta\to\delta_l}\left(\frac{\psi^x_{ijk}}{\xi^x}\right) = w_{,xx} - \phi_{x,x} \quad \lim_{\delta\to\delta_l}\left(\frac{\psi^y_{ijk}}{\xi^y}\right) = w_{,yy} - \phi_{y,y} \tag{4.59e}$$

$$\lim_{\delta\to\delta_l}\left(\psi^x_{ijk}\left(\hat{n}^{\,x}_{iij} + \hat{n}^{\,x}_{iik}\right) - \psi^x_{jki}\left(\hat{n}^{\,x}_{iij}\right) - \psi^x_{kij}\left(\hat{n}^{\,x}_{iik}\right)\right) = w_{,x} - \phi_x \tag{4.59f}$$

$$\lim_{\delta\to\delta_l}\left(\psi^y_{ijk}\left(\hat{n}^{\,y}_{iij} + \hat{n}^{\,y}_{iik}\right) - \psi^y_{jki}\left(\hat{n}^{\,y}_{iij}\right) - \psi^y_{kij}\left(\hat{n}^{\,y}_{iik}\right)\right) = w_{,y} - \phi_y \tag{4.59g}$$

$$\tag{4.59h}$$

Therefore, the localized form of the equations could be given as:

$$\rho\ddot{u} + 2z\rho\ddot{\phi_x} = \left(K^{\epsilon_{xx}}V_T^2\right)u_{,xx} + 2\left({}^1K^{\epsilon_{xy}}V_T^2\right)u_{,yy} + \left[\left({}^1K^{\epsilon_{xy}} + {}^2K^{\epsilon_{xy}}\right)V_T^2\right]v_{,xy} \tag{4.60a}$$

$$\rho\ddot{v} + 2z\rho\ddot{\phi_y} = \left(K^{\epsilon_{yy}}V_T^2\right)v_{,yy} + 2\left({}^2K^{\epsilon_{xy}}V_T^2\right)v_{,xx} + \left[\left({}^1K^{\epsilon_{xy}} + {}^2K^{\epsilon_{xy}}\right)V_T^2\right]u_{,xy} \tag{4.60b}$$

$$\rho\ddot{w} = \left(K^{\psi_x}V_T^2\right)(w_{,xx} - \phi_{x,x}) + \left(K^{\psi_y}V_T^2\right)(w_{,yy} - \phi_{y,y}) \tag{4.60c}$$

$$\rho\frac{I}{A}\ddot{\phi_x} + 2z\rho\ddot{u} = \left(K^{\phi^{xx}}V_T^2\right)\phi_{x,xx} + 2\left({}^1K^{\phi^{xy}}V_T^2\right)\phi_{x,yy} + \left[\left({}^1K^{\phi^{xy}} + {}^2K^{\phi^{xy}}\right)V_T^2\right]\phi_{y,xy} \tag{4.60d}$$

$$+ \left(K^{\psi_x}V_T^2\right)(w_{,x} - \phi_x) \tag{4.60e}$$

$$\rho\frac{I}{A}\ddot{\phi_y} + 2z\rho\ddot{v} = \left(K^{\phi^{yy}}V_T^2\right)\phi_{y,yy} + 2\left({}^2K^{\phi^{xy}}V_T^2\right)\phi_{y,xx} + \left[\left({}^1K^{\phi^{xy}} + {}^2K^{\phi^{xy}}\right)V_T^2\right]\phi_{x,xy} \tag{4.60f}$$

$$+ \left(K^{\psi_y}V_T^2\right)(w_{,y} - \phi_y) \tag{4.60g}$$

where V_T denotes the total volume of the domain associated to the horizon and can be calculated through the following:

$$V_T = \sum_{j=1}^{M} V_j \tag{4.61}$$

Noting that V_T is equal to $4V$ in the local limit for the plate model. The Eq. 4.61 is valid to be used in governing equations if we have "m" as upper bounds for both series. Noting that the classical EOMs for first-order plate theory can be given as:

$$\rho\ddot{u} + 2z\rho\ddot{\phi_x} = \left(\frac{E}{1-\nu^2}\right)u_{,xx} + \mu u_{,yy} + \left(\frac{E\nu}{1-\nu^2} + \mu\right)v_{,xy} \tag{4.62a}$$

$$\rho\ddot{v} + 2z\rho\ddot{\phi_y} = \left(\frac{E}{1-\nu^2}\right)v_{,yy} + \mu v_{,xx} + \left(\frac{E\nu}{1-\nu^2} + \mu\right)u_{,xy} \tag{4.62b}$$

$$\rho\ddot{w} = \kappa_s\mu\left(w_{,xx} - \phi_{x,x} + w_{,yy} - \phi_{y,y}\right) \tag{4.62c}$$

$$\rho\frac{I}{A}\ddot{\phi^x} + 2z\rho\ddot{u} = \frac{EI}{A\left(1-\nu^2\right)}\phi_{x,xx} + \frac{\mu I}{A}\phi_{x,yy} + \left(\frac{EI\nu}{A\left(1-\nu^2\right)} + \frac{\mu I}{A}\right)\phi_{y,xy} \tag{4.62d}$$

$$+ \kappa_s\mu\left(w_{,x} - \phi_x\right) \tag{4.62e}$$

$$\rho\frac{I}{A}\ddot{\phi^y} + 2z\rho\ddot{v} = \frac{EI}{A\left(1-\nu^2\right)}\phi_{y,yy} + \frac{\mu I}{A}\phi_{y,xx} + \left(\frac{EI\nu}{A\left(1-\nu^2\right)} + \frac{\mu I}{A}\right)\phi_{x,xy} \tag{4.62f}$$

$$+ \kappa_s\mu\left(w_{,y} - \phi_y\right) \tag{4.62g}$$

where κ_s is the shear correction coefficient and depends on the cross-section of the plate. This value for a rectangular cross-section is 5/6. The material parameters can be obtained by comparing the localized form of the tridynamics plate EOMs with the classical FSDT plate theory as:

$$\begin{aligned}
&K^{\epsilon_{xx}} = K^{\epsilon_{yy}} = \frac{E}{(1-\nu^2)\,{V_T}^2} \\
&{}^1K^{\epsilon_{xy}} = \frac{\mu}{2V_T^2},\ {}^2K^{\epsilon_{xy}} = \frac{1}{V_T^2}\left(\frac{E\nu}{1-\nu^2} + \frac{\mu}{2}\right) \\
&K^{\psi^x} = K^{\psi^y} = \frac{\kappa_s \mu}{V_T^2} \\
&K^{\phi^{xx}} = K^{\phi^{yy}} = \frac{EI}{A\,(1-\nu^2)\,{V_T}^2} \\
&{}^1K^{\phi_{xy}} = \frac{\mu I}{2AV_T^2},\ {}^2K^{\phi_{xy}} = \frac{1}{V_T^2}\left(\frac{EI\nu}{A\,(1-\nu^2)} + \frac{\mu I}{2A}\right)
\end{aligned} \tag{4.63}$$

Here, E, μ, A and I are respectively Young's modulus, shear modulus, cross-sectional area and the second moment of inertia of the plate.

4.6 Dispersion Analysis

To see how the model performs in comparison to classical and peridynamics, we will carry out dispersion analysis. Noting that we try to derive our dispersion equations without setting $z_i = 0$ in the EOMs i.e. the plate has thickness. Since our equations are written in discrete form, we are interested in using the discrete format of wave propagation for all

DOFs as follows:

$$
\begin{aligned}
&u_i = u(\mathbf{x}_i,t) = u_0 e^{\hat{i}(\kappa x_i - \omega t + \hat{n}_{iii}\kappa\xi_{ii})} = u_0 X_i \Lambda_{ii}, \quad v_i = v(\mathbf{x}_i,t) = v_0 e^{\hat{i}(\kappa x_i - \omega t + \hat{n}_{iii}\kappa\xi_{ii})} = v_0 X_i \Lambda_{ii} \\
&u_j = u(\mathbf{x}_j,t) = u_0 e^{\hat{i}(\kappa x_i - \omega t + \hat{n}_{iij}\kappa\xi_{ij})} = u_0 X_i \Lambda_{ij}, \quad v_j = u(\mathbf{x}_j,t) = v_0 e^{\hat{i}(\kappa x_i - \omega t + \hat{n}_{iij}\kappa\xi_{ij})} = v_0 X_i \Lambda_{ij} \\
&u_k = u(\mathbf{x}_k,t) = u_0 e^{\hat{i}(\kappa x_i - \omega t + \hat{n}_{iik}\kappa\xi_{ij})} = u_0 X_i \Lambda_{ij}, \quad v_k = u(\mathbf{x}_k,t) = v_0 e^{\hat{i}(\kappa x_i - \omega t + \hat{n}_{iik}\kappa\xi_{ik})} = v_0 X_i \Lambda_{ik}
\end{aligned}
$$

$$
\begin{aligned}
&\phi_i^x = \phi^x(\mathbf{x}_i,t) = \phi_0^x e^{\hat{i}(\kappa X_i - \omega t + \hat{n}_{iii}\kappa\xi_{ii})} = \phi_0^x X_i \Lambda_{ii}, \quad \phi_i^y = \phi^y(\mathbf{x}_i,t) = \phi_0^y e^{\hat{i}(\kappa X_i - \omega t + \hat{n}_{iii}\kappa\xi_{ii})} = \phi_0^y X_i \Lambda_{ii} \\
&\phi_j^x = \phi^x(\mathbf{x}_j,t) = \phi_0^x e^{\hat{i}(\kappa X_i - \omega t + \hat{n}_{iij}\kappa\xi_{ij})} = \phi_0^x X_i \Lambda_{ij}, \quad \phi_j^y = \phi^y(\mathbf{x}_j,t) = \phi_0^y e^{\hat{i}(\kappa X_i - \omega t + \hat{n}_{iij}\kappa\xi_{ij})} = \phi_0^y X_i \Lambda_{ij} \\
&\phi_k^x = \phi^x(\mathbf{x}_k,t) = \phi_0^x e^{\kappa(iX_i - \omega t + \hat{n}_{iik}\kappa\xi_{ik})} = \phi_0^x X_i \Lambda_{ik}, \quad \phi_k^y = \phi^y(\mathbf{x}_k,t) = \phi_0^y e^{\hat{i}(\kappa X_i - \omega t + \hat{n}_{iik}\kappa\xi_{ik})} = \phi_0^y X_i \Lambda_{ik}
\end{aligned}
$$

$$
\begin{aligned}
&w_i = w(\mathbf{x}_i,t) = w_0 e^{\hat{i}(\kappa x_i - \omega t + \hat{n}_{iii}\kappa\xi_{ii})} = w_0 X_i \Lambda_{ii} \\
&w_j = w(\mathbf{x}_j,t) = w_0 e^{\hat{i}(\kappa x_i - \omega t + \hat{n}_{iij}\kappa\xi_{ij})} = w_0 X_i \Lambda_{ij} \\
&w_k = w(\mathbf{x}_k,t) = w_0 e^{\hat{i}(\kappa x_i - \omega t + \hat{n}_{iik}\kappa\xi_{ik})} = w_0 X_i \Lambda_{ik}
\end{aligned}
\tag{4.64}
$$

where κ is the wave number and ω is the wave frequency. The axial coordinate of particles is shown by x_i and the variable t indicates time. u_0, v_0, w_0 and ϕ_0^x and ϕ_0^x are the amplitude of the waves in the x direction, y direction, z direction and rotation in x and y planes. Here $\hat{i}$ is showing the imaginary part ($\hat{i} = \sqrt{-1}$) . It should be noted that $X_i = e^{\hat{i}(\kappa x_i - \omega t)}$ is the wave equation associate to i^{th} particle. The phase difference of the particle i with particle j and k could be given by $\kappa\hat{n}_{iij}\xi_{ij}$ and $\kappa\hat{n}_{iik}\xi_{ik}$ respectively. Form the definition of $\Lambda_{i\alpha} = e^{i(\kappa\hat{n}_{ii\alpha}\xi_{i\alpha}t)}$ where $\alpha = i, j, k$, one can easily find that $\Lambda_{ii} = 1$ i.e, no phase difference with the ith particle. Substituting Eq. 4.64, in definition of stretch (Eq. 4.1) results into;

$$
\epsilon^{xx}_{\alpha\beta\gamma} = u_0 X_i \left(\frac{1}{\xi^x_{\alpha\beta}} \left(\Lambda_{i\beta} - \Lambda_{i\alpha} \right) + \frac{1}{\xi^x_{\alpha\gamma}} \left(\Lambda_{i\gamma} - \Lambda_{i\alpha} \right) \right) = u_0 X_i T^x_{\alpha\beta\gamma} \tag{4.65}
$$

$$
\epsilon^{yy}_{\alpha\beta\gamma} = v_0 X_i \left(\frac{1}{\xi^y_{\alpha\beta}} \left(\Lambda_{i\beta} - \Lambda_{i\alpha} \right) + \frac{1}{\xi^y_{\alpha\gamma}} \left(\Lambda_{i\gamma} - \Lambda_{i\alpha} \right) \right) = v_0 X_i T^y_{\alpha\beta\gamma} \tag{4.66}
$$

$$\begin{aligned}\epsilon^{xy}_{\alpha\beta\gamma} =& u_0 X_i \left(\frac{1}{\xi^y_{\alpha\beta}} \left(\Lambda_{i\beta} - \Lambda_{i\alpha}\right) + \frac{1}{\xi^y_{\alpha\gamma}} \left(\Lambda_{i\gamma} - \Lambda_{i\alpha}\right) \right) + v_0 X_i \left(\frac{1}{\xi^x_{\alpha\beta}} \left(\Lambda_{i\beta} - \Lambda_{i\alpha}\right) + \frac{1}{\xi^x_{\alpha\gamma}} \left(\Lambda_{i\gamma} - \Lambda_{i\alpha}\right) \right) \\ =& X_i \left(u_0 T^y_{\alpha\beta\gamma} + v_0 T^x_{\alpha\beta\gamma} \right)\end{aligned} \tag{4.67}$$

Noting that $T^e_{\alpha\beta\gamma} = \frac{1}{\xi^e_{\alpha\beta}} \left(\Lambda_{i\beta} - \Lambda_{i\alpha}\right) + \frac{1}{\xi^e_{\alpha\gamma}} \left(\Lambda_{i\gamma} - \Lambda_{i\alpha}\right)$ where e could be x or y. The set of equations could be rewritten in terms of particle i, j and k particle. For instance, we could have the following equations in x direction when α, β and γ are i, j and k respectively:

$$\begin{aligned}\epsilon^{xx}_{ijk} =& u_0 X_i \left(\frac{1}{\xi^x_{ij}} \left(\Lambda_{ij} - 1\right) + \frac{1}{\xi^x_{ik}} \left(\Lambda_{ik} - 1\right) \right) = u_0 X_i T^x_{ijk} \\ \epsilon^{xx}_{jki} =& u_0 X_i \left(\frac{1}{\xi^x_{jk}} \left(\Lambda_{ik} - \Lambda_{ij}\right) + \frac{1}{\xi^x_{ji}} \left(1 - \Lambda_{ij}\right) \right) = u_0 X_i T^x_{jki} \\ \epsilon^{xx}_{kij} =& u_0 X_i \left(\frac{1}{\xi^x_{ki}} \left(1 - \Lambda_{ik}\right) + \frac{1}{\xi^x_{kj}} \left(\Lambda_{ij} - \Lambda_{ik}\right) \right) = u_0 X_i T^x_{kij}\end{aligned} \tag{4.68}$$

Similarly, we can find it for $\kappa_{\alpha\beta\gamma}$ and $\psi_{\alpha\beta\gamma}$ by substituting ϕ and w in 4.64 and into their definitions (Eqs. 4.7 and 4.11) as:

$$\kappa^{xx}_{\alpha\beta\gamma} = \phi^x_0 X_i \left(\frac{1}{\xi^x_{\alpha\beta}} \left(\Lambda_{i\beta} - \Lambda_{i\alpha}\right) + \frac{1}{\xi^x_{\alpha\gamma}} \left(\Lambda_{i\gamma} - \Lambda_{i\alpha}\right) \right) = \phi^x_0 X_i J^x_{\alpha\beta\gamma} \tag{4.69}$$

$$\kappa^{yy}_{\alpha\beta\gamma} = \phi^x_0 X_i \left(\frac{1}{\xi^x_{\alpha\beta}} \left(\Lambda_{i\beta} - \Lambda_{i\alpha}\right) + \frac{1}{\xi^x_{\alpha\gamma}} \left(\Lambda_{i\gamma} - \Lambda_{i\alpha}\right) \right) = \phi^x_0 X_i J^y_{\alpha\beta\gamma} \tag{4.70}$$

$$\begin{aligned}\kappa^{xy}_{\alpha\beta\gamma} =& \phi^x_0 X_i \left(\frac{1}{\xi^y_{\alpha\beta}} \left(\Lambda_{i\beta} - \Lambda_{i\alpha}\right) + \frac{1}{\xi^y_{\alpha\gamma}} \left(\Lambda_{i\gamma} - \Lambda_{i\alpha}\right) \right) + \phi^y_0 X_i \left(\frac{1}{\xi^x_{\alpha\beta}} \left(\Lambda_{i\beta} - \Lambda_{i\alpha}\right) + \frac{1}{\xi^x_{\alpha\gamma}} \left(\Lambda_{i\gamma} - \Lambda_{i\alpha}\right) \right) \\ =& X_i \left(\phi^x_0 J^y_{\alpha\beta\gamma} + \phi^y_0 J^x_{\alpha\beta\gamma} \right)\end{aligned} \tag{4.71}$$

Noting that $J^e_{\alpha\beta\gamma} = \frac{1}{\xi^e_{\alpha\beta}}(\Lambda_{i\beta} - \Lambda_{i\alpha}) + \frac{1}{\xi^e_{\alpha\gamma}}(\Lambda_{i\gamma} - \Lambda_{i\alpha})$. For instance, we have the following for κ^{xx} for the indices i, j and k:

$$\begin{aligned}
\kappa^{xx}_{ijk} =& \phi^x_0 X_i \left(\frac{1}{\xi^x_{ij}}(\Lambda_{ij} - 1) + \frac{1}{\xi^x_{ik}}(\Lambda_{ik} - 1) \right) = \phi^x_0 X_i J^x_{ijk} \\
\kappa^{xx}_{jki} =& \phi^x_0 X_i \left(\frac{1}{\xi^x_{jk}}(\Lambda_{ik} - \Lambda_{ij}) + \frac{1}{\xi^x_{ji}}(1 - \Lambda_{ij}) \right) = \phi^x_0 X_i J^x_{jki} \\
\kappa^{xx}_{kij} =& \phi^x_0 X_i \left(\frac{1}{\xi^x_{ki}}(1 - \Lambda_{ik}) + \frac{1}{\xi^x_{kj}}(\Lambda_{ij} - \Lambda_{ik}) \right) = \phi^x_0 X_i J^x_{kij}
\end{aligned} \tag{4.72}$$

Also, we can get the following relations for $\psi^x_{\alpha\beta\gamma}$

$$\psi^x_{\alpha\beta\gamma} = w_0 X_i P^x_{\alpha\beta\gamma} + \phi^x_0 X_i Q^x_{\alpha\beta\gamma} \tag{4.73}$$

$$\psi^y_{\alpha\beta\gamma} = w_0 X_i P^y_{\alpha\beta\gamma} + \phi^y_0 X_i Q^y_{\alpha\beta\gamma} \tag{4.74}$$

where

$$\begin{aligned}
P^x_{\alpha\beta\gamma} &= \frac{1}{\xi^x_{\alpha\beta}}(\Lambda_{i\beta} - \Lambda_{i\alpha}) + \frac{1}{\xi^x_{\alpha\gamma}}(\Lambda_{i\gamma} - \Lambda_{i\alpha}) \\
Q^x_{\alpha\beta\gamma} &= -\frac{n^x_{\alpha\beta}}{2}(\Lambda_{i\alpha} + \Lambda_{i\beta}) - \frac{n^x_{\alpha\gamma}}{2}(\Lambda_{i\gamma} + \Lambda_{i\alpha})
\end{aligned} \tag{4.75}$$

$$\begin{aligned}
P^y_{\alpha\beta\gamma} &= \frac{1}{\xi^y_{\alpha\beta}}(\Lambda_{i\beta} - \Lambda_{i\alpha}) + \frac{1}{\xi^y_{\alpha\gamma}}(\Lambda_{i\gamma} - \Lambda_{i\alpha}) \\
Q^y_{\alpha\beta\gamma} &= -\frac{n^y_{\alpha\beta}}{2}(\Lambda_{i\alpha} + \Lambda_{i\beta}) - \frac{n^y_{\alpha\gamma}}{2}(\Lambda_{i\gamma} + \Lambda_{i\alpha})
\end{aligned} \tag{4.76}$$

For instance, $\psi^x_{ijk}, \psi^x_{jki}$ and ψ^x_{kij} can be given as:

$$\begin{aligned}
\psi^x_{ijk} =& w_0 X_i \left(\frac{1}{\xi^x_{ij}}(\Lambda_{ij} - 1) + \frac{1}{\xi^x_{ik}}(\Lambda_{ik} - 1) \right) + \phi^x_0 X_i \left(-\frac{\hat{n}^x_{iij}}{2}(1 + \Lambda_{ij}) - \frac{\hat{n}^x_{iik}}{2}(1 + \Lambda_{ik}) \right) \\
\psi^x_{jki} =& w_0 X_i \left(\frac{1}{\xi^x_{jk}}(\Lambda_{ik} - \Lambda_{ij}) + \frac{1}{\xi^x_{ji}}(1 - \Lambda_{ij}) \right) + \phi^x_0 X_i \left(-\frac{\hat{n}^x_{ijk}}{2}(\Lambda_{ij} + \Lambda_{ik}) - \frac{\hat{n}^x_{iji}}{2}(1 + \Lambda_{ij}) \right) \\
\psi^x_{kij} =& w_0 X_i \left(\frac{1}{\xi^x_{ki}}(1 - \Lambda_{ik}) + \frac{1}{\xi^x_{kj}}(\Lambda_{ij} - \Lambda_{ik}) \right) + \phi^x_0 X_i \left(-\frac{\hat{n}^x_{iki}}{2}(1 + \Lambda_{ik}) - \frac{\hat{n}^x_{ikj}}{2}(\Lambda_{ij} + \Lambda_{ik}) \right)
\end{aligned} \tag{4.77}$$

Substituting Eqs. 4.68, 4.72 and 4.77 in the EOMs 4.48,4.49 ,4.50, 4.51,4.52 gives:

$$
\begin{aligned}
&\left(\rho\omega^2 + K^{\epsilon_{xx}} A_1^{x,x} + 2\left({}^1K^{\epsilon_{xy}} A_1^{y,y}\right)\right) u_0 + \left({}^1K^{\epsilon_{xy}} + {}^2K^{\epsilon_{xy}}\right) A_1^{x,y} v_0 + \left(B_1\omega^2\right)\phi_0^x = 0 \\
&\left(\rho\omega^2 + K^{\epsilon_{yy}} A_1^{y,y} + 2\left({}^2K^{\epsilon_{xy}} A_1^{x,x}\right)\right) v_0 + \left({}^2K^{\epsilon_{xy}} + {}^1K^{\epsilon_{xy}}\right) A_2^{x,y} u_0 + \left(B_1\omega^2\right)\phi_0^y = 0 \\
&\left(\rho\omega^2 + K^{\psi_x} C_2^x + K^{\psi_y} C_2^y\right) w_0 + \left(K^{\psi_x} C_3^x\right)\phi_0^x + \left(K^{\psi_y} C_3^y\right)\phi_0^y = 0 \\
&\left(B_2\rho\omega^2\right) u_0 + \left(K^{\psi^x} C_2^x\right) w_0 + \left(\frac{\rho I}{A}\omega^2 + K^{\phi_{xx}} C_1^{x,x} + 2K C_1^{y,y} + K^{\psi^x} C_2^y\right)\phi_0^x \\
&+ \left[\left({}^1K^{\phi_{xy}} + {}^2K^{\phi_{xy}}\right) C_1^{x,y}\right]\phi_0^y = 0 \\
&\left(B_2\rho\omega^2\right) v_0 + \left(K^{\psi^y} C_2^y\right) w_0 + \left(\frac{\rho I}{A}\omega^2 + K^{\phi_{yy}} C_1^{y,y} + 2K C_1^{x,x} + K^{\psi^y} C_2^x\right)\phi_0^y \\
&+ \left[\left({}^1K^{\phi_{xy}} + {}^2K^{\phi_{xy}}\right) C_1^{y,x}\right]\phi_0^x = 0
\end{aligned}
\tag{4.78}
$$

where:

$$A_1^{x,x} = \frac{1}{3}\sum_{j=1}^{M}\sum_{k=1}^{M}\left[\left(\frac{1}{\xi_{ij}^x}+\frac{1}{\xi_{ik}^x}\right)T_{ijk}^x - \left(\frac{1}{\xi_{ij}^x}\right)T_{jki}^x - \left(\frac{1}{\xi_{ik}^x}\right)T_{kij}^x\right]V_kV_j$$

$$A_1^{y,y} = \frac{1}{3}\sum_{j=1}^{M}\sum_{k=1}^{M}\left[\left(\frac{1}{\xi_{ij}^y}+\frac{1}{\xi_{ik}^y}\right)T_{ijk}^y - \left(\frac{1}{\xi_{ij}^y}\right)T_{jki}^y - \left(\frac{1}{\xi_{ik}^y}\right)T_{kij}^y\right]V_kV_j$$

$$A_1^{x,y} = \frac{1}{3}\sum_{j=1}^{M}\sum_{k=1}^{M}\left[\left(\frac{1}{\xi_{ij}^y}+\frac{1}{\xi_{ik}^y}\right)T_{ijk}^x - \left(\frac{1}{\xi_{ij}^y}\right)T_{jki}^x - \left(\frac{1}{\xi_{ik}^y}\right)T_{kij}^x\right]V_kV_j$$

$$A_1^{y,x} = \frac{1}{3}\sum_{j=1}^{M}\sum_{k=1}^{M}\left[\left(\frac{1}{\xi_{ij}^x}+\frac{1}{\xi_{ik}^x}\right)T_{ijk}^y - \left(\frac{1}{\xi_{ij}^x}\right)T_{jki}^y - \left(\frac{1}{\xi_{ik}^x}\right)T_{kij}^y\right]V_kV_j$$

$$B_1 = B_2 = 2z$$

$$C_1^{x,x} = \frac{1}{3}\sum_{j=1}^{M}\sum_{k=1}^{M}\left[\left(\frac{1}{\xi_{ij}^x}+\frac{1}{\xi_{ik}^x}\right)J_{ijk}^x - \left(\frac{1}{\xi_{ij}^x}\right)J_{jki}^x - \left(\frac{1}{\xi_{ik}^x}\right)J_{kij}^x\right]V_kV_j$$

$$C_1^{y,y} = \frac{1}{3}\sum_{j=1}^{M}\sum_{k=1}^{M}\left[\left(\frac{1}{\xi_{ij}^y}+\frac{1}{\xi_{ik}^y}\right)J_{ijk}^y - \left(\frac{1}{\xi_{ij}^y}\right)J_{jki}^y - \left(\frac{1}{\xi_{ik}^y}\right)J_{kij}^y\right]V_kV_j \tag{4.79}$$

$$C_1^{x,y} = \frac{1}{3}\sum_{j=1}^{M}\sum_{k=1}^{M}\left[\left(\frac{1}{\xi_{ij}^y}+\frac{1}{\xi_{ik}^y}\right)J_{ijk}^x - \left(\frac{1}{\xi_{ij}^y}\right)J_{jki}^x - \left(\frac{1}{\xi_{ik}^y}\right)J_{kij}^x\right]V_kV_j$$

$$C_1^{y,x} = \frac{1}{3}\sum_{j=1}^{M}\sum_{k=1}^{M}\left[\left(\frac{1}{\xi_{ij}^x}+\frac{1}{\xi_{ik}^x}\right)J_{ijk}^y - \left(\frac{1}{\xi_{ij}^x}\right)J_{jki}^y - \left(\frac{1}{\xi_{ik}^x}\right)J_{kij}^y\right]V_kV_j$$

$$C_2^x = \frac{1}{6}\sum_{j=1}^{M}\sum_{k=1}^{M}\left[\left(\hat{n}_{iij}^{\ x}+\hat{n}_{iik}^{\ x}\right)P_{ijk}^x - \left(\hat{n}_{iij}^{\ x}\right)P_{jki}^x - \left(\hat{n}_{iik}^{\ x}\right)P_{kij}^x\right]V_kV_j$$

$$C_2^y = \frac{1}{6}\sum_{j=1}^{M}\sum_{k=1}^{M}\left[\left(\hat{n}_{iij}^{\ y}+\hat{n}_{iik}^{\ y}\right)P_{ijk}^y - \left(\hat{n}_{iij}^{\ y}\right)P_{jki}^y - \left(\hat{n}_{iik}^{\ y}\right)P_{kij}^y\right]V_kV_j$$

$$C_3^x = \frac{1}{6}\sum_{j=1}^{M}\sum_{k=1}^{M}\left[\left(\hat{n}_{iij}^{\ x}+\hat{n}_{iik}^{\ x}\right)Q_{ijk}^x - \left(\hat{n}_{iij}^{\ x}\right)Q_{jki}^x - \left(\hat{n}_{iik}^{\ x}\right)Q_{kij}^x\right]V_kV_j$$

$$C_3^y = \frac{1}{6}\sum_{j=1}^{M}\sum_{k=1}^{M}\left[\left(\hat{n}_{iij}^{\ y}+\hat{n}_{iik}^{\ y}\right)Q_{ijk}^y - \left(\hat{n}_{iij}^{\ y}\right)Q_{jki}^y - \left(\hat{n}_{iik}^{\ y}\right)Q_{kij}^y\right]V_kV_j$$

4.7 Conclusion

In this section, we provide the tridynamic model of FSDT plate using the a meaningful kinematic of the element. The governing equation were derived by constructing the Lagrangian of the system and the nonlocal parameters are determined. We also provided the polynomial equation for dispersion analysis.

5. A DERIVATIVE-FREE UPSCALED THEORY FOR ANALYSIS OF DEFECTS [1]

5.1 Introduction

With their striking mechanical properties [44, 45, 46, 47], carbon nanotubes (CNTs) find myriad applications – from nano-engineering to large-scale engineering materials, where they appear as impregnates [48, 49, 50, 51, 52, 53, 54]. Recently, employing advanced nano-technology in communication circuits leads to high-performance designs for 5G and satellite applications [55, 55, 56]. Akbarzadeh et al. [57] studied the effect of nano-step size topography on flow transport behavior, e.g., surface wetting, was studied. They showed that nano-scale steps have significant effect on flow characterestics such as shear stress on the surface. Optimal manufacturing [58, 59, 60, 61] and utilization of CNTs in an application demands better predictive models to determine their mechanical properties. Experiments have thus been supplemented with numerous computational studies, mostly through molecular dynamic simulations[62]. With manifold increase in the usage of CNT especially for macroscopic systems, an accurate macroscopic predictive model is indeed a state-of-the-art necessity. It is obvious that MD simulation being computationally intensive, may not always be of much use in this context.

Since material properties of CNTs may vary significantly with their changing chirality, the macroscopic law that underlies such a model must preserve the essential molecular information such as chirality. Of some relevance are the efforts by Arroyo and Belytschko [63], Guo *et al* [64], Yang and Weinan [65] who have developed higher order Cauchy–Born rules to arrive at useful continuum laws by upscaling from the molecular potential. Note that the classical Cauchy–Born rule (CBR), suitable for bulk materials, does not capture the out-of-plane deformation of the CNT, constructed by wrapping a single-layer graphene sheet. This has required the development of higher-order variants of the CBR [66, 64]. Elegant

[1] Reprinted with permission from, "A derivative-free upscaled theory for analysis of defects.", by Mohsen, Saikat Sarkar, J. N. Reddy, and Debasish Roy, 2019, *Journal of the Mechanics and Physics of Solids* 122, 489-501. Copyright 2019 by Elsivier.

and useful as these approaches are, the localized continuum laws are in the form of partial differential equations (PDEs), thus imposing strict smoothness restrictions on the field variables. The inevitable upshot is that the upscaled laws struggle to model a defective CNT experiencing crack growth and material failure via fragmentation. Indeed, there appears to be a conceptual gap – a rock-cleft region in need of attention. Saikat et al [33] proposed a direct Lagrangian based approach, designed at a length scale of interest, to characterize the response of a body within a framework which relaxes the requirement of differentiability of field variables

We set ourselves to addressing this question based on a stochastic projection principle that enables the macroscopic law to preserve certain microscopic information. On the basis of the upscaled information, presently employed as a discrete Cauchy–Born rule (DCBR), we derive, from the molecular potential, the evolution laws at a higher length scale of interest. Specifically, while MD simulations take into account the detailed motion of each atom in a lattice, we aim to characterize the collective behavior of atoms at a higher length scale. Using the upscaled law, we present a macroscopic study of the CNT, which may experience multiple cracks, crack branching and subsequent fragmentation.

5.2 The Stochastic Projection Principle

While coarse-grained variables typically evolve with slowly varying time scales, the corresponding microscopic phenomena occur over faster scales and hence wider range of frequencies. Accordingly, for an observer at coarser (macroscopic) spatio-temporal scales, certain fluctuations in the microscopic quantities of relevance remain unaccounted so they may be treated as stochastic processes. With this worldview, a microscopic displacement vector could, for instance, be represented as a zero mean Gaussian random variable at a coarser scale. This calls for suitable conditioning of the macroscopically evolving states, meaningful in classical continuum mechanics, on such representations of any non-trivial microscopic information. We expect such conditioning to retain some aspects of the microscopic information even when the unaccounted fluctuations have zero mean.

To begin with, consider the fundamental problem of characterizing a macroscopic field variable $\mathbf{u}(\mathbf{x})$ by exploiting its neighborhood information. Prior to conditioning based on any microscopically inspired information, we may not have a guidance on imposing a specific structure on the field. Thus we may simply add a zero-mean noise term, $\Delta\boldsymbol{\eta}$ to $\mathbf{u}(\mathbf{x})$ in order to obtain $\mathbf{u}(\mathbf{y})$, $\mathbf{y} \neq \mathbf{x}$, i.e.

$$\mathbf{u}(\mathbf{y}) = \mathbf{u}(\mathbf{x}) + \Delta\boldsymbol{\eta} \tag{5.1}$$

In a differential setting parameterized in time t, Eq. (5.1) has an equivalent form,

$$d(\mathbf{u}(\mathbf{y}_t) - \mathbf{u}(\mathbf{x}_t)) = d\boldsymbol{\eta}_t \tag{5.2}$$

The method of conditioning via representative microscopic information must act as a micro-to-macro bridge whilst preferably encapsulating within it the notion of a representative volume element (RVE). The constraining information from the micro-scale, sampled at a time instant t, may be written in the following form:

$$d\mathbf{Y}_t = \mathbf{h}(\mathbf{x}_t, \mathbf{y}_t)\, dt + \boldsymbol{\sigma} d\mathbf{W}_t \tag{5.3}$$

$\mathbf{h}(\cdot,\cdot)$ is a vector-valued function that returns, say, the undeformed, unsigned distance components between two (macroscopic) points. Since the value of $\mathbf{h}(\cdot,\cdot)$ is only macroscopically resolvable, we assume that the function returns zero whenever acting on $\mathbf{x}_t, \mathbf{y}_t$ such that $|\mathbf{x}_t - \mathbf{y}_t| \leq |\Delta|$; Δ may denote the vector of atomic bonds at a lattice point, thus describing an aspect of the material microstructure. $\mathbf{Y}_t$ is then the noisy function value detected by a macroscopic observer, where the source of the noise term $\boldsymbol{\sigma} d\mathbf{W}_t$ is traced to the surjective push-forward mapping of $\mathbf{x} - \mathbf{y}$ in terms its microscopic counterpart and the macroscopically time-sampled $\mathbf{Y}_t$. In this setting, the size of the RVE is given by $|\Delta|$ and $\boldsymbol{\sigma}$ is related, via a fluctuation relation, to kinetic-vibrational temperature. In order to introduce microscop-

ically informed spatial variation in the field $\mathbf{u}$, we describe it in terms of its conditional expectation $\pi_t(\mathbf{u}) = E_P[\mathbf{u}(\mathbf{x})|\mathcal{F}_t]$, where $\mathcal{F}_t$ is an increasing sequence of sigma algebras constructed using $\mathbf{Y}_t$ up to time t. The setting as above resembles that of the well known problem of stochastic filtering, provided we define all the processes measurable within a probability space $(\Omega, \mathcal{F}, P)$ and adapted to the increasing filtration $\mathcal{F}_t$, with $\boldsymbol{W}_t$ being a vector Brownian motion independent of $\boldsymbol{\eta}_t$. Note that the current macroscopic time t is only resolvable up to a microscopic time interval $\delta\hat{t}$, and hence the integration pending in equations (5.2) and (5.3) must be performed at least over this interval.

Since we intend to characterize $\mathbf{u}(\mathbf{x})$ through the distribution $\pi_t(\mathbf{u}) = E_P[\mathbf{u}(\mathbf{x})|\mathcal{F}_t]$, our immediate goal is to obtain an expression for the latter. For this, we exploit the Kallianpur–Striebel formula [67], a generalized Bayes' rule which we exploit in describing the conditional distribution under a different probability measure Q, which is absolutely continuous with respect to P and under which the process $\mathbf{Y}(t)$ behaves as a drift-removed Brownian motion. The formula states that, for a twice continuously differentiable function ϕ, we may express the conditional distribution as

$$\pi_t(\phi) = \frac{\sigma(\phi)}{\sigma(1)} := \frac{E_Q[\phi_t \Lambda_t | \mathcal{F}_t]}{E_Q[1\Lambda_t | \mathcal{F}_t]} \tag{5.4}$$

where

$$\Lambda_t = \frac{dP}{dQ} = \exp\left(\sum_i \left(\int_0^t \mathbf{h}^i(\mathbf{x}_s)\, d\mathbf{Y}_s^i - \int_0^t \mathbf{h}^i(\mathbf{x}_s)^2\, ds\right)\right)$$

is a Radon–Nikodym derivative [68] pertaining to the change of measures[69]; Λ_t may be shown to evolve according to the following stochastic differential equation (SDE):

$$d\Lambda_t = \Lambda_t \mathbf{h}_t^T d\mathbf{Y}_t \tag{5.5}$$

Based on this formalism, we may arrive at the following evolution equation for the normalized

conditional law $\pi_t(\phi)$ [70, 71].

$$d\pi_t(\phi) = \left(\pi_t\left(\phi\mathbf{h}^T\right) - \pi_t(\mathbf{h})^T \pi_t(\phi)\right)\left(\boldsymbol{\sigma}\boldsymbol{\sigma}^T\right)^{-1}(d\mathbf{Y}_t - \pi_t(\mathbf{h})\,dt) \tag{5.6}$$

We refer to the Appendix B for a derivation. When $\phi(\cdot) = Id(\cdot)$, Eq. (5.6) may be rewritten as:

$$d\pi_t(\mathbf{y}-\mathbf{x}) = \left(\pi_t\left((\mathbf{y}-\mathbf{x})\,\mathbf{h}^T\right) - \pi_t(\mathbf{h})^T \pi_t(\mathbf{y}-\mathbf{x})\right).\left(\boldsymbol{\sigma}\boldsymbol{\sigma}^T\right)^{-1}(d\mathbf{Y}_t - \pi_t(\mathbf{h})\,dt) \tag{5.7}$$

On the right hand side of the equation above, the coefficient matrix multiplying the incremental observation error (innovation) term $d\mathbf{Y}_t - \pi_t(\mathbf{h})dt$ is called the gain matrix.

We denote by t_0 the initial time when no force is applied on the body so it is undeformed. Since, by our postulate, the macroscopic observer cannot resolve, beyond a zero-mean Gaussian random variable, a vector whose length is smaller than that of $|\Delta|$ – the microscopic bond vector, Eq. (5.7) assumes the following form in the specific case of $\mathbf{y}_{t_0} - \mathbf{x}_{t_0} = \Delta$:

$$(\mathbf{y}_t - \mathbf{x}_t) = (\mathbf{y}_{t_0} - \mathbf{x}_{t_0}) + \int_{\hat{t}_0}^{\hat{t}} \left(\pi_s\left((\mathbf{y}-\mathbf{x})\,\mathbf{h}^T\right) - \pi_s(\mathbf{h})^T \pi_t(\mathbf{y}-\mathbf{x})\right)\left(\boldsymbol{\sigma}\boldsymbol{\sigma}^T\right)^{-1}(d\mathbf{Y}_t - 0) \tag{5.8}$$

Here the assignment $\mathbf{h}(\mathbf{x},\mathbf{y}) = \mathbf{0}$ for $|\mathbf{x}-\mathbf{y}| \leq |\Delta|$ has been used. In order to ensure that solutions to the SDEs involved exist, we choose the function $\mathbf{h}$ smooth whilst requiring that $\mathbf{h}(\mathbf{x},\mathbf{y}) = \mathbf{0}$ for $|\mathbf{y}-\mathbf{x}| \leq |\Delta|$ and that $\mathbf{h}(\mathbf{x},\mathbf{y})$ is non-zero otherwise. The same function is then used to empirically compute the gain matrix by macroscopically averaging over many points. In writing Eq. (5.8) we have adopted the specific observation $\mathbf{Y}_t = \mathbf{Y}_{t'} + \int_{\delta\hat{t}} \Delta d\hat{s}$, where t' is the just preceding macroscopic time at which it is possible to sample our observation.

Following the form of Eq. (5.3), we construct an empirical approximation to the macroscopic observation variance as $\boldsymbol{\sigma}\boldsymbol{\sigma}^T = \pi_t\left(\mathbf{h}\mathbf{h}^T\right)\delta\hat{t}$. Moreover, since the integration is carried

out within the least macroscopically resolvable time interval $\delta\hat{t}$, macroscopic temporal variations in the integrand are unresolvable and hence driftless. Accordingly, we arrive at the following simplified approximation.

$$(\mathbf{y}_t - \mathbf{x}_t) \approx \Delta + \mathbf{G}\Delta \tag{5.9}$$

where

$$\mathbf{G} = \left(\pi_t\left((\mathbf{y}-\mathbf{x})\,\mathbf{h}^T\right) - \pi_t\left(\mathbf{y}-\mathbf{x}\right)\pi_t\left(\mathbf{h}\right)^T\right)\left(\mathrm{Var}\left(\mathbf{h}\right)\right)^{-1}$$

. The gain matrix $\mathbf{G}$ may also be interpreted as a nonlocal counterpart to the deformation gradient that governs the motion of a continuum body under external forcing[34]. Clearly, $\mathbf{G}$ is a nonlocal term as it uses information from a non-infinitesimal neighborhood in its construction and yet provides directional information to propagate a line element in the body as it deforms. Alternatively, by way of an analogy with non-Euclidean differential geometry, it may be considered equivalent to the connection used to transport vectors in the material manifold. Moreover, exploiting its algebraic structure, the formula in (5.9) may also be interpreted as a generalized CBR depending on the application. Since $\mathbf{G}$ does not involve any derivatives, it admits ready computation even when there are discontinuities in the field variable. In line with the stochastic setting, the integrals appearing in $\mathbf{G}$ may be numerically evaluated through a Monte Carlo approach.

Of interest is the observation that the directionality term indeed approaches Newton's gradient term in the infinitesimal limit. This is readily varifiable via a Taylor's expansion of the neighboring deformed coordinates around the point of interest. A discussion on this is included in Appendix A. Note that the probabilistically founded and measure-theoretically consistent notion of various strain measures emerging out of this work provides for a basis to quantify the modified metric, which in turn is helpful in understanding various non-classical features of wave propagation through inherently heterogenous (and possibly discontinuous) solids. The gain matrix, which is crucial to our theory, also indicates a novel route to parallel

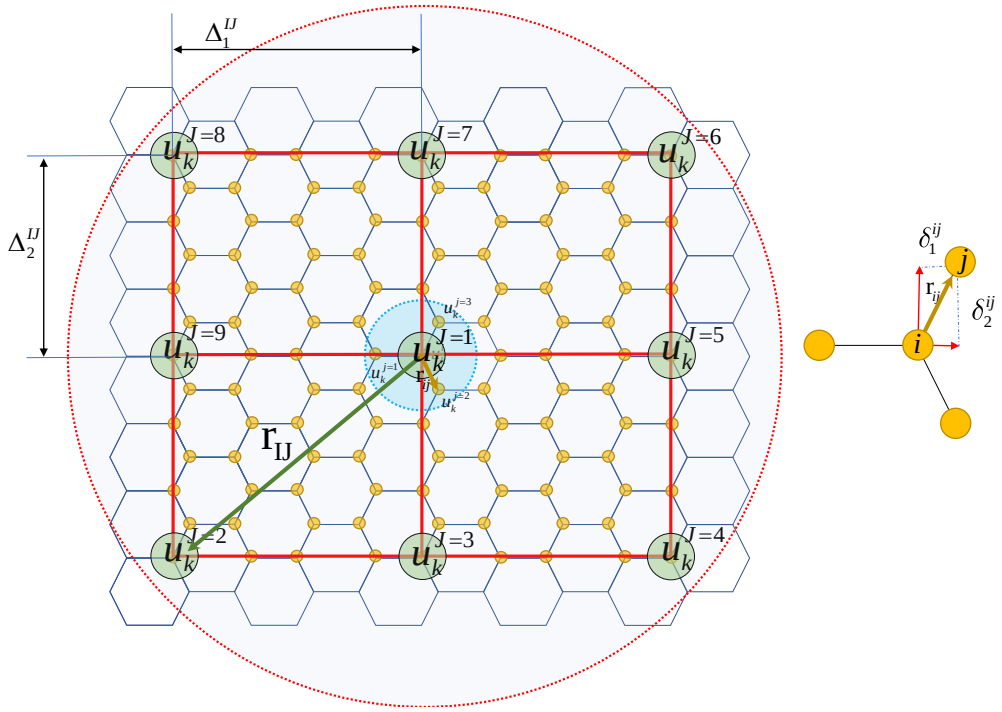

Figure 5.1: Molecular and coarse-grained computational lattices

transport of vectors, i.e. it corresponds to the notion of a connection (and hence non-locality through higher order derivatives of strain) in non-Euclidean differential geometry. However, unlike the differential geometric standpoint, the present approach is derivative-free and guided through a probabilistic (i.e. measure-theoretic) notion of uncertainty that arises in the specification of the microstructure at a higher scale. One could exploit the structure of noise that is inherent in this formulation to suitably define 'temperature' and thus weave into the theory an appropriate thermodynamic framework. None of these possibilities, which are yet to be explored, arise in an MD setting.

A separate study should ideally be carried out involving an increasing number of non-nearest neighbours in the calculations for the derivative-free directionality term, $\mathbf{G}$. As the molecular potential is approximated using $\mathbf{G}$, the upscaled potential is rendered strongly coupled involving far-off interactions in addition to the neighboring interactions among the

macroscopic particles. For a reduction of the computational cost, we may ignore the very far-off interaction using an influence function with finite radius. Moreover, depending on the level of upscaling, finer and finer discretizations (computational lattices) could be employed with a resolution up to the actual lattice level. Such details are however left for a future study oriented mostly along such numerical lines.

5.3 Numerical Experiments

5.3.1 Upscaled Simulation of an SWCNT

We now show the deformation profile of an SWCNT using the proposed formalism at a larger scale. Recall that the usual CBR fails to capture such phenomena properly [72] and, to this end, we need higher order versions of CBR. However, all these methods are derivative based and may not be useful as fracture emerges in the body. Our simulation of the deformation of a fractured SWCNT using a macroscopic law is a first-of-its-kind, to the best of our knowledge. While, for bulk crystals, the link between atomistic and continuum models is given by the well-known CBR, our primary focus is to provide a systematic generalization of the CBR to a low-dimensional surface. Using the proposed principle, we continualize the Tersoff–Brenner's potential [73] and write the macroscopic law for an SWCNT. The Tersoff–Brenner potential is written as:

$$V(\mathbf{r}_{ij}) = V_R(\mathbf{r}_{ij}) - B_{ij}V_A(\mathbf{r}_{ij}) \tag{5.10}$$

where B_{ij} is an empirical function, which represents multi-body coupling from bond i to bond j:

$$V_R\left(\mathbf{r}_{ij}\right) = f\left(\mathbf{r}_{ij}\right)\frac{D_e}{S-1}e^{-\sqrt{2s}\beta(\mathbf{r}_{ij}-\mathbf{r}_e)} \tag{5.11}$$

$$V_A\left(\mathbf{r}_{ij}\right) = f\left(\mathbf{r}_{ij}\right)\frac{D_eS}{S-1}e^{-\sqrt{2/s}\beta(\mathbf{r}_{ij}-r_e)} \tag{5.12}$$

The terms V_R and V_A are repulsive and attractive potential pairs, and $f\left(\mathbf{r}_{ij}\right)$ is a cutoff function. Using the proposed projection map, the upscalled representation, $\mathbf{r}_{IJ}$ of $\mathbf{r}_{ij}$ is

given below.

$$\mathbf{r}_{IJ} = \delta_1^{ij}\left(1 + G_1^{IJ}\right)\mathbf{e}_1 + \delta_2^{ij}\left(1 + G_2^{IJ}\right)\mathbf{e}_2 + \delta_3^{ij}\left(1 + G_3^{IJ}\right)\mathbf{e}_3 \tag{5.13}$$

The lower and upper case subscripts denote quantities computed at the atomistic and macroscopic (or coarser) scales respectively. $\delta^{ij} := \{\delta_1^{ij}, \delta_2^{ij}, \delta_3^{ij}\}^T$ is the microscopic lattice vector, Δ and $\{\mathbf{e}_1, \mathbf{e}_2, \mathbf{e}_3\}$ the canonical basis. G_1^{IJ}, G_2^{IJ}, G_3^{IJ} are the components deducible from $\mathbf{G}$ in a straightforward manner.

Therefore, the upscaled form of the total potential energy (integrated over the continuum domain Ω) may be written in the following form:

$$\mathscr{V} = \int_\Omega \int_\Omega \phi\left(\hat{r}_{IJ}\right)\left(V_R\left(\mathbf{r}_{IJ}\right) - B_{IJ}V_A\left(\mathbf{r}_{IJ}\right)\right) d\Omega_I d\Omega_J \tag{5.14}$$

where ϕ is the influence function that assumes the value 1 within the radius of influence domain $\hat{r}_{IJ}$ and zero outside of it. This influence function is introduced to discard interactions from very far off particles that may not contribute significantly. Note that while the lattice parameter Δ corresponds to microstructure length scale information, the upscaled (i.e. macroscopic) length scale is characterized by the radius of the influence domain ($\hat{r}_{IJ}$). Upon a discretization of the interaction terms, we can write the potential energy term as:

$$\mathscr{V} = \sum_{I=1}^{N}\sum_{J=1}^{M} \phi\left(\hat{r}_{IJ}\right)\left(V_R\left(\mathbf{r}_{IJ}\right) - B_{IJ}V_A\left(\mathbf{r}_{IJ}\right)\right) V_I V_J \tag{5.15}$$

Here N is the total number of macroscopic particles and M the number of neighbouring particles interacting with the I^{th} particle; M is not necessarily a constant. V_I is the volume assigned to particle I. We presently demonstrate the tension simulation of two giant SWCNT-s with two different chiralities (50,50) and (30,60). A region with axial length of 50 Å is defined at the ends of each CNT to apply the boundary conditions. To simulate the tensile test, the CNTs are stretched from both ends at a constant velocity of 1 Å/ps.

In all of our configurations, a 4-atom vacancy defect at $(L/2, R, 0)$ is created, where L and R are the length and radius of the tube. To remove dependency of the simulated results on the geometrical parameters such as radius, length of the SWCNT and radius of vacancy, nanotubes of same length have been considered. The defect is also kept the same in all the cases. Deformation profiles of the nanotubes are shown in Figs. 5.2,5.3,5.4 and5.5. To see the influence of chirality on crack growth in CNTs, a series of chiral vectors have been examined in the simulation, of which only a few are reported here. We validate the results from the proposed discrete Cauchy-Born rule (DCBR) via molecular dynamics simulations with LAMMPS. The molecular interactions are characterized using the Tersoff potential Eq. (5.10). A small enough time step (0.001 ps) is selected for numerical time integration so as to ensure quasi-static loading conditions. The damage index of one means that a particle has lost all its links, whereas the index of zero indicates a particle that has all its links intact. This parameter is given as:

$$\mu = 1 - \frac{R}{T} \tag{5.16}$$

where R is the number of remaining bonds and T the total number of bonds before the loading is applied. The color bars in Figures 5.2, 5.3, 5.4 and 5.5 show the extent of damage to a particle. The black tubes correspond to simulations from LAMMPS and the blue tubes are the results via DCBR. Due to stress concentration at the location of vacancies, the crack starts growing in the middle of the tubes. The fracture of the armchair SWCNT (50,50) starts at a measured strain of 5%, whereas 4% strain is recorded for the tube with the chiral vector (30,60). The brittle crack patterns from DCBR simulations in Figs. 5.2, 5.3, 5.4 and 5.5 (blue tubes) agree satisfactorily with the MD simulations (black tubes). A uniformly rectangular arrangement of coarse-grained particles are considered for simulation, even as the original molecular arrangement is hexagonal. The proposed scheme recovers MD results with a reduced number of particles. Indeed, the number of coarse-grained particles may readily be drastically reduced away from the crack zone. An elaborate demonstration addressing the precise reduction in the computing costs and related numerical issues will be communicated

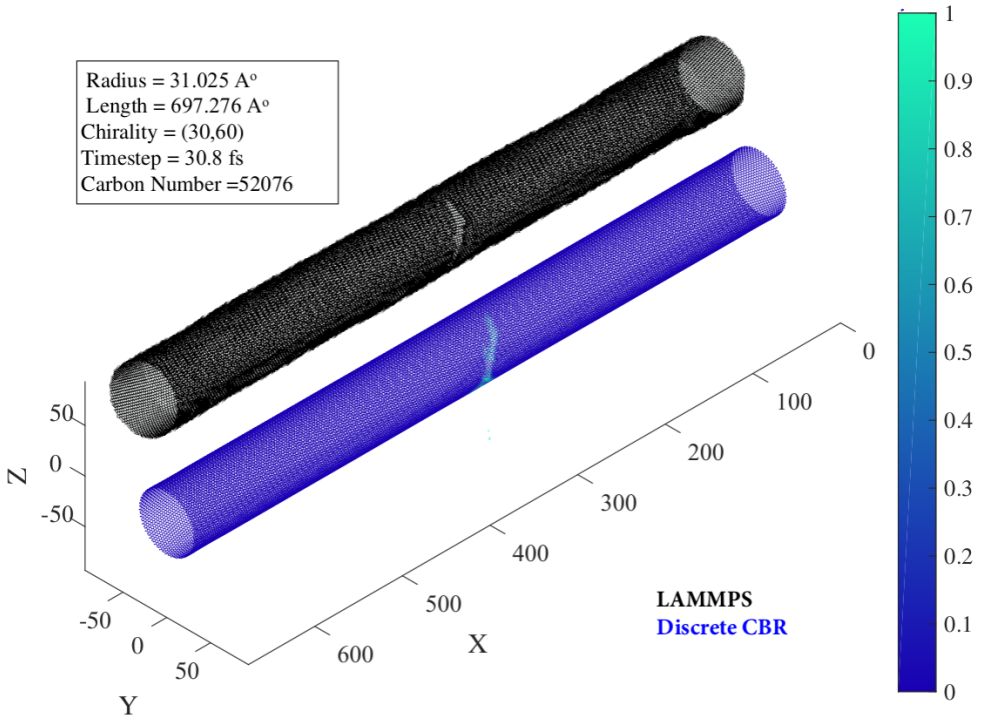

Figure 5.2: Crack propagation in tension test of SWCNT with chiral vector of (30,60)

separately.

Figures 5.6 and 5.7 show the developed stresses for uniaxial tensile tests of SWCNTs (30,60) and (50,50) computed through DCBR and LAMMPS. The DCBR results show tensile strengths of 58.75 GPA and 70.124 GPA respectively for CNTs (30,60) and (50,50) which are in agreement with the recorded numbers from LAMMPS simulation, namely 61.67 GPA and 72.07 GPA respectively.

Irrespective of how efficient the present-day computing systems are, MD simulations will remain limited by the very small size of the system in the foreseeable future and the importance of suitably upscaled continuum field models can hardly be over-emphasized for purposes of computational feasibility in the macroscale. Field theories are also very insightful in that the notions of metric, strain, connection etc. give a transparent geometrical meaning, along with a wave propagation-based perspective, to the evolving response of solids.

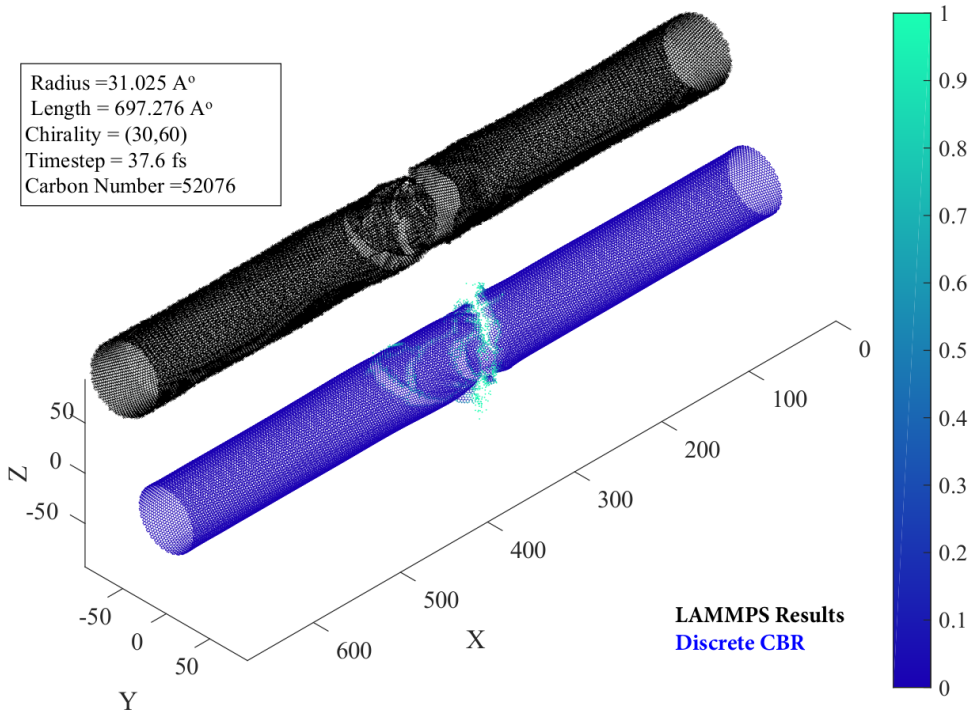

Figure 5.3: Crack propagation in tension test of SWCNT with chiral vector of (30,60)

Our present work has indeed been so motivated and we have, in the process, reported a microstructure-sensitive and probabilistically founded continuum principle – a first of its kind – that has presently been shown to faithfully simulate fracture in agreement with MD simulations. In the specific context of the examples presented in this work, the proposed continuum principle relaxes the requirement of working with the original hexagonal lattice, thus offering a scope for a drastic reduction in computation, especially by considering fewer particles away from the crack zone. The numerical procedure for accomplishing such a task may be readily borrowed from the quasi-continuum theory. While extensions of the basic idea in terms of interpretations, better implementation and myriad applications are possible, our current goal has solely been to set up a barebones mathematical framework for the basic idea itself. For the record, a brief comparative statement with the quasi-continuum (QC) method [74, 75, 76] will be in order. With a view to reducing the problem dimension away

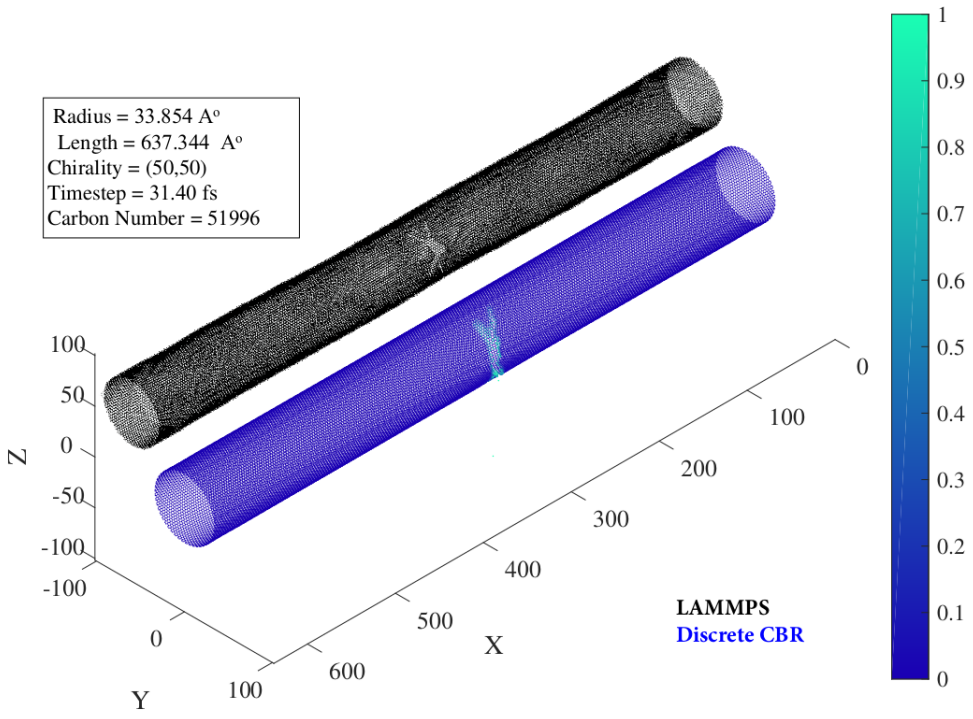

Figure 5.4: Crack propagation in tension test of SWCNT with chiral vector of (50,50)

from the so called critical zone (e.g. a dislocation site), the QC undertakes conventional minimization of the atomistic potential and enforces continualization of a discrete atomic structure through deterministic interpolation of the atomic displacement vector. Unlike the QC, our projection principle naturally obtains the directionality information strictly consistent with the discrete atomic configuration, successfully works even with a coarse graining of the critical zones and brings in the notion of temperature through the noise intensity terms.

5.3.2 Upscaled Simulation of a Bundle of SWCNT

In this section, in order to highlight the capability of the new discrete upscaling technique in the reduction of computational costs, we simulate the tensile test of two bundles of SWCNTs with different chirality. (see Figure. 5.8 and 5.9). The bundles consist of seven tubes of which the central tube is modeled in the actual molecular level, and it is surrounded by six SWCNTs (blue tubes). The blue tubes are the upscaled model of the red tubes on a

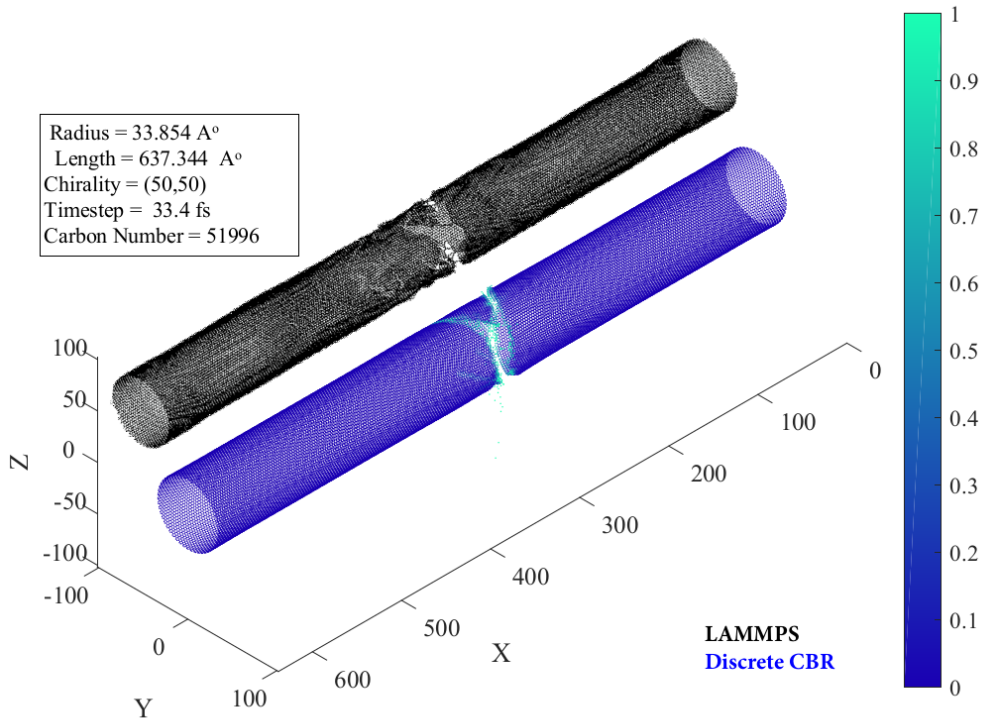

Figure 5.5: Crack propagation in tension test of SWCNT with chiral vector of (50,50)

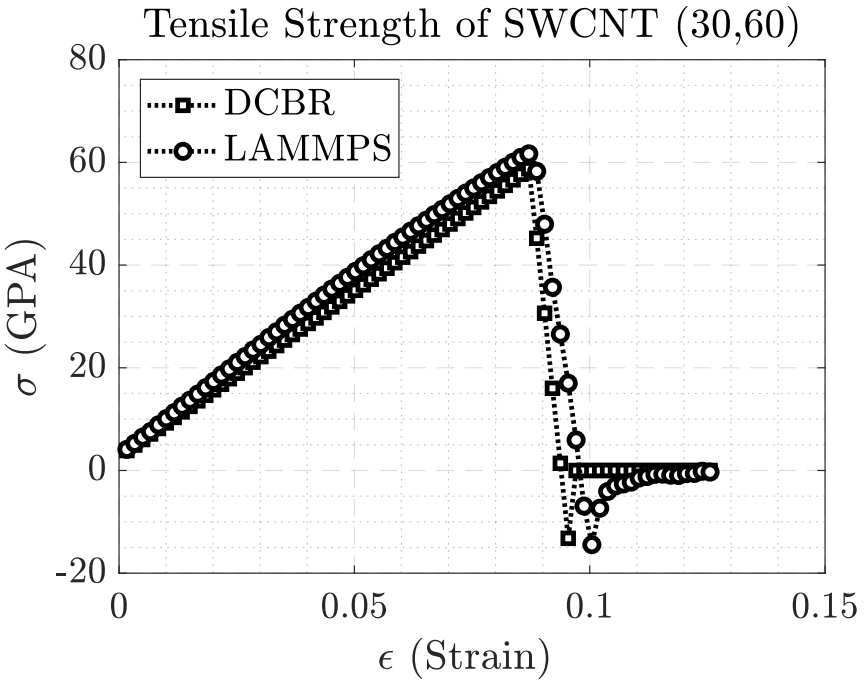

Figure 5.6: Variation of axial stress of SWCNT with the chiral vector of (30,60)

coarser mesh with a twice larger lattice distance. The center line of the surrounding tubes lies on the vertices of a hexagon with side length of $2.2R$ where R is the radius of the central tube. The central tube (red) of bundles with chiral vectors of (7,13) and (10,10) is made of 2472 and 2400 carbon atoms respectively. The red tube (in both cases) has 4 atoms vacancy defect at $(L/2, R, 0)$. The (7,13) and (10,10) tubes have lengths of 149.64 Åand 146.34 $\mathring{A}$ respectively. Accordingly, the number of particles of (7,13) and (10,10) upscaled tubes are 608 and 600. The LAMMPS simulations for both cases were carried out, and the results are shown in Figures 5.8 and 5.9. In the case of the bundle with chiral vector (7,13), the number of degree of freedoms decreased by 65 % in comparison to LAMMPS simulation. This reduction is computed as 63% for the bundle with the chiral vector of (10,10). With a closer look at the changes in each tube of the bundle during tensile loading, we observe that the failure initially starts from the central tube, with subsequent failure of the lateral

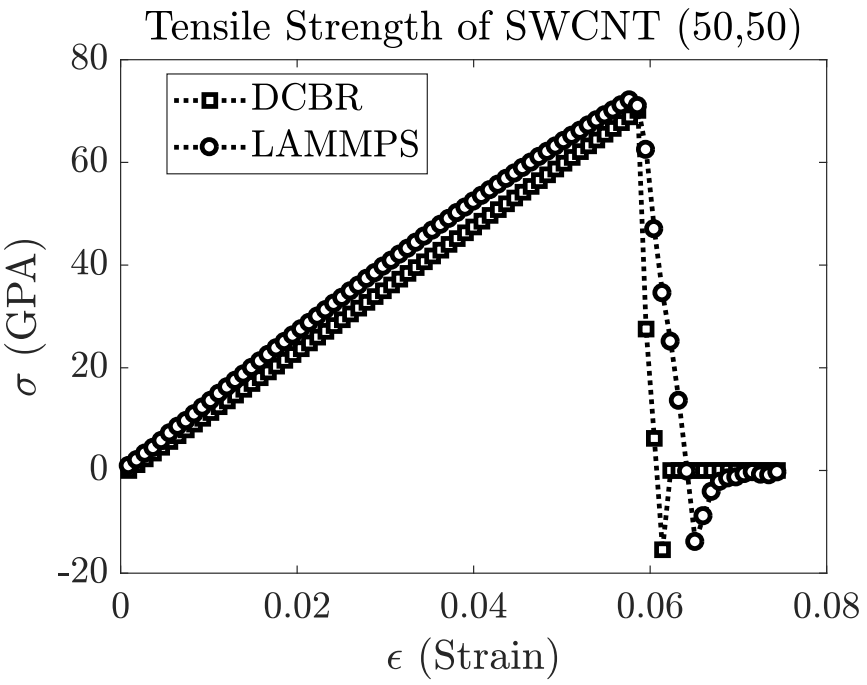

Figure 5.7: Variation of axial stress of SWCNT with the chiral vector of (50,50)

tubes. Figures 5.10 and 5.11 show the stress-strain profile of the bundle of SWCNT with chiral vectors of (7,13) and (10,10) for two different simulations. The results of DCBR are compared with LAMMPS simulations which should provide a decent prediction of 7-tube bundle behavior undergoing a tensile test. The DCBR simulation shows that the (7,13) and (10,10) bundles reach the maximum strengths of 51.92 GPa and 58.02 GPa. However, the LAMMPS simulation predicts 58.93 Gpa and 62.44 GPa for the (7,13) and (10,10) bundles respectively. As the central tube starts failing, the stress decreases slightly and then fluctuates around a value lower than the maximum strength. At this point, the lateral tubes carry the major part of the tensile load. Eventually, the surrounding tubes begin fracturing which is followed by a rapid decrease in the bundle strength.

In this study, a new nonlocal derivative-free framework based on the discrete Cauchy-Born rule was formulated. The new approach granted a systematic procedure to generate all

nonlocal version of classical continuum definitions such as deformation gradient, strain, and stresses from the local counterparts. For such a purpose, a compact matrix was constructed to transform surface-based forces to body-based ones. The new integral form of equation enables us to investigate mechanical problems having a discontinuity in the field variables. Instead of using conventional definition of bond, we introduced a more generic term to represent micro-interaction of particles. As an application of this study, a mixed-mode fracture analysis of PMMA semi-circular bend specimens was done. The results showed a remarkable improvement in prediction of fracture toughness in comparison to MTS method. Although GMTS performed much better than MTS, the simulation results showed that the new development still has a better determination of mode II fracture toughness compared to GMTS. Finally, a comparison of the experimental observation with the simulated crack trajectory confirms an acceptable agreement.

- Bundle tensile forces are slightly less than single CNT at failure, • This indicates inter-CNT vdW interaction in bundle does not affect the CNT tensile strength significantly. • Failure starts at the end of the bundle with fixed displacements. End tearing also observed in previous studies with standalone CNTs.

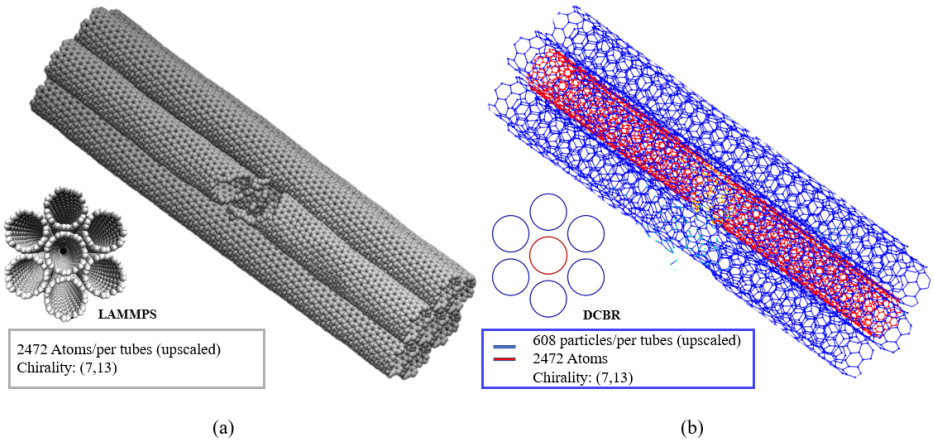

Figure 5.8: Tensile test of 6 tube bundle of SWCNTs with chiral vector of (7,13)

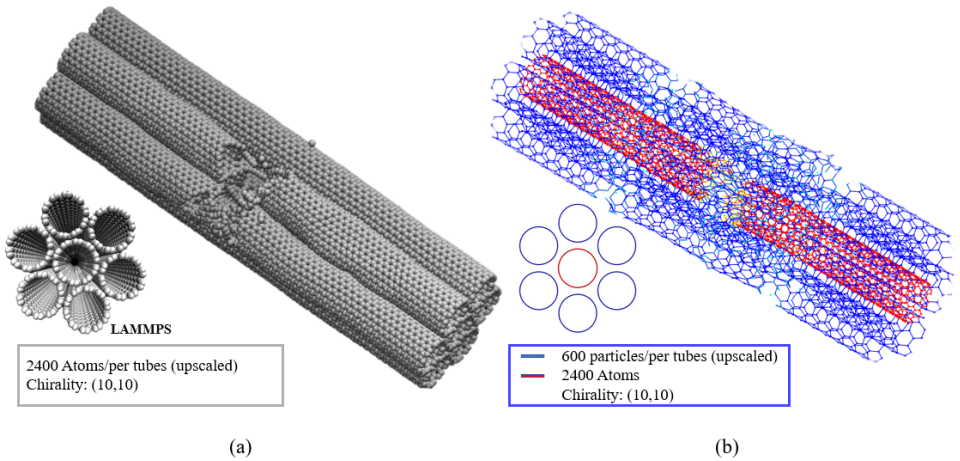

Figure 5.9: Tensile test of 6 tube bundle of SWCNTs with chiral vector of (10,10)

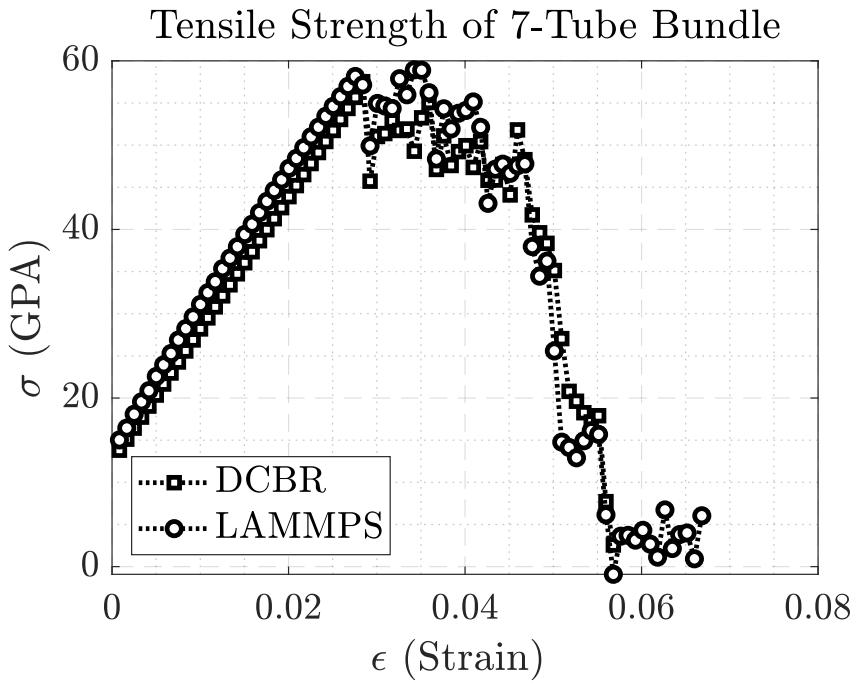

Figure 5.10: Tensile test of 6 tube bundle of SWCNTs with chiral vector of (7,13)

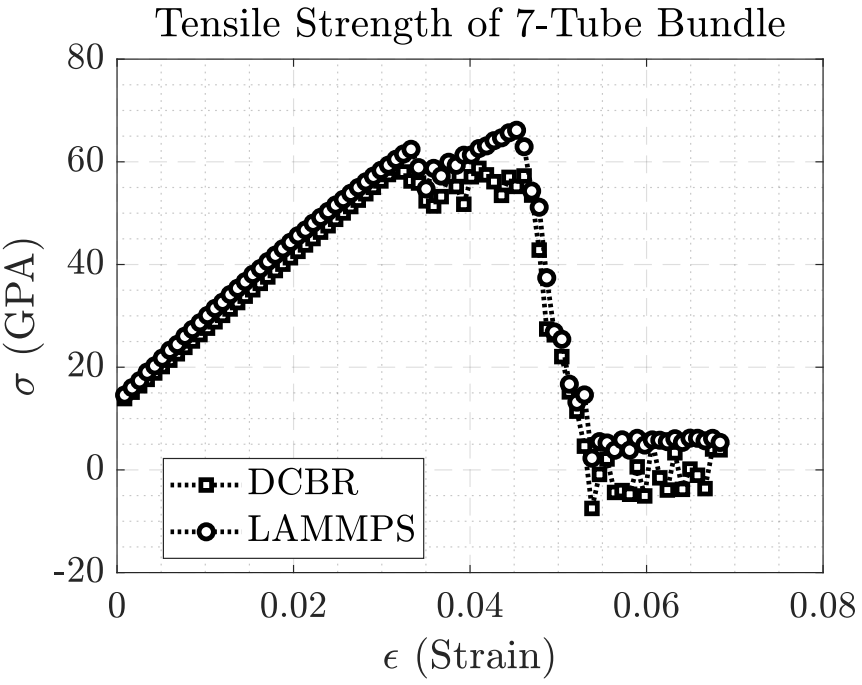

Figure 5.11: Tensile test of 6 tube bundle of SWCNTs with chiral vector of (10,10)

6. UNIFICATION OF LOCAL AND NONLOCAL MODELS WITHIN A STABLE INTEGRAL FORMULATION FOR ANALYSIS OF DEFECTS [1]

6.1 Introduction

The recent advancements in developing new materials with a broader application made scholars to revisit conventional constitutive models and frameworks. Besides, the description of empirical data challenges them to have a closer look at materials in lower scale. Classical Continuum Theories (CCTs) allow a continuous spread of matter in the body and sets the equations of motion holding the local action solely. In additions, CCTs are based on partial differential equations (PDE). These assumptions narrow the validity of the CCT to those macro-level responses where the loading length scale is much larger than the physical length scales. But in the case of loading with microscopic length scale, the classical prediction differs from experimental observation. Short wavelength excitations, analysis of porous media and state-of-the-art nanomaterial such as carbon nanotube are some examples that CCT failed to describe them accurately. [41]. Nanotube also plays an important role in fluid transport. In a carbon nanotubes, water molecules transport faster compared to the predicted values from classic continuum theory [77]. Moreover, several experiments showed that mediums with smaller cracks have higher fracture resistance than a body with a larger one, while the CCT does not consider the effect of crack dimensions. To avoid such restrictions of the CCT, Voigt [78] added a couple- forces to the conventional force-traction to model nonlocal interaction. Eringen verified that a nonlocal description is proficient at predicting a broad range of wavelengths [79]. The nonlocal theory was improved to be capable of predicting crack growth. Eringen pointed that unlike the CCT, the stress distribution close to the crack tip is bounded. Eringen [79] proposed a failure criterion by comparing cohesive stress to atomic bonds strength. Although the suggested nonlocal theory points the bounded stresses

[1] Reprinted with permission from "Unification of local and nonlocal models within a stable integral formulation for analysis of defects.", by Nowruzpour, Mohsen, and J. N. Reddy. 2018 *International Journal of Engineering Science*, 132, 45-59, Copyright 2018 by Elsivier

at the crack tips, the derivatives of the field variables are preserved in the formulation. Eringen [80] improved their nonlocal theory to model Griffith crack and later, he [81] noted that the results of nonlocal Griffith crack model are in a good agreement with Elliott 's lattice model [82]. Nevertheless, the governing equations were written based on the partial differential equations which are still ill-defined on discontinuity. Generally, the nonlocality comes into the picture by adding strain derivative to the standard constitutive relation or defining strain averaging [80]. Despite other nonlocal theories which use derivative of field variable, Rogula [83] proposed a nonlocal theory based on field variable. But the model was written for one-dimensional problems. Silling [20] proposed a derivative-free framework capable of analyzing multi-dimensional problems. The PD framework may be considered as an intermediate route between the classical and molecular dynamics (MD) approaches. Since it characterizes spatial interaction via integration, a PD equation can solve problems with discontinuities without resorting to any special treatment [20]. Based on this advantage, the PD framework finds its application not only in mechanics [20] but also in areas like thermo-mechanics [21], electromigration [22], heat conduction in a body involving discontinuity [23] etc. However, its original bond-based (BBPD) version faces a serious limitation because of its restriction on Poisson's ratio. Besides, the BBPD does not distinguish between volumetric and distortional deformation. The reason behind such limitations in BBPD is traced back to its assumption of equal and opposite pairwise forces between two particles within a bond. As an important step forward, Silling came up with a modification of the BBPD formalism and proposed state-based peridynamics (SBPD) (more precisely ordinary SBPD) in [24], which could resolve many of the issues associated with the original BBPD approach. Unlike the BBPD, the forces in a bond are unequal in ordinary SBPD [25]. However, the interaction forces within a bond are still considered as collinear. The SBPD framework is successfully applied in different areas of mechanics, e.g. plasticity [24], visco-elasticity [26], visco-plasticity [27], [28], dynamic brittle fracture [29], delamination in composite material [30], branching phenomena [31] etc. But owing

to its assumption of collinear forces along a bond, the ordinary SBPD is not applicable to non-linear anisotropic materials [25]. Such limitation has led to further development, and non-ordinary SBPD has been proposed [25]. Unfortunately, the non-ordinary SBPD is also scourged with difficulties in implementations. It may suffer from instability arising from the weak coupling of particles in the definition of deformation gradient. Responses via the non-ordinary SBPD may also show zero energy modes [32]. Other work done by Asadi [84] provided framework to study two different rupturing mechanisms of a membrane under liquid pressure loading introduced, which differ in time scale and loacation of the rupture. Tajdari and Tai [85] implements Smoothed Particle Hydrodynamics (SPH) in solid mechanics as a comparison to the traditional Finite Element approaches. Later, B Takabi et al [86], implemented SPH for orthogonal cutting for ductile and brittle material and compared the results with those obtained by FEM. Mei et al. [87] used inverse problem for partially known elastic modulus domain. Despite all the effort to improve laws and models [88, 89, 90, 91] a consistent connection between microscale and continuum level is not well defined. Most of the developed continuum models are not capable of capturing the evolution of microscopic defects such as crack within the framework. The existence of defects, such as imperfection and voids may affect the susceptibility of structure because of inception and growth of defects from an atomic level to the macroscopic scale. Several studies show that evolution of fracturing of brittle materials may not be presented via linear fracture mechanics.[92, 93, 94, 95, 96]. Other novel models in literature such as stress-based [97] and strain-based [98] criteria have been developed by Mirsayar to investigate mixed mode interfacial fracture behavior in strong interfaces where the interface crack kinks to one of the base materials. Kramer et al. [99] conducted an extensive study on different phenomenological numerical model to predict stress, strain, and failure mechanisms in additively manufactured materials. The numerical models are calibrated based on dogbone and notched samples and are applied on a new complex geometry. Blind predictions are compared against test data. They also introduced and provided an optimized mesh structure which is validated by experimental data [100].

It started with bond-based peridynamics [101] which brought up some obstacles to have realistic modeling due to the extreme simplification of particle interactions in the domain. The concept of state in peridynamics framework was introduced to remove some of the restrictions [24, 102]. However, the new concept required advanced mathematical tools to be implemented in the framework. Moreover, it has been shown that there is huge instability in the response of the problem [32]. Our recent study proposed a discrete Lagrangian-based framework to characterize the response of an elastic body at a length scale of interest [33]. A great benefit of adopting the Lagrangian description is its flexibility in characterizing coupled multibody-interaction. In this section, we present a systematic approach to constructing new nonlocal derivative-free formulation from classical constitutive models. This study could be an effort for the unification of local and nonlocal framework to analyze problems incorporating discontinuities and defects. In Section 6.2, we present nonlocal deformation in a body based on Discrete Cauchy-Born Rule (DCBR). The new definition compacts the state of deformation at a point of a discrete system into a second-order tensor. In Section 6.3, we derive a nonlocal derivative-free energetically-conjugate pair using nonlocal rate of work done in the continuum. In Section 6.4, a transformation matrix is introduced to map surface-based forces (conventional stress) to body-based ones. This transformation makes the continuum particle capable of interacting with the nonlocal region. In Section 6.5, using peridynamics approach for calculation of strain energy release rate (G), we present a new suitable energy-based criterion for the framework to predicts failure in brittle materials. In Section 6.6, a numerical investigation is done to show the credibility of the new development in analyzing mixed-mode fracture toughness of the semi-circular bend specimen made of PMMA.

6.2 Directionality Operator

Here, we present a projection principle for upscaling microscopic information, which allows non-trivial directional information to develop a variable in a continuous or discrete system. The principal was obtained by employing a stochastic projection method, uses certain microscopic details. The directionality operator can be defined as;

$$\mathbf{G} = [\mathbf{\Theta} - \mathbf{\Lambda}] \cdot \mathbf{\Upsilon} \tag{6.1}$$

$$\mathbf{\Upsilon} = \mathbf{\Delta}^{-1} \tag{6.2}$$

The gain matrix, $\mathbf{G}$ might be described as a nonlocal equivalent of the deformation gradient that dictates the motion of a continuum body under external loading. Numerically it can be shown that such definition converges to conventional deformation gradient for the local limit. A discretized version of each term in equation (6.1) can be given as;

$$\mathbf{\Theta}^{nc} = \left(\sum_{n=1}^{m} \kappa^{nc} \left(\bar{u}_i^n - \bar{u}_i^c \right) \left(x_j^n - x_j^c \right) v^n \right) \mathbf{e}_i \otimes \mathbf{e}_j \tag{6.3}$$

$$\mathbf{\Lambda}^{nc} = \frac{1}{\sum\limits_{n=1}^{m} v^n} \left(\sum_{n=1}^{m} \kappa^{nc} \left(\bar{u}_i^n - \bar{u}_i^c \right) v^n \sum_{n=1}^{m} \kappa^{nc} \left(x_j^n - x_j^c \right) v^n \right) \mathbf{e}_i \otimes \mathbf{e}_j \tag{6.4}$$

$$\mathbf{\Upsilon}^{nc} = \left(\sum_{n=1}^{m} \kappa^{nc} \left(x_i^n - x_i^c \right) \left(x_j^n - x_j^c \right) v^n \mathbf{e}_i \otimes \mathbf{e}_j \right)^{-1} \tag{6.5}$$

where, $\bar{u}_i^n$ can be given;

$$\bar{u}_i^c = \frac{1}{\sum\limits_{n=1}^{m} v^n} \sum_{n=1}^{m} \kappa^{nc} u_i^n v^n \tag{6.6}$$

Superscripts n and c indicate the neighboring and the central particle. u and x show the displacement and location of particles. v_n is the associated volume of the n^{th} particle. The subscripts i and j are showing the direction of Cartesian coordinates. κ is the non-local smoothing function. A stabilized displacement field of the c^{th} particle is defined in Eq. (6.6) that is dependent on the displacement of the neighbors to avoid weak coupling of particles; Such definition stabilizes the framework and avoids zero-mode energy in the solution. A continulized version of the $\mathbf{\Theta}$, $\mathbf{\Lambda}$ and $\mathbf{\Upsilon}$ can be given as;

$$\Theta_{ij} = \int_S \kappa \alpha_i \beta_j ds' \tag{6.7}$$

$$\Lambda_{ij} = \frac{1}{S}\int_S \kappa\alpha_i ds' \int_S \kappa\beta_j ds' \tag{6.8}$$

$$\Upsilon_{ij} = \int_S \kappa\beta_i\beta_j ds' \tag{6.9}$$

where α_i and β_j are;

$$\begin{aligned} \alpha_i &= u_i' - u_i \\ \beta_j &= x_j' - x_j \end{aligned} \tag{6.10}$$

Here, S is the scope or influence domain of the point of interest. Note that the prime symbol ($\prime$) implies the points in the neighborhood of central one.

6.3 Nonlocal Energetically-Conjugate Pair

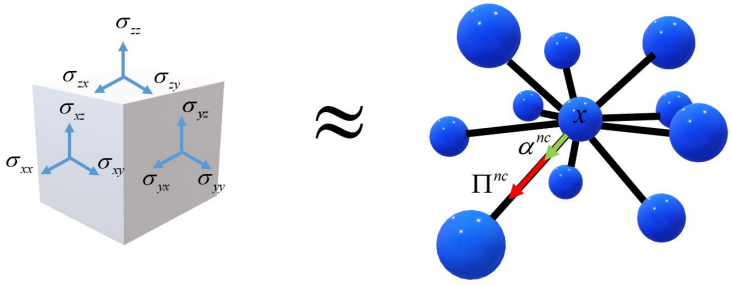

Figure 6.1: Energetically representation of continuum element in a discrete model

To get the new nonlocal energetically-conjugate pair suitable for the new framework, we go through a consistent energy approach. The rate of internal work done in a continuum in the current configuration can be equated to the rate of stored energy in the bonds connected from neighbors to central particle. The statement might be mathematically expressed as;

$$W = \frac{1}{2}\int_V (\boldsymbol{\sigma} : \mathbf{d})\, dv = \frac{1}{2}\int_\Omega \left(\int_S \mathbf{\Pi}.\dot{\boldsymbol{\alpha}} dS\right) d\Omega; \quad \mathbf{d} = \frac{1}{2}\left[\nabla\mathbf{v} + (\nabla\mathbf{v})^T\right] \tag{6.11}$$

where $\mathbf{d}$ is the symmetric part of the velocity gradient tensor, $\boldsymbol{\sigma}$ is the Cauchy stress tensor,

$\mathbf{\Pi}$ is the force vector developed between the particle of interest and the neighboring particle. The lattice deformation rate is shown by $\dot{\boldsymbol{\alpha}}$. Since $\mathbf{\Pi}$ creates the micro-potential density of a particle, and micro-potentials are defined with respect to a volume, $\mathbf{\Pi}$ may be called Body-Based (BB) forces. On other hands, classical stresses might be renamed to Surface-Based (SB) forces, because they are always described with respect to a surface. Due to the symmetry of the stress tensor;

$$W = \frac{1}{2}\int_V \boldsymbol{\sigma} : \mathbf{l} dv = \frac{1}{2}\int_\Omega \boldsymbol{P} : \dot{\mathbf{F}} dv \tag{6.12}$$

where $\mathbf{l}$ is velocity gradient and could be determined via $\mathbf{l} = \dot{\mathbf{F}}\mathbf{F}^{-1}$; Here $\mathbf{F}$ is deformation gradient and $\mathbf{P}$ is the local first Piola-Kirchhoff stress. To build up a nonlocal description of the deformation, we approximate $\mathbf{F}$ with the Gain function, $\boldsymbol{G}$. Hence, the rate of work done in a continuum can be rewritten in a nonlocal setting as;

$$W = \frac{1}{2}\int_\Omega \boldsymbol{\psi} : \dot{\mathbf{G}} dV \tag{6.13}$$

Accordingly, $\boldsymbol{\psi}$ might be interpreted as the nonlocal counterpart of First Piola-Kirchhoff Stress (NFPS). Because $\mathbf{\Upsilon}$ is calculated in the initial configuration, the time derivative of the Gain function can be given;

$$\dot{\mathbf{G}} = \left(\dot{\mathbf{\Theta}} - \dot{\mathbf{\Lambda}}\right)\mathbf{\Upsilon} \tag{6.14}$$

For the simplicity of summation over same indices, we use Einstein's notation ;

$$\left(\dot{\mathbf{\Theta}} - \dot{\mathbf{\Lambda}}\right) = \frac{1}{S}\left(\int_S \kappa \dot{\alpha}_i \gamma_j ds^{'}\right)\mathbf{e}_i \otimes \mathbf{e}_j; \quad \gamma_j = \beta_j - \frac{1}{\tau}\int_\tau \beta_j d\tau' \tag{6.15}$$

where γ is a new lower scale component that naturally rises in the formulation. The parameter quantifies the Average Deviation of Lattice (ADL) vector in the region of influence. Unlike the usual practice of mapping of the undeformed bond vector into the deformed configuration [25, 32, 103], here the ADL parameter will be evolved into the new configuration.

Therefore, in our derivation, γ may represent the notion of bond in a more generic manner. For a symmetric selection of τ, γ_j is equal to βj (lattice vector) which is widely used in previous studies, mainly, Nonordinary State-Based Peridynamic (NSBP) [32, 104, 105]. But in the case of selection of asymmetric influence domain, or an asymmetric distribution of particle in a symmetric scope like boundaries or discontinuities, γ_j differs significantly from β_j. Note that τ is independent of S and could be equal or smaller than S. Using Eq.(6.9) and (6.15) in Eq.(6.14) to get the rate of gain function and substituting the results in Eq. (6.13) gives;

$$W = \frac{1}{2}\int_{\Omega}\left(\psi_{ki}\Upsilon_{jk}\left(\int_{S}\kappa\dot{\alpha}_i\gamma_j dS\right)\right)dV = \frac{1}{2}\int_{\Omega}\left(\int_{S}\Pi_i\dot{\alpha}_i dS\right)dV \tag{6.16}$$

From Equation (6.16), the structure of nonlocal BB force, $\mathbf{\Pi}$, could be found. The transformation equation could be written in an indicial format as. Eq. (6.17)

$$\Pi_i = \psi_{ki}\Upsilon_{jk}\gamma_j \tag{6.17}$$

The obtained equation provides a connection from nonlocal surface-based (SB) interaction system to a nonlocal body-based (BB) one. It takes the undeformed ADL vector γ from the initial configuration with the nonlocal stress field ψ and returns the corresponding nonlocal BB force.

6.4 Body-Based Transformation Matrix

To facilitate the use of achieved results in previous section, we intend to prepare a matrix that could turn the nonlocalized derivative-free model from classical theory to the nonlocal BB model. Here, it should be noted that this framework cannot take every nonlocalized model, instead, the models that are constructed based on Gain function are suitable to be

implemented in this framework. The vectorial form of the Eq.(6.17) can be presented as:

$$\boldsymbol{\Pi} = (\boldsymbol{\Upsilon} \cdot \boldsymbol{\psi})^T \cdot \boldsymbol{\gamma} = \boldsymbol{\psi} \cdot^T \boldsymbol{\Upsilon}^T \cdot \boldsymbol{\gamma} = \left(\boldsymbol{\gamma}^T \cdot \boldsymbol{\Upsilon} \cdot \boldsymbol{\psi}\right)^T \tag{6.18}$$

Given the fact that definition of $\boldsymbol{\psi}$ is built on the Gain function that converges to the classical counterpart in a localized view, to measure stresses in large deformation problems, NFPK could be written in terms of; $\boldsymbol{\psi} = \boldsymbol{G}.\boldsymbol{\varphi}$ where $\boldsymbol{\varphi}$ might be interpreted as Nonlocal Second Piola Kirchhoff (NSPK) stress. Rewriting Eq. (6.18) in gives;

$$\boldsymbol{\Pi}^T = \boldsymbol{\gamma}^T \cdot \boldsymbol{\Upsilon} \cdot \boldsymbol{G} \cdot \boldsymbol{\varphi} \tag{6.19}$$

To find a transformation matrix capable of mapping of NSPK stress into BB forces, the following matrices are introduced;

$$\begin{bmatrix} T_1 & T_2 & T_3 \end{bmatrix} = \begin{bmatrix} \gamma_1 & \gamma_2 & \gamma_3 \end{bmatrix} \begin{bmatrix} \Upsilon_{11} & \Upsilon_{12} & \Upsilon_{13} \\ \Upsilon_{21} & \Upsilon_{22} & \Upsilon_{23} \\ \Upsilon_{31} & \Upsilon_{32} & \Upsilon_{33} \end{bmatrix} \tag{6.20}$$

It is noteworthy to mention that $\mathbf{T}$ vector solely depends upon the initial configuration of the body. Matrix $\hat{\mathbf{T}}$ that follows from the union of the $\mathbf{T}$ and $\mathbf{G}$ can be created as;

$$\begin{bmatrix} \hat{T}_1 & \hat{T}_2 & \hat{T}_3 \end{bmatrix} = \begin{bmatrix} T_1 & T_2 & T_3 \end{bmatrix} \begin{bmatrix} G_{11} & G_{12} & G_{13} \\ G_{21} & G_{22} & G_{23} \\ G_{31} & G_{32} & G_{33} \end{bmatrix} \tag{6.21}$$

using the $\hat{\mathbf{T}}$, Eq. (6.18) might be shown in matrix form;

$$\begin{bmatrix} \Pi_1 \\ \Pi_2 \\ \Pi_3 \end{bmatrix} = \underbrace{\begin{bmatrix} \hat{T}_1 & 0 & 0 & 0 & \hat{T}_3 & \hat{T}_2 \\ 0 & \hat{T}_2 & 0 & \hat{T}_3 & 0 & \hat{T}_1 \\ 0 & 0 & \hat{T}_3 & \hat{T}_2 & \hat{T}_1 & 0 \end{bmatrix}}_{\hat{\mathbf{T}}} \begin{bmatrix} \varphi_{11} \\ \varphi_{22} \\ \varphi_{33} \\ \varphi_{23} \\ \varphi_{13} \\ \varphi_{12} \end{bmatrix} \tag{6.22}$$

$\hat{\mathbf{T}}$ matrix might be named as a transformation matrix that converts nonlocal classical constitutive model to a generalized nonlocal derivative-free one. An evolution of SB force to BB forces are shown in Fig.6.2. Note that Π_1, Π_2, Π_3 should not be confused with the resultant of stress tensor in the classical model. In fact, they are new quantities which are associated with the volume of the body and resultant of microscopic interaction with the local and nonlocal medium. This is in contrast to the definition of stress as a quantity that can only communicate through the surface (local definition of interaction). The given formulation can be directly applied to the orthotropic linear elastic material;

$$\begin{bmatrix} \varphi_{11} \\ \varphi_{22} \\ \varphi_{33} \\ \varphi_{23} \\ \varphi_{31} \\ \varphi_{12} \end{bmatrix} = \begin{bmatrix} C_{11} & C_{12} & C_{13} & 0 & 0 & 0 \\ C_{21} & C_{22} & C_{23} & 0 & 0 & 0 \\ C_{31} & C_{32} & C_{33} & 0 & 0 & 0 \\ 0 & 0 & 0 & C_{44} & 0 & 0 \\ 0 & 0 & 0 & 0 & C_{55} & 0 \\ 0 & 0 & 0 & 0 & 0 & C_{66} \end{bmatrix} \begin{bmatrix} \xi_{11} \\ \xi_{22} \\ \xi_{33} \\ \xi_{23} \\ \xi_{31} \\ \xi_{12} \end{bmatrix} \tag{6.23}$$

where $\boldsymbol{\xi}$ is nonlocal derivative-free Green strain and it could be written based upon $\boldsymbol{G}$ as follows;

$$\boldsymbol{\xi} = \frac{1}{2}\left(\mathbf{G}^T \cdot \mathbf{G} - \mathbf{I}\right) \tag{6.24}$$

Ultimately, using the equation of motion (EOM) for a two-body interaction system, developed in the previous study, [33], EOM could be rewritten in the following form:

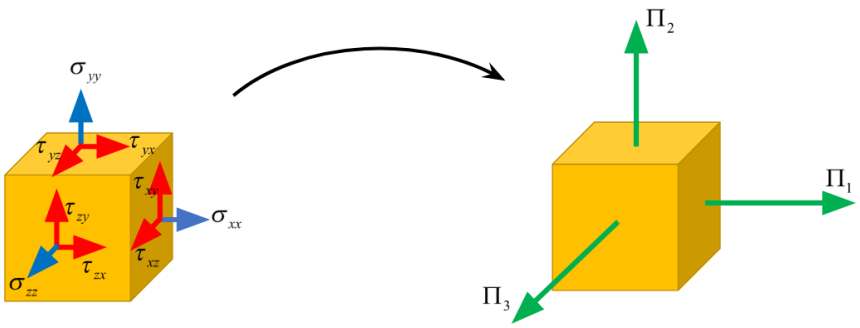

Figure 6.2: Conversion of local SB forces to nonlocal BB forces

$$\boldsymbol{\phi} + \mathbf{f} = \rho \ddot{\mathbf{u}} \;\; ; \quad \boldsymbol{\phi} = \int_S \left(\mathbf{\Pi} - \mathbf{\Pi}' \right) dS \tag{6.25}$$

where ρ, $\mathbf{f}$ and $\mathbf{u}$ are density, body force vector and displacement vector respectively. $\mathbf{\Pi}$ is generalized nonlocal body-based force vector. One of the major distinctions of such a framework with classical continuum theory is that the new nonlocal forces are not any longer interacting through the surface, since they are volume-dependent quantity and they can fix the restriction of reaching nonlocal region.

6.5 Failure Criteria

In this section, we try to develop an energy-based failure criterion for the framework. Zhou and Wang [106] provided a stress-based failure criterion in a discrete system. They proposed an extra criterion in addition to the tensile failure to incorporate shear failure of the bonds. Silling and Askari [107] calculated the summation of the required work per unit length to eliminate every interaction between particles on the symmetric line below the crack surface (P_i) and particles above the crack surface (P_j) that are in the influence domain of

particle (P_i) (see Fig. 6.3). Using this calculation, an energy-based failure approach which relaxes the need for an extra criterion is proposed. The strain energy release rate can be calculated once all the critical failure energy of bonds that cross the crack surface are summed up (see colored area in Fig. 6.4). Note that as we move downward, the area above the crack gets smaller. For a thin linear isotropic elastic material, the strain energy can be calculated via:

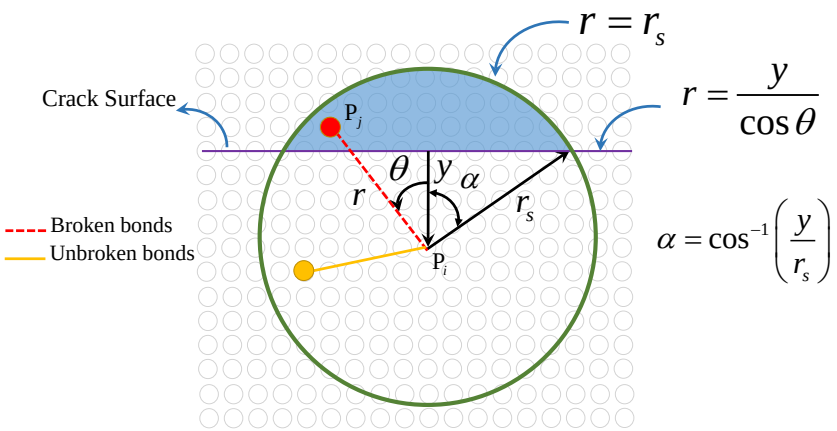

Figure 6.3: Calculation of nonlocal strain energy dissipated during formation of unite fracture surface area

$$U = \int_S U^* dv = \frac{1}{2}\int_S \varphi_{ij}\xi_{ij} dv \tag{6.26}$$

where U^* is strain energy density. Note that ξ_{ij} is the Green strain. For a two dimensional analysis, G can be calculated as follows;

$$G = U^{nc} = \frac{t}{2}\int_{y=0}^{y=r_s}\int_{\theta=-\alpha}^{\theta=\alpha}\int_{r=\frac{y}{cos(\theta)}}^{r=r_s}\left(\varphi_{ij}^{nc}\xi_{ij}^{nc}\right) r dr d\theta dy \tag{6.27}$$

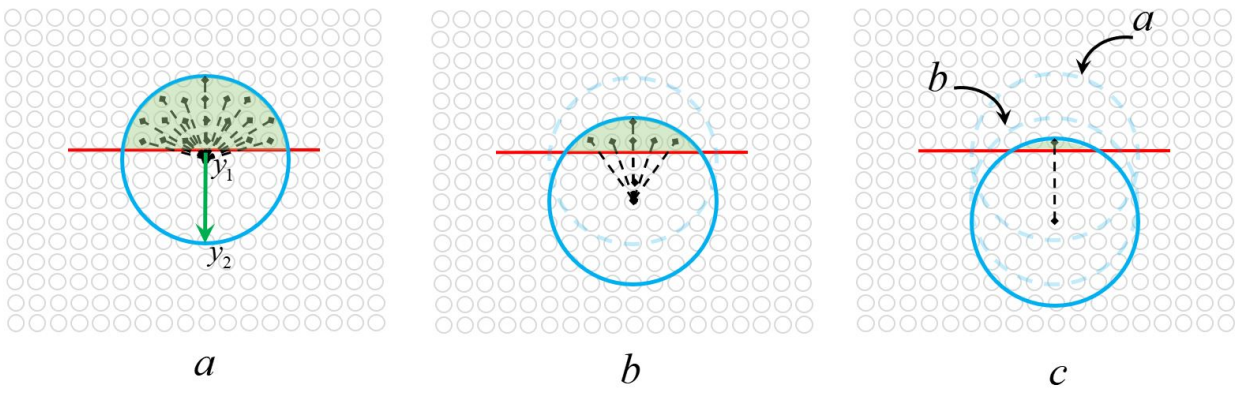

Figure 6.4: Areas representing particles with broken bonds connected to central particles lying on green axis

where t is the thickness. Assuming a symmetric distribution of particles i.e. $\frac{1}{\tau}\int_\tau \beta_j d\tau' = 0 \Rightarrow \gamma_j = \beta_j$, the strain energy for particles under the crack surface

$$G^{nc} = \frac{t}{2}\varphi_{ij}^{nc}\xi_{ij}^{nc}\left(r_s^2\, y\cos^{-1}\left(\frac{y}{r_s}\right) - \frac{r_s\, y^2\sqrt{1-\frac{y^2}{r_s^2}}}{3} - \frac{2\, r_s^3\sqrt{1-\frac{y^2}{r_s^2}}}{3}\right)_{y=0}^{y=r_s} = \frac{t}{3}r_s^3\varphi_{ij}^{nc}\xi_{ij}^{nc} \tag{6.28}$$
$$= \frac{t}{3}r_s^3\left[\varphi_{11}^{nc}\xi_{11}^{nc} + \varphi_{22}^{nc}\xi_{22}^{nc} + \varphi_{33}^{nc}\xi_{33}^{nc} + 2\left(\varphi_{23}^{c}\xi_{23}^{nc} + \varphi_{31}^{c}\xi_{31}^{nc} + \varphi_{12}^{nc}\xi_{12}^{nc}\right)\right]$$

Here, r_s is a nonlocal parameter that emerges in the definition of the nonlocal strain energy release rate. Since the calculation of energy can be repeated for particles on the line above the crack surface (i.e., G^{cn}), the total strain energy release rate cab be given;

$$G = f_1\left(\gamma^{nc}\right)G^{nc} + f_2\left(\gamma^{cn}\right)G^{cn} \tag{6.29}$$

In general, we are differentiating between the connections from n to c particle and c to n particle. To show this difference, we use f_1 and f_2 function as a coefficient of G. In this section, for $f_1 = f_2 = 1$, we are still able to get acceptable results. Here, the failure criterion states that the connection between two bonds fails if the strain energy calculated based upon

two ends of a bond exceeds the critical amount.

6.6 Numerical Results and Discussion

6.6.1 Calculation of Mode I/II Fracture Toughness Using SCB Specimens

Chong and Kuruppu [108] suggested semi-circular bend (SCB) specimen for measuring mode I of brittle materials such as rock or other geological material. Many factors such as convenient of running test, minimal machining labor for preparation of specimens and stability of results made it a popular test specimen. The tests have been done in normal room temperature, therefore we ignore the effect of thermal sresses. The effect of different driving factors on induced thermal stress in geological materials is studied by Ravaji [109, 110]. They showed how small values of thermal stress can lead to fatigue and crack propagation in rocks, a mechanism that plays a crucial role in the surface evolution in our Solar system. Figure. 6.5 depicts a scheme of the SCB of radius R which is resting on two supports. The length of the distance from one support to another is 2S. Each specimen has a crack of length a, that creates an angle with the line of symmetry. With different crack inclination (α), different crack modes or a mixture of them can be obtained. For instance, when $\alpha = 0$, the specimen is subjected to pure mode I. As we increase α, mode II contributes more to the failure of specimen. To calculate the stress state close to the tip of the crack, stress intensity factor in mode I and II are given;

$$Y_I\left(\alpha, \frac{a}{R}, \frac{S}{R}\right) = \frac{K_I}{\sqrt{\pi a}} \frac{2Rt}{P_{cr}} \tag{6.30}$$

$$Y_{II}\left(\alpha, \frac{a}{R}, \frac{S}{R}\right) = \frac{K_{II}}{\sqrt{\pi a}} \frac{2Rt}{P_{cr}} \tag{6.31}$$

where t and P_{cr} are thickness and critical applied force on the top of specimen respectively. Y_I, Y_{II} are geometry factors associated with mode I and mode II. The geometry factor parameters are a function of crack angle (α), crack length ratio, a/R, and support length ratio S/R. Ayatollahi [111] has provided a wide range of experimental data of Y_I and Y_{II} for

various geometrical ratios. Figure 6.6 shows values of Y_I and Y_{II} for a SCB with dimensional ratio of $a/R = 0.3$ and $S/R = 0.43$ for different inclination angles [112]

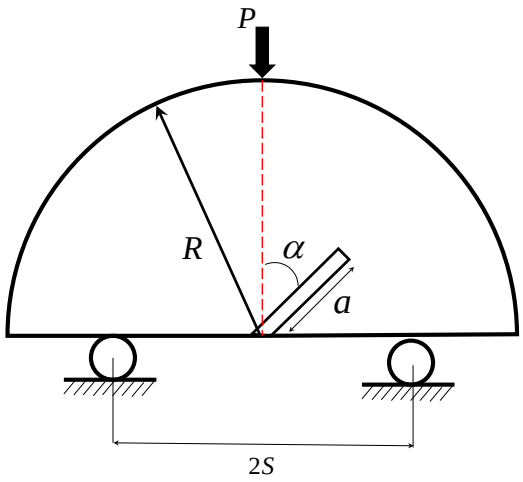

Figure 6.5: Scheme of SCB specimen with inclination crack angle, α

6.6.2 Numerical Method; Verlet Scheme

To solve equation of the motion numerically, the body is discretized into number of nodes. a discretized form of the the governing equations could be given as;

$$\boldsymbol{\phi}^c + \boldsymbol{f}^c = \rho \ddot{\boldsymbol{u}}^c \;\; ; \quad \boldsymbol{\phi}^c = \sum_{n=1}^{m} \left(\boldsymbol{\Pi}^c - \boldsymbol{\Pi}^n \right) v^n \tag{6.32}$$

$$\boldsymbol{\Pi}^c = \left(\boldsymbol{\Upsilon}^c \cdot \boldsymbol{\psi}^c \right)^T \cdot \boldsymbol{\gamma}^c \tag{6.33}$$

$$\boldsymbol{\Pi}^n = \left(\boldsymbol{\Upsilon}^n \cdot \boldsymbol{\psi}^n \right)^T \cdot \boldsymbol{\gamma}^n \tag{6.34}$$

$$\boldsymbol{\gamma}^{nc} = \boldsymbol{\beta}^{nc} - \frac{1}{S} \sum_{n=1}^{m} \boldsymbol{\beta}^{nc} v^n \tag{6.35}$$

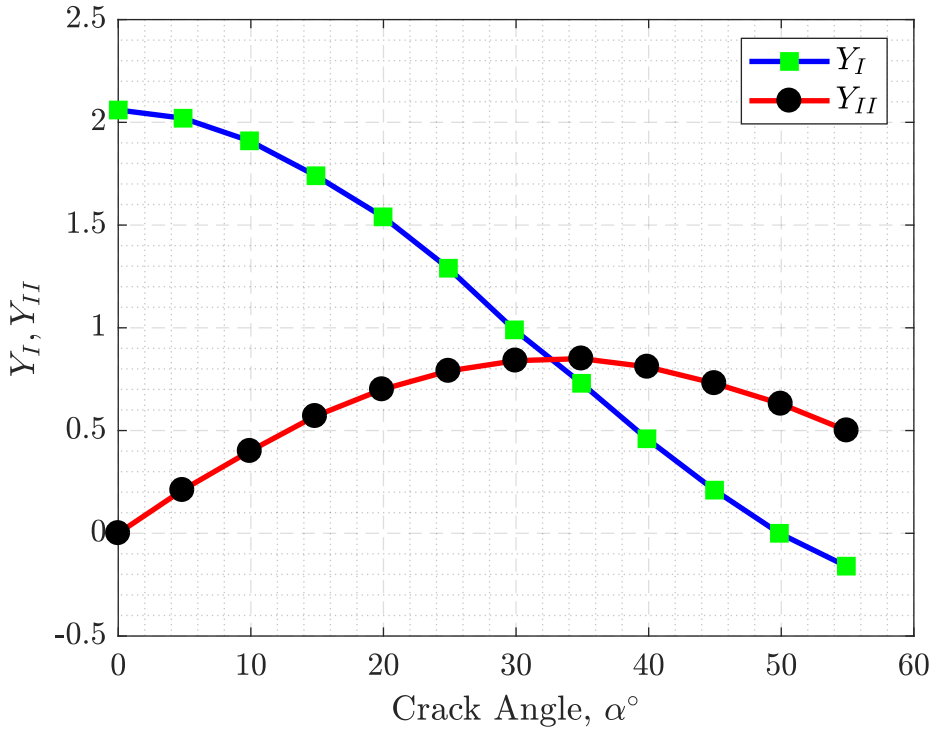

Figure 6.6: Geometry factor values of mode I and mode II for different inclination angles.

A flowchart of the developed code is shown in Fig. 6.8. Since we have a discrete structure, we try to pick one of the powerful methods for numerical integration of the equation of motion. Verlet scheme is a fascinating method particularly for researchers in molecular dynamics area. The method is offered in three version; Velocity, position [113] and Leapfrog [114] type. This algorithm provides acceptable stability along with simplicity. To update position at time t and velocity at time $(t+\frac{1}{2}\delta t)$ and t, Taylor expansion series is employed:

$$\mathbf{X}(t+\delta t) = \mathbf{X}(t) + \dot{\mathbf{X}}(t)\,\delta t + \frac{1}{2}\ddot{\mathbf{X}}(t)\,\delta t^2 + \cdots \tag{6.36}$$

$$\dot{\mathbf{X}}\left(t+\frac{1}{2}\delta t\right) = \dot{\mathbf{X}}(t) + \frac{1}{2}\ddot{\mathbf{X}}(t)\,\delta t + \cdots \tag{6.37}$$

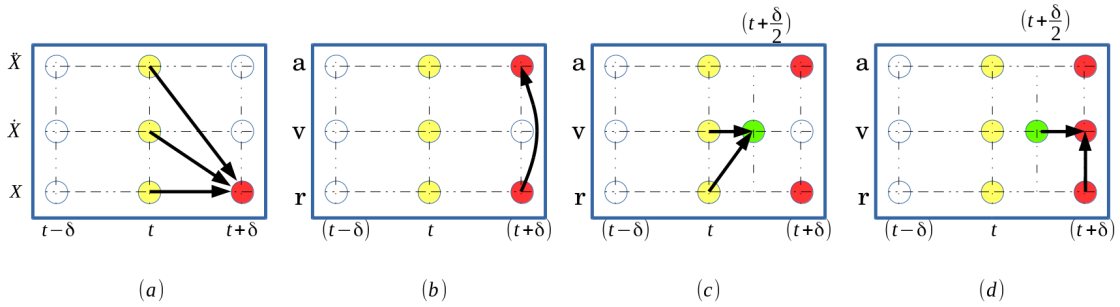

Figure 6.7: Algorithm of Verlet-Velocity method

$$\ddot{\mathbf{X}}(t+\delta t) = \frac{\boldsymbol{\phi}(t)}{\rho} \tag{6.38}$$

$$\dot{\mathbf{X}}(t+\delta t) = \dot{\mathbf{X}}\left(t+\frac{1}{2}\delta t\right) + \frac{1}{2}\ddot{\mathbf{X}}(t+\delta t)\,\delta t + \cdots \tag{6.39}$$

The new configuration can be updated using position, velocity, and acceleration at the previous step (see Fig. 6.7, a). The nonlocal forces can be calculated by updating new position vectors (see Fig. 6.7, b). Finally, to get velocity at time $(t+\delta t)$, the velocity at the middle of time increment is determined (Fig. 6.7, c), and then the velocity can be determined from the updated position and velocity at previous half-step.

6.6.3 Numerical Simulation of Dynamic Crack Growth and Fracture Analysis of SCB Rock Specimen

Failure of engineering parts due to crack propagation is a topic that attracts much attention. Maiti and Prasad [115] studied the prediction of the unstable crack path using the stress distribution before the crack starts propagating in the body. Oliver [116] developed a numerical technique by injecting a discontinuous displacement to simulate the evolution of crack in materials. In this model, the evolution of crack is investigated without applying any external criteria to dictate crack path. As a benchmark problem, we implemented a numerical simulation of a cracked SCB made of Polymethylmethacrylate (PMMA) with the

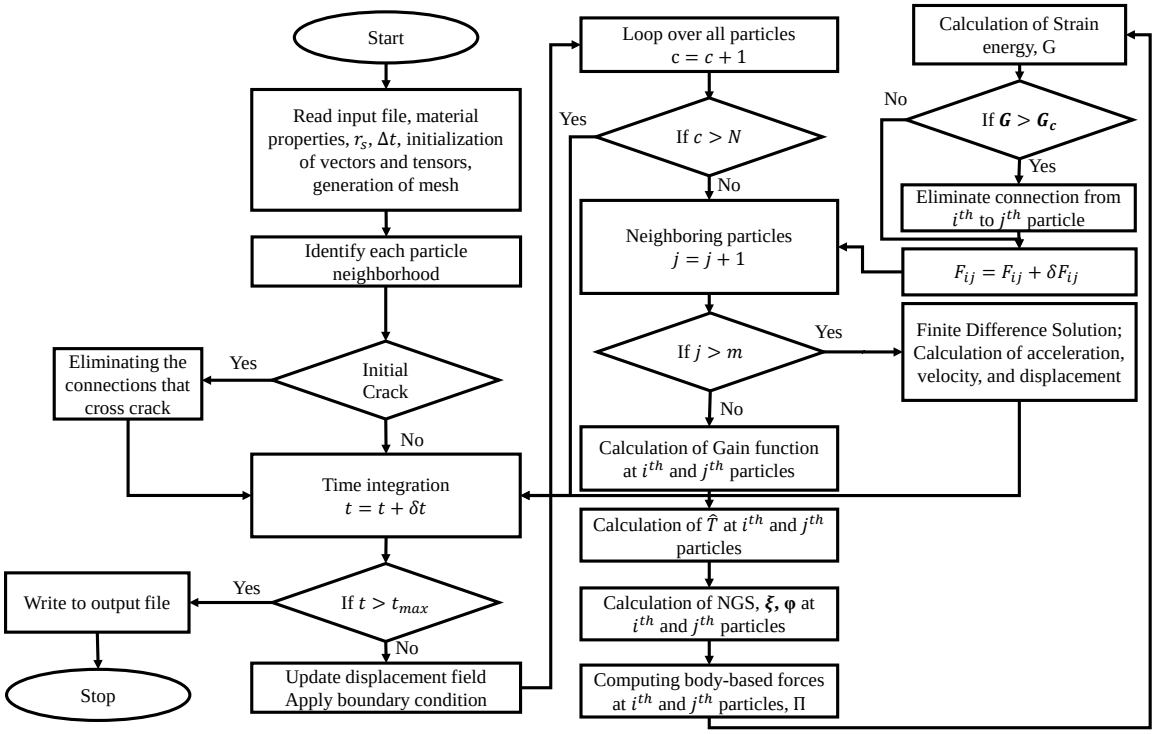

Figure 6.8: Flowchart of the developed code.

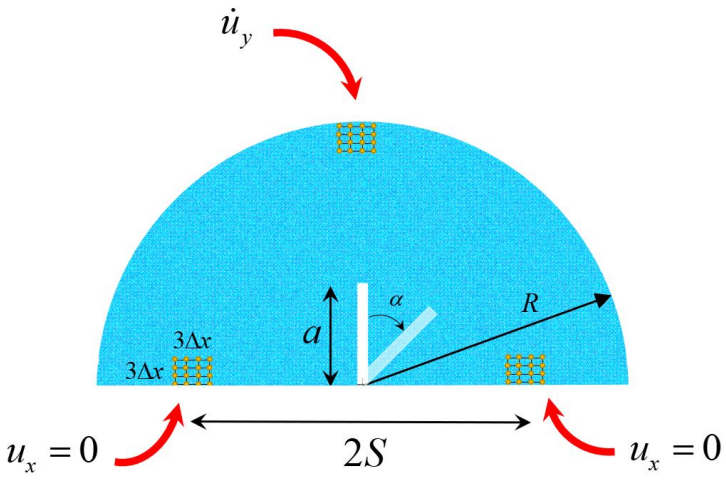

Figure 6.9: Semi-Circular Bend specimen under mode I ($\alpha = 0$) or mixed mode loading ($\alpha \neq 0$)

different inclination angles. The mechanical properties of PMMA are given in the table6.1. The domain is discretized into 16366 particle uniformly ($\Delta x = \Delta y$) with the particle spacing of $\Delta x = 0.0005$.

Table 6.1: Mechanical properties of PMMA

Parameter	Value	Units
E (Young's Modulus)	3.75	GPa
ν (Poisson's ratio)	0.35	-
ρ (Density)	1.41	Mg/m^3
K_{Ic} (Fracture Toughness I)	2.13	$MPa\sqrt{m}$

Fig. 6.9 depicts a discretized SCB with constraints and loading condition. The SCB is constrained vertically on both supports, and a constant displacement rate is applied on the top of the specimen. For the sake of stability and avoiding fracture at supports, all constraints and loading (on the top) are applied to an area of $3\Delta x \times 3\Delta x$. The following dimensions and loading condition are considered for the simulation;

$$\begin{aligned} &R = 50\ mm,\ a = 0.3R,\ S = 0.43R,\ t = 5mm, \\ &\Delta t = 5 \times 10^{-8} s, V_y\left(0, R\right) = -0.005\ \text{mm/min},\ u_x\left(\pm S, 0\right) = 0.0 \end{aligned} \tag{6.40}$$

Since r_s is a new nonlocal parameter, it can be determined by comparison of the fracture results for different r_s with the experimental values. Fig. 6.10 displays the critical load associated with different crack angles. It can be seen that for $r_s = 2\Delta x$, the simulation's results have a closer prediction to experiment. Therefore, the remaining results are presented based on $r_s = 2\Delta x = 0.001$. It is noteworthy to mention that r_s is not a mesh dependent parameter, but it is material property, and it has a unique value for each material.

Fig.6.11 and Fig. 6.12 illustrate the final status of specimens after the crack is fully grown. The color bar in these figures shows the extent of damage to a particle. The damage

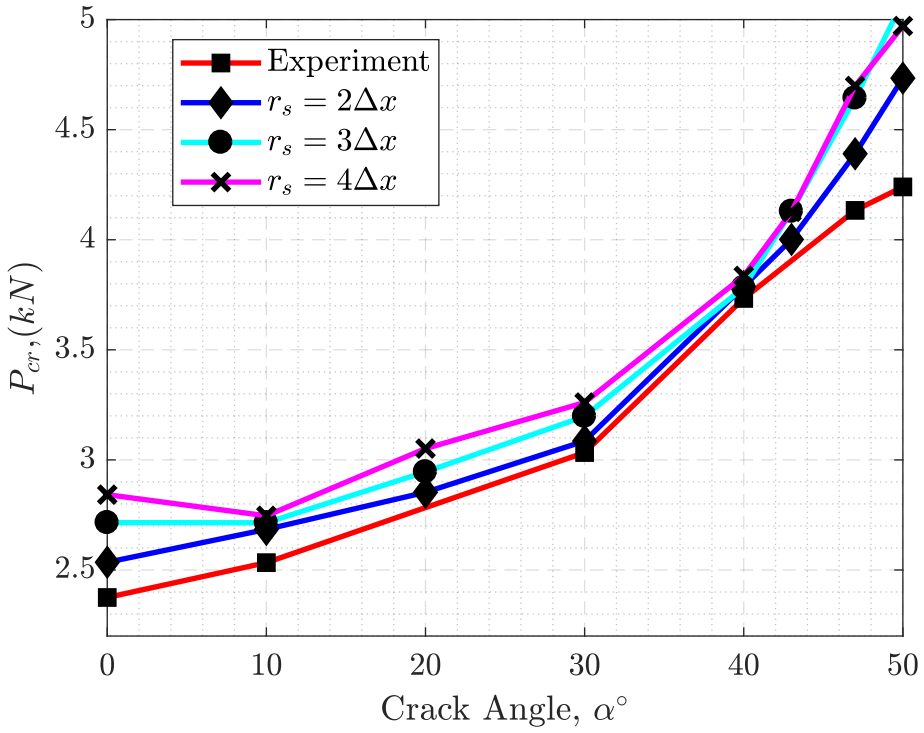

Figure 6.10: Variation of critical load with crack inclination angles for different r_s

index of one implies that a particle has missed all its links, whereas the index of zero indicates a particle that preserves all of its connections. This parameter is given as:

$$\mu = 1 - \frac{R}{T} \tag{6.41}$$

where R is the number of remaining bonds and T is the total number of connected bonds before the loading starts. When $\alpha = 0.0^\circ$ (pure mode I), The crack starts propagating on a straight line, along the direction of initial crack till it reaches the top of the SCB. As the inclination angle increases, cracks trajectory deviates from the direction of initial flaw due to the contribution of mode II loading. It can be clearly seen for angles greater than 10°, the propagation starts from the tip, and it eventually aligns with the symmetry line

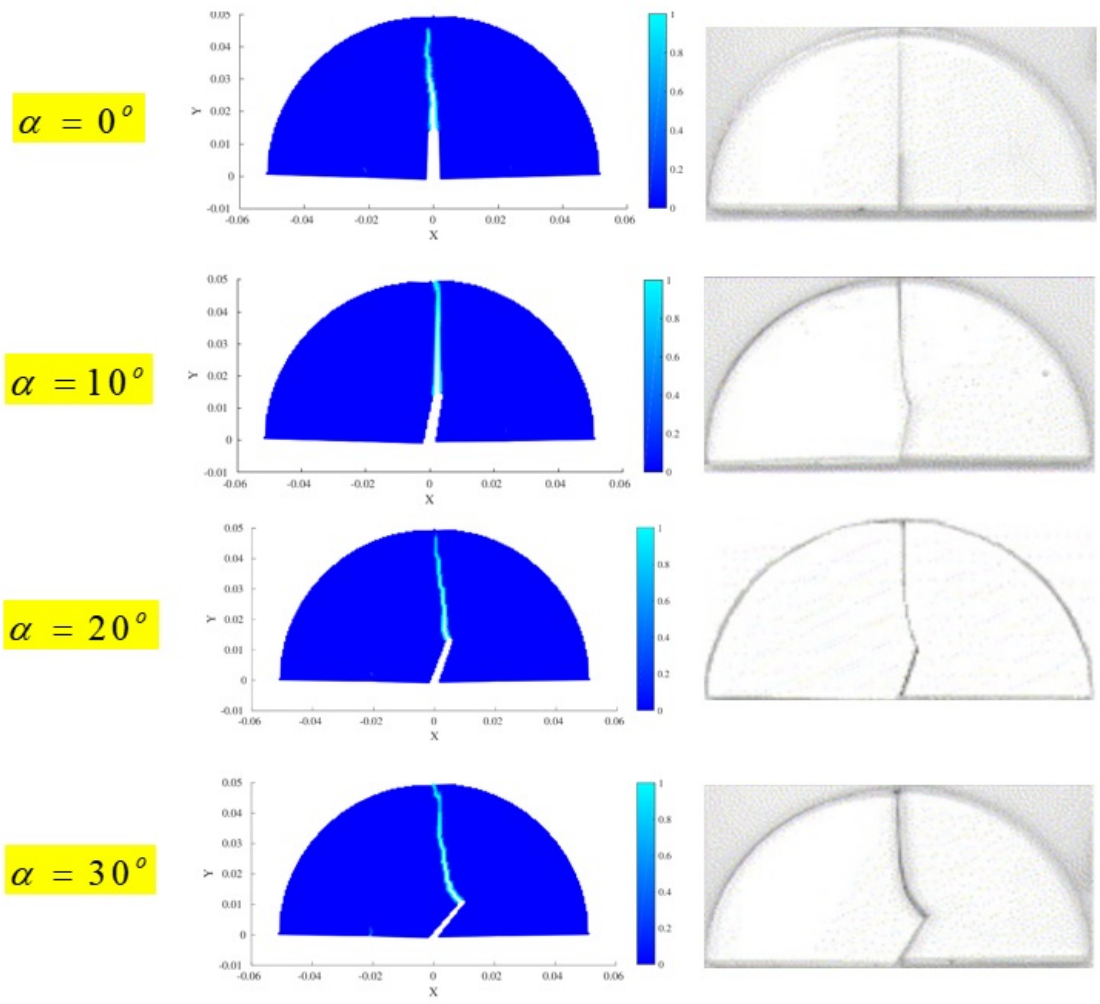

Figure 6.11: Crack trajectory in SCB specimen made of PMMA with initial crack and inclination angle of $\alpha = 0°, 10°, 20°, 30°$

of semi-circle. This is in agreement with the Ayatollahi's experiments[112] and Xie and Wang's reports [117] for SCB with length ratio $a/r = 0.3$. The mean values of experimental and theoretical fracture toughness along with their corresponding critical load are listed in table 6.2. The magnitude of the error for K_{IC}, K_{IIC} and P are relatively low, except at $\alpha = 20, 43$. According to the trend of P_c, it is expected to get a value more than 2.53 kN at $\alpha = 20$, but the experimental data is showing lower magnitude. Such inconsistency might be a result of manufacturing flaws or measurement errors. Note that Ayatollahi [112] has

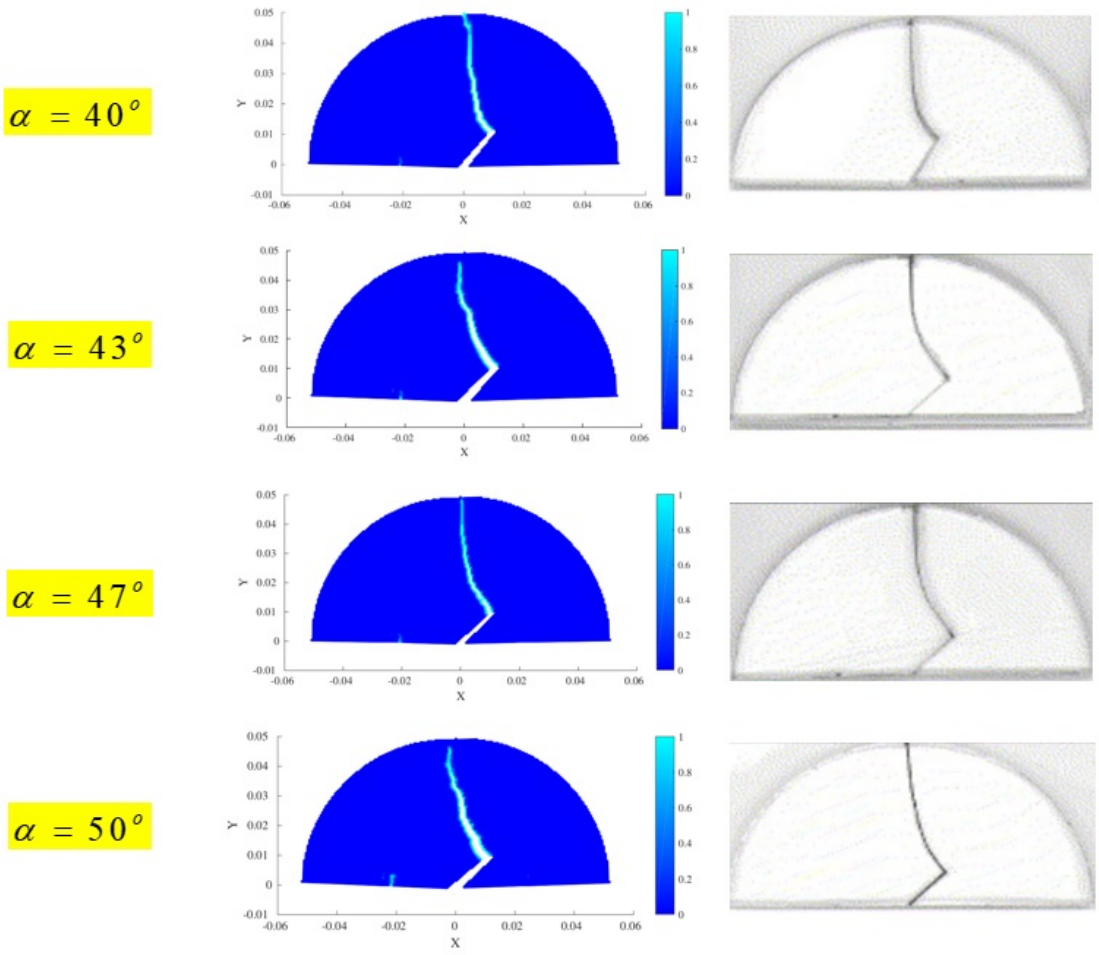

Figure 6.12: Crack trajectory in SCB specimen made of PMMA with initial crack and inclination angle of $\alpha = 40°, 43°, 47°, 50°$.

dropped these values from their graphical results to get a decent trend in their curve fitting. Fig. 6.13 and 6.14 are showing the theoretical and experimental fracture toughness of mode I and II for each specimen. The results are compared with the maximum tangential stress (MTS) method[118] and generalized MTS (GMTS) [119] that are commonly used in the analysis of mixed-mode fracture. Note that MTS only takes the first term (singular term) of the series expansion of tangential stress around the crack tip. However, GMTS includes singular and nonsingular terms of the series to predict the start of crack propagation. In both developments, the crack propagates along a direction perpendicular to the maximum

Table 6.2: Experimental and Numerical fracture results for SCB with a length ratio of $S/R = 0.43$ and $a/R = 0.3$ subjected to a three-point bending

	Experimental[112]			Theorical			Error %		
$\alpha(^\circ)$	K_I	K_{II}	$P_c\ (kN)$	K_I	K_{II}	$P_c\ (kN)$	K_I	K_{II}	$P_c\ (kN)$)
0	2.13	0.00	2.38	2.27	0.00	2.54	6.74	6.66	0.00
10	2.10	0.47	2.53	2.22	0.47	2.68	5.96	5.95	0.05
20	1.63	0.75	2.45	1.91	0.87	2.85	16.44	17.12	16.30
30	1.30	1.07	3.03	1.32	1.13	3.09	1.73	1.24	4.73
40	0.75	1.31	3.73	0.75	1.33	3.79	1.45	0.04	1.33
43	0.53	1.22	3.63	0.53	1.33	4.00	10.13	0.97	9.02
47	0.23	1.24	4.13	0.22	1.32	4.39	6.22	1.61	6.47
50	0.00	1.12	4.24	0.00	1.29	4.73	11.65	0.00	15.74

of the tangential stress, σ_θ. The simulation from current study predicts mode I fracture toughness at $\alpha = 10^\circ, 20^\circ, 40^\circ$ with better accuracy (see Fig. 6.13). It also performs better in determining the magnitude of mode II fracture toughness at $20^\circ, 30^\circ, 40^\circ$ in comparison to both conventional and generalized MTS [112] (see Fig. 6.14).

It is common practice to present the fracture toughness results from mixed mode loading in terms of normalized fracture toughness i.e. K_I/K_{Ic} and K_{II}/K_{Ic}. The mean value of experimental data [112] for pure mode I fracture toughness of PMMA is $2.1258MPa\sqrt{m}$. In Fig. 6.15, the simulation results of mode I and mode II fracture toughness are plotted along with the experimental data, MTS and GMTS simulation. Each of the green squares is showing an initial crack inclination angle (given in the table. 6.2) that starts from zero as we move on the curve from right to left. The red dash line is showing the average of the experimental value (red dots) for mode I and mode II normalized fracture toughness. It can be seen from the figure that the current study has better estimation than other two methods (MTS, GMTS), especially, once the specimen is undergoing pure mode II (i.e., $K_I = 0$). This is consistent with the studies on mixed mode I/II strain-based criteria were developed by Mirsayar to predict onset of fracture and crack propagation angle in different specimen geometries and materials. [120, 121, 122, 123, 124, 125, 126]

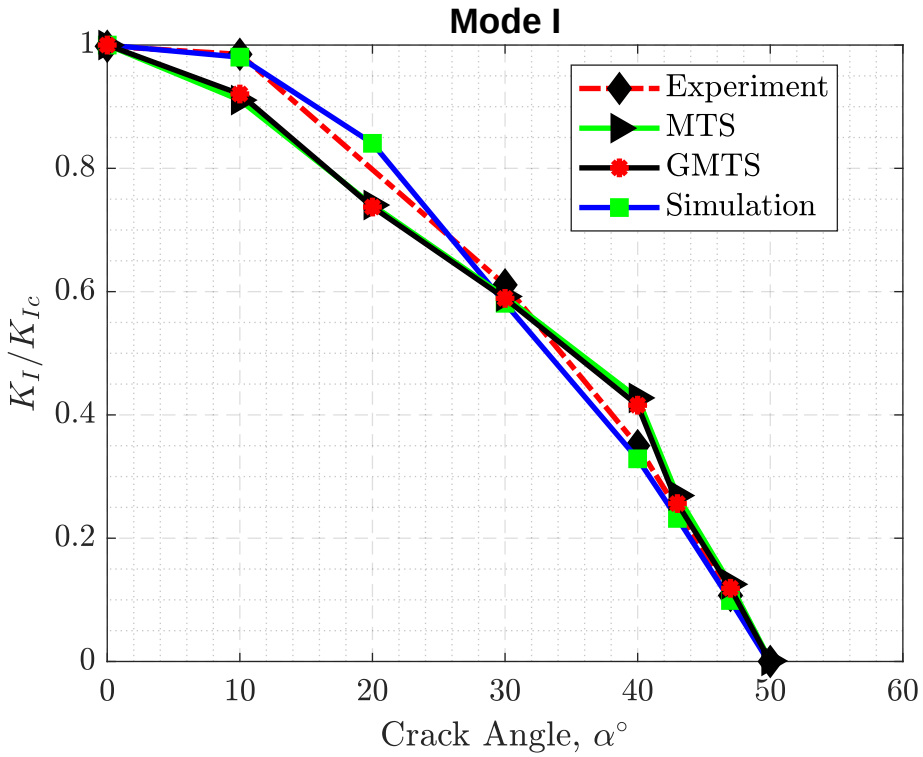

Figure 6.13: Comparison of the mode I normalized fracture toughness of different crack angle obtained from experiment and conventional criteria with the predicted results from the present study

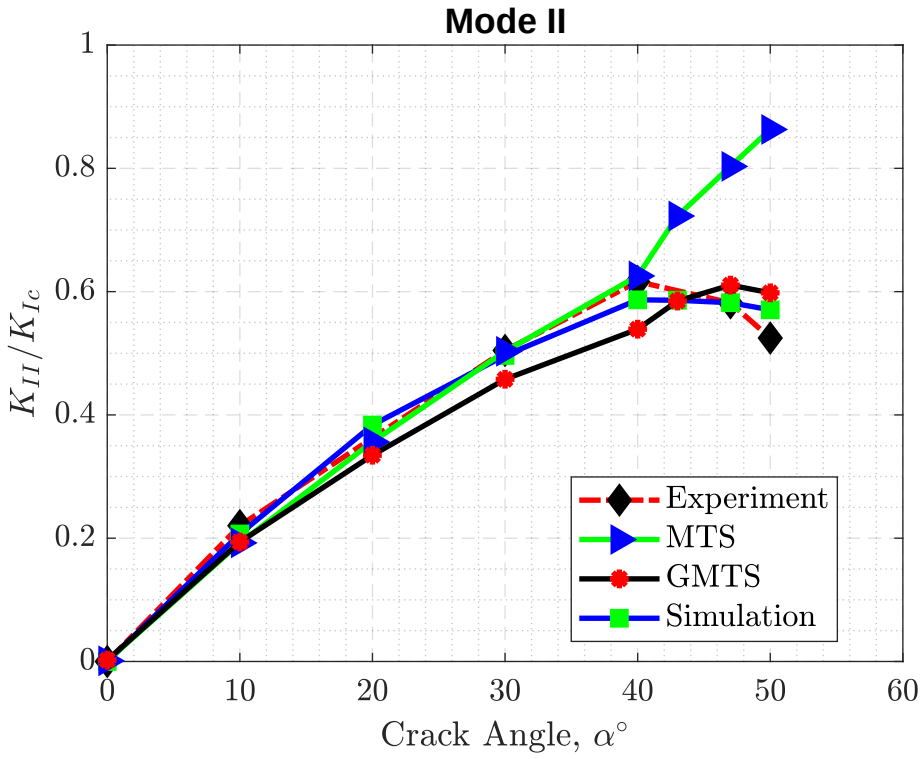

Figure 6.14: Comparison of the mode II normalized fracture toughness of different crack angle obtained from experiment and conventional criteria with the predicted results from the present study

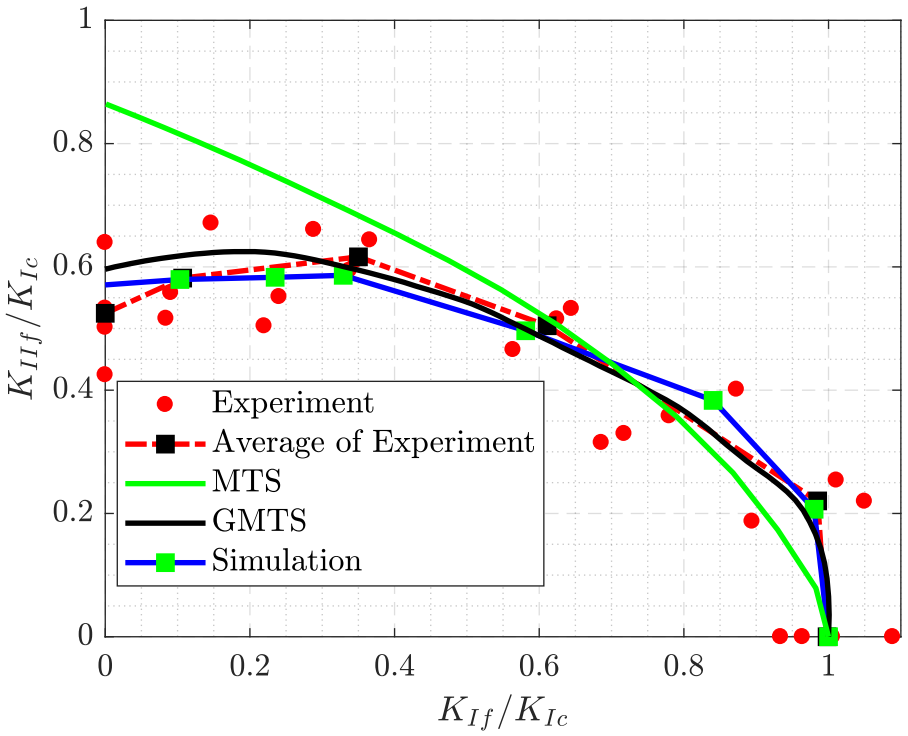

Figure 6.15: Comparison of mode I/II normalized fracture toughness from the experiment and conventional criteria with the predicted results from the present study

7. SUMMARY AND CONCLUSIONS, AND FUTURE WORK

7.1 Summary and Concluding Remarks

The dissertation mainly consists of three interconnected developments: (i) Tridynamics; a Lagrangian-based approach to macroscopic modeling, (ii) A derivative-free upscaled theory for analysis of defects, and (iii) Unification of local and nonlocal models within a stable formulation. In the following, a brief review of each development is presented:

In Section 1, an general introduction on the nonlocal theories and motivation to develop a new nonlocal framework has been given.

In Section 2, a discrete Lagrangian-based approach for dynamic systems at a length scale of interest is presented. Another aspect of the present work is the introduction of a triangular surface element as the basic unit to characterize interactions between particles, which might be helpful in incorporating finer length scale information. The discrete framework is applied to derive equivalent Euler–Bernoulli beam model. The numerical evidence suggests that the present equation models beam as a stiffer system in comparison to its classical version. Numerical simulations for crack propagation on isotropic and anisotropic materials have also been included to illustrate the utility of the present approach.

In Section 3 and 4, we provide the tridynamic model of Timoshenko beam and FSDT plate using the a meaningful kinematic of the element. The governing equations have been derived by constructing the Lagrangian of the system. The dispersion analysis of the beam model were carried out and the results were compared with the classical and peridynamics models. Unlike the other approaches, the developed model predicts a nonlinear wave frequency for the first mode of vibration which is in agreement with the molecular dynamics model.

In Section 5, a rationally grounded stochastic projection principle is proposed for upscaling atomistic information, thus yielding non-trivial directional information to evolve the state variables in a discrete or continuous setting. For completeness, some details on the stochastic

projection used to develop the proposed method are included in the supplementary material. The upscaling principle is strictly non-local and allows one to write the microstructure dependent upscaled law without any spatial derivative, such as the deformation gradient in the Cauchy–Born rule. The upscaled simulation of the fractured CNT shows the effect of chirality – perhaps a first-of-its-kind result.

While the SWCNT modeling problem is analyzed as an illustration, it is likely that the upscaling technique should find applications in myriad problems involving multiple scales, wherein phenomena at the microscopic scales non-trivially affect those at a macroscopic level. With its derivative-free directional term drawing upon the microscopic information and enabling the construction of a discrete or continuum macroscopic model, the approach perhaps holds the key to a resolution of the discrete-to-continuum conundrum whilst offering a modeling route to designing engineered material with a targeted response via appropriate inversion. The authors intend to explore this important application elsewhere.

In Section 6, a new nonlocal derivative-free framework based on the discrete Cauchy-Born rule was formulated. The new approach granted a systematic procedure to generate all nonlocal version of classical continuum definitions such as deformation gradient, strain, and stresses from the local counterparts. For such a purpose, a compact matrix was constructed to transform surface-based forces to body-based ones. The new integral form of equation enables us to investigate mechanical problems having a discontinuity in the field variables. Instead of using conventional definition of bond, we introduced a more generic term to represent micro-interaction of particles. As an application of this study, a mixed-mode fracture analysis of PMMA semi-circular bend specimens was done. The results showed a remarkable improvement in prediction of fracture toughness in comparison to MTS method. Although GMTS performed much better than MTS, the simulation results showed that the new development still has a better determination of mode II fracture toughness compared to GMTS. Finally, a comparison of the experimental observation with the simulated crack trajectory confirms an acceptable agreement.

7.2 Further Work

Through this dissertation, we have shown the application of the developed framework in analyses of problems, which involves nonlocal effects or discontinuities in the field variable. The promising results bring several exciting problems that could be carried out in the future study:

All developed models in this study neglect the energy dissipation in the system. This is due to the fact that the interactions of material particles were defined through elastic bonds (Section 2, 3 and 4). However, they could be revised by introducing parallel and series combination of springs and dash-pot to represent both elastic and viscous behaviors. The revision may help to develop the well-known viscoelastic models such as Maxwell, Kelvin-Voigt, and Standard Solid Model.

The presented beam and plate models in Sections 2, 3 and 4 could be extended for inhomogeneous materials such as functionally graded or composite materials through constructing the forces A, B, and C. Noting that these forces are developed so that it accounts for anisotropic materials. But it could be still challenging to determine nonlocal material properties. Also, to model fracture and failure in FSDT plate, it is required to calculate the critical stretch which remained unsolved in this study.

All problems through this study have been analyzed under low-speed loading (LSL) condition. Noting that the algorithm, given in Section 6 shows stability under LSL condition. Further study could be done to investigate the stability of the method for problems under high-speed loading such as impact.

REFERENCES

[1] S. Plimpton, "Fast parallel algorithms for short-range molecular dynamics," *Journal of Computational Physics*, vol. 117, no. 1, pp. 1–19, 1995.

[2] L. Kalé, R. Skeel, M. Bhandarkar, R. Brunner, A. Gursoy, N. Krawetz, J. Phillips, A. Shinozaki, K. Varadarajan, and K. Schulten, "Namd2: greater scalability for parallel molecular dynamics," *Journal of Computational Physics*, vol. 151, no. 1, pp. 283–312, 1999.

[3] A. C. Eringen, "Nonlocal polar elastic continua," *International Journal of Engineering Science*, vol. 10, no. 1, pp. 1–16, 1972.

[4] S. Sarkar, S. R. Chowdhury, D. Roy, and R. M. Vasu, "Internal noise-driven generalized langevin equation from a nonlocal continuum model," *Physical Review E*, vol. 92, no. 2, p. 022150, 2015.

[5] A. C. Eringen, "On differential euations of nonlocal elasticity and solutions of screw dislocation and surface waves," *Journal of Applied Physics*, vol. 54, no. 9, pp. 4703–4710, 1983.

[6] P. Lu, P. Zhang, H. Lee, C. Wang, and J. N. Reddy, "Non-local elastic plate theories," *Proceedings of the Royal Society of London A: Mathematical, Physical and Engineering Sciences*, vol. 463, no. 2088, pp. 3225–3240, 2007.

[7] J. N. Reddy, J. Romanoff, and J. A. Loya, "Nonlinear finite element analysis of functionally graded circular plates with modified couple stress theory," *European Journal of Mechanics-A/Solids*, vol. 56, pp. 92–104, 2016.

[8] S. Sarkar and J. N. Reddy, "Exploring the source of non-locality in the euler–bernoulli and timoshenko beam models," *International Journal of Engineering Science*, vol. 104, pp. 110–115, 2016.

[9] A. Samaei, S. Abbasion, and M. Mirsayar, "Buckling analysis of a single-layer graphene sheet embedded in an elastic medium based on nonlocal mindlin plate theory," *Mechanics Research Communications*, vol. 38, no. 7, pp. 481–485, 2011.

[10] J. N. Reddy, "Nonlocal theories for bending, buckling and vibration of beams," *International Journal of Engineering Science*, vol. 45, no. 2, pp. 288–307, 2007.

[11] R. Jastrow, "Many-body problem with strong forces," *Physical Review*, vol. 98, no. 5, p. 1479, 1955.

[12] M. Finnis and J. Sinclair, "A simple empirical n-body potential for transition metals," *Philosophical Magazine A*, vol. 50, no. 1, pp. 45–55, 1984.

[13] D. W. Brenner, O. A. Shenderova, J. A. Harrison, S. J. Stuart, B. Ni, and S. B. Sinnott, "A second-generation reactive empirical bond order (rebo) potential energy expression for hydrocarbons," *Journal of Physics: Condensed Matter*, vol. 14, no. 4, p. 783, 2002.

[14] J. Hahn and H.-R. Trebin, "Molecular dynamics of covalent crystals," in *High Performance Computing in Science and Engineering'99*, pp. 92–99, Springer, 2000.

[15] J. Anta, E. Lomba, and M. Lombardero, "Exploring the influence of three-body classical dispersion forces on phase equilibria of simple fluids: An integral-equation approach," *Physical Review E*, vol. 49, no. 1, p. 402, 1994.

[16] G. Marcelli and R. J. Sadus, "A link between the two-body and three-body interaction energies of fluids from molecular simulation," *The Journal of Chemical Physics*, vol. 112, no. 14, pp. 6382–6385, 2000.

[17] L. Wang and R. J. Sadus, "Effect of three-body interactions on the vapor-liquid phase equilibria of binary fluid mixtures," *The Journal of Chemical Physics*, vol. 125, no. 7, p. 074503, 2006.

[18] L. Wang and R. J. Sadus, "Three-body interactions and solid-liquid phase equilibria: Application of a molecular dynamics algorithm," *Physical Review E*, vol. 74, no. 3, p. 031203, 2006.

[19] G. Zhao, M. B. Carson, and H. Lu, "Prediction of specific protein-dna recognition by knowledge-based two-body and three-body interaction potentials," in *2007 29th Annual International Conference of the IEEE Engineering in Medicine and Biology Society*, pp. 5017–5020, IEEE, 2007.

[20] S. A. Silling, "Reformulation of elasticity theory for discontinuities and long-range forces," *Journal of the Mechanics and Physics of Solids*, vol. 48, no. 1, pp. 175–209, 2000.

[21] B. Kilic and E. Madenci, "Peridynamic theory for thermomechanical analysis," *Advanced Packaging, IEEE Transactions on*, vol. 33, no. 1, pp. 97–105, 2010.

[22] W. Gerstle, S. Silling, D. Read, V. Tewary, and R. Lehoucq, "Peridynamic simulation of electromigration," *Comput Mater Continua*, vol. 8, no. 2, pp. 75–92, 2008.

[23] F. Bobaru and M. Duangpanya, "A peridynamic formulation for transient heat conduction in bodies with evolving discontinuities," *Journal of Computational Physics*, vol. 231, no. 7, pp. 2764–2785, 2012.

[24] S. A. Silling, M. Epton, O. Weckner, J. Xu, and E. Askari, "Peridynamic states and constitutive modeling," *Journal of Elasticity*, vol. 88, no. 2, pp. 151–184, 2007.

[25] T. L. Warren, S. A. Silling, A. Askari, O. Weckner, M. A. Epton, and J. Xu, "A non-ordinary state-based peridynamic method to model solid material deformation and fracture," *International Journal of Solids and Structures*, vol. 46, no. 5, pp. 1186–1195, 2009.

[26] B. Kilic, *Peridynamic theory for progressive failure prediction in homogeneous and heterogeneous materials*. ProQuest, 2008.

[27] M. J. Taylor, *Numerical simulation of thermo-elasticity, inelasticity and rupture in membrane theory*. University of California, Berkeley, 2008.

[28] J. T. Foster, S. A. Silling, and W. W. Chen, "Viscoplasticity using peridynamics," *International Journal for Numerical Methods in Engineering*, vol. 81, no. 10, pp. 1242–1258, 2010.

[29] Y. D. Ha and F. Bobaru, "Characteristics of dynamic brittle fracture captured with peridynamics," *Engineering Fracture Mechanics*, vol. 78, no. 6, pp. 1156–1168, 2011.

[30] J. Xu, A. Askari, O. Weckner, and S. Silling, "Peridynamic analysis of impact damage in composite laminates," *Journal of Aerospace Engineering*, vol. 21, no. 3, pp. 187–194, 2008.

[31] A. Agwai, I. Guven, and E. Madenci, "Predicting crack propagation with peridynamics: a comparative study," *International Journal of Fracture*, vol. 171, no. 1, pp. 65–78, 2011.

[32] M. Breitenfeld, P. Geubelle, O. Weckner, and S. Silling, "Non-ordinary state-based peridynamic analysis of stationary crack problems," *Computer Methods in Applied Mechanics and Engineering*, vol. 272, pp. 233–250, 2014.

[33] S. Sarkar, M. Nowruzpour, J. Reddy, and A. Srinivasa, "A discrete lagrangian based direct approach to macroscopic modelling," *Journal of the Mechanics and Physics of Solids*, vol. 98, pp. 172–180, 2017.

[34] M. Nowruzpour and J. Reddy, "Unification of local and nonlocal models within a stable integral formulation for analysis of defects," *International Journal of Engineering Science*, vol. 132, pp. 45–59, 2018.

[35] M. Nowruzpour, S. Sarkar, J. Reddy, and D. Roy, "A derivative-free upscaled theory for analysis of defects," *Journal of the Mechanics and Physics of Solids*, vol. 122, pp. 489–501, 2019.

[36] V. I. Arnol'd, *Mathematical methods of classical mechanics*, vol. 60. Springer Science & Business Media, 2013.

[37] J. N. Reddy, *Energy Principles and Variational Methods in Applied Mechanics*. John Wiley & Sons (3rd ed. to appear), 2002.

[38] I. Newton, D. Bernoulli, C. MacLaurin, and L. Euler, *Philosophiae naturalis principia mathematica*, vol. 1. excudit G. Brookman; impensis TT et J. Tegg, Londini, 1833.

[39] F. Riewe, "Nonconservative lagrangian and hamiltonian mechanics," *Physical Review E*, vol. 53, no. 2, p. 1890, 1996.

[40] F. Riewe, "Mechanics with fractional derivatives," *Physical Review E*, vol. 55, no. 3, p. 3581, 1997.

[41] A. C. Eringen, *Continuum Physics. Vol. Iii: Mixtures and Em Field Theories*. Academic Press, 1976.

[42] C. Diyaroglu, E. Oterkus, S. Oterkus, and E. Madenci, "Peridynamics for bending of beams and plates with transverse shear deformation," *International Journal of Solids and Structures*, vol. 69, pp. 152–168, 2015.

[43] O. Serrano, R. Zaera, J. Fernández-Sáez, and M. Ruzzene, "Generalized continuum model for the analysis of nonlinear vibrations of taut strings with microstructure," *International Journal of Solids and Structures*, vol. 164, pp. 157–167, 2019.

[44] S. Iijima and T. Ichihashi, "Single-shell carbon nanotubes of 1-nm diameter," *Nature*, vol. 363, no. 6430, pp. 603–605, 1993.

[45] M. J. Treacy, T. Ebbesen, and J. Gibson, "Exceptionally high young's modulus observed for individual carbon nanotubes," *Nature*, vol. 381, no. 6584, p. 678, 1996.

[46] A. Krishnan, E. Dujardin, T. Ebbesen, P. Yianilos, and M. Treacy, "Young's modulus of single-walled nanotubes," *Physical Review B*, vol. 58, no. 20, p. 14013, 1998.

[47] E. Hernandez, C. Goze, P. Bernier, and A. Rubio, "Elastic properties of c and b x c y n z composite nanotubes," *Physical Review Letters*, vol. 80, no. 20, p. 4502, 1998.

[48] L. Ci, J. Suhr, V. Pushparaj, X. Zhang, and P. Ajayan, "Continuous carbon nanotube reinforced composites," *Nano Letters*, vol. 8, no. 9, pp. 2762–2766, 2008.

[49] C. De las Casas and W. Li, "A review of application of carbon nanotubes for lithium ion battery anode material," *Journal of Power Sources*, vol. 208, pp. 74–85, 2012.

[50] W. Zhang, Z. Zhang, and Y. Zhang, "The application of carbon nanotubes in target drug delivery systems for cancer therapies," *Nanoscale Research Letters*, vol. 6, no. 1, p. 555, 2011.

[51] G. Yu, M. Xue, Z. Zhang, J. Li, C. Han, and F. Huang, "A water-soluble pillar [6] arene: synthesis, host–guest chemistry, and its application in dispersion of multiwalled carbon nanotubes in water," *Journal of the American Chemical Society*, vol. 134, no. 32, pp. 13248–13251, 2012.

[52] S. Nardecchia, D. Carriazo, M. L. Ferrer, M. C. Gutiérrez, and F. del Monte, "Three dimensional macroporous architectures and aerogels built of carbon nanotubes and/or graphene: synthesis and applications," *Chemical Society Reviews*, vol. 42, no. 2, pp. 794–830, 2013.

[53] R. Khare and S. Bose, "Carbon nanotube based composites-a review," *Journal of Minerals and Materials Characterization and Engineering*, vol. 4, no. 01, p. 31, 2005.

[54] U. Narkiewicz, I. Peech, Z. Rosaniec, M. Kwiatkowska, and W. Arabczyk, "Preparation of nanocrystalline iron–carbon materials as fillers for polymers," *Nanotechnology*, vol. 18, no. 40, p. 405601, 2007.

[55] M. H. Naderi, S. Prakash, and J. Silva-Martinez, "Operational transconductance amplifier with class-b slew-rate boosting for fast high-performance switched-capacitor circuits," *IEEE Transactions on Circuits and Systems I: Regular Papers*, vol. 65, no. 11, pp. 3769–3779, 2018.

[56] V. Natarajan, M. H. Naderi, and J. Silva-Martinez, "Low noise rf quadrature vco using tail-switch network-based coupling in 40 nm cmos," in *2018 IEEE Custom Integrated Circuits Conference (CICC)*, pp. 1–4, IEEE, 2018.

[57] A. M. Akbarzadeh, A. Moosavi, and A. Moghimi Kheirabadi, "Dewetting of evaporating thin films over nanometer-scale topographies," *Physical Review E*, vol. 90, no. 1, p. 012409, 2014.

[58] K. Patil, S. Rashidi, H. Wang, and W. Wei, "Recent progress of graphene-based photoelectrode materials for dye-sensitized solar cells," *International Journal of Photoenergy*, vol. 2019, 2019.

[59] S. Rashidi, Z. Zheng, and B. Li, "Enhancement of discharged energy density of poly (ethylene oxide) by soy protein isolate," *Journal of Applied Polymer Science*, vol. 134, no. 34, p. 45214, 2017.

[60] Z. Zheng, D. Ma, S. Rashidi, and B. Li, "Study of denaturation and composition-dependent poly (ethylene oxide)–soy protein interactions: Structures and dielectric polarization," *Journal of Applied Polymer Science*, vol. 135, no. 31, p. 46561, 2018.

[61] S. Rashidi, A. Caringula, A. Nguyen, I. Obi, C. Obi, and W. Wei, "Recent progress in mos 2 for solar energy conversion applications," *Frontiers in Energy*, pp. 1–18, 2019.

[62] A. Vashisth and M. Mirsayar, "A combined atomistic-continuum study on the temperature effects on interfacial fracture in *SiC SiO2* composites," *Theoretical and Applied Fracture Mechanics*, vol. 105, p. 102399, 2020.

[63] M. Arroyo and T. Belytschko, "An atomistic-based finite deformation membrane for single layer crystalline films," *Journal of the Mechanics and Physics of Solids*, vol. 50, no. 9, pp. 1941–1977, 2002.

[64] X. Guo, J. Wang, and H. Zhang, "Mechanical properties of single-walled carbon nanotubes based on higher order cauchy–born rule," *International Journal of Solids and Structures*, vol. 43, no. 5, pp. 1276–1290, 2006.

[65] J. Z. Yang and E. Weinan, "Generalized cauchy-born rules for elastic deformation of sheets, plates, and rods: Derivation of continuum models from atomistic models," *Physical Review B*, vol. 74, no. 18, p. 184110, 2006.

[66] R. Sunyk and P. Steinmann, "On higher gradients in continuum-atomistic modelling," *International Journal of Solids and Structures*, vol. 40, no. 24, pp. 6877–6896, 2003.

[67] G. Kallianpur and C. Striebel, "Estimation of stochastic systems: Arbitrary system process with additive white noise observation errors," *The Annals of Mathematical Statistics*, vol. 39, no. 3, pp. 785–801, 1968.

[68] G. Kallianpur, *Stochastic filtering theory*, vol. 13. Springer Science & Business Media, 2013.

[69] I. V. Girsanov, "On transforming a certain class of stochastic processes by absolutely continuous substitution of measures," *Theory of Probability & Its Applications*, vol. 5, no. 3, pp. 285–301, 1960.

[70] H. J. Kushner, "On the differential equations satisfied by conditional probablitity densities of markov processes, with applications," *Journal of the Society for Industrial and Applied Mathematics, Series A: Control*, vol. 2, no. 1, pp. 106–119, 1964.

[71] D. Roy and G. V. Rao, *Stochastic Dynamics, Filtering and Optimization*. Cambridge University Press, 2017.

[72] Y. Sun and K. M. Liew, "The buckling of single-walled carbon nanotubes upon bending: the higher order gradient continuum and mesh-free method," *Computer Methods in Applied Mechanics and Engineering*, vol. 197, no. 33, pp. 3001–3013, 2008.

[73] J. Tersoff, "New empirical approach for the structure and energy of covalent systems," *Physical Review B*, vol. 37, no. 12, p. 6991, 1988.

[74] E. B. Tadmor, M. Ortiz, and R. Phillips, "Quasicontinuum analysis of defects in solids," *Philosophical Magazine A*, vol. 73, no. 6, pp. 1529–1563, 1996.

[75] E. Tadmor, G. Smith, N. Bernstein, and E. Kaxiras, "Mixed finite element and atomistic formulation for complex crystals," *Physical Review B*, vol. 59, no. 1, p. 235, 1999.

[76] R. E. Miller and E. B. Tadmor, "The quasicontinuum method: Overview, applications and current directions," *Journal of Computer-Aided Materials Design*, vol. 9, no. 3, pp. 203–239, 2002.

[77] A. M. Kheirabadi, A. Moosavi, and A. M. Akbarzadeh, "Nanofluidic transport inside carbon nanotubes," *Journal of Physics D: Applied Physics*, vol. 47, p. 065304, jan 2014.

[78] W. Voigt, "Theoretische studien fiber die elastizit˜ itsverh˜ iltnisse der kristalle," *Abh. Geschichte Wissenschaften*, vol. 34, 1887.

[79] A. C. Eringen, "Linear theory of nonlocal elasticity and dispersion of plane waves," *International Journal of Engineering Science*, vol. 10, no. 5, pp. 425–435, 1972.

[80] A. C. Eringen, C. Speziale, and B. Kim, "Crack-tip problem in non-local elasticity," *Journal of the Mechanics and Physics of Solids*, vol. 25, no. 5, pp. 339–355, 1977.

[81] N. Ari and A. C. Eringen, "Nonlocal stress field at griffith crack.," tech. rep., PRINCETON UNIV NJ DEPT OF CIVIL AND GEOLOGICAL ENGINEERING, 1980.

[82] H. Elliott, "An analysis of the conditions for rupture due to griffith cracks," *Proceedings of the Physical Society*, vol. 59, no. 2, p. 208, 1947.

[83] D. Rogula, "Introduction to nonlocal theory of material media," in *Nonlocal Theory of Material Media*, pp. 123–222, Springer, 1982.

[84] H. Asadi, M. Taeibi-Rahni, A. M. Akbarzadeh, K. Javadi, and G. Ahmadi, "Investigation of hydrodynamically dominated membrane rupture, using smoothed particle hydrodynamics–finite element method," *Fluids*, vol. 4, no. 3, p. 149, 2019.

[85] M. Tajdari and B. L. Tai, "Modeling of brittle and ductile materials drilling using smoothed-particle hydrodynamics," in *ASME 2016 11th international manufacturing*

science and engineering conference, American Society of Mechanical Engineers Digital Collection, 2016.

[86] B. Takabi, M. Tajdari, and B. L. Tai, "Numerical study of smoothed particle hydrodynamics method in orthogonal cutting simulations–effects of damage criteria and particle density," *Journal of Manufacturing Processes*, vol. 30, pp. 523–531, 2017.

[87] Y. Mei, M. Tajderi, and S. Goenezen, "Regularizing biomechanical maps for partially known material properties," *International Journal of Applied Mechanics*, vol. 9, no. 02, p. 1750020, 2017.

[88] S. Ghosh and M. Arroyo, "An atomistic-based foliation model for multilayer graphene materials and nanotubes," *Journal of the Mechanics and Physics of Solids*, vol. 61, no. 1, pp. 235–253, 2013.

[89] T. Chang, "A molecular based anisotropic shell model for single-walled carbon nanotubes," *Journal of the Mechanics and Physics of Solids*, vol. 58, no. 9, pp. 1422–1433, 2010.

[90] X. Zhang, K. Jiao, P. Sharma, and B. Yakobson, "An atomistic and non-classical continuum field theoretic perspective of elastic interactions between defects (force dipoles) of various symmetries and application to graphene," *Journal of the Mechanics and Physics of Solids*, vol. 54, no. 11, pp. 2304–2329, 2006.

[91] R. Maranganti and P. Sharma, "A novel atomistic approach to determine strain-gradient elasticity constants: tabulation and comparison for various metals, semiconductors, silica, polymers and the (ir) relevance for nanotechnologies," *Journal of the Mechanics and Physics of Solids*, vol. 55, no. 9, pp. 1823–1852, 2007.

[92] A. Mattoni, L. Colombo, and F. Cleri, "Atomic scale origin of crack resistance in brittle fracture," *Physical Review Letters*, vol. 95, no. 11, p. 115501, 2005.

[93] J. J. Remmers, R. de Borst, and A. Needleman, "The simulation of dynamic crack propagation using the cohesive segments method," *Journal of the Mechanics and Physics of Solids*, vol. 56, no. 1, pp. 70–92, 2008.

[94] M. J. Buehler, A. C. van Duin, and W. A. Goddard III, "Multiparadigm modeling of dynamical crack propagation in silicon using a reactive force field," *Physical Review Letters*, vol. 96, no. 9, p. 095505, 2006.

[95] H. Yukutake, "Fracturing process of granite inferred from measurements of spatial and temporal variations in velocity during triaxial deformations," *Journal of Geophysical Research: Solid Earth*, vol. 94, no. B11, pp. 15639–15651, 1989.

[96] T. Mura, "Micromechanics: overall properties of heterogeneous solids," 1993.

[97] M. Mirsayar, "On fracture of kinked interface cracks–the role of t-stress," *Materials & Design*, vol. 61, pp. 117–123, 2014.

[98] M. Mirsayar, "T-strain effects in kinked interfacial fracture of bonded composites," *Theoretical and Applied Fracture Mechanics*, vol. 104, p. 102381, 2019.

[99] S. L. Kramer, A. Jones, A. Mostafa, B. Ravaji, T. Tancogne-Dejean, C. C. Roth, M. G. Bandpay, K. Pack, J. T. Foster, M. Behzadinasab, *et al.*, "The third sandia fracture challenge: predictions of ductile fracture in additively manufactured metal," *International Journal of Fracture*, vol. 218, no. 1-2, pp. 5–61, 2019.

[100] B. Ravaji, S. Mashadizade, and A. Hashemi, "Introducing optimized validated meshing system for wellbore stability analysis using 3d finite element method," *Journal of Natural Gas Science and Engineering*, vol. 53, pp. 74–82, 2018.

[101] S. A. Silling, M. Zimmermann, and R. Abeyaratne, "Deformation of a peridynamic bar," *Journal of Elasticity*, vol. 73, no. 1-3, pp. 173–190, 2003.

[102] S. Silling and R. Lehoucq, "Peridynamic theory of solid mechanics," *Advances in Applied Mechanics*, vol. 44, pp. 73–168, 2010.

[103] J. A. Mitchell, "A nonlocal ordinary state-based plasticity model for peridynamics.," tech. rep., Sandia National Laboratories (SNL-NM), Albuquerque, NM (United States), 2011.

[104] C. Wu and B. Ren, "A stabilized non-ordinary state-based peridynamics for the nonlocal ductile material failure analysis in metal machining process," *Computer Methods in Applied Mechanics and Engineering*, vol. 291, pp. 197–215, 2015.

[105] J. Amani, E. Oterkus, P. Areias, G. Zi, T. Nguyen-Thoi, and T. Rabczuk, "A non-ordinary state-based peridynamics formulation for thermoplastic fracture," *International Journal of Impact Engineering*, vol. 87, pp. 83–94, 2016.

[106] X.-P. Zhou and Y.-T. Wang, "Numerical simulation of crack propagation and coalescence in pre-cracked rock-like brazilian disks using the non-ordinary state-based peridynamics," *International Journal of Rock Mechanics and Mining Sciences*, vol. 89, pp. 235–249, 2016.

[107] S. A. Silling and E. Askari, "A meshfree method based on the peridynamic model of solid mechanics," *Computers & Structures*, vol. 83, no. 17, pp. 1526–1535, 2005.

[108] M. D. Kuruppu and K. P. Chong, "Fracture toughness testing of brittle materials using semi-circular bend (scb) specimen," *Engineering Fracture Mechanics*, vol. 91, pp. 133–150, 2012.

[109] C. El Mir, K. Ramesh, and M. Delbo, "The efficiency of thermal fatigue in regolith generation on small airless bodies," *Icarus*, vol. 333, pp. 356–370, 2019.

[110] B. Ravaji, V. Alí-Lagoa, M. Delbo, and J. W. Wilkerson, "Unraveling the mechanics of thermal stress weathering: Rate-effects, size-effects, and scaling laws," *Journal of Geophysical Research: Planets*.

[111] M. Ayatollahi and M. Aliha, "Wide range data for crack tip parameters in two disc-type specimens under mixed mode loading," *Computational Materials Science*, vol. 38, no. 4, pp. 660–670, 2007.

[112] M. Ayatollahi, M. Aliha, and M. Hassani, "Mixed mode brittle fracture in pmma—an experimental study using scb specimens," *Materials Science and Engineering: A*, vol. 417, no. 1-2, pp. 348–356, 2006.

[113] L. Verlet, "Computer" experiments" on classical fluids. i. thermodynamical properties of lennard-jones molecules," *Physical Review*, vol. 159, no. 1, p. 98, 1967.

[114] W. C. Swope, H. C. Andersen, P. H. Berens, and K. R. Wilson, "A computer simulation method for the calculation of equilibrium constants for the formation of physical clusters of molecules: Application to small water clusters," *The Journal of Chemical Physics*, vol. 76, no. 1, pp. 637–649, 1982.

[115] S. Maiti and K. Prasad, "A study on the theories of unstable crack extension for the prediction of crack trajectories," *International Journal of Solids and Structures*, vol. 16, no. 6, pp. 563–574, 1980.

[116] J. Oliver, I. Dias, and A. E. Huespe, "Crack-path field and strain-injection techniques in computational modeling of propagating material failure," *Computer Methods in Applied Mechanics and Engineering*, vol. 274, pp. 289–348, 2014.

[117] Y. Xie, P. Cao, J. Jin, and M. Wang, "Mixed mode fracture analysis of semi-circular bend (scb) specimen: A numerical study based on extended finite element method," *Computers and Geotechnics*, vol. 82, pp. 157–172, 2017.

[118] F. Erdogan and G. Sih, "On the crack extension in plates under plane loading and transverse shear," *Journal of Basic Engineering*, vol. 85, no. 4, pp. 519–525, 1963.

[119] D. Smith, M. Ayatollahi, and M. Pavier, "The role of t-stress in brittle fracture for linear elastic materials under mixed-mode loading," *Fatigue & Fracture of Engineering Materials & Structures*, vol. 24, no. 2, pp. 137–150, 2001.

[120] M. Mirsayar, "Mixed mode fracture analysis using extended maximum tangential strain criterion," *Materials & Design*, vol. 86, pp. 941–947, 2015.

[121] M. Mirsayar, F. Berto, M. Aliha, and P. Park, "Strain-based criteria for mixed-mode fracture of polycrystalline graphite," *Engineering Fracture Mechanics*, vol. 156, pp. 114–123, 2016.

[122] M. Mirsayar, "On fracture analysis of dental restorative materials under combined tensile-shear loading," *Theoretical and Applied Fracture Mechanics*, vol. 93, pp. 170–176, 2018.

[123] M. Mirsayar, A. Razmi, M. Aliha, and F. Berto, "Emtsn criterion for evaluating mixed mode i/ii crack propagation in rock materials," *Engineering Fracture Mechanics*, vol. 190, pp. 186–197, 2018.

[124] M. Mirsayar, A. Razmi, and F. Berto, "Tangential strain-based criteria for mixed-mode i/ii fracture toughness of cement concrete," *Fatigue & Fracture of Engineering Materials & Structures*, vol. 41, no. 1, pp. 129–137, 2018.

[125] M. Mirsayar and P. Park, "Mixed mode brittle fracture analysis of high strength cement mortar using strain-based criteria," *Theoretical and Applied Fracture Mechanics*, vol. 86, pp. 233–238, 2016.

[126] M. Mirsayar, "On the low temperature mixed mode fracture analysis of asphalt binder–theories and experiments," *Engineering Fracture Mechanics*, vol. 186, pp. 181–194, 2017.

[127] M. E. Gurtin, *An introduction to continuum mechanics*, vol. 158. Academic press, 1982.

[128] M. Mohammadsalehi, O. Zargar, and M. Baghani, "Study of non-uniform viscoelastic nanoplates vibration based on nonlocal first-order shear deformation theory," *Meccanica*, vol. 52, no. 4-5, pp. 1063–1077, 2017.

[129] M. H. Jalali, O. Zargar, and M. Baghani, "Size-dependent vibration analysis of fg microbeams in thermal environment based on modified couple stress theory," *Iranian*

Journal of Science and Technology, Transactions of Mechanical Engineering, vol. 43, no. 1, pp. 761–771, 2019.

[130] M. H. Jalali, B. Shahriari, O. Zargar, M. Baghani, and M. Baniassadi, "Free vibration analysis of rotating functionally graded annular disc of variable thickness using generalized differential quadrature method," *Scientia Iranica. Transaction B, Mechanical Engineering*, vol. 25, no. 2, pp. 728–740, 2018.

[131] R. Hosseini, M. Hamedi, H. Golparvar, and O. Zargar, "Analytical and experimental investigation into increasing operating bandwidth of piezoelectric energy harvesters," *AUT Journal of Mechanical Engineering*, vol. 3, no. 1, pp. 113–122, 2019.

[132] R. Hosseini, O. Zargar, and M. Hamedi, "Improving power density of piezoelectric vibration-based energy scavengers," *Journal of Solid Mechanics*, vol. 10, no. 1, pp. 98–109, 2018.

APPENDIX A

DERIVATION OF PD EQUATION OF MOTION

Denoting the force states as:

$$\mathcal{F}_{1i} := -\frac{\partial}{\partial \mathbf{u}_i}\left(a_{jk}\omega_{ijk}\right), \quad \mathcal{F}_{2i} := -\frac{\partial}{\partial \mathbf{u}_i}\left(a_{ki}\omega_{jki}\right), \quad \mathcal{F}_{3i} := -\frac{\partial}{\partial \mathbf{u}_i}\left(a_{ij}\omega_{kij}\right)$$

we take a continuum limit on Eq. (2.8) to arrive at the following integro-differential equations involving double integrals:

$$\begin{aligned} \frac{\partial}{\partial t}\left(\frac{\partial \tau\left(\dot{\mathbf{u}}\right)}{\partial \dot{\mathbf{u}}}\right) &= \int_{\overline{\Omega}}\int_{\overline{\Omega}} \mathcal{F}_1\left(\mathbf{x}, \mathbf{x}', \mathbf{x}''\right) dV' dV'' \\ + \int_{\overline{\Omega}}\int_{\overline{\Omega}} \mathcal{F}_2\left(\mathbf{x}, \mathbf{x}', \mathbf{x}''\right) dV' dV'' &+ \int_{\overline{\Omega}}\int_{\overline{\Omega}} \mathcal{F}_3\left(\mathbf{x}, \mathbf{x}', \mathbf{x}''\right) dV' dV'' + \mathbf{f} \end{aligned} \tag{A.1}$$

Variables $\mathbf{u}$, $\mathbf{f}$, $\mathbf{x}$, $\mathbf{x}'$, $\mathbf{x}''$, $\mathcal{F}_1$, $\mathcal{F}_2$ and $\mathcal{F}_3$ in Eq. (A.1) are continuum versions of their respective discrete counterparts. dV' and dV'' are infinitesimal volume elements at $\mathbf{x}'$ and $\mathbf{x}''$. $\overline{\Omega}$ denotes the influence domain. Putting:

$$\begin{aligned} T_1\left(\mathbf{x}, \mathbf{x}'\right) &= \int_{\overline{\Omega}} \mathcal{F}_1\left(\mathbf{x}, \mathbf{x}', \mathbf{x}''\right) dV'' \\ T_2\left(\mathbf{x}, \mathbf{x}'\right) &= \int_{\overline{\Omega}} \mathcal{F}_2\left(\mathbf{x}, \mathbf{x}', \mathbf{x}''\right) dV'' \\ T_3\left(\mathbf{x}, \mathbf{x}'\right) &= \int_{\overline{\Omega}} \mathcal{F}_3\left(\mathbf{x}, \mathbf{x}', \mathbf{x}''\right) dV'' \end{aligned} \tag{A.2}$$

We can rewrite Eq. (A.1) as:

$$\frac{\partial}{\partial t}\left(\frac{\partial \tau\left(\dot{\mathbf{u}}\right)}{\partial \dot{\mathbf{u}}}\right) = \int_{\overline{\Omega}} \left(T_1\left(\mathbf{x}, \mathbf{x}'\right) + T_2\left(\mathbf{x}, \mathbf{x}'\right) + T_3\left(\mathbf{x}, \mathbf{x}'\right)\right) dV' + \mathbf{f} \tag{A.3}$$

By putting $T_2(\mathbf{x},\mathbf{x}') + T_3(\mathbf{x},\mathbf{x}')$ as $-T_4(\mathbf{x},\mathbf{x}')$, Eq. (A.3) may be written as,

$$\frac{\partial}{\partial t}\left(\frac{\partial \tau(\dot{\mathbf{u}})}{\partial \dot{\mathbf{u}}}\right) = \int_{\overline{\Omega}} \left(T_1(\mathbf{x},\mathbf{x}') - T_4(\mathbf{x},\mathbf{x}')\right) dV' + \mathbf{f} \tag{A.4}$$

$T_1(\mathbf{x},\mathbf{x}')$ and $T_4(\mathbf{x},\mathbf{x}')$ as a force field operator, $T[.]$ acting on points $\mathbf{x}$ and $\mathbf{x}'$ respectively along a *bond* $< \mathbf{x} - \mathbf{x}' >$. Hence, Eq. (A.4) may be written as,

$$\frac{\partial}{\partial t}\left(\frac{\partial \tau(\dot{\mathbf{u}})}{\partial \dot{\mathbf{u}}}\right) = \int_{\overline{\Omega}} \left(T[\mathbf{x}] < \mathbf{x} - \mathbf{x}' > - T[\mathbf{x}'] < \mathbf{x} - \mathbf{x}' >\right) dV' + \mathbf{f} \tag{A.5}$$

Eq. (A.5) is the PD equation of motion [24].

APPENDIX B

DIRECTIONALITY INFORMATION BASED ON STOCHASTIC PROJECTION TECHNIQUE

Here we derive the evolution equation for the normalized conditional law $\pi_t(\phi)$ [70]

$$d\pi_t(\phi) = \left(\pi_t\left(\phi \mathbf{h}^T\right) - \pi_t(\phi)\,\pi_t(\mathbf{h})^T\right)\left(\boldsymbol{\sigma}\boldsymbol{\sigma}^T\right)^{-1}\left(d\mathbf{Y}_t - \pi_t(\mathbf{h})\,dt\right)$$

where ϕ is a twice continuously differentiable bounded function of $\mathbf{x}$ and $\mathrm{Var}(\mathbf{h}) := \left(\boldsymbol{\sigma}\boldsymbol{\sigma}^T\right)$ is the spatial variance of $\mathbf{h}$.

Proof: The conditioned equation for a bounded and at least twice continuously differentiable function $\phi_t := \phi(\mathbf{x}_t)$ of $\mathbf{x}_t$ may be arrived at by expanding $\phi(\mathbf{x}_t)\Lambda_t$, where $\tau \in (t_{i-1}, t_i]$, using Ito's formula:

$$d(\phi_t\Lambda_t) = \phi_t d\Lambda_t + d\phi_t\Lambda_t + \langle d\phi_t, d\Lambda_t\rangle \tag{B.1}$$

$\langle\cdot\rangle$ denotes the quadratic covariation. A further expansion leads to:

$$d(\phi_t\Lambda_t) = \phi_t\Lambda_t\Delta_t^T d\mathbf{Y}_t + \Lambda_t{\phi'}_t^T d\mathbf{u}_t + \frac{1}{2}\Lambda_t\left\langle d\mathbf{u}_t, \phi_t'' d\mathbf{u}_t\right\rangle \tag{B.2}$$

By explicitly writing out the term $\left\langle d\mathbf{u}_t, \phi_t'' d\mathbf{u}_t\right\rangle$ we get:

$$\begin{aligned} d(\phi_t\Lambda_t) =& \phi_t\Lambda_t\Delta_t^T d\mathbf{Y}_t + \Lambda_t{\phi'}_t^T d\mathbf{u}_t \\ &+ \frac{1}{2}\sum_{j,k=1}^{n}\sum_{l=1}^{d}\left(\frac{\partial^2\phi}{\partial u^j\partial u^k}\right)_t \sigma^{jl}\sigma^{kl}dt \end{aligned} \tag{B.3}$$

The incremental form in Eqn. (B.3) may be given the following integral representation:

$$\begin{aligned}\phi_t\Lambda_t =&\phi_{i-1}\Lambda_{i-1} + \int_{t_{i-1}}^{t} \phi_s\Lambda_s\mathbf{h}_s^T d\mathbf{Y}_s + \int_{t_{i-1}}^{t} \Lambda_s{\phi'}_s^T d\mathbf{u}_s \\ &+ \frac{1}{2}\sum_{j,k=1}^{n}\sum_{l=1}^{d}\int_{t_{i-1}}^{t}\left(\frac{\partial^2\phi}{\partial u^j\partial u^k}\right)_s \sigma^{jl}\sigma^{kl}ds\end{aligned} \tag{B.4}$$

Taking conditional expectation with respect to $\mathcal{F}_t$ under Q, and using Fubini's theorem:

$$\begin{aligned}E_Q\left[\phi_t\Lambda_t|\mathcal{F}_t\right] = E_Q\left[\phi_{i-1}\Lambda_{i-1}\right] &+ \int_{t_{i-1}}^{t} E_Q\left[\phi_s\Lambda_s\mathbf{h}_s^T|\mathcal{F}_s\right] d\mathbf{Y}_s \\ &+ \int_{t_{i-1}}^{t} E_Q\left[\Lambda_s{\phi'}_s^T|\mathcal{F}_s\right] d\mathbf{u}_s + \\ &\frac{1}{2}\sum_{j,k=1}^{n}\sum_{l=1}^{d}\int_{t_{i-1}}^{t} E_Q\left[\left(\frac{\partial^2\phi}{\partial u^j\partial u^k}\right)_s \sigma^{jl}\sigma^{kl}|\mathcal{F}_s\right] ds\end{aligned} \tag{B.5}$$

Noting that $\int_{t_{i-1}}^{t} E_Q\left[\Lambda_s{\phi'}_s^T|\mathcal{F}_s\right] d\mathbf{u}_s = 0$ and for notational convenience denoting the unnormalized conditional expectation operator, $E_Q\left((\centerdot)_t\Lambda_t|\mathcal{F}_t\right)$ as $\theta_t\left(\centerdot\right)$ we arrive at the following equation:

$$\begin{aligned}\theta_t\left(\phi_t\Lambda_t\right) =&\theta_t\left(\phi_{i-1}\Lambda_{i-1}\right) + \int_{t_{i-1}}^{t} \theta_s\left(\phi_s\Lambda_s\mathbf{h}_s^T\right) d\mathbf{Y}_s \\ &+ \frac{1}{2}\sum_{j,k=1}^{n}\sum_{l=1}^{d}\int_{t_{i-1}}^{t}\theta_s\left(\left(\frac{\partial^2\phi}{\partial u^j\partial u^k}\right)_s \sigma^{jl}\sigma^{kl}\right) ds\end{aligned} \tag{B.6}$$

An incremental representation of Eqn. (B.6) may be given as:

$$\begin{aligned}d\theta_t\left(\phi_t\Lambda_t\right) =&\theta_t\left(\phi_t\Lambda_t\mathbf{h}_t^T\right) d\mathbf{Y}_s \\ &+ \frac{1}{2}\sum_{j,k=1}^{n}\sum_{l=1}^{d}\theta_t\left(\left(\frac{\partial^2\phi}{\partial u^j\partial u^k}\right)_t \sigma^{jl}\sigma^{kl}\right) dt\end{aligned} \tag{B.7}$$

In order to obtain the normalized conditional law, i.e. $\pi_t\left(\phi\right) = \frac{\theta_t(\phi)}{\theta_t(1)}$, it is expanded using

Ito's formula as given below:

$$d\pi_t(\phi) = \frac{d\theta_t(\phi)}{\theta_t(1)} + \theta_t(\phi)\, d\left(\frac{1}{\theta_t(1)}\right) + \left\langle d\theta_t(\phi), d\left(\frac{1}{\theta_\tau(1)}\right)\right\rangle \tag{B.8}$$

$d\left(\frac{1}{\theta_t(1)}\right)$ may be expanded as:

$$d\left(\frac{1}{\theta_t(1)}\right) = -\frac{1}{\theta_t^2(1)} d\theta_t(1) + \frac{1}{\theta_t^3(1)} \langle d\theta_t(1), d\theta_t(1)\rangle \tag{B.9}$$

Putting $\phi = 1$ in Eqn. (B.7), we get an Ito expansion for $d\theta_t(1)$, which is given below:

$$d\theta_t(1) = \theta_t\left(\mathbf{h}^T\right) d\mathbf{Y}_t \tag{B.10}$$

Using Eqn. (B.10) in Eqn. (B.9):

$$d\left(\frac{1}{\theta_t(1)}\right) = -\frac{\pi_t\left(\mathbf{h}^T\right)}{\theta_t(1)} d\mathbf{Y}_t + \frac{\pi_t\left(\mathbf{h}^T\right)\pi_t(\mathbf{h})}{\theta_t(1)} dt \tag{B.11}$$

After some more calculation, we arrive at the evolution of the normalized conditional estimate $\pi_t(\phi)$ given in Eqn.(B.12):

$$d\pi_t(\phi) = \left(\pi_t\left(\phi\mathbf{h}^T\right) - \pi_t(\phi)\,\pi_t(\mathbf{h})^T\right)(\mathrm{Var}(\mathbf{h}))^{-1}\left(d\mathbf{Y}_t - \pi_t(\mathbf{h})\, dt\right) \tag{B.12}$$

B.1 Correspondences with Classical Strain Measures

We can recover the classical deformation gradient from our derivative-free directionality term, $\mathbf{G}$ in an infinitesimal neighborhood ($\Omega \to \omega$) around a spatial point $\mathbf{x}_t$. Upon a Taylor's expansion of $\mathbf{y}_t$ around $\mathbf{x}_t$ only up to the first order approximation we get,

$$\mathbf{y}_t = \mathbf{x}_t + \nabla_{\mathbf{x_t}} \mathbf{y}_t \mathbf{h} \tag{B.13}$$

where $\nabla_{\mathbf{x_t}}$ is the usual gradient operator acting on $\mathbf{y}_t$. Incorporating Eq. (B.13) in Eq. (5.9) we have,

$$(\mathbf{y}_t - \mathbf{x}_t) \approx \Delta + \mathbf{G}\Delta \tag{B.14}$$

where

$$\begin{aligned}
&\lim_{\Omega\to\omega} \mathbf{G} = \lim_{\Omega\to\omega} \left(\pi_t\left((\mathbf{y}-\mathbf{x})\,\mathbf{h}^T\right) - \pi_t\left(\mathbf{y}-\mathbf{x}\right)\pi_t\left(\mathbf{h}\right)^T\right)\left(\mathrm{Var}\left(\mathbf{h}\right)\right)^{-1} \\
&\qquad \text{Using Taylor's expansion of } \mathbf{y} \text{ around } \mathbf{x} \text{ within the } \pi_t \text{ operator} \\
&\lim_{\Omega\to\omega} \mathbf{G} \approx \left(\pi_t\left(\nabla_{\mathbf{x}}\mathbf{y}\mathbf{h}\mathbf{h}^T\right) - \pi_t\left(\nabla_{\mathbf{x}}\mathbf{y}\mathbf{h}\right)\pi_t\left(\mathbf{h}\right)^T\right)\mathrm{Var}\left(\mathbf{h}\right)^{-1} \\
&\qquad \text{Since } \nabla_{\mathbf{x}}\mathbf{y} \text{ provides point information at } \mathbf{x}\text{, it does dont vary with different} \\
&\qquad \text{sample points within the expectation operator } \pi_t. \\
&\qquad \text{Hence } \nabla_{\mathbf{x}}\mathbf{y} \text{ comes out of } \pi_t. \\
&\lim_{\Omega\to\omega} \mathbf{G} = \nabla_{\mathbf{x}}\mathbf{y}\left(\pi_t\left(\mathbf{h}\mathbf{h}^T\right) - \pi_t\left(\mathbf{h}\right)\pi_t\left(\mathbf{h}\right)^T\right)\mathrm{Var}\left(\mathbf{h}\right)^{-1} \\
&\qquad = \nabla_{\mathbf{x}}\mathbf{y}\mathrm{Var}\left(\mathbf{h}\right)\mathrm{Var}\left(\mathbf{h}\right)^{-1} \\
&\qquad = \nabla_{\mathbf{x}}\mathbf{y}
\end{aligned} \tag{B.15}$$

Since $\nabla_{\mathbf{x}_t}\mathbf{y}$ is the deformation gradient, we label it with its standard notation $\mathbf{F}$ for convenience. Similarly we can show correspondences in the infinitesimal limit among different classical strain measures with our respective derivative-free counterparts:

$$\begin{aligned}
&\lim_{\Omega\to\omega} \mathbf{G}^T\mathbf{G} \to \text{Right Cauchy-Green strain tensor, } \mathbf{C} = \mathbf{F}^T\mathbf{F} \\
&\lim_{\Omega\to\omega} \frac{1}{2}\left(\mathbf{G}^T\mathbf{G} - \mathbf{I}\right) \to \text{Green strain tensor, } \mathbf{E} = \frac{1}{2}\left(\mathbf{C}^T\mathbf{C} - \mathbf{I}\right)
\end{aligned} \tag{B.16}$$

$\mathbf{G}$ is assumed to be nonsingular with a positive determinant. This should hold given the specific scheme of computing sample averages using non-identical sample points. However a detailed mathematical study on this would be carried out elsewhere. With such a property of $\mathbf{G}$, it can be uniquely written as a product of a proper orthogonal tensor $\mathbf{G_R}$ and a

symmetric positive tensor $\mathbf{G_U}$ as given below [127],

$$\mathbf{G} = \mathbf{G_R}\mathbf{G_U}$$

$$\mathbf{G_U} = \left(\mathbf{G}^T\mathbf{G}\right)^{\frac{1}{2}}$$

$$\mathbf{G_R} = \mathbf{G}{\mathbf{G_U}}^{-1}$$

Using $\mathbf{G_U}$, we can show the following correspondence between classical strain measures with our respective derivative-free counterparts:

$$\begin{aligned}
&\lim_{\Omega\to\omega} \frac{1}{2}\left({\mathbf{G_U}}^2 - \mathbf{I}\right) \rightarrow \text{Green strain tensor, } \frac{1}{2}\left(\mathbf{U}^2 - \mathbf{I}\right) \\
&\lim_{\Omega\to\omega} \frac{1}{m}\left({\mathbf{G_U}}^m - \mathbf{I}\right) \rightarrow \text{Generalized Green strain tensor, } \frac{1}{m}\left(\mathbf{U}^m - \mathbf{I}\right) \\
&\lim_{\Omega\to\omega} \ln\left(\mathbf{G_U}\right) \rightarrow \text{Hencky strain tensor, } \ln\left(\mathbf{U}\right)
\end{aligned} \tag{B.17}$$

Accordingly, derivative-free stress tensor and energy of the system can be readily designed that recover appropriate classical formulations.

APPENDIX C

LOCALIZATION OF THE TRIDYNAMICS EQUATIONS FOR BEAM

C.1 Localization of the Tridynamics Equations for Beam

Note that M for all series in local limit is 2. A particle i interact only with a particle before and a particle after itself. Thus, values j and k can only be equal to 1 and 2. Now, by replacing values 1 and 2 in place of j and k, the series can be dropped and Eqs. 3.5, 3.5 and 3.5 can be written out in expanded forms as:

$$\rho\ddot{u}_i = \frac{K^{\epsilon}}{\xi}\left(\epsilon_{i11} + \epsilon_{i12} + \epsilon_{i21} + \epsilon_{i22}\right)V^2 \tag{C.1}$$

$$\rho\ddot{w}_i = \frac{K^{\psi}}{\xi}\left(\psi_{i11} + \psi_{i12} + \psi_{i21} + \psi_{i22}\right)V^2 \tag{C.2}$$

$$\begin{aligned}\rho\frac{I}{A}\ddot{\phi}_i = \frac{K^{\phi}}{\xi}\left(\kappa_{i11} + \kappa_{i12} + \kappa_{i21} + \kappa_{i22}\right)V^2 + \frac{K^{\psi}}{\xi}[2\hat{n}_{i1}\psi_{i11} - \hat{n}_{i1}\psi_{11i} - \hat{n}_{i1}\psi_{1i1} \\ +(\hat{n}_{i2} + \hat{n}_{i1})\psi_{i21} - \hat{n}_{i2}\psi_{21i} - \hat{n}_{i1}\psi_{1i2} + (\hat{n}_{i1} + \hat{n}_{i2})\psi_{i12} - \hat{n}_{i1}\psi_{12i} - \hat{n}_{i2}\psi_{2i1} \\ 2\hat{n}_{i2}\psi_{i22} - \hat{n}_{i2}\psi_{22i} - \hat{n}_{i2}\psi_{2i2}]V^2\end{aligned} \tag{C.3}$$

$$\rho\ddot{u}_i = \frac{4K^{\epsilon}V^2}{\xi}\left(\hat{u}_{i1} + \hat{u}_{i2}\right) \tag{C.4}$$

$$\rho\ddot{w}_i = \frac{4K^{\psi}V^2}{\xi}\left(\theta_{i1} + \bar{\phi}_{i1} + \theta_{i2} - \bar{\phi}_{i2}\right) \tag{C.5}$$

$$\rho\frac{I}{A}\ddot{\phi}_i = \frac{4K^{\phi}V^2}{\xi}\left(\hat{\phi}_{i1} + \hat{\phi}_{i2}\right) + \frac{K^{\psi}V^2}{6}\left(8\theta_{1i} - 8\theta_{2i} + 8\theta_{12} - 8\bar{\phi}_{1i} - 8\bar{\phi}_{2i} - 8\bar{\phi}_{12}\right) \tag{C.6}$$

Since the present formulation utilizes the interaction between particles j and k (while this particular interaction does not exist in the other particle-based nonlocal theories), the value of 2 should be multiplied by terms θ_{12} and $\hat{n_{12}}$ to remove the effect of localization. The

following relations are exploited to obtain Eqs. C.5 and C.6:

$$\left.\begin{gathered}\hat{n}_{i1}=-\hat{n}_{1i}=\hat{n}_{2i}=-\hat{n}_{i2}=\hat{n}_{21}=-\hat{n}_{12}=-1,\\ \psi_{ijk}+\psi_{jki}+\psi_{kij}=0\\ \psi_{ijk}=\psi_{ikj}\end{gathered}\right\}\rightarrow \psi_{i11}=-2\psi_{11i},\ \psi_{i22}=-2\psi_{22i} \tag{C.7}$$

From the above equations, one can get:

$$\rho\ddot{u}_i=\frac{4K^{\epsilon}V^2}{\xi}\left(u_2-2u_i+u_1\right) \tag{C.8}$$

$$\rho\ddot{w}_i=\frac{4K^{\psi}V^2}{\xi}\left(\frac{w_2-2w_i+w_1}{\xi}-\left(\frac{\phi_2-\phi_1}{2}\right)\right) \tag{C.9}$$

$$\rho\frac{I}{A}\ddot{\phi}_i=\frac{4K^{\phi}V^2}{\xi}\left(\frac{\phi_2-2\phi_i+\phi_1}{\xi}\right)+\frac{K^{\psi}V^2}{6}\left(12\frac{w_2-w_1}{\xi}-8\phi_i-8(\phi_2+\phi_1)\right) \tag{C.10}$$

Thus Eqs. C.8, C.9 and C.10 yield to the local EOMs of Timoshenko beams.

Other methods to characterize material properties are available in literature. Mohammadsalehi et. al. [128] investigated vibration characteristics of viscoelastic nanoplates by considering nonlocal equations. They found that the nonlocal parameter has a negative effect on the natural frequencies of the nanoplates. Researchers have also studied the effect of thermal environments on the vibration of FG microbeams [129] and rotating FG disks [130]. They evaluated the effect of various thickness, angular velocity, and geometric parameters on the natural frequencies and critical speeds of these structures in thermal environment. Furthermore, several studies showed the improvment of mechanical behavior using micro/nano piezoelectric layers. Hosseini et. al. [131, 132] analyzed the vibration energy harvesting through piezoelectric unimorph and bimorph structures. They found that among different geometries, triangular cantilever beams improve the total vibration and generate more energy than the other geometries.

C.2 Classical Dispersion

In the case of classical theory:

$$\begin{aligned} u =& u(x,t) = u_0 e^{\hat{i}(\kappa x - \omega t)} = u_0 X \\ w =& w(x,t) = w_0 e^{\hat{i}(\kappa x - \omega t)} = w_0 X \\ \phi =& \phi(x,t) = \phi_0 e^{\hat{i}(\kappa x - \omega t)} = \phi_0 X \end{aligned} \tag{C.11}$$

where $X = e^{\hat{i}(\kappa x - \omega t)}$, substituting u, w, ϕ in classical EOMs yields to the following determinant of coefficient:

$$\begin{vmatrix} \rho\omega^2 - E\kappa^2 & 0 & 2z\rho\omega^2 \\ 0 & \rho\omega^2 - \kappa_s G\kappa^2 & -i\kappa_s G\kappa \\ 2z\rho\omega^2 & i\kappa_s G\kappa & \rho\frac{I}{A}\omega^2 - E\frac{I}{A}\kappa^2 - \kappa_s G \end{vmatrix} = 0 \tag{C.12}$$

Therefore, the characteristic equation can be found as:

$$\begin{aligned} &\left(G\kappa\kappa_s\left(I\rho^3 - 4A\rho^3 z^2\right)\right)\omega^6 + \left(-G\kappa\kappa_s\left(AG\kappa_s\rho^2 + EI\kappa^2\rho^2 + AEI\kappa^2\rho^2\right)\right)\omega^4 \\ &+ \left(G\kappa\kappa_s\left(G\kappa_s\rho A^2 E\kappa^2 + I\rho AE^2\kappa^4 - 1G\kappa_s\rho A\kappa\right)\right)\omega^2 + A^2 EG^2\kappa^4{\kappa_s}^2 = 0 \end{aligned} \tag{C.13}$$

With the assumption of thin beam, we would get the following frequency for the axial direction:

$$\omega = \kappa\sqrt{\frac{E}{\rho}} \tag{C.14}$$

The following determinant could be defined for the rest of frequencies:

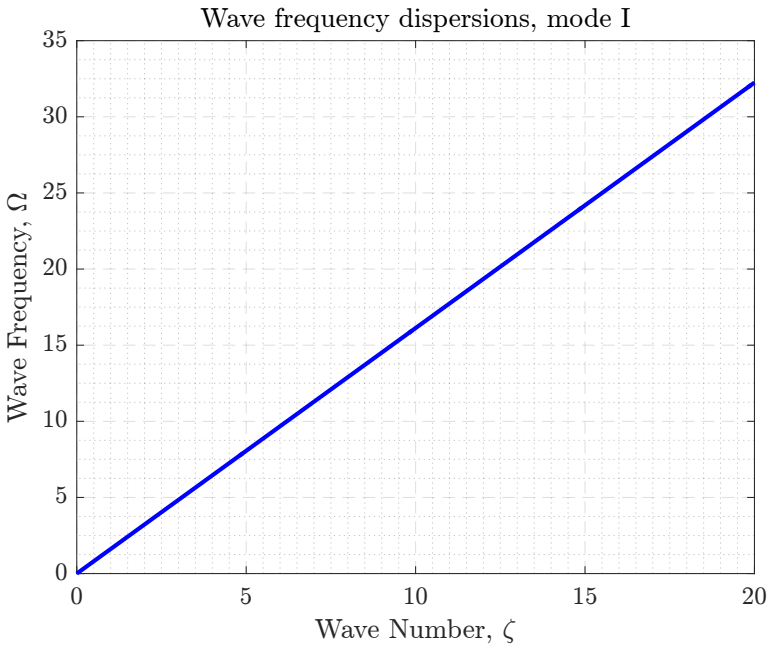

Figure C.1: Variation of wave frequency versus the normalized wave number for classical model.

$$\begin{vmatrix} \rho\omega^2 - \kappa_s G\kappa^2 & -i\kappa_s G\kappa \\ i\kappa_s G\kappa & \rho\frac{I}{A}\omega^2 - E\frac{I}{A}\kappa^2 - \kappa_s G \end{vmatrix} = 0 \tag{C.15}$$

which conclude the following set of solutions as follows:

$$\begin{aligned} \omega_1 &= \frac{1}{\sqrt{2\rho I}}\left(S_a + S_b^{\frac{1}{2}}\right)^{\frac{1}{2}} \\ \omega_2 &= \frac{1}{\sqrt{2\rho I}}\left(S_a - S_b^{\frac{1}{2}}\right)^{\frac{1}{2}} \end{aligned} \tag{C.16}$$

where S_a and S_b are:

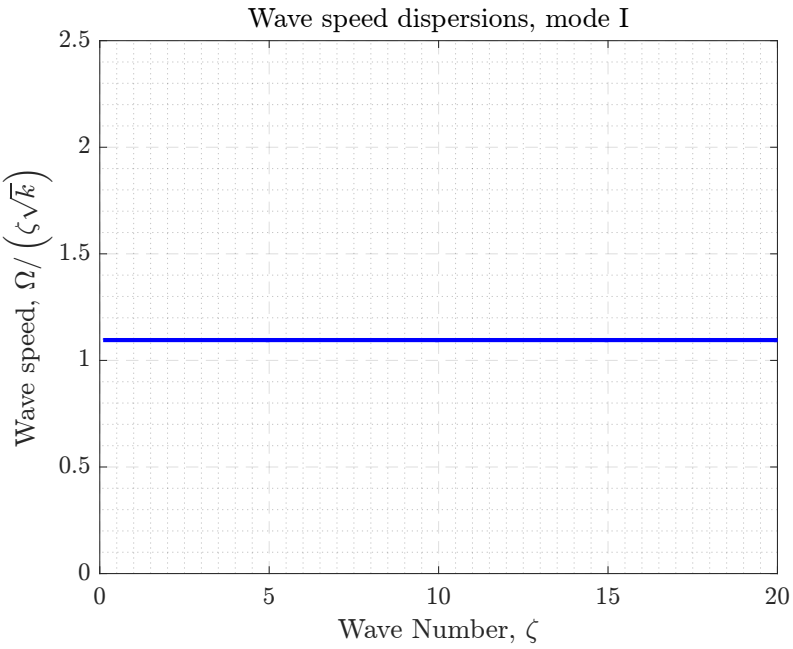

Figure C.2: Variation of wave frequency versus the normalized wave number for classical model (mode I).

$$
\begin{aligned}
S_a =& AG\kappa_s + EI\kappa^2 + GI\kappa^2\kappa_s \\
S_b =& A^2G^2{\kappa_s}^2 + 2AEGI\kappa^2\kappa_s + 2AG^2I\kappa^2{\kappa_s}^2 \\
&+ E^2I^2\kappa^4 - 2EGI^2\kappa^4\kappa_s + G^2I^2\kappa^4{\kappa_s}^2
\end{aligned}
\tag{C.17}
$$

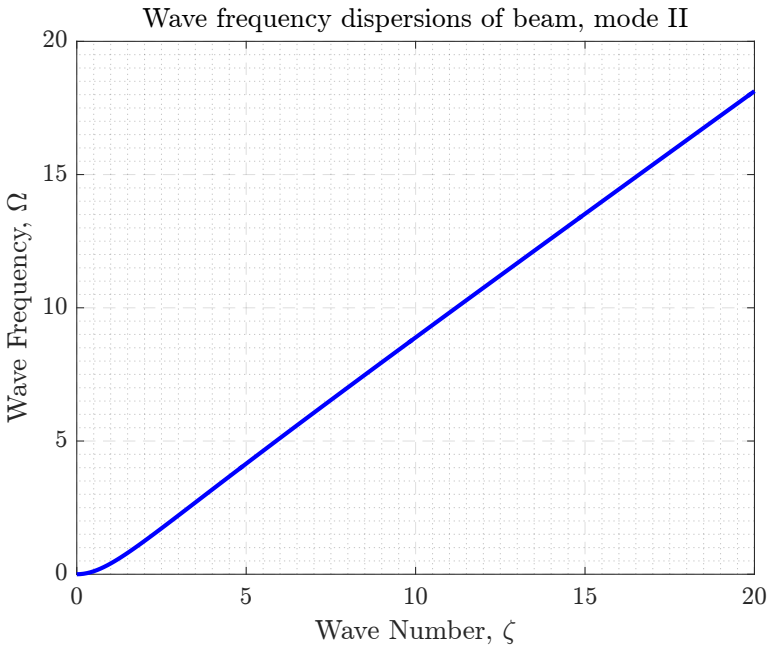

Figure C.3: Variation of wave frequency versus the normalized wave number for classical model (mode II).

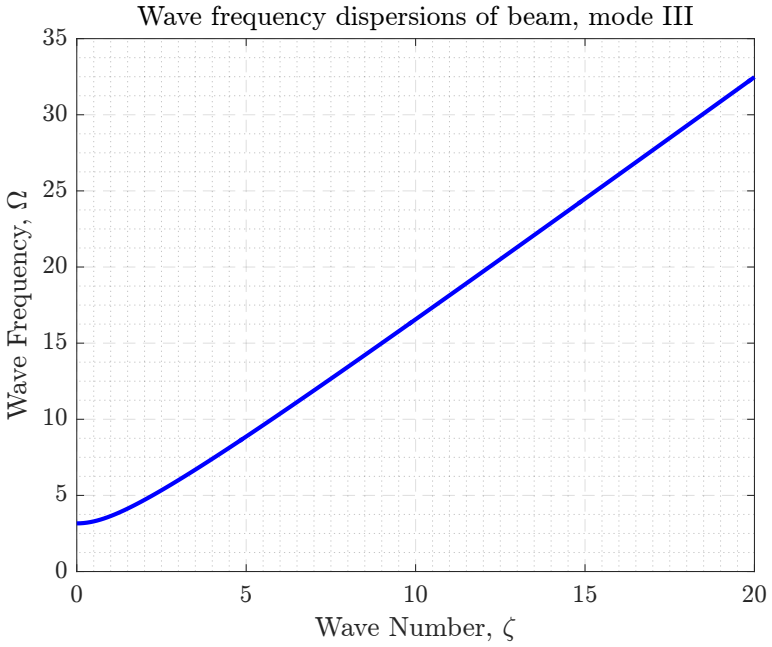

Figure C.4: Variation of wave speed versus the normalized wave number for classical model (mode III).

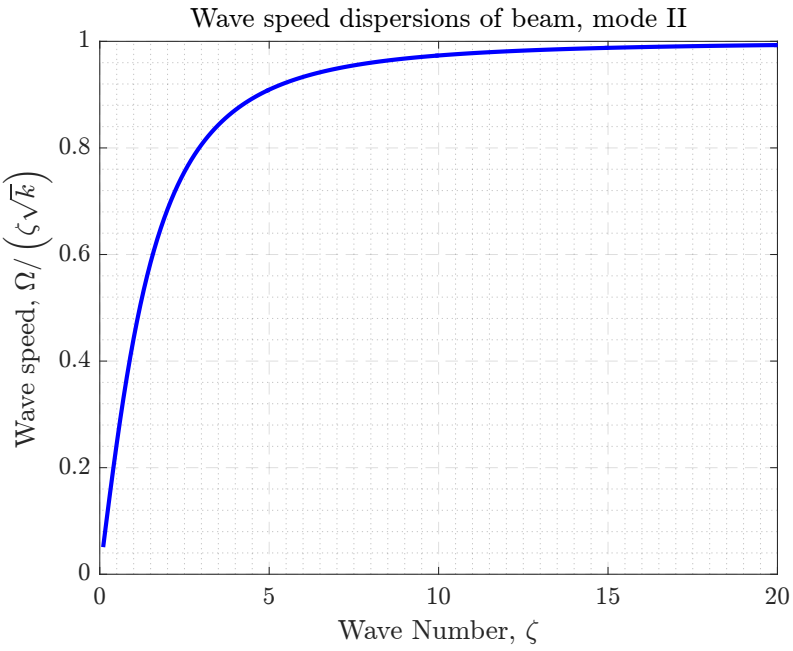

Figure C.5: Variation of wave speed versus the normalized wave number for classical model (mode II).

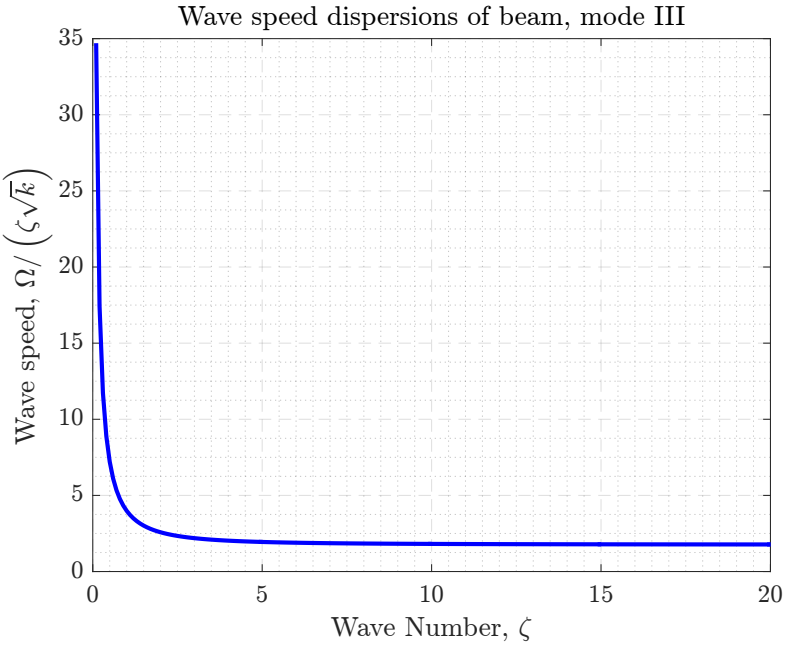

Figure C.6: Variation of wave speed versus the normalized wave number for three models: tridynamics, peridynamics and classical model (mode III).

C.3 Peridynamics Dispersion Analysis

The Peridynamics equation of motion for a bar can be given as;

$$\rho\ddot{u} = \int_{\Omega} c\left(\frac{u(x',t) - u(x,t)}{\xi}\right) dV + b \tag{C.18}$$

using Taylor series $u(x',t) = u(x,t) + u'(x,t)\xi n + 1/2u''(x,t)\xi^2 n^2 + ...$, the equation of motion leads to:

$$\rho\ddot{u} = cu'(x,t)A\int_{-\delta}^{\delta} nd\xi + \frac{1}{2}cu''A\int_{-\delta}^{\delta} \xi d\xi + b \tag{C.19}$$

where $\xi = (x' - x)$ and $n = sign\,(x' - x)$. Due to symmetry of the horizon, $\int_{-\delta}^{\delta} nd\xi = 0$. Comparing the localized equation with the equation of motion will gives:

$$c = \frac{2E}{A\delta^2} \tag{C.20}$$

Now to do the dispersion analysis, we find the frequency analytically as:

$$u(x,t) = u_0 e^{\hat{i}(\kappa x - \omega t + \hat{n}_0\kappa\xi_0)} = u_0 X\Lambda_0 = u_0 X \tag{C.21}$$

$$u(x',t) = u_0 e^{\hat{i}(\kappa x - \omega t + \hat{n}_1\kappa\xi_1)} = u_0 X\Lambda_1 \tag{C.22}$$

substituting Eq. u and u' in EOM gives:

$$-\rho\omega^2 u_0 X = cu_0 XA\int_{-\delta}^{+\delta} \frac{(\Lambda - 1)}{\xi} d\xi \tag{C.23}$$

We may rewrite Λ as $\Lambda = e^{i(n\kappa\xi)} = cos(n\kappa\xi) + i\sin(n\kappa\xi)$, therefor due to symmetry of interaction in the specified horizon, we could drop the odd terms in the integral as following:

$$\int_{-\delta}^{+\delta} \frac{i\sin(n\kappa\xi)}{\xi} d\xi = 0 \tag{C.24}$$

Noting that the Taylor series of cos term could be written as $\cos(n\kappa\xi) = 1 - \frac{\kappa^2\xi^2}{2!} + \frac{\kappa^4\xi^4}{4!} + ...$

Therefore, Eq. C.23 could be simplified to:

$$-\rho\omega^2 u_0 X = 2cu_0 XA \int_0^{+\delta} \left(\frac{-\kappa^2\xi}{2!} + \frac{\kappa^4\xi^3}{4!} \right) d\xi \tag{C.25}$$

Therefore the axial frequency could be found as follows;

$$\omega = \sqrt{\frac{cA}{\rho}} \left[\frac{\kappa^2\delta^2}{2} - \frac{\kappa^4\delta^4}{48} \right]^{1/2} = \kappa\sqrt{\frac{E}{\rho}} \left[1 - \frac{\kappa^2\delta^2}{24} \right]^{1/2} \tag{C.26}$$

Noting that the classical wave frequency could be discover by letting $\delta \to 0$.

APPENDIX D

DERIVATION OF THE TERMS IN EOM FOR PARTICLE J^{TH} AND K^{TH} PARTICLES

$$\begin{aligned}\frac{\partial \omega_i^{\epsilon_j^{xx}}}{\partial u_i} &= \frac{1}{6}\sum_{j=1}^{N}\sum_{k=1}^{N}\frac{\partial\left(A^1_{jki}\epsilon^{xx}_{jki}\right)}{\partial u_i}V_kV_j = \frac{1}{6}\sum_{j=1}^{N}\sum_{k=1}^{N}\frac{\partial\left(A^1_{jki}\epsilon^{xx}_{jki}\right)}{\partial \epsilon^{xx}_{jki}}\frac{\partial \epsilon^{xx}_{jki}}{\partial u_i}V_kV_j \\ &= +\frac{1}{3}\sum_{j=1}^{N}\sum_{k=1}^{N}\left[K^{\epsilon_{xx}}_{jki}\epsilon^{xx}_{jki}\left(\frac{1}{\xi^x_{ij}}\right)\right]V_kV_j\end{aligned} \tag{D.1}$$

$$\begin{aligned}\frac{\partial \omega_i^{\epsilon_k^{xx}}}{\partial u_i} &= \frac{1}{6}\sum_{j=1}^{N}\sum_{k=1}^{N}\frac{\partial\left(A^1_{kij}\epsilon^{xx}_{kij}\right)}{\partial u_i}V_kV_j = \frac{1}{6}\sum_{j=1}^{N}\sum_{k=1}^{N}\frac{\partial\left(A^1_{kij}\epsilon^{xx}_{kij}\right)}{\partial \epsilon^{xx}_{kij}}\frac{\partial \epsilon^{xx}_{kij}}{\partial u_i}V_kV_j \\ &= +\frac{1}{3}\sum_{j=1}^{N}\sum_{k=1}^{N}\left[K^{\epsilon_{xx}}_{kij}\epsilon^{xx}_{kij}\left(\frac{1}{\xi^x_{ik}}\right)\right]V_kV_j\end{aligned} \tag{D.2}$$

$$\begin{aligned}\frac{\partial \omega_i^{\epsilon_j^{yy}}}{\partial v_i} &= \frac{1}{6}\sum_{j=1}^{N}\sum_{k=1}^{N}\frac{\partial\left(A^2_{jik}\epsilon^{yy}_{jik}\right)}{\partial v_i}V_kV_j = \frac{1}{6}\sum_{j=1}^{N}\sum_{k=1}^{N}\frac{\partial\left(A^2_{jik}\epsilon^{yy}_{jik}\right)}{\partial \epsilon^{yy}_{jik}}\frac{\partial \epsilon^{yy}_{jik}}{\partial v_i}V_kV_j \\ &= +\frac{1}{3}\sum_{j=1}^{N}\sum_{k=1}^{N}\left[K^{\epsilon_{yy}}_{jik}\epsilon^{yy}_{jik}\left(\frac{1}{\xi^y_{ij}}\right)\right]V_kV_j\end{aligned} \tag{D.3}$$

$$\begin{aligned}\frac{\partial \omega_i^{\epsilon_k^{yy}}}{\partial v_i} &= \frac{1}{6}\sum_{j=1}^{N}\sum_{k=1}^{N}\frac{\partial\left(A^2_{kij}\epsilon^{yy}_{kij}\right)}{\partial v_i}V_kV_j = \frac{1}{6}\sum_{j=1}^{N}\sum_{k=1}^{N}\frac{\partial\left(A^2_{kij}\epsilon^{yy}_{kij}\right)}{\partial \epsilon^{yy}_{kij}}\frac{\partial \epsilon^{yy}_{kij}}{\partial v_i}V_kV_j \\ &= +\frac{1}{3}\sum_{j=1}^{N}\sum_{k=1}^{N}\left[K^{\epsilon_{yy}}_{kij}\epsilon^{yy}_{kij}\left(\frac{1}{\xi^y_{ik}}\right)\right]V_kV_j\end{aligned} \tag{D.4}$$

$$\begin{aligned}\frac{\partial \omega_i^{\epsilon_j^{xy}}}{\partial u_i} &= \frac{1}{6}\sum_{j=1}^{N}\sum_{k=1}^{N}\frac{\partial\left(A^3_{jik}\epsilon^{xy}_{jik}\right)}{\partial v_i}V_kV_j = \frac{1}{6}\sum_{j=1}^{N}\sum_{k=1}^{N}\frac{\partial\left(A^3_{jik}\epsilon^{xy}_{jik}\right)}{\partial \epsilon^{xy}_{jik}}\frac{\partial \epsilon^{xy}_{jik}}{\partial u_i}V_kV_j \\ &= +\frac{1}{3}\sum_{j=1}^{N}\sum_{k=1}^{N}\left[\left(K^{1_{\epsilon^{xy}1}}_{jki}\epsilon^{xy}_{jki} + \left(K^{1_{\epsilon^{xy}}}_{jki} + K^{2_{\epsilon^{xy}}}_{jki}\right)^2\epsilon^{xy}_{jki}\right)\left(\frac{1}{\xi^y_{ij}}\right)\right]V_kV_j\end{aligned} \tag{D.5}$$

$$\begin{aligned}\frac{\partial \omega_i^{\epsilon_k^{xy}}}{\partial u_i} &= \frac{1}{6}\sum_{j=1}^{N}\sum_{k=1}^{N}\frac{\partial\left(A^3_{kij}\epsilon^{xy}_{kij}\right)}{\partial v_i}V_kV_j = \frac{1}{6}\sum_{j=1}^{N}\sum_{k=1}^{N}\frac{\partial\left(A^3_{kij}\epsilon^{xy}_{kij}\right)}{\partial \epsilon^{xy}_{kij}}\frac{\partial \epsilon^{xy}_{kij}}{\partial u_i}V_kV_j \\ &= +\frac{1}{3}\sum_{j=1}^{N}\sum_{k=1}^{N}\left[\left(K^{1_{\epsilon^{xy}1}}_{kij}\epsilon^{xy}_{kij} + \left(K^{1_{\epsilon^{xy}}}_{kij} + K^{2_{\epsilon^{xy}}}_{kij}\right)^2\epsilon^{xy}_{kij}\right)\left(\frac{1}{\xi^y_{ik}}\right)\right]V_kV_j\end{aligned} \tag{D.6}$$

$$\begin{aligned}\frac{\partial \omega_i^{\epsilon_j^{xy}}}{\partial v_i} &= \frac{1}{6}\sum_{j=1}^{N}\sum_{k=1}^{N}\frac{\partial\left(A_{jik}^{3}\epsilon_{jik}^{xy}\right)}{\partial v_i}V_kV_j = \frac{1}{6}\sum_{j=1}^{N}\sum_{k=1}^{N}\frac{\partial\left(A_{jik}^{3}\epsilon_{jik}^{xy}\right)}{\partial \epsilon_{jik}^{xy}}\frac{\partial \epsilon_{jik}^{xy}}{\partial v_i}V_kV_j \\ &= +\frac{1}{3}\sum_{j=1}^{N}\sum_{k=1}^{N}\left[\left(K_{jki}^{{}^1\epsilon^{xy}{}1}\epsilon_{jki}^{xy} + \left(K_{jki}^{{}^1\epsilon^{xy}} + K_{jki}^{{}^2\epsilon^{xy}}\right)^2\epsilon_{jki}^{xy}\right)\left(\frac{1}{\xi_{ij}^{x}}\right)\right]V_kV_j\end{aligned} \tag{D.7}$$

$$\begin{aligned}\frac{\partial \omega_i^{\epsilon_k^{xy}}}{\partial v_i} &= \frac{1}{6}\sum_{j=1}^{N}\sum_{k=1}^{N}\frac{\partial\left(A_{kij}^{3}\epsilon_{kij}^{xy}\right)}{\partial v_i}V_kV_j = \frac{1}{6}\sum_{j=1}^{N}\sum_{k=1}^{N}\frac{\partial\left(A_{kij}^{3}\epsilon_{kij}^{xy}\right)}{\partial \epsilon_{kij}^{xy}}\frac{\partial \epsilon_{kij}^{xy}}{\partial v_i}V_kV_j \\ &= +\frac{1}{3}\sum_{j=1}^{N}\sum_{k=1}^{N}\left[\left(K_{kij}^{{}^1\epsilon^{xy}{}1}\epsilon_{kij}^{xy} + \left(K_{kij}^{{}^1\epsilon^{xy}} + K_{kij}^{{}^2\epsilon^{xy}}\right)^2\epsilon_{kij}^{xy}\right)\left(\frac{1}{\xi_{ik}^{x}}\right)\right]V_kV_j\end{aligned} \tag{D.8}$$

$$\begin{aligned}\frac{\partial \omega_i^{\psi_j^{y}}}{\partial w_i} &= \frac{1}{6}\sum_{j=1}^{N}\sum_{k=1}^{N}\frac{\partial\left(C_{jki}^{2}\psi_{jki}^{y}\right)}{\partial w_i}V_kV_j = \frac{1}{6}\sum_{j=1}^{N}\sum_{k=1}^{N}\frac{\partial\left(C_{jki}^{2}\psi_{jki}^{y}\right)}{\partial \psi_{jki}^{y}}\frac{\partial \psi_{jki}^{y}}{\partial w_i}V_kV_j \\ &= -\frac{1}{3}\sum_{j=1}^{N}\sum_{k=1}^{N}\left[K_{jki}^{\psi^y,w}\psi_{jki}^{y}\left(\frac{1}{\xi_{ij}^{y}}\right)\right]V_kV_j\end{aligned} \tag{D.9}$$

$$\begin{aligned}\frac{\partial \omega_i^{\psi_k^{y}}}{\partial w_i} &= \frac{1}{6}\sum_{j=1}^{N}\sum_{k=1}^{N}\frac{\partial\left(C_{kij}^{2}\psi_{kij}^{y}\right)}{\partial w_i}V_kV_k = \frac{1}{6}\sum_{j=1}^{N}\sum_{k=1}^{N}\frac{\partial\left(C_{kij}^{2}\psi_{kij}^{y}\right)}{\partial \psi_{kij}^{y}}\frac{\partial \psi_{kij}^{y}}{\partial w_i}V_kV_k \\ &= -\frac{1}{3}\sum_{j=1}^{N}\sum_{k=1}^{N}\left[K_{kij}^{\psi^y,w}\psi_{kij}^{y}\left(\frac{1}{\xi_{ik}^{y}}\right)\right]V_kV_k\end{aligned} \tag{D.10}$$

$$\begin{aligned}\frac{\partial \omega_i^{\psi_j^{x}}}{\partial \phi_i^{x}} &= \frac{1}{6}\sum_{j=1}^{N}\sum_{k=1}^{N}\frac{\partial\left(C_{jki}^{1}\psi_{jki}^{x}\right)}{\partial \phi_i^{x}}V_kV_j = \frac{1}{6}\sum_{j=1}^{N}\sum_{k=1}^{N}\frac{\partial\left(C_{jki}^{1}\psi_{jki}^{x}\right)}{\partial \psi_{jki}^{x}}\frac{\partial \psi_{jki}^{x}}{\partial \phi_i^{x}}V_kV_j \\ &= +\frac{1}{6}\sum_{j=1}^{N}\sum_{k=1}^{N}\left[K_{jki}^{\psi^x}\psi_{jki}^{x}\left(\hat{e}_{iij}^{\,x}\right)\right]V_kV_j\end{aligned} \tag{D.11}$$

$$\begin{aligned}\frac{\partial \omega_i^{\psi_k^{x}}}{\partial \phi_i^{x}} &= \frac{1}{6}\sum_{j=1}^{N}\sum_{k=1}^{N}\frac{\partial\left(C_{kij}^{1}\psi_{kij}^{x}\right)}{\partial \phi_i^{x}}V_kV_j = \frac{1}{6}\sum_{j=1}^{N}\sum_{k=1}^{N}\frac{\partial\left(C_{kij}^{1}\psi_{kij}^{x}\right)}{\partial \psi_{kij}^{x}}\frac{\partial \psi_{kij}^{x}}{\partial \phi_i^{x}}V_kV_j \\ &= +\frac{1}{6}\sum_{j=1}^{N}\sum_{k=1}^{N}\left[K_{kij}^{\psi^x}\psi_{kij}^{x}\left(\hat{e}_{iik}^{\,x}\right)\right]V_kV_j\end{aligned} \tag{D.12}$$

$$\begin{aligned}\frac{\partial \omega_i^{\psi_j^{y}}}{\partial \phi_i^{y}} &= \frac{1}{6}\sum_{j=1}^{N}\sum_{k=1}^{N}\frac{\partial\left(C_{jki}^{2}\psi_{jki}^{y}\right)}{\partial \psi_i^{y}}V_kV_j = \frac{1}{6}\sum_{j=1}^{N}\sum_{k=1}^{N}\frac{\partial\left(C_{jki}^{2}\psi_{jki}^{y}\right)}{\partial \psi_{jki}^{y}}\frac{\partial \psi_{jki}^{y}}{\partial \psi_i^{y}}V_kV_j \\ &= +\frac{1}{6}\sum_{j=1}^{N}\sum_{k=1}^{N}\left[K_{jki}^{\psi^y}\psi_{jki}^{y}\left(\hat{e}_{iij}^{\,y}\right)\right]V_kV_j\end{aligned} \tag{D.13}$$

$$\begin{aligned}\frac{\partial \omega_i^{\psi_k^y}}{\partial \phi_i^y} &= \frac{1}{6}\sum_{j=1}^{N}\sum_{k=1}^{N}\frac{\partial\left(C_{kij}^2\psi_{kij}^y\right)}{\partial\psi_i^y}V_kV_j = \frac{1}{6}\sum_{j=1}^{N}\sum_{k=1}^{N}\frac{\partial\left(C_{kij}^2\psi_{kij}^y\right)}{\partial\psi_{kij}^y}\frac{\partial\psi_{kij}^y}{\partial\psi_i^y}V_kV_j \\ &= +\frac{1}{6}\sum_{j=1}^{N}\sum_{k=1}^{N}\left[K_{kij}^{\psi^y}\psi_{kij}^y\left(\hat{e}_{iik}{}^y\right)\right]V_kV_j\end{aligned} \tag{D.14}$$

$$\begin{aligned}\frac{\partial \omega_i^{\kappa_j^{xx}}}{\partial \phi_i^x} &= \frac{1}{6}\sum_{j=1}^{N}\sum_{k=1}^{N}\frac{\partial\left(B_{jki}^1\kappa_{jki}^{xx}\right)}{\partial\phi_i^x}V_kV_j = \frac{1}{6}\sum_{j=1}^{N}\sum_{k=1}^{N}\frac{\partial\left(B_{jki}^1\kappa_{jki}^{xx}\right)}{\partial\kappa_{jki}^{xx}}\frac{\partial\kappa_{jki}^{xx}}{\partial\phi_i^x}V_kV_j \\ &= +\frac{1}{3}\sum_{j=1}^{N}\sum_{k=1}^{N}\left[K_{jki}^{\phi^{xx}}\kappa_{jki}^{xx}\left(\frac{1}{\xi_{ij}^x}\right)\right]V_kV_j\end{aligned} \tag{D.15}$$

$$\begin{aligned}\frac{\partial \omega_i^{\kappa_k^{xx}}}{\partial \phi_i^x} &= \frac{1}{6}\sum_{j=1}^{N}\sum_{k=1}^{N}\frac{\partial\left(B_{kij}^1\kappa_{kij}^{xx}\right)}{\partial\phi_i^x}V_kV_j = \frac{1}{6}\sum_{j=1}^{N}\sum_{k=1}^{N}\frac{\partial\left(B_{kij}^1\kappa_{kij}^{xx}\right)}{\partial\kappa_{kij}^{xx}}\frac{\partial\kappa_{kij}^{xx}}{\partial\phi_i^x}V_kV_j \\ &= +\frac{1}{3}\sum_{j=1}^{N}\sum_{k=1}^{N}\left[K_{kij}^{\phi^{xx}}\kappa_{kij}^{xx}\left(\frac{1}{\xi_{ik}^x}\right)\right]V_kV_j\end{aligned} \tag{D.16}$$

$$\begin{aligned}\frac{\partial \omega_i^{\kappa_j^{xy}}}{\partial \phi_i^x} &= \frac{1}{6}\sum_{j=1}^{N}\sum_{k=1}^{N}\frac{\partial\left(B_{jki}^3\kappa_{jki}^{xy}\right)}{\partial\phi_i^x}V_kV_j = \frac{1}{6}\sum_{j=1}^{N}\sum_{k=1}^{N}\frac{\partial\left(B_{jki}^3\kappa_{jki}^{xy}\right)}{\partial\kappa_{jki}^{xy}}\frac{\partial\kappa_{jki}^{xy}}{\partial\phi_i^x}V_kV_j \\ &= +\frac{1}{3}\sum_{j=1}^{N}\sum_{k=1}^{N}\left[\Gamma_1 K_{jki}^{\phi^{xx}}\kappa_{jki}^{xy}\left(\frac{1}{\xi_{ij}^y}\right)\right]V_kV_j\end{aligned} \tag{D.17}$$

$$\begin{aligned}\frac{\partial \omega_i^{\kappa_k^{xy}}}{\partial \phi_i^x} &= \frac{1}{6}\sum_{j=1}^{N}\sum_{k=1}^{N}\frac{\partial\left(B_{kij}^3\kappa_{kij}^{xy}\right)}{\partial\phi_i^x}V_kV_j = \frac{1}{6}\sum_{j=1}^{N}\sum_{k=1}^{N}\frac{\partial\left(B_{kij}^3\kappa_{kij}^{xy}\right)}{\partial\kappa_{kij}^{xy}}\frac{\partial\kappa_{kij}^{xy}}{\partial\phi_i^x}V_kV_j \\ &= +\frac{1}{3}\sum_{j=1}^{N}\sum_{k=1}^{N}\left[\Gamma_1 K_{kij}^{\phi^{xx}}\kappa_{kij}^{xy}\left(\frac{1}{\xi_{ij}^y}\right)\right]V_kV_j\end{aligned} \tag{D.18}$$

$$\begin{aligned}\frac{\partial \omega_i^{\kappa_j^{yy}}}{\partial \phi_i^y} &= \frac{1}{6}\sum_{j=1}^{N}\sum_{k=1}^{N}\frac{\partial\left(B_{jki}^2\kappa_{jki}^{yy}\right)}{\partial\phi_i^y}V_kV_j = \frac{1}{6}\sum_{j=1}^{N}\sum_{k=1}^{N}\frac{\partial\left(B_{jki}^2\kappa_{jki}^{yy}\right)}{\partial\kappa_{jki}^{yy}}\frac{\partial\kappa_{jki}^{yy}}{\partial\phi_i^y}V_kV_j \\ &= +\frac{1}{3}\sum_{j=1}^{N}\sum_{k=1}^{N}\left[K_{jki}^{\phi^{yy}}\kappa_{jki}^{yy}\left(\frac{1}{\xi_{ij}^y}\right)\right]V_kV_j\end{aligned} \tag{D.19}$$

$$\begin{aligned}\frac{\partial \omega_i^{\kappa_k^{yy}}}{\partial \phi_i^y} &= \frac{1}{6}\sum_{j=1}^{N}\sum_{k=1}^{N}\frac{\partial\left(B_{kij}^2\kappa_{kij}^{yy}\right)}{\partial\phi_i^y}V_kV_j = \frac{1}{6}\sum_{j=1}^{N}\sum_{k=1}^{N}\frac{\partial\left(B_{kij}^2\kappa_{kij}^{yy}\right)}{\partial\kappa_{kij}^{yy}}\frac{\partial\kappa_{kij}^{yy}}{\partial\phi_i^y}V_kV_j \\ &= +\frac{1}{3}\sum_{j=1}^{N}\sum_{k=1}^{N}\left[K_{kij}^{\phi^{yy}}\kappa_{kij}^{yy}\left(\frac{1}{\xi_{ik}^y}\right)\right]V_kV_j\end{aligned} \tag{D.20}$$

$$\begin{aligned}\frac{\partial \omega_i^{\kappa_j^{xy}}}{\partial \phi_i^y} &= \frac{1}{6}\sum_{j=1}^{N}\sum_{k=1}^{N}\frac{\partial\left(B_{jki}^2\kappa_{jki}^{xy}\right)}{\partial\phi_i^y}V_kV_j = \frac{1}{6}\sum_{j=1}^{N}\sum_{k=1}^{N}\frac{\partial\left(B_{jki}^2\kappa_{jki}^{xy}\right)}{\partial\kappa_{jki}^{xy}}\frac{\partial\kappa_{jki}^{xy}}{\partial\phi_i^y}V_kV_j \\ &= +\frac{1}{3}\sum_{j=1}^{N}\sum_{k=1}^{N}\left[\Gamma_2 K_{jki}^{\phi^{yy}}\kappa_{jki}^{xy}\left(\frac{1}{\xi_{ij}^y}\right)\right]V_kV_j\end{aligned} \tag{D.21}$$

$$\begin{aligned}\frac{\partial \omega_i^{\kappa_k^{xy}}}{\partial \phi_i^y} &= \frac{1}{6}\sum_{j=1}^{N}\sum_{k=1}^{N}\frac{\partial\left(B_{kij}^2\kappa_{kij}^{xy}\right)}{\partial\phi_i^y}V_kV_j = \frac{1}{6}\sum_{j=1}^{N}\sum_{k=1}^{N}\frac{\partial\left(B_{kij}^2\kappa_{kij}^{xy}\right)}{\partial\kappa_{kij}^{xy}}\frac{\partial\kappa_{kij}^{xy}}{\partial\phi_i^y}V_kV_j \\ &= +\frac{1}{3}\sum_{j=1}^{N}\sum_{k=1}^{N}\left[\Gamma_2 K_{ijk}^{\phi^{yy}}\kappa_{ijk}^{xy}\left(\frac{1}{\xi_{ik}^y}\right)\right]V_kV_j\end{aligned} \tag{D.22}$$